

Design and Performance Analysis of Indoor Visible Light Communication System Considering Human Blockages

A THESIS

SUBMITTED IN PARTIAL FULFILLMENT OF THE REQUIREMENTS

FOR THE DEGREE OF

Doctor of Philosophy

By

Anand Singh

PhD17107

under the guidance of

Prof. Anand Srivastava

Professor, IIIT-Delhi

Prof. Vivek Ashok Bohara

Professor, IIIT-Delhi



INDRAPRASTHA INSTITUTE *of*
INFORMATION TECHNOLOGY **DELHI**

Department of Electronics & Communication Engineering

Indraprastha Institute of Information Technology, Delhi

January, 2023

©Indraprastha Institute of Information Technology Delhi

Acknowledgments

My Ph.D. journey was full of unexpected events. It had many ups and downs. Apart from research and technical skills, it has taught me valuable lessons that would help me in life. It has taught me how to handle unexpected situations and multiple tasks while maintaining a balance between professional and personal life. The journey would not have been possible without the support of many people. I take this opportunity to express my sincere gratitude to all those who made this **Ph.D.** thesis possible.

First and foremost, I would like to express my special thanks to my advisers, **Prof. Anand Srivastava** and **Prof. Vivek Ashok Bohara**, for believing in me and agreeing to guide me as their **Ph.D.** student. They have helped me to improve in both technical and non-technical aspects. Now, when I look back, from where I started and where I am right now, I can certainly say I am much more confident and comfortable to drive any research project independently. I feel very fortunate to have been advised by them. Their dedicated approach toward any task is very inspiring. I truly enjoyed their many conversations that forced me to think critically. Their support throughout this work is highly appreciable. They truly have an eye for detail. Without them, this thesis would have been nothing but a distant dream.

This work would not have been possible without support from **Cognizant, India**, thank you for providing me with a **Ph.D.** fellowship. I acknowledge and express my gratitude to **Dr. G. Subrahmanya VRK Rao** and **Mr. Anand Kumar Jagadeesan**. Dr. Raos and Mr. Kumar's guidance helped me a lot to grow in both technical and industrial aspects.

I want to thank my **Ph.D.** monitoring committee members, **Dr. Gourab Ghatak (IIT-Delhi)**, **Dr. Abhijit Mitra**, and **Dr. Abhishek Dixit (IIT-Delhi)**, for their fruitful comments throughout my **Ph.D.** journey. I express my gratitude to the admin staff of IIIT-D, for being extremely helpful in the fast resolution of all admin related matters.

I want to express my gratitude to my amazing **IIIT-D** friends and labmates, **Dr. Dhananjay Kimothi**, **Dr. Parag Aggarwal**, **Dr. Ambuj Mehrish**, **Dr. Naveen Gupta**, **Dr. Mansi Peer**, **Dr. Rizwana Ahmad**, **Dinashin Anwar**, **Gurinder Singh**, **Neelam**, **Hamza**, **Rana Kumar Jana**, **Rahul**, **Akshita**, **Neetu**, **Saumya**, **Priyanaka**, **Rishu Raj (IIT-Delhi)**, **Yash Gupta**, **Tathagat Pal**, **Aranya Chakraborty (IISc Bangalore)**, for their constant support and motivation. I also want to thank my childhood friends **Rupendra**, **Sachin**, **Ashish**, **Ritesh**, **Divye**, **Atul**, and **Shailendra** for being with me in the ups and downs of life. Having friends like them is a blessing.

I express my most profound appreciation for my parents, **Maya** and **Late. Gopal Singh**, my brother **Aniruddha Singh** and my wife **Pragya Singh** for their unconditional love, support, and belief in me. They are the source of my motivation.

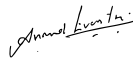


Anand Singh

PhD17107

Certificate

This is to certify that the thesis titled “**Design and Performance Analysis of Indoor Visible Light Communication System Considering Human Blockages**” being submitted by **Anand Singh** to **Indraprastha Institute of Information Technology, Delhi**, for the award of the **Doctor of Philosophy**, is an original research work carried out under our supervision. In our opinion, the thesis has reached the standards fulfilling the requirements of the regulations relating to the degree. The results contained in this thesis have not been submitted in part or full to any other university or institute for the award of any degree/diploma.



Prof. Anand Srivastava

**Department of Electronics & Communication Engineering
Indraprastha Institute of Information Technology, Delhi**



Prof. Vivek Ashok Bohara

**Department of Electronics & Communication Engineering
Indraprastha Institute of Information Technology, Delhi**

Declaration

This is to be certified that the dissertation entitled “**Design and Performance Analysis of Indoor Visible Light Communication System Considering Human Blockages**” being submitted by **Anand Singh** to the **Indraprastha Institute of Information Technology, Delhi**, for the award of degree of **Doctor of Philosophy**, is a bonafide work carried out by me. This research work has been carried out under the supervision of **Prof. Anand Srivastava** and **Dr. Vivek Ashok Bohara**. The study pertains to this dissertation has not been submitted in part or in full, to any other University or Institution for the award of any other degree.



Prof. Anand Srivastava

**Department of Electronics & Communication Engineering
Indraprastha Institute of Information Technology, Delhi**



Prof. Vivek Ashok Bohara

**Department of Electronics & Communication Engineering
Indraprastha Institute of Information Technology, Delhi**

Dedication

To My Parents & Teachers

for giving me the strength and support to pursue my dreams

ABSTRACT

Most of the current wireless networks are radio frequency (RF) based, however, these networks are regularly confronted with growing demand for higher data rates. Watching high-definition live stream videos and accessing cloud-based services are the main user activities that rapidly consume the data capacity. The higher data rates also lead to a significant increase in energy consumption. Further, the demand is much more intense for indoor communication, where the maximum data usage occurs. This leads to extra load on the base station (BTS) and poor quality of services (QoS) at the end-users. Furthermore, the indoor radio channel heavily depends on factors such as building structure, room layout, and construction materials used. Consequently, there is severe attenuation of RF waves at the receiver. Furthermore, for multi-storey buildings, floor-wise attenuation factor (FAF) increases toward lower floors. FAF for each successive floor is reduced by a factor of 6 dB. Therefore, in conjunction with RF communication, visible light communication (VLC) can provide potential solutions to address the issues as mentioned above faced by RF communication in the indoor environment.

Motivated by the above, this thesis first aims to reduce the power consumption at BTS caused due to strong attenuation of radio signals in an indoor environment by proposing a hybrid cellular-VLC link. This is achieved by replacing the end-user connection with a VLC link in the indoor environment. VLC access points (AP) act as a decode-and-forward (DF) relays, which decode the received signal transmitted from the BTS and forward it to the indoor user using LEDs. Earlier work on hybrid RF-VLC systems has not considered the amount of power saving achieved by using VLC as an indoor link. Further, the existing works have not optimized the Lambertian order for uniform delay spread and high average received optical power inside the room. The recent research also ignored the effect of dimming on the VLC link. Additionally, the analysis so far has used a static VLC channel model and has not considered the impact of user movement, type of room, or shadow objects in the room on the performance of the hybrid RF-VLC system. Hence, in this thesis, we have proposed a hybrid cellular-VLC downlink framework and have analyzed its performance for indoor environments by considering all the above parameters. This work also analyze hybrid RF-VLC system performance for a single user between RF and VLC modulation schemes of the same order. For example, VLC on-off-keying (OOK) with RF binary-phase-shift-keying (BPSK) and VLC modified color-shift-keying (M-CSK) with RF M-ary quadrature amplitude modulation (M-QAM) schemes of the same order. Further, this work also calculates the amount of power saving in the VLC link as compared to the RF link.

Light-emitting-diode (LED) deployment also plays an essential role in the VLC system, as the received optical power distribution (ROPD) varies with respect to the LED's placement and the user's location inside the room. Consequently, ROPD can be improved by optimizing the placement of LEDs inside the room. Hence, in our subsequent work, this thesis utilizes the Matern hardcore point (MHCP) process to propose a random placement of LEDs in an indoor scenario to achieve uniform signal-to-noise-ratio (SNR) and improve bit-error-

rate (BER) performance at the receiver. It has been shown that MHCP is the desirable and more appropriate process for LED placement since it results in the minimum separation between any two LEDs for better coverage and reduced interference. The system is analyzed under two receiver configurations, i.e., with the non-imaging receiver (1-FOV and 2-FOV) and with the imaging receiver.

Studies show that the received optical power in the indoor VLC system depends on the distance between the transmitting LEDs and the desired user inside the room and the presence of static and dynamic blockages. In a multi-user scenario, the other users inside the room act as blockages for the desired user. These blockages result in a sudden fall in the received optical power as it can block both the line-of-sight (LoS) and the non-line-of-sight (NLoS) signals from the LED to the desired user. The amount of power reduction will depend on the height and width of the blockage. In order to analyze the impact of static and dynamic human blockages on indoor VLC systems performance, as our third objective in this thesis, we adopt a stochastic-geometry-based approach to study the performance of an indoor VLC system in the presence of human blockages. In particular, we consider two types of blockages: static and mobile, and characterize the impact of the density of the blockages on the received signal strength of a receiver uniformly placed inside the room. Contrary to the existing studies on indoor VLC systems, which typically ignore the impact of human blockages, our investigation reveals that the blockages considerably impact the propagation environment and significantly alter the system design insights.

Moreover, unlike conventional RF communication systems, the optical wireless communication (OWC) channel is not isotropic, meaning that the user equipment (UE) orientation and obstacles significantly affect the gain of VLC. Specifically, the performance of VLC may severely deteriorate when the LoS link gets blocked due to other users/obstacles. Further, the received power may also fluctuate due to the random orientation of UE as NLoS power varies. In this thesis, in order to combat the shadowing due to obstacles and the UE orientation, as our fourth objective, we employ optical intelligent reflecting surfaces (OIRS) in indoor VLC systems in the presence of multiple human blockages. Moreover, we propose the UE orientation model of users for an OIRS-aided indoor VLC system. The LoS channel gain statistics are calculated, and the orientation of UE is modeled as a random process. By utilizing the above, the impact of the random UE orientation and human blockages on SNR performance of VLC systems is evaluated. In addition, the probability distribution function (PDF) of received SNR with OIRS is also calculated. The proposed analysis also deduces the optimum LED semiangle and the receiver FOV for the OIRS-aided indoor VLC system.

The recent interest in using visible light as a means of communication has opened up possibilities for using visible light for other applications as well, such as indoor positioning. Visible light offers higher bandwidth, immunity from electromagnetic radiation, and most importantly, it can be seamlessly integrated into the existing lighting infrastructure. As this thesis's fifth objective, we propose a visible light-based positioning system for estimating an object's three-dimensional (3-D) parameters, such as height and radius, in addition to the location in an indoor environment. The model is built using neural networks, trained by simulating multiple object scenarios in an indoor environment as well. It also takes into account the shadowing effects so it can be implemented in a multiple obstacle environment. The proposed algorithm has numerous applications, such as positioning assisted communication, suspicious object monitoring, and surveillance in an indoor environment.

Further, in earlier work, utilization of this location information for indoor communication has not been explored. We believe that this position information can be exploited to improve communication performance in the presence of different obstacles inside the room. Moreover, the LED power allocation can be optimized to maximize the data rate or minimize the BER by exploiting this location information. Hence in this thesis as a final objective, we propose a location-assisted indoor VLC system, wherein the location information is exploited to enhance the communication performance of the user. Specifically, we propose an optimal LED power allocation framework to maximize the average data rate across the room subject to predefined communication constraints as well as a number of blockages inside the room.

List Of Publications

The following papers are the outcome of the work done towards this thesis:

Journals

1. **A. Singh**, A. Srivastava, V. A. Bohara and A. K. Jagadeesan, "Optimal LED Power Allocation Framework for a Location-Assisted Indoor Visible Light Communication System," in IEEE Photonics Journal, vol. 14, no. 3, pp. 1-14, June 2022, Art no. 7329814, doi: 10.1109/JPHOT.2022.3173435. (**Published**)
2. **A. Singh**, G. Ghatak, A. Srivastava, V. A. Bohara and A. K. Jagadeesan, "Performance Analysis of Indoor Communication System Using Off-the-Shelf LEDs With Human Blockages," in IEEE Open Journal of the Communications Society, vol. 2, pp. 187-198, 2021, doi: 10.1109/OJCOMS.2020.3048954. (**Published**)
3. **A. Singh**, A. Srivastava, V. A. Bohara and A. K. Jagadeesan, "Performance of Indoor VLC System Under Random Placement of LEDs With Nonimaging and Imaging Receiver," in IEEE Systems Journal, vol. 16, no. 1, pp. 868-879, March 2022, doi: 10.1109/JSYST.2020.3019823. (**Published**)
4. **A. Singh**, A. Srivastava, V. A. Bohara and G. S. V. Rao, "Performance of hybrid cellular-vlc link for indoor environments under dynamic user movement", Physical Communication, vol. 36, pp. 100816, 2019. (**Published**)
5. A. Chakraborty, **A. Singh**, V. A. Bohara and A. Srivastava, "On Estimating the Location and the 3-D Shape of an Object in an Indoor Environment Using Visible Light," in IEEE Photonics Journal, 2022, doi: 10.1109/JPHOT.2022.3186793. (**Published**)
6. **A. Singh**, A. Srivastava, V. A. Bohara, and Marcos Katz, " Optical IRS-aided Indoor VLC System in the Presence of Human Blockages with Random User Equipment Orientation," in IEEE Journal of Optical Communication and Networking, 2022. (**Under Review**).
7. T. Pal, **A. Singh**, A. Srivastava, and V. A. Bohara, "Impact of Time-Varying Dynamic Human Blockages on Indoor Visible Light Communication System" in IEEE Transaction on Wireless Communication, 2022. (**Under Review**).

Conferences

1. **A. Singh**, A. Srivastava, and V. A. Bohara, "Optimum LED semi angle and the receiver FOV selection for Indoor VLC System with Human Blockages," VTC-Spring, Helsinki, Finland, 2022.
2. Y. Gupta, **A. Singh**, A. Bansal, V. Bohara and A. Srivastava, "Deploying Visible Light Communication for Alleviating Light Pollution," 2020 IEEE International Conference on Advanced Networks and Telecommunications Systems (ANTS), 2020, pp. 1-4, doi: 10.1109/ANTS50601.2020.9342830.
3. A. Chakraborty, **A. Singh**, V. A. Bohara and A. Srivastava, "A Visible Light Communication based predictive system for the height and location estimation of an obstacle," 2020 IEEE International Conference on Advanced Networks and Telecommunications Systems (ANTS), 2020, pp. 1-6.
4. **A. Singh**, Y. Gupta, A. Bansal, A. Srivastava, V. A. Bohara and A. K. Jagadeesan, "A Smart User-Centric Visible Light Communication System," 2020 22nd International Conference on Transparent Optical Networks (ICTON), 2020, pp. 1-5, doi: 10.1109/ICTON51198.2020.9203054.
5. S. Pandey, **A. Singh**, V. A. Bohara and A. Srivastava, "Visible Light Communication Modulation Toolkit using Reconfigurable GNU Radio Framework," 2019 IEEE International Conference on Advanced Networks and Telecommunications Systems (ANTS), 2019, pp. 1-4, doi: 10.1109/ANTS47819.2019.9118103.
6. Y. Gupta, A. Bansal, **A. Singh**, V. A. Bohara, A. Srivastava and K. Joshi " A Smart User-Centric Visible Light Communication system " accepted to 2019 IEEE International Conference on Advanced Networks and Telecommunications Systems (ANTS), Goa, India, 2019.
7. S. Agarwal, **A. Singh**, V. A. Bohara, and A. Srivastava " SDR Compatible Constant Current LED Driver Circuit Design for Visible Light Communication Applications " accepted to 2019 IEEE International Conference on Advanced Networks and Telecommunications Systems (ANTS), Goa, India, 2019.
8. **A. Singh**, A. Srivastava, V. A. Bohara and G. Subrahmanya VRK Rao, "Performance of Indoor Visible Light Communication System Under Random Placement of LEDs," 2019 21st International Conference on Transparent Optical Networks (ICTON), Angers, France, 2019, pp. 1-5.
9. **A. Singh**, A. Srivastava, V. A. Bohara, G. S. V. Rao et al., "Power and SER analysis of VLC-and RF-based links in indoor environment," in Broadband Access Communication Technologies XIII, vol. 10945. International Society for Optics and Photonics, 2019, p. 109450R.
10. **A. Singh**, A. Srivastava, V. A. Bohara and G. S. V. R. K. Rao, "Outage and Power Saving Analysis for Hybrid Cellular-Visible Light Communication and Direct Cellular Downlink," 2018 20th International Conference on Transparent Optical Networks (ICTON), 2018, pp. 1-4, doi: 10.1109/ICTON.2018.8473972.

Contents

Publication	viii
List of Figures	xvi
List of Tables	xix
1 Introduction	1
1.1 Introduction to VLC	2
1.1.1 Advantages of VLC	3
1.2 VLC System Architecture	4
1.2.1 VLC Transmitter	4
1.2.2 VLC Receiver	5
1.3 Noise Sources in VLC	6
1.3.1 Thermal Noise	6
1.3.2 Shot Noise	6
1.3.3 Ambient Noise	7
1.4 Applications of VLC	7
1.4.1 Human-Computer Interaction	7
1.4.2 Vehicular Systems	8
1.4.3 Indoor Localization	8
1.5 Research Challenges in VLC	8
1.5.1 Effect of Multipath Reflections	8
1.5.2 Dimming Control	9
1.5.3 Flicker Mitigation	9
1.5.4 ISI Mitigation	10
1.5.5 Low Modulation Bandwidth of LEDs	10
1.5.6 Augmentation with RF Systems	10
1.5.7 Shadowing	10
1.6 Related works	11
1.6.1 Recent Progress in VLC	11
1.6.2 Hybrid RF/VLC system	11
1.6.3 Placement of LEDs	13

1.6.4	Shadowing	14
1.6.5	IRS-aided Indoor VLC system	15
1.6.6	Indoor Positioning	16
1.6.7	VLC Power Optimization	17
1.7	Research Contributions	18
1.7.1	Research Gap	18
1.7.2	Contributions	19
1.8	Thesis organization	21
2	Modelling and Characterization of Multipath VLC Channels	22
2.1	Operation of Visible Light Communication System	22
2.2	VLC Channel Modelling	23
2.2.1	Source Modelling	23
2.2.2	Receiver Modelling	24
2.2.3	LoS Channel Gain	24
2.2.4	NLoS Channel Gain	24
2.2.5	Integrating Sphere VLC Channel Model	25
2.3	VLC Channel Model with User Movement	26
2.4	Indoor VLC with Human Blockage System Model	27
2.4.1	Spatial Model	28
2.5	UE Orientation	28
2.6	Modulation Technique	29
2.7	Detection Technique	29
2.8	Delay Spread	29
2.9	Summary	30
3	Hybrid cellular-VLC link for indoor environments under dynamic user movement	31
3.1	Motivation and Contribution	31
3.1.1	Motivation	31
3.1.2	Contribution	32
3.2	Hybrid RF-VLC System Model	32
3.2.1	Optimal Lambertian Order (OLO)	33
3.2.2	WINNER-II Pathloss Model	34
3.3	BER Expression in Hybrid Cellular-VLC Link Under VLC Channel with User Movement Inside the Room	34
3.4	Outage Probability in Hybrid Cellular-VLC Link	36
3.5	Power and SER Analysis of VLC and RF Based Links in Indoor Environment	37
3.5.1	Comparison of VLC and RF Based Links in Indoor VLC System Model	37

3.6	Results and Discussion	37
3.6.1	Received Optical Power Distribution	38
3.6.2	RMS Delay Spread	39
3.6.3	Outage Region for Indoor Room Using Static VLC Channel Model	40
3.6.4	Outage Analysis Under VLC Channel Model with User Movement	40
3.6.5	BER Performance Under VLC Channel Model with User Movement	42
3.6.6	Performance Under Dimming	43
3.6.7	Power Saving with respect to Cellular-VLC Link	43
3.6.8	SER Performance	44
3.6.9	Power saving with respect to Modulation Schemes	45
3.7	Summary	46
4	Indoor VLC System Under Random Placement of LEDs with Non-imaging and Imaging Receiver	48
4.1	Motivation and Contribution	48
4.1.1	Motivation	48
4.1.2	Contribution	49
4.2	System Model	49
4.2.1	Random Placement of LEDs	49
4.2.2	Receiver Structure	51
4.3	LED Power Allocation Schemes	52
4.3.1	Equal Power Allocation	52
4.3.2	Distance-based Power Allocation	52
4.3.3	Optimum Power Allocation	53
4.4	BER Performance	54
4.4.1	BER for Equal Power Allocation	54
4.4.2	BER for Distance-based Power Allocation	55
4.4.3	BER for Optimal Power Allocation	55
4.5	Results and Discussion	56
4.5.1	Received SNR Profile	56
4.5.2	BER Performance	60
4.6	Summary	61
5	Indoor Visible Light Communication System with Human Blockages	62
5.1	Motivation and Contribution	62
5.1.1	Motivation	62
5.1.2	Contributions	63
5.2	Characterization of Static Human Blockages Using MHCP	63

5.2.1	Intensity of Homogeneous Blockages Using MHCP	64
5.2.2	Intensity Calculation of Heterogeneous Blockages Using MHCP	64
5.3	Characterization of Dynamic Blockages using RWP	65
5.4	SNR Model	66
5.5	Results and Discussion	67
5.5.1	Received SNR Profile with Human Blockage	67
5.5.2	Received Power with Varying Homogeneous Blockage Intensity	68
5.5.3	Received Power with Heterogeneous Blockage Intensity Using MHCP	69
5.5.4	Received Power with Heterogeneous Blockage Intensity Using RWP	70
5.5.5	Received Power with Varying Blockage Radius and Height	71
5.6	Summary	72
6	Optimum LED semiangle and the receiver FOV selection for Indoor VLC System with Human Blockages	73
6.1	Motivation and Contribution	73
6.1.1	Motivation	73
6.1.2	Contribution	74
6.2	Multipath VLC System Model with Human Blockage	75
6.2.1	Impact of Human Body	75
6.2.2	Modeling of Human Blockages using MHCP	75
6.3	VLC Parameter Optimization	76
6.3.1	FOV Optimization	76
6.3.2	LED Semiangle Optimization	78
6.3.3	Joint Optimization	78
6.4	Results and Discussion	78
6.4.1	VLC Channel Gain as a Function of LED Semiangle and Receiver FOV	79
6.4.2	Average Received Power with Varying FOV in the Presence of Blockage	80
6.4.3	Average Received Power and the Received Quality Factor with Varying LED Semiangle	80
6.4.4	Delay Spread with and without Blockage	81
6.4.5	Quality Factor and Delay Spread Trade-off	82
6.5	Summary	83
7	Optical IRS-aided Indoor VLC System with Human Blockages Considering Random User Equipment Orientation	84
7.1	Motivation and Contribution	84
7.1.1	Motivation	84
7.1.2	Contribution	85
7.2	OIRS-aided Indoor VLC System Model	86

7.2.1	OIRS-aided VLC channel	86
7.2.2	UE Orientation	87
7.3	Orientation Model of Users for OIRS-Aided Indoor VLC System	88
7.4	PDF of the Received SNR with OIRS	90
7.5	Optimal LED Semiangle and the Receiver FOV for OIRS-aided Indoor VLC System	92
7.5.1	Optimal LED Semiangle	92
7.5.2	FOV Optimization	93
7.6	Results and Discussion	93
7.6.1	Received Power	94
7.6.2	Standalone Contribution of OIRS and NLoS (wall) Link in Received Power	95
7.6.3	Effect of OIRS Mirror Size on the Received Power	95
7.6.4	Effect of Varying LED Semiangle and the Receiver FOV on Received Power	96
7.6.5	Optimization of LED Semiangle and the Receiver FOV	97
7.6.6	Number of IRS Elements Required	98
7.6.7	BER Performance	99
7.6.8	Data Rate Performance	100
7.7	Summary	100

8 On estimating the Location and the 3-D shape of an Object in an Indoor Environment

	Using Visible Light	102
8.1	Motivation and Contribution	102
8.1.1	Motivation	102
8.1.2	Contribution	103
8.2	VLC Positioning System Model	104
8.3	Spatial Model	105
8.3.1	Regression Model	105
8.3.2	Multiple Object Environment	106
8.4	Proposed Visible Light Positioning (VLP) Model	107
8.4.1	VLP Model	107
8.4.2	Performance of VLP Algorithm	108
8.5	Results and Discussion	108
8.5.1	Received Power Profile with infinitely thin object	109
8.5.2	Received Power Profile with an object of finite radius	109
8.5.3	Variation of VLP System Performance with System Parameters	110
8.6	Shape Estimation using Visible Light	112
8.6.1	Height Estimation Model	112
8.6.2	Radius Estimation Model	114
8.7	Optimising VLP by changing Power Allocation to LED's	116

8.8	Summary	119
9	Optimal LED Power Allocation Framework for a Location-Assisted Indoor VLC system	120
9.1	Motivation and Contribution	120
9.1.1	Motivation	120
9.1.2	Contribution	121
9.2	System Model	121
9.3	LED Power Allocation Optimization Problem	122
9.3.1	Power Saving Optimization	124
9.4	BER Performance	124
9.5	Results and Discussion	125
9.5.1	Optimal LED Power Allocation	127
9.5.2	Convergence of the Proposed LED Power Allocation Framework	128
9.5.3	Optimal LED power allocation framework for 4 and 8 LED configuration with varying room size	128
9.5.4	Maximum Achieved Data Rate for Different Localization Error with respect to Number of Blockages	129
9.5.5	Effect of LED Semiangle in the Maximum Allowed Localization Error	130
9.5.6	Power Saving with and without Illumination Constraint Under the Effect of Dimming	131
9.5.7	BER Performance with Optimal LED Power Allocation	132
9.5.8	BER Performance with Random UE orientation	133
9.6	Summary	134
10	Conclusion	135
10.1	Conclusion	135
10.2	Future Work	138
	References	140

List of Figures

1.1	The electromagnetic spectrum [1]	2
1.2	VLC System Architecture.	4
1.3	Development of illumination technology.	4
1.4	Simplified circuit diagram of a FET-based transimpedance preamplifier [2].	6
2.1	Propagation Model	23
2.2	NLoS VLC Propagation Model [3].	25
2.3	Decrease in normalized received power distribution for VLC channel with user movement.	26
2.4	Indoor VLC System Model with Human Blockages	27
2.5	Schematic for calculation of shadow length due to blockage	28
3.1	Hybrid RF-VLC System Model	33
3.2	VLC and RF Based Links System Model	38
3.3	Received optical power distribution in rectangular configuration without and with OLO.	38
3.4	RMS channel delay spread inside the room without and with OLO.	40
3.5	Outage region contours inside the room with 4 LED and using OLO with different FOV.	41
3.6	Outage area comparison without and with OLO.	41
3.7	Outage Probability	42
3.8	BER Performance	42
3.9	BER performance at different dimming level.	43
3.10	Power saving at different BER with user movement.	44
3.11	SNR vs BER for indoor VLC and RF link for 2 constellation points modulation scheme	44
3.12	SNR vs SER for indoor VLC 4-CSK and RF 4-QAM Rayleigh.	45
3.13	SNR vs SER for 4-CSK in indoor VLC Dynamic channel with varying people density	46
3.14	SNR vs SER for indoor VLC 4-QAM DCO-OFDM and RF 4-QAM OFDM RF.	46
3.15	Power saving of different VLC modulation schemes over different channel models over RF link.	46
3.16	Power saving of different VLC modulation schemes over different channel models over RF link in dBm.	47
4.1	Indoor VLC System Model	50
4.2	Realization of MHCP with 16 LEDs	50

4.3	Non-imaging receiver structure with four PDs in 1-FOV and 2-FOV configuration.	51
4.4	Imaging receiver	52
4.5	Received SNR distribution for 1-FOV and 2-FOV receiver with equal power allocation.	56
4.6	Received SNR distribution for 1-FOV and 2-FOV receiver with distance based power allocation.	57
4.7	Optimal distribution of total transmit power across source LEDs.	57
4.8	Received SNR profile for 1-FOV and 2-FOV receiver with 16 LEDs in MHCP with optimal power allocation	58
4.9	Received SNR profile for 1-FOV and 2-FOV receiver with 13 LEDs in MHCP with optimal power allocation	58
4.10	CDF of received power in MHCP with equal power (EP), distance-based power (DBP) and optimal power allocation (OP).	59
4.11	BER performance of the MHCP with non-imaging 1-FOV and 2-FOV receiver	60
4.12	BER performance of the MHCP with non-imaging and imaging receiver	61
5.1	Stationary RWP model location PDF	65
5.2	Received optical power distribution profile with human blockage intensity.	68
5.3	Received power with varying homogeneous blockage intensity	69
5.4	Average Received power with varying heterogeneous blockage density inside the room with 4 and 8 LEDs.	70
5.5	Average Received power with varying heterogeneous blockage density inside the room with 4 and 8 LEDs using RWP.	71
5.6	Comparison of average Received power with heterogeneous blockage density inside the room with 4 and 8 LEDs using MHCP and RWP.	71
5.7	Average received power with varying blockage height and radius	72
6.1	Multipath VLC System model	74
6.2	Variation in VLC Channel gain as a function of PD's position	79
6.3	Effect of varying FOV and the separation distance between the blockages on the received power	80
6.4	Effect of varying LED semiangle on received power and the quality factor	81
6.5	Delay spread Comparison without and with blockage	81
7.1	OIRS-aided Indoor VLC System with Multiple Human Blockages	86
7.2	OIRS-aided Indoor Visible light Propagation System with UE Orientation [4]	88
7.3	Effect on the received power without blockages	94
7.4	Effect on the received power with and without OIRS in the presence of blockages and random UE orientation	95
7.5	Effect of mirror size on the received power	96
7.6	Effect of mirror size on the received power with varying LED irradiance angle and the receiver FOV	97

7.7	Effect of mirror size on the received power with optimized FOV and LED irradiance angle	98
7.8	Minimum number of OIRS elements required with blockages	98
7.9	BER performance without blockages	99
7.10	BER Performance with Blockages	99
7.11	Average data rate performance	100
8.1	Indoor VLP System Model	104
8.2	Received power profile of the room in the absence of any objects.	105
8.3	Parameter training using Linear Regression	106
8.4	Predictive Algorithm obtained from the results of Linear Regression	106
8.5	Differential power profile for an object at (0.6507,-1.2414) with height of 1.4806 which is used to predict the height of the obstacle	107
8.6	Infinitely thin obstacle is at (-0.6,-0.5) with height = 1m for single LED setup	109
8.7	Obstacle having finite width(=0.05m) is at (-0.6,-0.5) with height = 1m for single LED setup	109
8.8	Variation of location error with grid size	111
8.9	Variation of location error with the number of obstacles	111
8.10	Structure of the shallow neural network[5, 6] used for shape estimation	112
8.11	Training the neural network	113
8.12	Distribution of error (in meters) in prediction by the NN	114
8.13	R values for the data in each of the training, validation and test set as well as the entire dataset	115
8.14	Training the neural network	115
8.15	Distribution of error (in meters) in prediction by the NN	116
8.16	R values for the data in each of the training, validation and test set as well as the entire data set	117
8.17	Position of objects, power allocated to the LED's and the location error	118
9.1	Optimal LED power allocation in the presence of blockages with total power of 2 watts	126
9.2	Optimal LED power allocation with respect to shift in blockage location (the values in red color shows the updated LED power values due to shift)	127
9.3	Convergence of achieved average data rate for different localization error with respect to all possible solution (α)	128
9.4	Achieved average data rate with localization error for 4 and 8 LEDs and two room dimensions	129
9.5	Maximum achieved data rate for different localization error with 4 and 8 LEDs	129
9.6	Maximum allowed Localization error versus the LED semiangle with 4 and 8 LED configuration	130
9.7	Power saving and dimming performance with and without illumination constraints	131
9.8	BER Performance	132
9.9	BER Performance with DCO-OFDM and ACO-OFDM	132
9.10	BER performance with and without UE orientation	134

List of Tables

3.1 Hybrid RF-VLC System Model Parameters	39
4.1 SNR Performance of LEDs in Circular geometry	59
4.2 SNR Performance of LEDs with Non-imaging Receiver	59
4.3 SNR performance of LEDs in MHCP Configuration with Imaging Receiver	59
5.1 Indoor VLC System Model Parameters	68
6.1 VLC System Model Parameters	79
6.2 Quality Factor and Delay Spread performance with respect to proposed optimization techniques	82
7.1 OIRS-aided VLC System Model and Simulation Parameters	94
8.1 VLP System Model Parameters	105
8.2 Accuracy Matrix	110
8.3 Distributed Error in Prediction	113
8.4 Error in Prediction	116
9.1 System Model & Simulation Parameters	126
9.2 Performance Comparison	133

Chapter 1

Introduction

The shortage of spectrum in the conventional ultra-high frequency (UHF) bands coupled with increasing wireless data traffic has led the researchers to consider employing visible light communication (VLC) as one of the candidate technologies to facilitate high throughput communication in the next-generation wireless cellular standards. In this regard, integration of 5th generation (5G) New Radio (NR) with a VLC system to support the cellular downlink architecture has been proposed in the literature [7], [8]. Further, to cater these high throughput application scenarios, both back-haul and wireless front-ends need to be improved [9]. Recent studies have shown that the demand is much more severe in indoor scenarios, where the maximum data usage occurs [10]. The ambitious features envisioned for 6th generation (6G) require innovation, research, and the development of emerging communication technologies. To fulfill its challenging requirements (e.g., aggregated bit rates in the order of Tb/s), enhancing the 6G system capacity is inevitable. There are three approaches to increase the capacity of wireless communication systems. The first approach is to increase the spectral efficiency by employing better modulation schemes, improved channel coding, or a new modulation paradigm. Although the spectral efficiencies of wireless communication technologies have improved over the last few decades, but the growth has slowed down to less than 20 % in the last few years [11]. The second method is reusing the spectrum by reducing the cell size to increase the number of nodes. However, this is costly, and having two nodes does not double the capacity due to interference issues. The third approach is to acquire new sub-bands for more spectrum bandwidth (BW), but the use of radio frequency (RF) spectrum is strictly regulated by local and international authorities, and acquiring new RF sub-bands is an extremely costly affair. Moreover, the RF spectrum is finite, and it is already overcrowded.

A possible solution to address and overcome all these challenges is to use a complementary wireless communication technology operating in an entirely new band of the electromagnetic spectrum. One such promising technology is VLC, which uses the visible light signals from light-emitting-diodes (LEDs) for illumination as well as communication. Hence, VLC is an optical wireless communication (OWC) technology that can be used to fulfill the high capacity demand in indoor scenarios. In a VLC system, a LED is used as a transmitter, while a photo-detector (PD) is used as a receiver. The system operates on an intensity modulation/direct detection (IM/DD) scheme in which the intensity of LED is modulated to carry the information, and the optical signal is detected directly by a photodiode. License-free deployment and nearly universal LED availability make it an

attractive and inexpensive choice for the service providers [12].

Further, LEDs have a modulation bandwidth of up to 20 MHz [13, 14], which can support very high data rates. Moreover, it has been shown that one can achieve higher capacity and more secure communication using VLC [15–18]. It allows significant power savings as the visible light sources can serve the dual role of communications and illumination. However, despite its numerous advantages, it has a few drawbacks, such as it suffers from high interference from other light sources and is prone to significant losses due to blockage [19, 20].

This thesis focuses on the design and performance analysis of indoor VLC systems considering human blockages and random device orientation. This Chapter provides a detailed introduction and overview of VLC. It starts with a basic introduction to VLC in Section 1.1, followed by a description of the VLC system architecture in Section 1.2 and a brief discussion on the significant sources of noise in VLC systems in Section 1.3. Section 1.4 enumerates a few auxiliary applications of VLC. In Section 1.5, the major research challenges for VLC are discussed. Section 1.6 gives a brief overview of the related work. Finally, Section 1.7 provides the research contribution of this thesis. The overall thesis organization is provided in Section 1.8.

1.1 Introduction to VLC

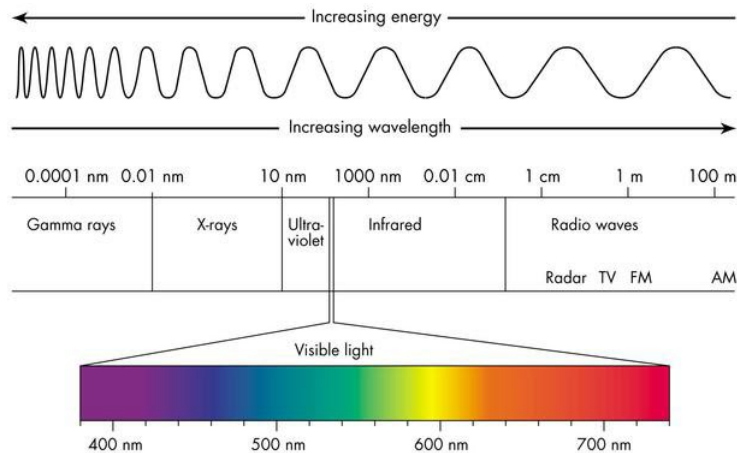


Figure 1.1: The electromagnetic spectrum [1]

VLC is an OWC technology in which data transmission is achieved by modulating carrier frequencies in the hitherto untapped visible range (380 – 750 nm) of the electromagnetic spectrum (ref. Fig. 1.1). It switches optical sources (such as LEDs) at a rate much faster than the response of the human eye, such that the light is effectively perceived as a steady glow. By combining illumination with communication, VLC provides an alternative to the over-crowded RF spectrum and promotes the judicious use of the available LED illumination

infrastructure.

1.1.1 Advantages of VLC

The interest in VLC as a complementary (and sometimes as a substitute) communication technology to RF communication is motivated by several factors as outlined below.

- **Over congested RF spectrum:** For decades, the term “wireless” had been synonymous with RF technologies, but, as explained earlier, the RF spectrum is now over stripped and dwindling. This has created a pressing need to explore and open up new and untapped regions of the electromagnetic spectrum. However, this would need creating and setting up an entirely new infrastructure compatible with the new frequency band. VLC circumvents this bottleneck because it uses LED as transmitters that are already widely used in the indoor illumination infrastructure. Moreover, visible light corresponds to the frequency band of around 400 THz to 780 THz, whereas the radio waves lie in the frequency band of approximately 3 kHz to 300 GHz [21, 22]. Hence, the VLC channel offers 400 THz of unlicensed BW, which is a 10,000 times wider spectrum than RF.
- **Less electromagnetic interference:** Unlike RF signals, visible light signals have no interference with electronic equipment and other sensing equipment like radar, etc. This makes VLC suitable for communication in hospitals and aeronautical applications.
- **Enhanced security:** Unlike RF and infrared (IR) signals, visible light cannot penetrate walls [23]. So the transmission of user data over visible light signals is confined to a room, making it difficult for eavesdroppers to intercept data, thereby enhancing security from malicious users.
- **Higher energy efficiency:** LEDs have higher energy efficiency and radiate less heat [24]. Therefore, using LEDs instead of conventional fluorescent light bulbs can significantly reduce energy consumption by up to 80 % in lighting applications [25]. Hence, the overall global energy consumption can be reduced by 50 % if all conventional light sources are replaced by LEDs [26]. This could, in turn, reduce CO2 emissions by 10 gigatons and the global crude oil consumption by 962 million barrels in the next decade [27]. The U.S. Department of Energy has reported [28] that LED technology can possibly save up to 217 terawatt-hours (TWh) of energy by 2025. Hence, the use of LEDs as transmitters has enabled VLC to become an eco-friendly green communication technology.
- **Easy and low-cost implementation:** Owing to their symbiotic relationship with indoor lighting systems, VLC can be easily implemented with a few upgrades of the illumination infrastructure, rather than setting up an entirely new communication infrastructure as required for RF communication. This drastically reduces the initial implementation cost and complexity of VLC.
- **Possibility of spatial reuse:** The confined nature of LED illumination facilitates the coexistence of closely located cells and links with minimal interference. This allows spatial reuse of modulation BW leading to higher data density.

1.2 VLC System Architecture

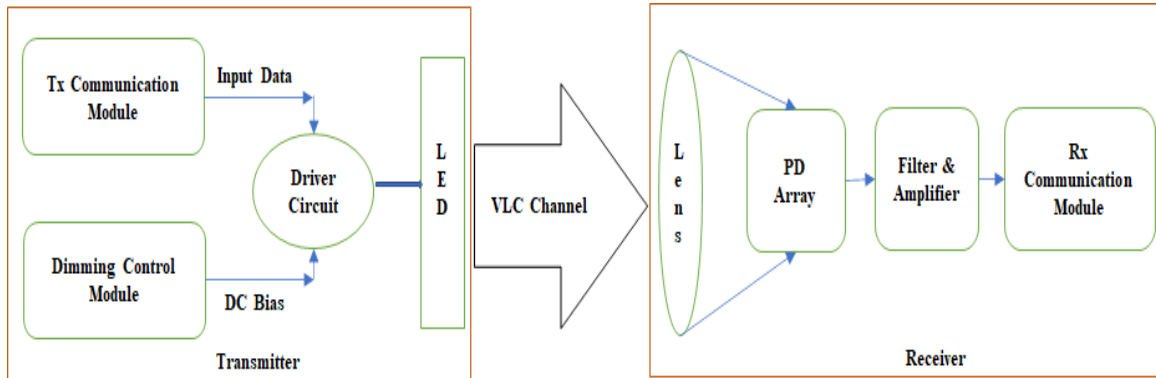


Figure 1.2: VLC System Architecture.

The basic schematic architecture of a VLC link is depicted in Fig. 1.2. Like any other communication system, VLC also consists of a transmitter, channel, and receiver. The channel in a VLC system is inherently multipath in nature. The modeling and characterization of VLC channels are discussed in detail in Chapter 2. In the following subsections, we discuss the characteristics of VLC transmitters and receivers.

1.2.1 VLC Transmitter

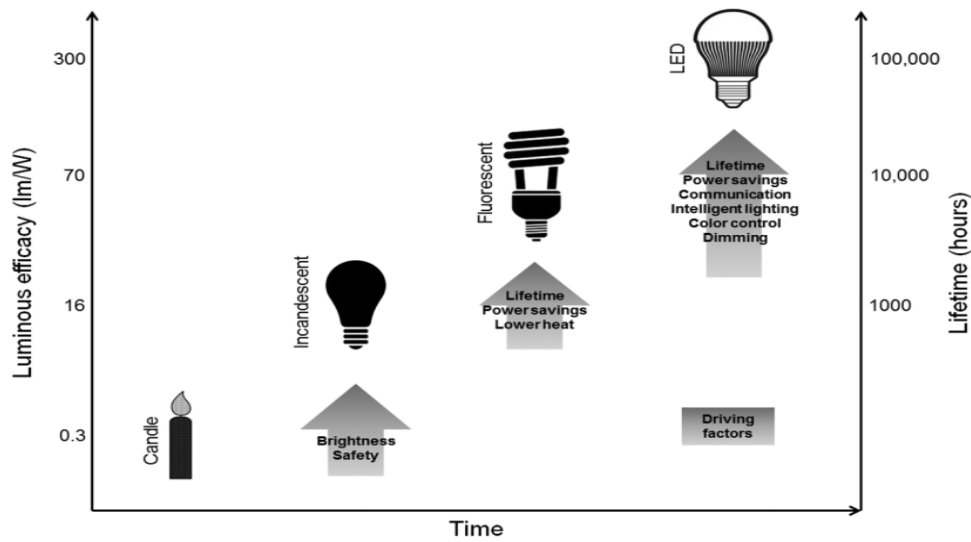


Figure 1.3: Development of illumination technology.

An LED luminaire is used as the transmitter¹ in a VLC system. It consists of an LED panel (which contains one or more LEDs), a driver circuit, housing, ballast, and other auxiliary components. Today, LEDs are the first

¹Laser diodes (operating in the visible spectrum) can also be employed as transmitters in VLC. However, it is challenging to provide indoor illumination using laser diodes. This undermines the main advantages of VLC over RFC and IRC, and hence, laser diodes are not preferred as transmitters in VLC.

choice when it comes to indoor illumination. This is mainly due to the rapid advancements in LED technology, which has resulted in LED being the most energy-efficient lighting solution with the highest luminous efficacy and lifetime among all lighting technologies like incandescent bulbs, fluorescent bulbs, etc., as depicted in Fig. 1.3. The optical output of LEDs drops by only 30 % after they have been used for 25,000 – 50,000 hours, which means their lifetime is approximately 10 times higher than that of fluorescent lamps. Moreover, the luminous efficacy of white LEDs (produced by Cree Inc.) is 254 lm/W. This is significantly higher than the luminous efficacies of incandescent and fluorescent light bulbs, which are 14 lm/W and 74 lm/W, respectively [29]. Apart from this, LEDs have numerous other advantages over traditional lighting technologies. They are safe from chemicals like mercury used in other bulbs. They can be used to generate lights of diverse colors and intensities. Moreover, they have higher modulation BW (100s of MHz), thereby making them suitable for the dual purpose of illumination and communication [30]. Depending upon their physical construction, there are basically four types of LEDs available in the market these days, namely, blue LED with phosphor (BLP); multi-chip LEDs, which employ LED chips emitting red, green, and blue (RGB) lights; organic LEDs (OLEDs); and micro-LEDs (μ -LEDs).

1.2.2 VLC Receiver

The receiver used in a general VLC system consists of a detector, optical components, and a preamplifier. The detector is a thousand times greater in size than the constructive and destructive interference patterns [30]. Hence, these patterns can be easily averaged by the receiver, thereby enabling a simple PD to be used as a detecting element in the receiver circuitry. The PDs used in VLC can be broadly divided into two types: positive intrinsic negative (PIN) PDs and avalanche PDs (APDs). Shot noise is proportional to the incident optical power and hence would not be different, assuming the PD and the APD have the same bandwidth. It is the electronic noise which is in excess for APDs. Further, APDs have higher gain. Since the intensity of the received light in an indoor VLC system is usually very high, so PIN PDs are more commonly used in such systems. Moreover, PIN PDs are less expensive and more tolerant to high temperatures [29].

Depending upon the number of detecting elements employed in the receiver, the receiver architecture can be categorized into single element receivers (containing a single PD) or multielement receivers (containing multiple PDs). Due to their simplicity and ease of implementation, single element receivers are the most popularly used in the research on VLC. Multi-element receivers are further classified into three types: selective combining receivers, image diversity receivers, and angle diversity receivers. Selective combining receivers have been used in indoor [31] as well as outdoor [32] VLC systems. However, the performance improvement by using these receivers is only marginal at the expense of a significant increase in the complexity of the receiver. Hence, their practical implementation is often not feasible. In image diversity receivers, an array of PDs is employed along with a lens to filter out signals being received from different sources. Such receivers are highly suitable for multiple-input-multiple-output (MIMO) VLC systems [33]. The work presented in [34] employed four transmitters and nine receivers to achieve a data rate up to 1.1 Gb/s using the image diversity architecture. Angle diversity receivers have a wider field-of-view (FOV) and hence, promise higher channel gains which are particularly helpful in highly diffuse links. They also help reduce channel correlation in MIMO-VLC systems. However, they are

costly and large in size.

1.3 Noise Sources in VLC

In this subsection, we discuss the various sources of noise added at the receivers in VLC.

1.3.1 Thermal Noise

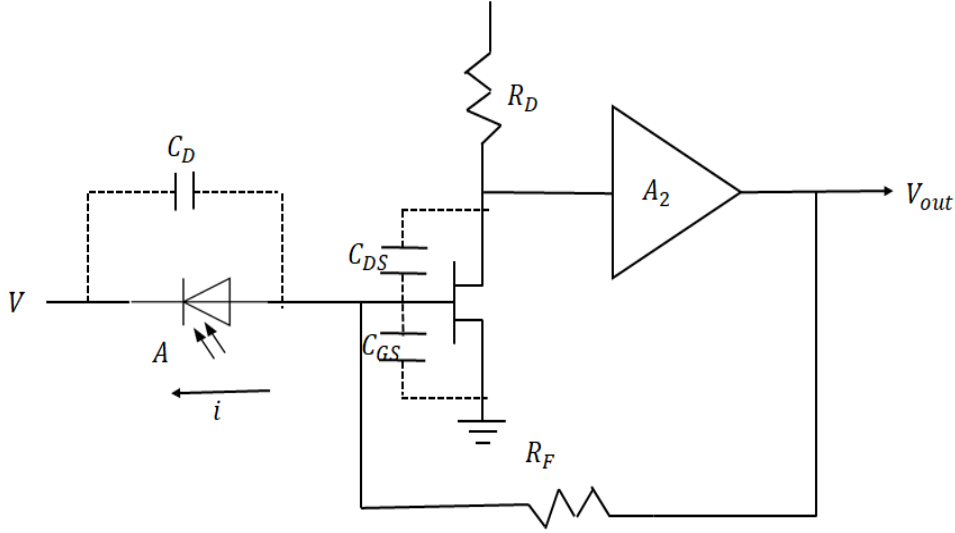


Figure 1.4: Simplified circuit diagram of a FET-based transimpedance preamplifier [2].

Thermal noise is majorly generated due to the random motion of free electrons as a result of the thermal agitation in an electrical circuit. The transimpedance type is the most preferred preamplifier circuit design in VLC receivers. Typically, superior noise performance is achieved if a field-effect transistor (FET) is used in the preamplifier circuit [2]. So, in the design of VLC systems, we generally assume a FET-based transimpedance preamplifier at the receiver front-end. Its simplified circuit diagram is shown in Fig. 1.4, where R_F and R_D are the feedback and drain resistances, respectively. C_D , C_{GD} , and C_{GS} are the capacitance's of the PD, FET drain and FET source, respectively; g_m is the FET transconductance; and V_{bis} and V_{out} are the biasing voltage and output voltage, respectively.

1.3.2 Shot Noise

Although the mean number of photons detected by the PD remains constant, the actual number of photons detected per second follows the Poisson distribution. Shot noise occurs due to the random arrival rate of photons resulting in an inherent statistical fluctuation in the number of photons detected. The effect of shot noise is significant in the indoor VLC system as shot noise is also the function of received power at the PD. In indoor scenarios, the received power is large because less distance between LED and the PD results in considerable shot noise, so the indoor VLC system is highly affected by shot noise.

1.3.3 Ambient Noise

Since VLC uses LEDs for communication as well as illumination, there is bound to be substantial interference from other artificial light sources and solar radiation. These sources contribute to the total shot noise at the receiver, as indicated in (1.2). The ambient noise sources are broadly classified into two categories:

- **Sunlight and Incandescent Lights:** These are background sources that produce a DC interference whose average power can be much larger than the desired signal power, even after optical filtering is employed [2]. Although it is mostly assumed that the DC photocurrent resulting from these sources remains stationary in time and space, but this is often not a realistic approximation. For example, solar radiation changes at different times of the day and also at different places in an indoor environment depending upon the location of the doors and windows. Moreover, the radiation from incandescent lights cannot be totally neglected unless we completely transition to LED sources for illumination.
- **Fluorescent Lamps:** Conventional fluorescent sources operate at power line frequency (50Hz or 60 Hz). However, when electronic RF ballasts are used in the driver circuitry for higher efficiency, the lamps are driven at frequencies reaching up to hundreds of kilohertz. Consequently, the spectrum of the detected electrical signal contains considerable energy at harmonics up to tens of megahertz [35]. Hence, these harmonics interfere with the useful optical power incident on the PD [36]. Unlike sunlight and incandescent lamps, the interference produced by florescent sources is not DC, and hence, they cannot be simply removed by using filters [2]. One way to tackle fluorescent light interference is to use differential detection for common-mode rejection [2] where, instead of using a single PD, we use two PDs, and the receiver recovers the signal by processing the difference between the currents generated by the two PDs. The transmitted signal is made incident only on one of the PDs. As such, while this PD receives the useful signal along with the ambient interference, the other receives only the ambient radiation. Ideally, the ambient radiation at both the PDs is the same.

1.4 Applications of VLC

Apart from indoor communication, which is its primary application, VLC also finds applications in some related areas like vehicular systems, human-computer interaction, and indoor localization. In this section, we describe these applications of VLC.

1.4.1 Human-Computer Interaction

Human-computer interaction (HCI) involves utilizing sensors for applications such as motion detection and gesture recognition. Many researchers [37],[38] have successfully applied wireless communication to enable efficient HCI, especially due to the growing interest in Internet-of-Things (IoT) for 5G and 6G networks. Lately, VLC-based HCI is being actively researched, and many related products are already commercially available. The most common example is the optical mouse which uses a small red LED that bounces off light from the surface on which the mouse is being moved. The reflected light is detected by a PD which captures an image

of the surface. Based on the changes over a sequence of images, the processing circuit sends the coordinates to the computer, which hovers the cursor accordingly. Another example is the Microsoft Kinect Sensor system [39] which performs accurate three-dimensional gesture recognition for gaming applications. However, it requires costly image sensors and highly advanced image processors, which makes this system expensive.

1.4.2 Vehicular Systems

Owing to the pervasive nature of LED technology, there is now an abundance of visible light LED sources on the roads, starting from traffic lights and streetlights to the headlights and taillights of vehicles. As such, it is an attractive option to apply VLC to vehicular systems for outdoor communication. The applications of VLC in vehicular communication can be broadly divided into three categories: vehicle to vehicle communication (V2V), vehicle to infrastructure (V2I), and infrastructure to vehicle (I2V). These are distinguished based on the transmitters and receivers being employed therein for communication. V2V systems [40], [41] utilize the headlights and taillights as transmitters, and PDs or image sensors as receivers for communication between vehicles.

1.4.3 Indoor Localization

Localization using visible light signals benefits from all the advantages of VLC over RF communication. Consequently, there has been an unprecedented interest in utilizing VLC for indoor positioning applications. Modern positioning-based applications are primarily dependent on global positioning system (GPS), which is inoperable indoors [42]. As such, there is a need to explore alternative technologies for indoor localization and positioning. In this context, indoor localization using VLC is advantageous over Wi-Fi due to many reasons. The number of LEDs is ten times more as compared to Wi-Fi access points in a typical indoor scenario [43]. This results in higher accuracy and precision of VLC based indoor positioning systems (IPSS).

1.5 Research Challenges in VLC

We now outline some of the basic system-level challenges and research gaps in the area of VLC. It is essential to address these issues in order to make VLC a feasible and viable high speed indoor communication technology.

1.5.1 Effect of Multipath Reflections

The non-penetrability of visible light signals means that they suffer reflections at the walls. These reflections create multiple paths from the LED source to the receiver, giving rise to the problem of delay spread because the light signals carrying the same data reach the receiver at different time instants. Furthermore, illumination LEDs used for VLC have a non-directed diffuse radiation pattern and are installed in the form of panels on the ceiling [44]. In such a system with a broadcasting scenario, where all LEDs transmit the same data, the presence of spatially distributed transmitters aggravates the delay spread. Hence, the presence of reflections and multiple transmitters creates the problem of delay spread, which is the primary reason for the origin of inter-symbol-interference (ISI) in indoor VLC systems. ISI is undesirable as it limits the achievable data rate

in VLC channels and entails deterioration in its bit-error-rate (BER) performance. To this end, there is a need to develop channel models that incorporate the effect of ISI caused by multiple reflections as well as the spatial distribution of transmitters. In this thesis, we have considered the effect of multipath on delay spread by considering the reflections from the wall up to the second order. We have tried to minimize the delay spread by optimizing the LED Lambertian order (Chapter 3). We have also studied the effect of multipath in the presence of blockages on delay spread (Chapter 6).

1.5.2 Dimming Control

In dual functionality applications such as VLC, where LEDs are employed both as a communication source and an illumination device, it is desirable to have efficient and reliable data communication and dimming control for brightness regulation. Different levels of luminance are required in different indoor environments [45]. For example, the illuminance range needed in public places is 30 – 100 lux, whereas offices and residential settings require almost ten times this illuminance in the range of 300 – 1000 lux [46]. Dimming control provides variable lighting levels and ensures that data communication is not hindered when a user arbitrarily changes the brightness level of the LEDs. Proper dimming support facilitates power savings, improves energy efficiency, and has ecological benefits. In fact, dimming control has been identified as an essential consideration for VLC by the the Institute of Electrical and Electronics Engineers (IEEE) 802.15.7 task group [47] [48, 49]. It is required to provide dimming support over a large range and, at the same time, maintain reliable data communication. To this end, the dual objective of dimming control and data transmission is achieved by incorporating dimming techniques into the modulation schemes popularly used in other optical wireless communication techniques like free space infrared communication (IRC). As such, it is crucial to study the power spectral densities (PSDs) and determine the BW requirement of these modulation schemes to ascertain their feasibility in practical scenarios. In this thesis, we formulate and study the effect of dimming in terms of power savings by maintaining the required quality of service and highlight the impact of dimming on their system performance (Chapter 3). Further, we have also analyzed the power saving with and without illumination constraints under the effect of dimming (Chapter 9).

1.5.3 Flicker Mitigation

Flickering is another challenge that arises due to the dual use of LEDs for illumination and communication in VLC systems. It refers to the fluctuation in the brightness of light perceived by the naked human eye and occurs due to on/off switching of the light source for data transmission. The modulation process in VLC must not introduce any noticeable flicker either during the data frame (called intraframe flickering) or between data frames (called interframe flickering) because flickering can cause detrimental physiological changes in humans [50], [51]. A switching frequency greater than 200 Hz is generally considered safe to avoid any discomfort or health risks, but long runs of 0s or 1s can reduce the rate at which intensity changes, and this could be a potential cause for flickering.

1.5.4 ISI Mitigation

ISI, which is caused due to the multipath propagation of signals, puts an upper limit on the achievable data rate in a communication system. However, the adverse effects of ISI are more severe in VLC as compared to other wireless communication technologies. This is due to the broadcasting nature of spatially distributed LED transmitters and the relatively closed and confined indoor environment in which VLC is employed [52]. These two factors result in a very large number of successive reflections, thereby leading to significant variations in the effective path lengths of different signal components carrying the same information. Hence, ISI is a serious concern for high data rate VLC systems as it behaves as a source of noise. In this thesis, in order to minimize the delay spread, we have found optimal Lambertian order (OLO). OLO maximizes the optical power from the LoS path and minimizes ISI by increasing the mean received optical power and making delay spread uniform across the room (Chapter 1).

1.5.5 Low Modulation Bandwidth of LEDs

Most of the advantages of VLC are attributed to the high efficiency, compact size, long life, and low cost of the white LEDs used therein [53]. However, these LEDs have a limited modulation BW (a few megahertz), creating a major bottleneck in developing a high-capacity VLC system. Multiplexing techniques are employed for the capacity enhancement of VLC systems to operate at this upper limit. Several orthogonal multiplexing techniques, such as optical orthogonal frequency division multiplexing (O-OFDM), have been proposed to support multi-user networks.

1.5.6 Augmentation with RF Systems

Since RF-based technologies like Wi-Fi are already omnipresent, especially in indoor scenarios, augmenting them with the VLC technology is an attractive option to expedite the practical implementation of VLC systems. The RF links can be used as a backup to provide uninterrupted connectivity when the VLC link fails, thereby preventing system outage. Another possibility is establishing RF links for inter-user communication while each user is connected to the VLC access point. This provides cooperative diversity and improves the reliability of the overall communication system. In this thesis, we propose a hybrid RF-VLC link in order to save the power at the RF base station (Chapter 1).

1.5.7 Shadowing

The received optical power in the indoor VLC system varies with respect to the distance from respective transmitting LEDs to the intended user inside the room. When there are multiple users inside the room, these users and other static obstacles like furniture acts as a blockage to the intended user and create shadowing. This shadowing results in a sudden fall in received optical power as it can block both the line-of-sight (LoS) and the non-line-of-sight (NLoS) signal from the LED to the intended user. The amount of power reduction will depend on the height and width of the obstacles [20]. In this thesis, we studied the effect of shadowing with static and dynamic blockages (chapter 5). We have also found the optimum VLC parameters, such as LED semiangle and

the receiver FOV, under the effect of shadowing (Chapter 6). Further, we have also analyzed the VLC-based indoor positioning system performance under the impact of shadowing due to blockages (Chapters 8 and 9).

1.6 Related works

In this Section, we discuss the state-of-the-art in VLC and present a brief survey on the related research literature in Section 1.6.1. We highlight some latest advancements in the field of hybrid RF/VLC technology in Section 1.6.2 and outline the importance of LED deployment and the multi-PD receiver for VLC systems in Section 1.6.3. Subsequently, in Section 1.6.3, 1.6.4, 1.6.5, 1.6.6, and 1.6.7, we describe the existing research work related to shadowing and the other challenges mentioned earlier in Section 1.5.

1.6.1 Recent Progress in VLC

Owing to the attractive benefits promised by VLC and a simultaneous boom in demand for LEDs, the research in VLC has experienced a massive thrust. Parallel to the efforts to standardize VLC, numerous research groups are working on developing high data rate VLC links. The earliest attempt to modulate visible light by fast switching of LEDs was presented in 1999 by Pang et al. [54]. Later, visible light beams were used to transmit data at 10 Mb/s over a distance of 1.4 km by the Reasonable Optical Joint Access (RONJA) group [55] in 2001. The use of white LEDs for the dual purpose of illumination and communication was pioneered by Tanaka et al. at the Keio University [56]. In 2003, Komine et al. demonstrated a VLC link in which they achieved data rates up to 200 Mb/s [33]. The European Union sponsored the hOME Gigabit Access (OMEGA) project to implement VLC in providing gigabit wireless access in the indoor environment. Using visible light, the OMEGA group demonstrated a data rate of 125 Mb/s in 2009 [57], followed by 513 Mb/s in 2010 [33], 803 Mb/s in 2011 [58] and 806 Mb/s in 2012 [59]. Around the same time, several other research groups began active research in this area.

1.6.2 Hybrid RF/VLC system

It is expected that the VLC system will be used primarily for indoor environments. However, recent studies have shown that it can also be employed for outdoor settings to provide hot-spots for internet access using street lighting, and cellular access as part of 5G cellular technology [60]. Recent studies have also explored the coexistence of VLC and RF in the indoor environment with the goal of power optimization. For instance, [61] proposes a hybrid radio-visible downlink to provide connectivity in RF protected areas such as hospitals and airplanes. An amplify-and-forward (AF) relay is used outside the building to receive the radio signal from BTS. However, [61] only considered a LoS link while calculating the signal-to-noise-ratio (SNR) distribution inside the room for evaluating the outage probability. In [62], a relay-assisted VLC system is proposed where a mobile user acts as a relay and forwards data from the source to the end mobile user. Both AF and DF relaying techniques were incorporated and compared. The results obtained in [62] showed that DF outperforms the AF relaying scheme for different irradiance angles. Further, DF relay-based system offered a more comprehensive coverage area compared to the AF scheme. Kizilirmak et al., in [63] presented a hybrid VLC system where an intermediate

light source receives the signal from the primary light source, and forwards it to the end user using relaying techniques such as AF and DF. The performance of the VLC system was measured in terms of SNR and BER. Further, the performance is optimized by optimal LED power allocation under illumination constraints. Results in [63], showed that under the same lighting requirements, DF relaying provides higher BER performance gains over AF. In [64], cooperative communication for orthogonal frequency division multiplexing (OFDM) based VLC systems with full-duplex (FD) relaying is investigated. Through analytical and simulation results, it is demonstrated that FD relaying is far more superior than half-duplex (HD) relaying, specifically for higher order modulation schemes. For lower order modulation schemes, HD relaying slightly outperforms FD relaying. It is also shown that both AF and DF relaying techniques significantly outperform the direct VLC link. In [65], authors shows that for a VLC system the user throughput can fluctuate widely in the room depending on the location of the receiver. To improve the performance of a standalone VLC system, an RF system is introduced where the system dynamically assigns users to either VLC or RF system based on the channel conditions of the user. Authors in [65], further optimizes the spectrum and power for the RF system to ensure certain outage and user data rate performance. In [66], a mathematical toolbox is proposed for performance analysis of hybrid RF/VLC systems that work under low latency conditions. It is shown that RF technology can be beneficial when there are lower average power constraints and lower QoS requirements. Further, VLC either alone or in a hybrid transmission strategy can potentially enhance the delay performance of the system. Hammouda et al., in [66] proposed a hybrid system design for wireless indoor access to reduce the power consumption of indoor networks. The system proposed in [66] contained both traditional RF APs along with the VLC APs. As the majority of indoor traffic is downlink, the proposed thesis focuses on minimizing the total downlink power consumption. In [67] and [68], the energy efficiency benefits of employing VLC in a heterogeneous wireless environment is investigated. The problem of maximizing the heterogeneous network energy efficiency constrained by the required data rates is analyzed. Specifically, it has been shown that integrating VLC and RF APs in heterogeneous wireless networking environments increases the energy efficiency.

Further, the idea of combining different modulation techniques has been recently proposed in the past. Liu et al. have introduced a new class of optical modulation formats based on combining M-ary pulse-position-modulation (M-PPM) or modified frequency-shift-keying (M-FSK) with additional polarization and phase modulation [69]. Also, they have presented the principle, implementation, and performance of high-sensitivity modulation format based on the combined use of polarization-division-multiplexed quadrature phase-shift-keying (PDM-QPSK) and M-PPM [70]. Selmy et al. have proposed hybrid BPSK-modified MPPM, which outperforms both traditional BPSK and MPPM techniques [71]. Also, they have introduced a new hybrid modulation technique based on both quadrature phase shift keying (QPSK) modulation and modified-MPPM technique. Their proposed scheme achieves much less bit error rate levels than that of traditional QPSK modulation [72]. Khallaf et al. have proposed a hybrid orthogonal frequency division multiplexing pulse-position modulation (OFDM-PPM) technique for turbulent free-space optical communications systems [73]. Hybrid quadrature amplitude modulation (QAM)-MPPM modulation technique has been introduced in [74], it shows that over turbulent channels in free-space optical communication systems, the BER performance of this technique out-

performs that of ordinary MPPM and conventional QAM techniques.

1.6.3 Placement of LEDs

LED deployment also plays an essential role in VLC system, as the received optical power distribution (ROPD) varies with respect to the placement of LED and the location of the user inside the room. Consequently, ROPD can be improved by optimizing the placement of LEDs inside the room. Lei et al., in [75], proposed an approach to obtain optimum spacing between LEDs in square geometry and maximum radius in case of circular geometry to achieve uniform SNR across the room. To find the optimum location of the LEDs, a numerical optimization based local search algorithm is employed. The solution is obtained by an iterative process and remains sub-optimal if the time bound expires. In [76], the relationship between the placement of LEDs and ROPD is studied, and a method is proposed to deploy the LED in a plane to improve the SNR at the receiver. Varma et al., in [77], proposed a binomial point process (BPP) to deploy the LEDs in a plane to achieve uniform illumination. Further, a simple heuristic power allocation scheme is also proposed to obtain uniform irradiance. In [78], an optimum placement of LEDs arrays is investigated for indoor VLC subject to maximization of average area spectral efficiency (ASE). Design parameters of the LED array such as the distance between two neighboring LEDs and the precise location of the LED arrays on the ceiling are obtained by solving an optimization problem. Due to the complexity of the optimization problem, a numerical optimization procedure is employed, and the maximization is carried out by using algorithms from MATLAB optimization toolbox. In [79], an ab initio design of a LED array for achieving uniform illumination is presented. Specifically, an optimization technique based on evolutionary programming has been developed to facilitate the search for an optimal array in the hyperspace formed by a number of LEDs and spacing among them.

As evident from above, most of the non-imaging literature has focused on the placement of LEDs with regular geometry and equal power allocation to the individual LED sources. While uniform illuminance is desirable, optimal power consumption is an essential factor in the deployment of the LEDs. To address this issue, recent literature has focused on power allocation, along with flexibility in the LED source geometry to achieve uniform irradiance. In [80], hyper-heuristics evolutionary algorithm (HypEA) is proposed to optimize the LED resources within an indoor room. Niaz et al., in [81], proposed an optimized LED deployment technique to provide a better ROPD across the room while keeping the power consumption to minimum. Specifically, the authors applied particle swarm optimization (PSO) technique to minimize the overall outage area of an indoor VLC system. In [82], a network planning tool is provided to maximize the average rate achieved by the users in a room by optimizing the LED footprint. The proposed tool also takes into account the signaling needed to accomplish the handover task. In this regard, it is shown that several parameters influence system performance starting from the download data rate, the movement of the user in the room as well as the handover time. In [83], a genetic algorithm is proposed to optimize the refraction indices of the concentrators on receivers to achieve a uniform distribution of the received power, without decreasing the illuminance quality. Simulation results show that the proposed method can effectively reduce the RPDP (the ratio of power deviation from peak) from 88% to 52%, with respect to the transmitted power.

1.6.4 Shadowing

In a VLC system, the availability of a LoS link between the LED and the PD is essential for successful data transmission. However, a direct LoS path between LED and the PD is not always guaranteed due to the presence of other users and objects (collectively called blockers). Therefore, the occurrence of LoS blockage is very frequent in indoor VLC systems, and according to [84], this can have detrimental effects on its performance. In [85], the authors have considered an O-OFDM based indoor attocell network and computed the outage probability and achievable rates for different network deployments. In [86], authors have characterized the rate as well as coverage of different RF and VLC systems under different configurations using stochastic geometry. Since VLC networks are generally confined to room boundaries, each user may not necessarily see a similar serving transmitter's distribution and interference field. This effect is more prominent in the presence of wall reflections and obstacles between the transmitter (LED) and the receiver (user). Therefore, it is essential to include the impact of users' locations and modeling of the blockages in the performance analysis. In [87], a novel and tractable model for characterizing the probability of human-body blockage is proposed. Specifically, they model the humans as cylindrical objects with arbitrarily distributed heights and radius, whereas the location of the center of the cylinder follows a Poisson Point Process (PPP) in two dimensions. A novel AP placement method that considers a stationary distribution of the users has been proposed in [88]. The novel optimization framework for approximately optimal VLC AP placement takes into account the stationary distribution of users for the first time. This distribution is the result of the mobility pattern of users in an indoor environment. The proposed method is independent of the resource allocation algorithm and eliminates the need for exhaustive simulations to find the optimal location for VLC APs. However, the authors in [88], overlooked the distribution of users inside the room in their proposed model. In an indoor environment, depending on their mobility pattern, the users may be reluctant to stay close to the walls, and the distribution of users is generally not uniform. For example, users' stationary distribution is well approximated by an elliptic paraboloid function if users obey the celebrated random waypoint mobility (RWP) model [89]. Dastgheib et al. have introduced the problem of mobility-aware optimization of resources in VLC networks using the T-step look-ahead policy and employing the notion of handover efficiency in [90]. It is shown that the handover efficiency can correlate the network's overall performance with future actions based on users' mobility. In [91], the authors investigated the deployment of light sources as well as proposed an optimization framework for power allocation to evaluate the BER and the required transmitted signal power under illumination constraints in presence of a blockage. The system performance is further optimized under lighting constraints, especially when a blockage impairs the LoS link. A low complexity optimization problem is formulated where a simplified power allocation is derived.

Further, to track the behavior of the mobile users, it is essential to use a mobility model such as random walk, Markovian models [92], Levy walk [93] and models based on product-form queuing networks [94], [95]. Amongst different models, the RWP is widely used, and hence is thoroughly studied [89]. In RWP model, each user moves at a uniform speed. Then it selects another destination randomly according to a uniform distribution and moves toward that point with another speed along a straight line [96]. As the users continue to move, the distribution of the position of users approaches a stationary distribution [89]. For the dynamic users inside the

room, the fact is that most of the users will prefer to stay at the center of the room rather than near the edge of the room or close to walls. The RWP model results in a distribution that concentrates more probability mass near the centre of the coverage area. Thus, since most of the optical power in VLC is concentrated near the placement of LED, it is more reasonable to employ the RWP mobility model rather than uniform spatial distribution.

1.6.5 IRS-aided Indoor VLC system

Prior studies on indoor VLC systems have shown that it is necessary to study the impact of obstacles and user equipment orientation for an indoor VLC system [20], [97]. As in both cases, the LoS path from the LED to the PD may be blocked, resulting in a significant reduction in the received SNR. Various system models have been used to characterize obstacles and user equipment orientation in an enclosed area. In [98], Soltani et al. considered three standard angles similar to those used in mobile devices to model the device orientation, namely yaw, pitch, and roll. The proposed orientation model investigates the effect of UE orientation on users' throughput and network load balancing. The impact of the receiver's tilted angle on the channel capacity of VLC is examined in [99]. The lower and upper bounds with the receiver's tilted angle of the channel capacity for the VLC system are presented. It is shown that we can improve the channel capacity by tilting the receiver plane correctly by considering an optimization problem in order to combat the LoS link blockages in the VLC system. However, the possibility of providing the NLoS channel gain to the blocked users (due to unavailability of LoS link) from the wall or using optical intelligent reflecting surfaces (OIRS) can be explored. The NLoS path generated through the walls is not guided, whereas we can guide the NLoS path coming from the OIRS if we have prior information on the location of the blockages.

Recently, increasing channels by adding design degrees of freedom by incorporating tunable IRS has received significant research attraction in RF systems [100–102]. Considerable efforts have been dedicated in order to model and investigate the potential gains of using IRS in RF networks performance enhancement [103], [104]. As for the VLC systems, OIRS are expected to participate effectively in boosting their performance by increasing the probability of LoS gain, and it is because most of the VLC systems rely on the existence of an LoS path between LED and the PD [105–107]. Incorporating OIRS in indoor VLC systems can provide significant gains in terms of resilience to LoS blockages, an improved trade-off between illumination and communications quality of service, interference mitigation, more efficient energy harvesting capabilities, and enhanced localization services. However, in [108] authors have investigated the application of IRS in VLC systems and focused on the derivation of irradiance expressions for IRS elements and studied their focusing capabilities. Similarly, an IRS-aided secured VLC system and the energy efficiency optimization model have been explored in [109], and [110], respectively. Authors in [111] presented a framework for integrating IRS in indoor VLC systems. It includes the overview of IRS, including its advantages and main applications for indoor VLC systems. Also, authors in [111] discuss critical factors about the design and integration of IRS in VLC systems, namely, the channel state information (CSI) acquisition, the deployment of IRSs, the optimization of IRS configuration, and the real-time IRS control. The authors also suggest several promising research directions that centers around the integration of IRS in indoor VLC systems.

In [112] authors explore the use of IRS to address the LoS link blockage issue in an indoor VLC system. It also considers observed user behaviors such as random UE orientation and obstructions in the direct link between the transmitter and the receiver. Specifically, a system model for an IRS-aided VLC system is proposed, and a rate maximization problem is considered to determine the optimal orientation of the IRS mirror array to establish robust non-LoS links. Najafi et al., in [113] investigate the use of IRS to relax the LoS requirement for free-space-optical (FSO) systems. They have considered a Gaussian laser beam and designed a phase-shift distribution across the IRS that enables the reflection of the incident beam in any desired direction, i.e., realizing the generalized law of reflection. Moreover, for the designed phase-shift profile, the authors demonstrated an equivalent mirror-assisted FSO system that generates a reflected electric field on a mirror identical to the IRS in the original system. Similarly, [114] in authors investigates the use of intelligent mirrors to relax the LoS requirement for the FSO systems. Here, the authors characterize the impact of the physical parameters of the IRS, such as IRS positioning, IRS mirror size, and the orientation of IRS (essentially the mirror angles), on the quality of the end-to-end FSO channel like, BER and the achieved data rates. In [110], Qian et al. investigate the energy efficiency maximization problem in a downlink using a re-configurable intelligent surface (RIS) assisted indoor VLC system. Further, they have also formulated an energy efficiency maximization problem through jointly optimizing power control, time allocation, and phase shift matrix subject to the total power constraints for indoor VLC systems [110].

1.6.6 Indoor Positioning

VLC has been widely used in indoor positioning, its suitability for indoor positioning comes from the fact that it offers large bandwidth, high positioning accuracy, and immunity from electromagnetic interference. In addition, it requires no large-scale costs for deployment as it can be integrated seamlessly into the existing illumination setup. Moreover, the LED-based VLP system can also be applied in other applications such as light assisted communication, suspicious obstacle monitoring, and surveillance in an indoor environment. VLC-based positioning techniques are of two types, PD and image sensor (IS) based systems [115]. The usage of PD based system is more because they have high sensitivity to light, and they are less expensive, whereas IS can spatially separate light sources. But preference is given to IS based positioning technique because it does not need multiplexing techniques, and also, positioning exactness will not be influenced by surrounding light interference. The basic methodology is trilateration which uses visible light sources as anchors. In Epsilon [116], each bulb, with its lighting function, also serves as a site mark. It transmits, using the light carrier; location signals carries the information, which means the stance of the bulb and its duty cycle, to enable positioning on the end of the receiver part. An intelligent cell is used as a receiver that uses light sensors to extract the signal's information, and the received signal strengths (RSS) are measured [117] from many LEDs, and distance is calculated from each bulb using the optical channel model. Then, from all light sources, beacon information is received, and distances are measured, which helps to estimate the location. There are different methods for triangulation's like received signal strength indicator (RSSI), time of arrival (TOA), angle of arrival (AOA), and time difference of arrival (TDOA). There are different probing signals depending on the positioning system, like ultrasound, ultra-wideband (UWB), and wireless local area network (WLAN). As ceiling lights are visible from

any place in an indoor environment, it works under LoS conditions, which is why the received signal strength ratio (RSSR) is preferred [117]. Here the RSSR is the ratio of the received signal power (strength) at the PD to the transmitted signal power from the LED. In an indoor VLC system, RSSR is determined by the LED transmission power, the distance between the LED and the PD, and the respective VLC parameters such as LED irradiance angle, receiver FOV.

The two primary components required for visible light-based indoor positioning are the LED as transmitters and PD as optical receivers. There is a constant link between the LED and PD, which is only interrupted in the presence of an object blocking the LoS. Thus the changes in the channel characteristics in the presence of an object can be used to gather information about the object such as its position, shape etc. However, multipath propagation, shadowing and interference from various noise sources as well as from other objects in the vicinity affect the LED's transmitted optical signals [118]. Thus, finding suitable models for the VLP to achieve high positioning accuracy is a source of a considerable amount of research. [119].

1.6.7 VLC Power Optimization

Earlier authors review the optimization techniques previously reported in the literature to improve the VLC network performance when the system consists of multiple users. In [120], authors considered four main issues are considered in this type of network, for maximizing the various objectives and achieving the various constraints, including power and resource allocation, users to APs association (APA), cell formation, and AP cooperation used for mitigating the disadvantages of VLC networks to improve performance. Similarly, in [121], with the help of a central controller, and by considering the arbitrary receiver orientation, Soltani et al. proposed an approach for APA to users, based on the strength of the received signal and the traffic of the APs, aimed at maximizing the system's throughput. It is shown that, when any user wants to join an network, the central controller calculates all the offered data rates from all APs and enables the user to select the best AP. Wu et al. in [122], jointly allocated time resources to the users and assigned APs to the users. They considered the resource allocation problem as a bidirectional allocation game, since the aim of APs is to select the only users that maximize the system throughput, and the users want to select APs providing better QoS. By considering mobile users in standalone VLC networks, Zhang et al. in [123], proposed a novel user-to-AP assignment based on anticipating the future users' locations and their traffic dynamics, and find a trade-off between the delay and the throughput in the dynamic VLC systems. Jiang et al. in [124], studied and formulated the joint power allocation and load balancing (LB) problems. Chen et al. in [125], investigated the effects of the cell size and network deployment on the performance of VLC systems by measuring the signal-to-noise and interference ratio (SINR) distributions. Cincotta et al., in [126] show that the introduction of luminaire reference points (LRPs) dismisses this limitation and allows the creation of a self-contained VLP system that requires only a single luminaire in its FOV. It is noted that the models presented in the existing literature focus on optimizing the location accuracy. Employing this location information to improve communication performance has been ignored. Also, how can we use this location information to improve the shadowing caused by obstacles inside the room.

1.7 Research Contributions

In this Section, we discuss the research contribution of this thesis based on the brief survey on the related research literature in Section 1.6. Section 1.7.1 discuss the possible research gap based on the literature survey. We highlight some major contributions of this thesis in Section 1.7.2.

1.7.1 Research Gap

Previous studies on indoor VLC systems have not considered the amount of power saving that can be achieved by using VLC for indoor communication scenarios. Further, the existing works have not optimized the Lambertian order for uniform delay spread, and high average received optical power inside the room. The existing work also ignored the effect of dimming on the VLC link. Further, the analysis so far have used static VLC channel model and have not considered the impact of user movement, type of room, shadow objects in the room on the performance of indoor VLC system. In indoor VLC system LEDs deployment plays an essential role, as the ROPD varies with respect to the placement of LEDs and the location of the user inside the room. Consequently, ROPD can be improved by optimizing the placement of LEDs inside the room. Motivated by these earlier works, in this article, we utilize MHCP to propose a random placement of LEDs in an indoor scenario to achieve uniform SNR and improved BER performance at the receiver. It has been shown that MHCP is a desirable and more appropriate approach for LED placement.

Further, earlier works on indoor VLC systems have not considered humans' impact as a blockage. The existing work also ignored the effect of static and dynamic human blockages inside the room. Also, the impact of NLoS links in indoor VLC systems with human blockages has not been explored previously in the literature. In addition, the recent study on indoor VLC does not provide any method to characterize the static and dynamic blockages inside the room. In a VLC system, the availability of a LoS link between the LED and the PD is essential for successful data transmission. However, a direct LoS path between LED and the PD is not always guaranteed due to the presence of other users and objects (collectively called blockers). Therefore, the occurrence of LoS blockage is very frequent in indoor VLC systems, and according to [84], this can have detrimental effects on its performance. Further, in many studies on VLC systems, it is assumed that the users' devices always face upward towards the ceiling where LED is located [127, 128]. However, such an assumption is impractical as users typically operate their smartphones by holding them in any comfortable position other than vertically upward. Hence, random user equipment (UE) orientation does affect the existence and availability of LoS links as demonstrated in [4, 97]. Therefore, it is crucial to consider random UE orientation in the design and analysis of indoor VLC systems. Further, in earlier work, utilization of this location information for indoor communication has not been explored. We believe that this position information can be exploited to improve communication performance in the presence of different obstacles inside the room. The LED power allocation can also be optimized to maximize the data rate or minimize the BER by exploiting this location information. Our study tries to address all the research gaps mentioned earlier in this thesis.

1.7.2 Contributions

The main contributions of this thesis are summarized as follows:

- To reduce the power consumption at BTS caused due to strong attenuation of radio signals in an indoor environment in this thesis, we have proposed a hybrid cellular-VLC link where the cellular link is followed by the VLC link, which acts as a DF relay. The performance of the hybrid link has been compared with a direct cellular link. Further, the closed-form expressions for BER and outage probability are derived by considering the movement of people and different indoor conditions. The proposed thesis also optimizes the Lambertian order of the LEDs in order to make delay spread uniform and increase average SNR through the LoS path inside the room, resulting in higher throughput and reduced outage in the room. It is observed that there is significant power saving when VLC is used as an indoor link. The effect of dimming on the VLC link is also investigated. It has been shown that it is possible to have a wide dimming range without compromising on BER performance.
- Further, to the best of the authors' knowledge, comparing RF and VLC modulation schemes as standalone technology under static and dynamic VLC environments has not been done so far with the objective of power-saving. This thesis aims to analyze indoor system performance for a single user between RF and VLC modulation schemes of the same order. For example, VLC on-off-keying (OOK) with RF BPSK and VLC modified-color-shift-keying (M-CSK) with RF M-QAM schemes of the same order. Also, this work calculates the amount of power saving in the VLC link as compared to the RF link.
- To provide the uniform received power across the room and improve BER performance, this thesis proposes a random placement scheme of LEDs using MHCP, which results in a more uniform SNR at the receiver throughout the room. The performance of the proposed method has been evaluated under two types of receiver structures, one with four PDs in 1-FOV and 2-FOV non-imaging receiver configuration and another with an imaging receiver. Further, an optimal and distance-based power allocation scheme is proposed to distribute the power across each LED. The proposed power allocation schemes have shown improved performance regarding equal power allocation schemes.
- In order to analyze the impact of static and dynamic human blockages on indoor VLC systems performance, in this thesis, we adopt a stochastic-geometry-based approach to study the performance of an indoor VLC system in the presence of human blockages. In particular, we consider two models of blockages: static and mobile, and characterize the impact of the density of the blockages on the received signal strength of a receiver uniformly placed inside the room. Contrary to the existing studies on indoor VLC systems, which typically ignore the impact of human blockages, our investigation reveals that the blockages considerably impact the propagation environment and significantly alter the system design insights. Then, we extend our study to the MHCP with different radii to emulate different sizes of the blockages. Further, to include blockages' movement, the RWP model with uniform velocity has been considered. The RWP model gives more practical realizations of blockages inside the room.

- With the objective of uniform received power across the room, this thesis optimizes the LED semiangle and the receiver FOV for an indoor VLC system in the presence of human blockages for 4 LEDs in a rectangular configuration in order to provide a high-quality factor (Q) and minimum delay spread across the room. In the analysis of Q inside the room, wall reflection up to second-order and reflections from the human body and the clothes are also considered. A Joint optimization framework along with single variable optimization have been proposed to provide us with the optimum value of the VLC parameter (LED semiangle and receiver FOV) considering the impact of human blockages. Moreover, We also analyze the trade-off between the required quality factor and the delay spread across the room with respect to the number of blockages, LED semiangle, and the receiver FOV.
- The received power in VLC may also fluctuate due to the random orientation of UE as a result of self-blockage. In this thesis, in order to combat the shadowing due to obstacles and the UE orientation, we employ optical IRS (OIRS) in indoor VLC systems. This thesis makes a novel contribution in investigating the impact of random UE orientation for OIRS-aided indoor VLC systems. The proposed framework also considers multiple human blockages. We have proposed a UE orientation model for an OIRS-aided indoor VLC system with multiple human blockages considering random UE orientation. The receiver statistics, such as critical elevation angle, rotated normal vector with respect to OIRS, and the multiple LEDs have been calculated. Additionally, this thesis also determined the optimum OIRS mirror size with respect to the varying LED semiangle and the receiver FOV for a given room size and the varying number of human blockages.
- Further, in this thesis, we propose a novel system model for VLP, which can be used to estimate the location of objects in a room. Unlike the conventional VLP models, the proposed model can be used to predict the location even in the presence of multiple objects. Further, we also construct and train a neural network (NN) to estimate the height as well as the radius of the objects. The NN, along with the VLP algorithm, can be employed together to construct a 3-D model of the objects in the room. In addition, we propose a method to optimize the power allocation to each LED by exploiting the objects' current location while maintaining the system's total power constraint. This will lead to efficient power allocation among LEDs based on the position of objects in the room for optimum communication performance.
- Finally, in this thesis, we propose a location-assisted indoor VLC system, wherein the location information is exploited to enhance the communication performance of the user. Specifically, we propose an optimal LED power management scheme to maximize the average data rate across the room subject to predefined communication constraints as well as the number of blockages inside the room. We have also formulated a power-saving optimization framework to maximize the power savings among the LEDs with respect to the number of blockages and permissible localization errors. The effect of dimming on the above is also investigated.

1.8 Thesis organization

In this thesis, we analyze the performance of an indoor VLC system in the presence of obstacles (both static and dynamic), considering the random device orientation. **Chapter 2** discusses the overall operation of a general LED-based VLC system and relevant background information. **Chapter 3** presents the performance of hybrid cellular-VLC links for indoor environments under dynamic user movement. Further, **Chapter 4** discusses the implementation of an indoor VLC system under the random placement of LEDs with non-imaging and imaging receivers. **Chapter 5** analyze the effect of static and dynamic blockages in an indoor VLC system using stochastic geometry. **Chapter 6** discusses the optimal VLC parameters like LED semiangle and the receiver FOV considering human blockages. **Chapter 7** analyze the optical IRS-aided indoor VLC system in the presence of human blockages. **Chapter 8** presents indoor localization on estimating the location and the 3-D shape of an object in an indoor environment using visible light. Further, we have exploited the location information and proposed a location-assisted optimal LED power allocation framework in **Chapter 9**. The conclusions and future research scope are discussed in **Chapter 10**.

Chapter 2

Modelling and Characterization of Multipath VLC Channels

Channel modeling is the first step in the analysis and performance evaluation of any communication system. Although the popularity of VLC has grown tremendously over the last few years [2], yet there is a lack of proper channel models that take into account the multipath nature of the indoor VLC link to emulate practical scenarios [129]. The VLC channel is inherently diffuse in nature because visible light signals from an LED can reach the PD via multiple paths [3].

In this Chapter, we study the multipath model for indoor VLC links. We study the effect of several practical factors like LED semi-angle, wall reflectivity, number of reflections, and user locations on the channel gain, channel delay parameters, namely RMS delay spread. In Section 2.1, we describe the operation of visible light communication. Section 2.2, describes the complete modelling of multipath VLC links using LoS, and NLoS paths. VLC channel model with user movement has been discussed in Section 2.3, followed by the modulation and detection techniques in Sections 2.4 and 2.5, respectively. We discuss the channel delay spread in Section 2.6, followed by the brief Summary of VLC channel modelling in Section 2.7.

2.1 Operation of Visible Light Communication System

Let us understand how the VLC system communicates with a simple example of transmitting data in the form of digital signals ‘0’s and ‘1’s. An ordinary light is used to send the data. It is turned on when ‘1’ is transmitted and turned off when ‘0’ is transmitted. But when ‘0’ is transmitted, the light is turned off and doesn’t meet the purpose of illumination. Now, if the light is switched on and off continuously at a high rate, then the light appears to be constant. However, the speed of data transmission is highly dependent on the speed of the flickering.

For this reason, LEDs are used as the primary light source in VLC systems. LED bulbs are semiconductors, giving them the ability to handle ultra-fast modulation of light occurring at speeds undetectable by the human eye. It serves the purpose of both illumination and communication at the same time. A human eye can perceive this flickering effect up to a frequency of 100 to 120 Hz. The fluorescent or ordinary lamps can transmit signals at 10 Kbps, and LEDs can reach up to 500 Mbps.

2.2 VLC Channel Modelling

In this section, we elaborately describe the modeling of VLC sources, receivers, and the channel in a multipath VLC link. We also discuss the parameters used to characterize a multipath channel.

2.2.1 Source Modelling

In VLC systems, the optical source is usually an LED, which is modeled as a generalized Lambertian source located at a distance d and its orientation is defined by the unit vector \mathbf{n}_s which is normal to its radiating surface with unit vector \mathbf{n}_r . LED radiant intensity is characterized by its radiation pattern, which is uniaxially symmetric with a radiation density given as [2, 12]:

$$R_0(\phi) = \frac{(m+1)\cos^m(\phi)}{2\pi}, \quad (2.1)$$

where ϕ is the angle of incidence of light on the surface and m is the order of Lambertian emission, with $\Phi_{\frac{1}{2}}$ being the LED semi-angle at half power, provided by the manufacturer. The Lambertian order m determines the shape of the radiation lobe and signifies the directionality of the source and is defined as:

$$m = \frac{-\ln(2)}{\ln(\cos(\Phi_{\frac{1}{2}}))}. \quad (2.2)$$

The shapes of the radiation lobes for different values of m is illustrated in Fig. 2.1. The desired radiation pattern can be obtained by proper designing of the lens used at the source. Note that, irrespective of the value of m the maximum radiant intensity is available at $\phi = 0^\circ$.

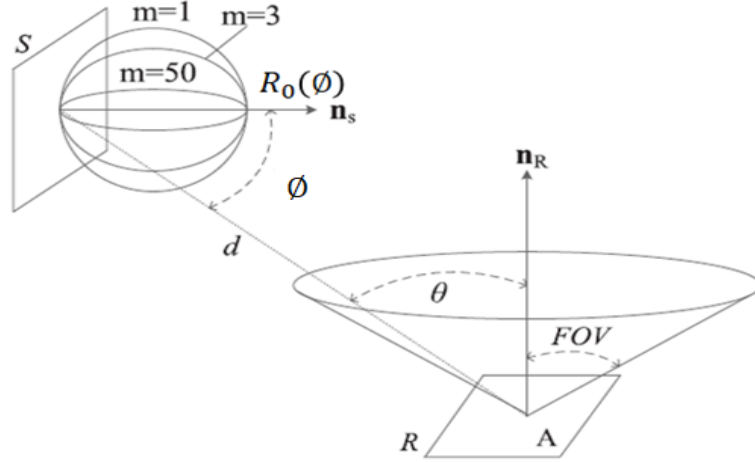


Figure 2.1: Propagation Model

In Fig. 2.1, the transmitter emits an axially symmetric radiation pattern described by the radiant intensity $P_T R_0(\phi)$. A receiver located at a distance d at an angle ϕ with respect to (w.r.t.) transmitter the irradiance is $\frac{P_T R_0(\phi)}{d^2}$. Ignoring reflection losses, a detector achieves an effective signal-collection area given as:

$$A_{eff} = A \cos(\theta), \quad (2.3)$$

where A is the detector physical area and θ is the angle of incidence with respect to the receiver axis.

The power received at the receiver using (2.1) and (2.3) is given by:

$$P_r = \frac{P_T R_0(\phi) A_{eff}}{d^2}, \quad (2.4)$$

The parameter that characterizes the channel is DC channel gain which can then be expressed as [2, 12]:

$$H = \frac{R_0(\phi) \cos(\theta) A}{d^2} = \frac{(m+1) \cos^m(\phi) A \cos(\theta)}{2\pi d^2}. \quad (2.5)$$

where θ is the inclination of the PD to the incident surface.

2.2.2 Receiver Modelling

A receiving element is modeled as a photosensitive detector located at the distance d with orientation defined by the unit vector \mathbf{n}_r normal to the photosensitive surface of area A_{PD} . Its FOV is denoted by Ψ_c . If the angle of incidence of light ψ with respect to \mathbf{n}_r greater than Ψ_c , then the light is not detected by the receiver. The limited value of receiver FOV may be a result of improper manufacturing or packaging of the PD. Moreover, it can be intentionally limited by a lens or aperture to reduce unwanted reflections or reduce noise by shielding excessive ambient light. Besides, an optical concentrator is commonly employed to increase the signal received. The gain of this optical concentrator is gain given as [2]:

$$g(\psi) = \begin{cases} \frac{n^2}{\sin^2(\Psi_c)}, & 0 \leq \Psi \leq \Psi_c, \end{cases} \quad (2.6)$$

where n is the optical concentrator's refractive index.

2.2.3 LoS Channel Gain

In this thesis, we have used a multipath VLC channel model considering LoS path and NLoS reflection up to second-order [130]. Lambert radiator is a typical radiation model that can model the LED light source in VLC. It has also suggested in [131] that the Lambertian model can accurately reproduce the LoS and NLoS luminous intensity pattern of the LEDs. Therefore, the overall VLC channel gain is a sum of both the LoS path (direct path between the LED and the user) and the NLoS path reflected by the walls.

Thus, the VLC channel response of the LoS component from LED H_{LoS}^{LED} , is given as:

$$H_{LoS}^{LED} = \begin{cases} \frac{(m+1)A_{PD}}{2\pi d^2} \cos^m(\phi) T_s g(\psi) \cos(\theta) & 0 \leq \Psi \leq \Psi_c, \end{cases} \quad (2.7)$$

here, A_{PD} represents the physical area of the PD, θ is the angle of incidence to the PD from LED, ϕ is the LED angle of irradiance, $T_s(\psi)$ is the optical filter's gain.

2.2.4 NLoS Channel Gain

The NLoS channel gain of the LED after reflections from the wall is defined as:

$$H_{NLoS}^{wall} = \begin{cases} \frac{\rho_{wall}(m+1)A_{PD}}{2\pi d_1^2 d_2^2} \cos^m(\phi) T_s(\psi) g(\psi) \cos(\alpha_{wall}) \cos(\beta_{wall}) & 0 \leq \Psi \leq \Psi_c, \end{cases} \quad (2.8)$$

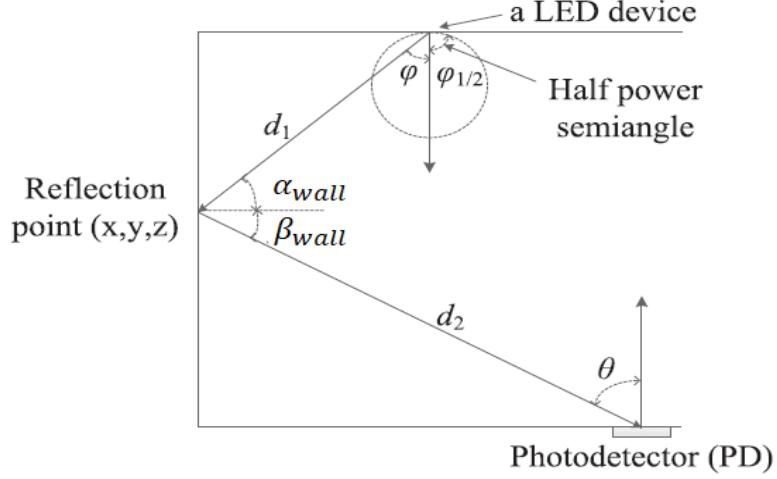


Figure 2.2: NLoS VLC Propagation Model [3].

here α_{wall} and β_{wall} are the incidence and reflectance angle non-line of sight link make with reflecting surface (wall) have reflection coefficient ρ_{wall} . d_1 , d_2 are the distance traveled by the NLoS link to reach the user from the wall as shown in Fig. 2.2.

The total received power at j_{th} receiver location from multiple LEDs including both LoS as well as NLoS path through the walls for a given transmission power (P_T), can be expressed as:

$$P_{r_j} = \sum_{i=1}^N \left[P_T H_{LoS}(i, j) + \sum_{k=1}^K P_T H_{NLoS}(i, j) \right], \quad (2.9)$$

Here, N is the number of transmitting LEDs, and K is the total number of reflective points on the wall, the total received power is obtained by summation both LoS the NLoS link from the walls across the room.

2.2.5 Integrating Sphere VLC Channel Model

In this thesis apart from Lambertian VLC channel model we have also used integrating-sphere model given in [132] was referenced in [117, 133–135]. The integrating-sphere model was originally used in infrared communications, and the most important feature of the model is that the same scattered signal gain is assumed throughout the room. The frequency response of the channel is given by:

$$H(f) = H(0) \exp(-j2\pi f \Delta\tau_{LoS}) + H_{DIFF} \frac{\exp(-j2\pi f \Delta\tau_{DIFF})}{1 + j \left(\frac{f}{f_0} \right)}, \quad (2.10)$$

where $\Delta\tau_{LoS}$ and $\Delta\tau_{DIFF}$ are the time delays of the transmitted signal taking the LoS and the NLoS path, respectively, f_0 denotes the cut-off frequency of scattering channel, and f represents the operating frequency in Hz.

The channel gain of LoS component, $H(0)$, is given as:

$$H(0) = \begin{cases} \frac{(m+1)A}{2\pi D_d^2} \cos^m(\phi) T_s(\psi) g(\psi) \cos(\psi) & 0 \leq \psi \leq \psi_c, \\ 0 & \psi > \psi_c \end{cases}, \quad (2.11)$$

The diffuse channel gain H_{DIFF} due to NLoS path is given as:

$$H_{DIFF} = \frac{A_R}{A_{walls}} \frac{\rho}{1 - \bar{\rho}} , \quad (2.12)$$

where,

$$\bar{\rho} = \frac{1}{A_{walls}} \sum_i A_i \rho_i , \quad (2.13)$$

$\bar{\rho}$ represents an average reflectance, ρ refers to instantaneous reflection, A_R is the area of reflection point on the wall from where the NLoS rays are reflected, A_i is the area of i_{th} grid on the wall and A_{walls} is the total area of the walls of the room over which the reflection is considered.

For a given transmission power (P_T), the total received power using multiple LEDs, including diffused path through the walls, can be obtained as:

$$P_r = \sum_{l=1}^L \left[P_T H(0) + \int_{walls} P_T H_{DIFF} \right] . \quad (2.14)$$

where L is the total number of transmitting LEDs and the total power is obtained by integrating both LoS the NLoS links across the room.

2.3 VLC Channel Model with User Movement

The movement of users within a room will certainly affect the channel characteristics and hence the link performance. Since the VLC technology is perceived to be mainly used for indoor application, the dynamic indoor environment with people will give us more practical measure of the link [129]. The movement of the users inside the room can be modeled in terms of effective people density (people/m²). The effective people density also considers the effect of shadowing and blocking of the signal path due to obstacles present in the room. Two different case have been considered for analysis: furnished room and non-furnished room. In the

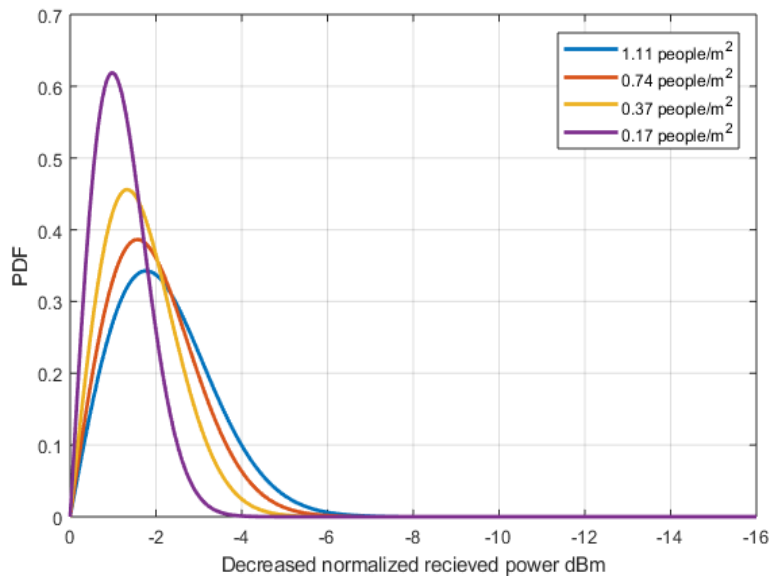


Figure 2.3: Decrease in normalized received power distribution for VLC channel with user movement.

VLC channel with user movement, decrease in the normalized received power can be empirically modeled to follow Rayleigh distribution given by [129]:

$$p(x) = \frac{x}{\sigma^2} \exp\left(\frac{-x^2}{2\sigma^2}\right), \quad (2.15)$$

where x is the normalized received power and σ represents the scale parameter. The scale parameters varies with the effective people density inside the room. For example, in furnished room with effective people density of 1.11 people/m², σ is 1.77 and in the case of non-furnished room with effective people density of 0.17 people/m², σ is 0.98.

The measured probability distribution function (PDF) of the normalized received power with user movement is depicted in Fig. 2.3 [129]. It is clear that for VLC systems a decrease in normalized received power can be approximated by Rayleigh distribution.

2.4 Indoor VLC with Human Blockage System Model

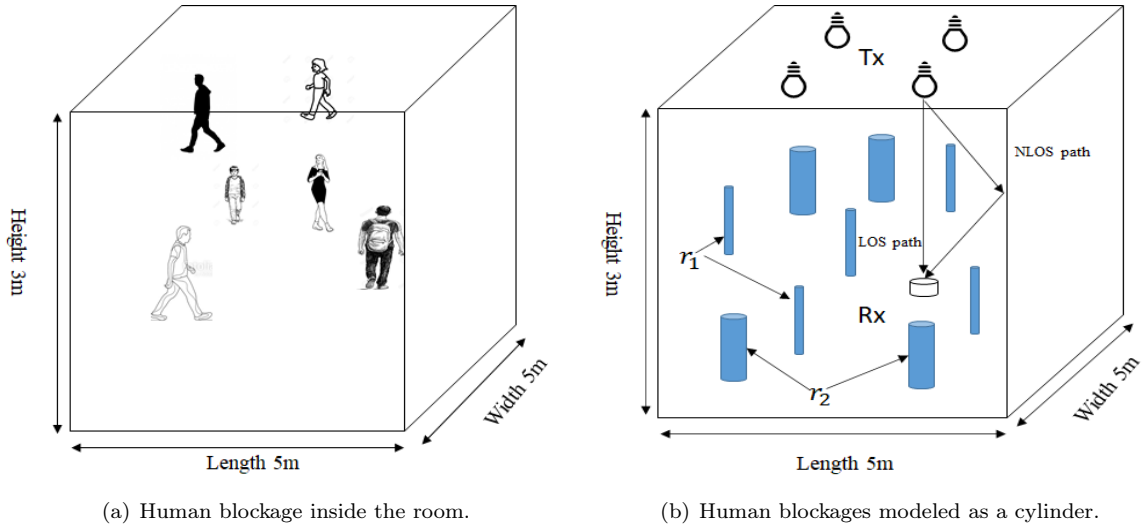


Figure 2.4: Indoor VLC System Model with Human Blockages

As mentioned before, we consider two scenarios of 4 and 8 LEDs in the rectangular configuration in a 5 m × 5 m × 3 m room. The receiver plane is assumed to be 0.85 m above the floor. Both LoS and NLoS paths are considered. The receiver plane is divided into a 25 × 25 grids to cover the whole room for analysis. We have used the Matern type-II process and RWP model to distribute the location of the static and dynamic blockages in a plane with an intensity of λ_B respectively. The blockages are assumed to be cylindrical with radius r and the height h_B , as shown in Fig. 2.4(a). For the proposed system model, two types of blockages of having radius r_1 and r_2 have been considered, which are equivalent to varying sizes of humans. We have assumed OOK modulation in the VLC link for deriving the BER expression as this is one of the standards modulation scheme defined in the VLC standard (IEEE 802.15.7) [49].

In the following subsection, we discuss in detail the the spatial model of human blockages.

2.4.1 Spatial Model

Consider the scenario illustrated in Fig. 2.5, where a transmitter (Tx) is located at a certain height h_T above the ground, and a receiver (Rx) is located at a height h_R . The potential human blockages are distributed over the receiver plane. As stated before, we model the blockages as cylinders [136] with a certain height, h_B , and the base diameter of D . The locations of the human blockages present inside the room are distributed as per the mobility aspects of humans.

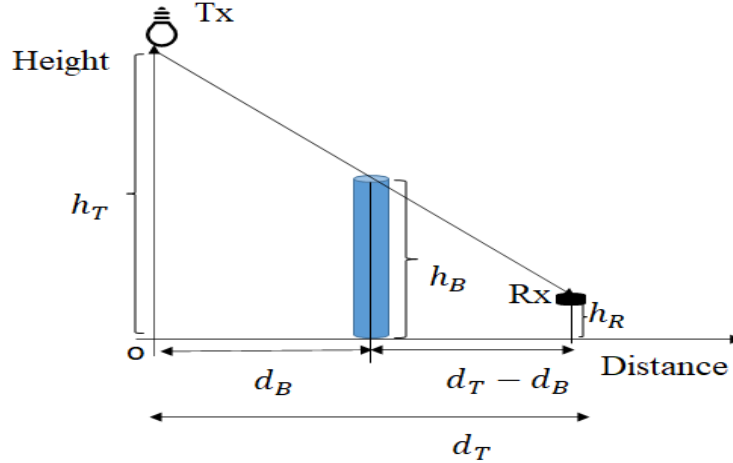


Figure 2.5: Schematic for calculation of shadow length due to blockage

As illustrated in Fig 2.5, a human body of height h_B is present between the LED and the receiver, which results in a communication link blockage. The distance of the human blockage and the intended user from LED is denoted by d_B and d_T , respectively. Using simple geometry, (Fig. 2.5) the length of shadow due to blockage form LED $d_T - d_B$ can be calculated as:

$$d_T - d_B = \frac{h_B}{h_T} d_T. \quad (2.16)$$

The region in shadow due to blockage will be a rectangle whose area can be calculated using (2.16), with a length equal to $d_T - d_B$, and a width similar to the blockage diameter D .

2.5 UE Orientation

The UE orientation can significantly impact the performance of an indoor VLC system. In most of the research on indoor VLC, the UE is always vertically up. Such assumptions are accurate only for a limited number of devices, such as laptops with LiFi dongles. However, most users use devices such as smartphones, and in reality, the user is mobile and tends to hold the device according to comfort. Therefore, considering a random device orientation is a more realistic assumption.

Only a few studies have considered the impact of random orientation in their analysis, see for instance [4, 97, 137] and references therein. All these works incorporate UE orientation. Another important indicator affecting system performance is an optical channel communication link blocked by the user, known as "self-blocking." Or it may be interrupted as a result by other users or objects. The blockage modeling has been done

in the prior literature for both millimeter-wave and LiFi systems [20, 138].

2.6 Modulation Technique

The modulation scheme employed for performance analysis in this thesis is OOK¹. OOK is one of the standard modulation schemes defined in the VLC standard (IEEE 802.15.7) [47], [139]. In VLC, the power to the LED transmitter is modulated to transmit '1's and '0's. Since the power is always non-negative, unlike conventional digital modulation techniques. The modulated signal is $P_t(1 + x_i)$, x_i assumes bipolar symbols +1 and -1 for bits '1' and '0' respectively. Here the former term (P_{t_i}) takes care of illumination while the latter term ($P_{t_i}x_i$) is for communication. Because in VLC, LED serves the dual role of illumination and communication. This power drives the source LEDs, which results in a change in intensity and hence the name intensity modulation (IM).

2.7 Detection Technique

The receivers used for detection are photo-diodes. The photons emitted by light sources hit the photo-diode, and electron-hole pairs are created in the depletion region of the photo-diode. This mechanism is called as the inner photoelectric effect. The holes in the depletion region move towards the anode, and electrons move towards the cathode producing a photocurrent. Thus the photo-diode converts the optical energy into an electrical signal. This is known as direct detection (DD). Note that if multiple sources transmit the signal, the signal at PD is the sum of all the received signals from individual sources.

2.8 Delay Spread

Due to the multipath nature of visible light channels, the transmitted signal gets divided into several paths. These signal components do not reach the receiver at the same time, which causes the spreading of the received signal in the time domain. Moreover, in a broadcasting set-up, where all the LED panels transmit the same information, the unequal path lengths from different transmitters to the receiver cause the signals to reach the receiver at different times. Hence, the non-symmetrical location of multiple transmitters with respect to the receiver also adds to the time-domain spreading of the received signal. Therefore, delay spread play a crucial role while analyzing the performance of an indoor system. The received signal in the case of NLoS link consists of various components arriving from different paths. The path length of these components differs in proportion to the room design which results in a broadening of the pulse [140]. The root mean square (RMS) delay spread D_{rms} is a parameter which is commonly used to quantify the time-dispersive properties of multipath channels which can be calculated as [19, 141]:

$$D_{rms} = \sqrt{\left[\frac{\int_{-\infty}^{\infty} (t - \mu)^2 h^2(t) dt}{\int_{-\infty}^{\infty} h^2(t) dt} \right]}, \quad (2.17)$$

¹Further, we have also used other standard VLC modulation techniques such as CSK, M-QAM, and M-PSK with DC-biased optical OFDM (DCO-OFDM) for comparison as per the necessity.

where $h(t)$ is a time domain representation of channel response expressed in (2.1) and μ is the mean delay spread given by:

$$\mu = \frac{\int_{-\infty}^{\infty} t \times h^2(t) dt}{\int_{-\infty}^{\infty} h^2(t) dt}. \quad (2.18)$$

2.9 Summary

In this Chapter, we presented the detailed formulation of the multipath channel model for VLC, including the modeling of transmitters, reflectors, and receivers. We infer that VLC parameter like LED semiangle, receiver FOV, and NLoS reflections plays an essential role in calculating the received power. Further, an increase in the LED semiangle and the FOV increases the delay spread, thereby indicating the existence of an optimum value of semiangle at which the delay spread is minimum and, correspondingly, the coherence BW is maximum. We deduce that it is adequate to incorporate up to second-order reflections of the signal to sufficiently emulate the multipath effect in channel characterization. In addition, it is found that people's movement and density have also been important in realizing the practical indoor VLC system.

Based on the known channel models, we identified the main parameters associated with the channel models, which include RMS delay spread that affects ISI directly, path loss related to the received power, and 3-dB bandwidth that is related to communication quality. In addition, we also found there is a need of VLC channel models, including the establishment of a general VLC channel model combining the effects of transmitter LED and room size, improvement in measuring channel reflection characteristics, and the research on multipath and Doppler effects in the channels.

Chapter 3

Hybrid cellular-VLC link for indoor environments under dynamic user movement

In this Chapter, we analyze the performance of a hybrid cellular-VLC downlink where the outdoor coverage is provided via cellular network, and the indoor coverage is provided through a VLC system. Multiple LED transmitters with rectangular deployment are considered for a VLC transmitter. The channel model for the VLC link has been modeled as an integrating sphere VLC channel, which includes both LoS and NLoS links.

The rest of the Chapter is organized as follows. We discuss the motivation behind this work and outline our contributions in Section 3.1. Section 3.2 describes the hybrid cellular-VLC system model followed by the BER calculation in Section 3.3. Further, Section 3.4 presents the outage probability for the proposed hybrid cellular-VLC system. Section 3.5 compares VLC and RF-based modulation schemes for hybrid RF-VLC systems. Finally, we discuss the results in Section 3.6 and briefly summarize the Chapter in Section 3.7.

3.1 Motivation and Contribution

3.1.1 Motivation

The indoor radio channel heavily depends on factors such as building structure, room layout, and construction materials used. As a consequence, there is severe attenuation of RF waves at the receiver. The motivation behind this work is to reduce the power consumption at BTS caused due to strong attenuation of radio signals in an indoor environment by proposing a hybrid cellular-VLC link. Earlier work on hybrid cellular-VLC systems (ref. Section 1.6.2) have not considered the amount of power saving that can be achieved by using VLC as an indoor link. Further, the existing works have not optimized the Lambertian order for uniform delay spread, and high average received optical power inside the room. The current work also ignored the effect of dimming on the VLC link. Further, the analysis so far have used a static VLC channel model and have not considered the impact of user movement, type of room, or shadow objects in the room on the performance of the hybrid cellular-VLC system.

To cater the above research gap in this chapter, we analyze the performance of hybrid cellular-VLC downlink

where the outdoor coverage is provided via cellular network, and the indoor coverage is provided through a VLC system. In the proposed framework, VLC AP helps to communicate the information between the base station (BTS) and user by acting as a decode-and-forward (DF) relay. The relay decodes the received signal from the base station and then uses the decoded signal to modulate the intensity of the optical transmitter. Multiple LED transmitters with rectangular deployment are considered for a VLC transmitter. The channel model for VLC link has been modeled as an integrating sphere VLC channel which includes both line-of-sight (LOS) and non-line-of-sight (NLOS) links.

3.1.2 Contribution

In this Chapter, we have proposed a hybrid cellular-VLC downlink framework and have analyzed its performance for indoor environments by considering all the above parameters. The main contributions of this Chapter are summarized as follows:

- We have proposed a hybrid cellular-VLC link where the cellular link is followed by the VLC link, which acts as a DF relay. The performance of the hybrid link has been compared with a direct cellular link. The closed-form expressions for BER and outage probability are derived by taking into consideration the movement of people and different indoor conditions.
- The proposed work also optimizes the Lambertian order of the LEDs in order to make delay spread uniform and increase average SNR through the LoS path inside the room, resulting in higher throughput and reduced outage in the room. Outage region for indoor room under static VLC channel for different FOV and optimal irradiance angle of LED have been investigated for the rectangular LED configuration.
- Further, this Chapter analyzes indoor system performance for a single user between RF and VLC modulation schemes of the same order. For example, VLC OOK with RF BPSK and VLC M-CSK with RF M-QAM schemes of the same order. Also, this work calculates the amount of power saving in the VLC link as compared to the RF link.
- The power-saving corresponding to the hybrid cellular-VLC link with respect to the direct cellular link has been evaluated. It is observed that there is significant power saving when VLC is used as an indoor link. The effect of dimming on the VLC link is also investigated. It has been shown that it is possible to have a wide dimming range without compromising on BER performance.

3.2 Hybrid RF-VLC System Model

The proposed system model considers a three-node network consisting of a BTS, a VLC AP which acts as a DF relay, and a user present in the indoor environment as shown in Fig. 3.1. The channel between the BTS and the VLC AP is modeled as a frequency non-selective Rayleigh faded channel having channel gain, assuming the channel delay spread for the given room dimensions (such as small office room) is smaller than the symbol duration h_{RF1} . Further, to address the frequency-selective channel, modulation schemes such as DCO-OFDM and ACO-OFDM can be used. After receiving the signal from the BTS, VLC AP decodes the signal and then

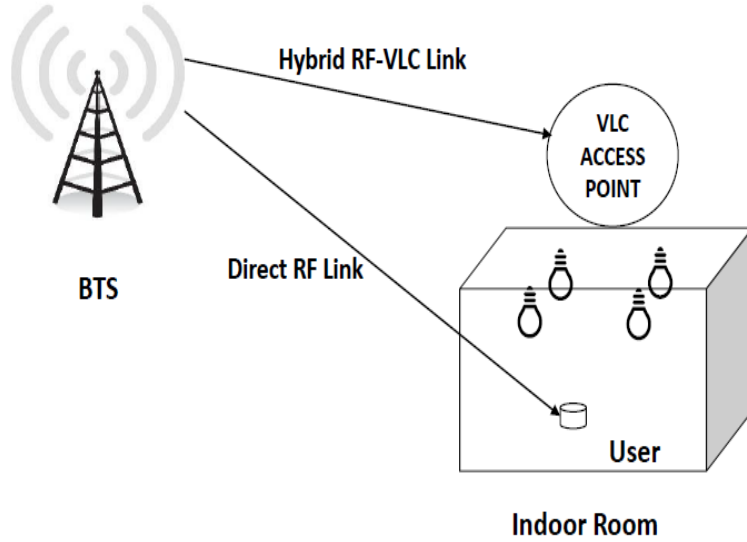


Figure 3.1: Hybrid RF-VLC System Model

transmits the signal inside the room via VLC link. The channel gain for the VLC link is denoted as, h_{VLC} . In the proposed work the end-user VLC link is modeled by employing two different channel models: first by using standard VLC static channel model as proposed in [3] and second a VLC channel model which takes into account the movement of the users under different indoor conditions (i.e., non-furnished room, furnished room) [129]. The direct RF link, from BTS to the indoor user is modeled as a frequency non-selective Rayleigh faded channel having channel gain, h_{RF2} . The indoor pathloss of the direct RF link is modeled using WINNER-II pathloss model, considering the effect of distance, number of floors in the building, shadowing, the height of transmitting and receiving antenna [142].

In the following subsections, we will provide brief overview of optimum Lambertian order (OLO) and WINNER-II pathloss model.

3.2.1 Optimal Lambertian Order (OLO)

In order to provide desired QoS to the user across the room, the required power and delay spread must be optimized across the room. To achieve this objective, OLO can be used because OLO maximizes the optical power from the LoS path and minimizes ISI, by increasing the mean received optical power and making delay spread uniform across the room.

The expression for the OLO m_{opt} is given as[143]:

$$m_{opt} = \frac{-1}{\ln(\cos(\phi_{max}))} - 1, \quad (3.1)$$

where ϕ_{max} is the maximum irradiance angle, which is given as:

$$\phi_{max} = \cos^{-1} \left(\frac{h}{d_{max}} \right). \quad (3.2)$$

where d_{max} is the maximum distance between the transmitter and receiver in each cell, and h denotes the room height.

In the proposed system, OLO is used to achieve nearly uniform delay spread across the room, and maximize the average received optical power. Using (3.1), the optimized irradiance angle of LED should be 56° and its corresponding OLO was found to be 5.57 for the given system model.

3.2.2 WINNER-II Pathloss Model

The direct RF link will go through both outdoor and indoor pathloss. Hence, to cater for outdoor-to-indoor, WINNER-II pathloss model has been employed to evaluate the total pathloss between BTS and user [144]. The pathloss for direct RF link can be expressed as [142]:

$$PL(\text{dB}) = [44.9 - 6.55\log_{10}(h_{\text{BS}})]\log_{10}(d) + 34.46 + 5.83\log_{10}(h_{\text{BS}}) + 23\log_{10}\left(\frac{f_c}{5.0}\right), \quad (3.3)$$

where f_c is the carrier frequency, h_{BS} is the height of base station, h_{MS} is the height of mobile station (MS) and is given by $h_{\text{MS}} = 3n_{\text{fl}} + 1.5$, n_{fl} denotes the floor number in the building and d is the distance between BTS and MS within the range of $50\text{m} \leq d \leq 5\text{km}$.

3.3 BER Expression in Hybrid Cellular-VLC Link Under VLC Channel with User Movement Inside the Room

We have assumed OOK modulation in the VLC link for deriving the BER expression as this is one of the standard modulation scheme defined in the VLC standard (IEEE 802.15.7) [47], [139]. For the hybrid cellular-VLC link using DF relaying the average BER can be expressed as [145]:

$$\text{BER}_{\text{RF1-VLC}}^{\text{DF}} = (1 - \text{PER}_{\text{SR}})\text{BER}_{\text{RD}} + \text{PER}_{\text{SR}}, \quad (3.4)$$

where PER_{SR} is a average packet error rate from source to relay RF link, BER_{RD} is the BER from relay to destination VLC link. For the N-bit packet, the PER_{SR} for the case of binary-phase-shift keying (BPSK) at BTS can be expressed in terms of BER_{SR} as:

$$\text{PER}_{\text{SR}} = 1 - (1 - \text{BER}_{\text{SR}})^N, \quad (3.5)$$

where BER_{SR} is the BER from source to relay RF link and can be expressed as:

$$\text{BER}_{\text{SR}} = \frac{1}{2} \left[1 - \sqrt{\frac{\overline{\gamma}_{\text{SR}}}{\overline{\gamma}_{\text{SR}} + 1}} \right]. \quad (3.6)$$

where $\overline{\gamma}_{\text{SR}} = \frac{E_b}{N_0} E[|h_{\text{RF1}}|^2]$ is the average SNR of BTS to relay link. For the calculation of BER_{RD} , for relay to destination which is a VLC link, we have used the VLC channel model with user movement. In VLC link the output optical signal from a LED for transmitting power P_{T} is given by:

$$P(t) = P_{\text{T}}(1 + M_{\text{I}}f(t)), \quad (3.7)$$

where M_{I} is the modulation index, $f(t)$ is the information signal. The received power at the PD is expressed as:

$$P_{\text{r}}(0) = H(0)P(t). \quad (3.8)$$

where $H(0)$ is the LoS channel gain describe in (2.7) and (2.11). After receiving the signal at the PD and filtering the DC signal, the output electrical signal is given by:

$$S(t) = \mathcal{R}H(0)P_{\text{T}}M_{\text{I}}f(t), \quad (3.9)$$

where \mathcal{R} is responsivity of the PD. The instantaneous signal-to-noise ratio for the VLC link, relay to destination is defined as the ratio of received signal power to the noise power [146]:

$$\gamma_{\text{RD}} = \frac{\overline{S(t)^2}}{P_{\text{noise}}}, \quad (3.10)$$

$$\gamma_{\text{RD}} = \frac{(\mathcal{R}M_{\text{I}}H(0)P_{\text{T}}\overline{f(t)})^2}{P_{\text{noise}}}, \quad (3.11)$$

where P_{noise} is the total noise power comprising of shot noise power (σ_{shot}^2) and thermal noise power ($\sigma_{\text{thermal}}^2$) which can be expressed as:

$$P_{\text{noise}} = \sigma_{\text{shot}}^2 + \sigma_{\text{thermal}}^2, \quad (3.12)$$

where

$$\sigma_{\text{shot}}^2 = 2e\mathcal{R}P_{\text{r}}B_{\text{s}} + 2eI_{\text{bg}}I_2B_{\text{s}}, \quad (3.13)$$

and

$$\sigma_{\text{thermal}}^2 = \frac{8\pi kT_{\text{k}}}{G}\eta A_{\text{r}}I_2B_{\text{s}}^2 + \frac{16\pi^2 kT_{\text{k}}\Gamma}{g_{\text{m}}}\eta^2 A_{\text{r}}^2 I_3 B_{\text{s}}^3, \quad (3.14)$$

where e is the electron charge, P_{r} is the average received optical power, B_{s} is the system bandwidth, I_{bg} is the received background noise current, k is Boltzmann's constant, T_{k} is the absolute temperature, G is the open loop voltage gain, η is the fixed capacitance of PD per unit area, Γ is the field effect transistor (FET) channel noise factor, g_{m} is the FET transconductance, I_2 is the noise bandwidth factor for background noise and I_3 is the noise bandwidth factor.

The measured probability distribution for decrease in received optical power in VLC follows Rayleigh distribution (2.2), i.e., SNR will be exponentially distributed in the VLC channel with user movement, and its pdf can be expressed as:

$$f_{\gamma_{\text{RD}}}(\gamma_{\text{RD}}) = \frac{1}{\overline{\gamma_{\text{RD}}}} \exp\left(\frac{-\gamma_{\text{RD}}}{\overline{\gamma_{\text{RD}}}}\right), \quad (3.15)$$

where $\overline{\gamma_{\text{RD}}} = \frac{(\mathcal{R}M_{\text{I}}\overline{f(t)})^2}{P_{\text{noise}}} E[|H(0)P_{\text{T}}|^2]$. As the decrease in normalized received power follows Rayleigh distribution see((2.2)) with variance equals to scale factor σ^2 , and replacing $(\mathcal{R}M_{\text{I}})^2$ with α . The pdf can be written as:

$$f_{\gamma_{\text{RD}}}(\gamma_{\text{RD}}) = \frac{1}{\alpha\sigma^2} \exp\left(\frac{-\gamma_{\text{RD}}}{\alpha\sigma^2}\right), \quad (3.16)$$

BER for VLC with OOK under additive white Gaussian noise (AWGN) can be defined as [146]:

$$\text{BER}_{\text{RD}} = Q\left(\sqrt{2\gamma_{\text{RD}}}\right) \cong \frac{1}{2} \text{erfc}\left(\sqrt{2\gamma_{\text{RD}}}\right), \quad (3.17)$$

The BER for fading channel can be obtained by averaging the error in AWGN channels over the fading probability density function. The average BER under VLC channel with user movement from VLC AP to the user inside the room can be expressed as:

$$\text{BER}_{\text{RD}} = \int_0^\infty \frac{1}{2} \text{erfc}(\sqrt{2\gamma_{\text{RD}}}) \frac{1}{\alpha\sigma^2} \exp\left(\frac{-\gamma_{\text{RD}}}{\alpha\sigma^2}\right) d\gamma_{\text{RD}}, \quad (3.18)$$

$$\text{BER}_{\text{RD}} = \frac{1}{2} \left[1 - \sqrt{\frac{\alpha\sigma^2}{\alpha\sigma^2 + 1}} \right]. \quad (3.19)$$

From (3.4) (3.5) (3.6) and (3.19), the closed-form BER expression for the hybrid cellular-VLC for OOK in VLC link and the BPSK in the cellular link is given as:

$$\begin{aligned} \text{BER}_{\text{RF1-VLC}}^{\text{DF}} = & \left[1 - \left\{ 1 - \frac{1}{2} \left(1 - \sqrt{\frac{\gamma_{\text{SR}}}{\gamma_{\text{SR}} + 1}} \right) \right\}^N \times \left(1 - \sqrt{\frac{\alpha\sigma^2}{\alpha\sigma^2 + 1}} \right) \right. \\ & \left. + 1 - \left\{ 1 - \frac{1}{2} \left(1 - \sqrt{\frac{\gamma_{\text{SR}}}{\gamma_{\text{SR}} + 1}} \right) \right\}^N \right]. \end{aligned} \quad (3.20)$$

The above analysis of BER expression in section 3.3 can be extended for other modulation techniques like QAM, PAM, etc.

3.4 Outage Probability in Hybrid Cellular-VLC Link

In this section, we have evaluated closed-form expression for the outage probability for the proposed hybrid cellular-VLC link. The message signal from BTS is received at the DF relay (VLC AP), which decodes the received signal and modulates the LED and sends it to the user via VLC link.

The maximum achievable instantaneous data rate (I_{DF}) for the hybrid cellular VLC link using decode-and-forward can be given as [147]:

$$I_{\text{DF}} = \min(R_1, R_2), \quad (3.21)$$

where R_1 and R_2 is the achievable data rate between BTS to VLC AP and VLC AP to the end user respectively, and can be expressed as:

$$R_1 = \frac{1}{2} \log_2(1 + \text{SNR}_{\text{RF1}} |h_{\text{RF1}}|^2), \quad (3.22)$$

$$R_2 = \frac{1}{2} \log_2(1 + \text{SNR}_{\text{VLC}} |h_{\text{VLC}}|^2), \quad (3.23)$$

SNR_{RF1} and SNR_{VLC} is the AWGN SNR for RF and VLC links in the hybrid cellular-VLC link respectively. The factor $\frac{1}{2}$ in the above equation accounts for the fact that the transmission is being divided into two phases.

The first term R_1 in (3.21), represents the maximum rate at which the VLC AP can reliably decode the source message, while the second term R_2 , represents the maximum rate at which the destination can reliably decode the source message given repeated transmission from the relay.

The outage probability for the proposed hybrid cellular-VLC link using DF relaying with the target data rate (R) can be computed according to [148]:

$$\begin{aligned} P_{\text{out}} &= P_r [I_{\text{DF}} < R] \\ &= 1 - P_r(R_1 > R) P_r(R_2 > R). \end{aligned} \quad (3.24)$$

For the RF link, h_{RF1} is frequency non selective Rayleigh faded channel gain with variance σ_{RF1}^2 and in VLC link decreased in normalized received power follows Rayleigh distribution with variance equals to square of the scale factor (σ).

The outage probability can be expressed as [147]:

$$P_{\text{out}} = \left[1 - \exp\left(\frac{-2^{2R} - 1}{\sigma_{\text{RF1}}^2 \text{SNR}_{\text{RF1}}}\right) \exp\left(\frac{-2^{2R} - 1}{\sigma_{\text{VLC}}^2 \text{SNR}_{\text{VLC}}}\right) \right], \quad (3.25)$$

where $\sigma_{\text{VLC}}^2 = \sigma^2$.

Under high SNR approximation (3.25) can be simplified to:

$$P_{\text{out}} \cong \left[\frac{2^{2R} - 1}{\sigma_{\text{RF1}}^2 \text{SNR}_{\text{RF1}}} + \frac{2^{2R} - 1}{\sigma^2 \text{SNR}_{\text{VLC}}} \right]. \quad (3.26)$$

Using (3.26), the outage for a given cellular-VLC system can be calculated for a given data rate of R.

3.5 Power and SER Analysis of VLC and RF Based Links in Indoor Environment

This Section analyses and compares the RF and VLC link for indoor communication with respect to symbol-error-rate (SER) performance and power saving. The RF link path loss inside the building is modeled using WINNER-II path loss model, and VLC channel is modeled including the movement of the people. The same constellation-based modulation schemes are used in both the links for fair comparison such as BPSK for RF and OOK for VLC, M-QAM for RF and M-CSK for VLC. VLC link provides better SER performance as compared to RF link at the same SNR for both BPSK (OOK) and 4-QAM (4-CSK) modulation schemes. There is an outstanding amount of power saving using VLC link as compared to RF link inside the room. Further, the SER gap between VLC and RF decreases as the constellation size increases.

3.5.1 Comparison of VLC and RF Based Links in Indoor VLC System Model

The proposed system model as shown in Fig. 3.2 compares RF communication link coming from the BTS, and VLC from rooftop LED for an indoor environment. The channel for RF is modeled as a frequency non-selective Rayleigh faded channel having channel gain, h_{RF} . The channel gain for the VLC link is denoted as, h_{VLC} . This work analyses VLC link for two different channel models; i.e. static and dynamic with respect to WINNER-II path loss modeled RF link. RF link with modulation schemes such as BPSK or M-QAM is compared with the VLC link with modulations such as OOK or M-CSK.

3.6 Results and Discussion

In this section, we present simulation and analytical results for the proposed hybrid cellular-VLC link inside a standard room size of 5 m × 5 m × 3 m. The room consists of four LED transmitters and a receiver. The locations and the orientations of the VLC transmitters and the receiver are provided in Table 3.1. Both LoS and NLoS (with one-point reflection because of higher data rate threshold) [149] signals are considered in the analysis.

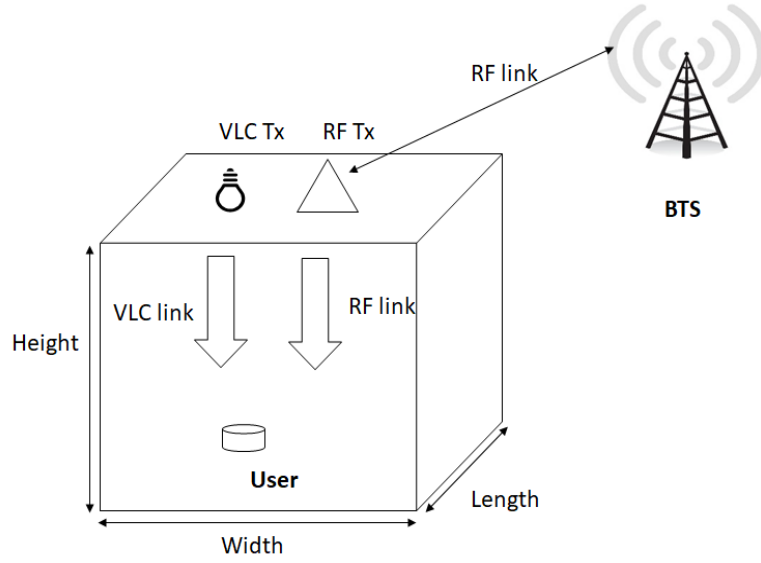


Figure 3.2: VLC and RF Based Links System Model

3.6.1 Received Optical Power Distribution

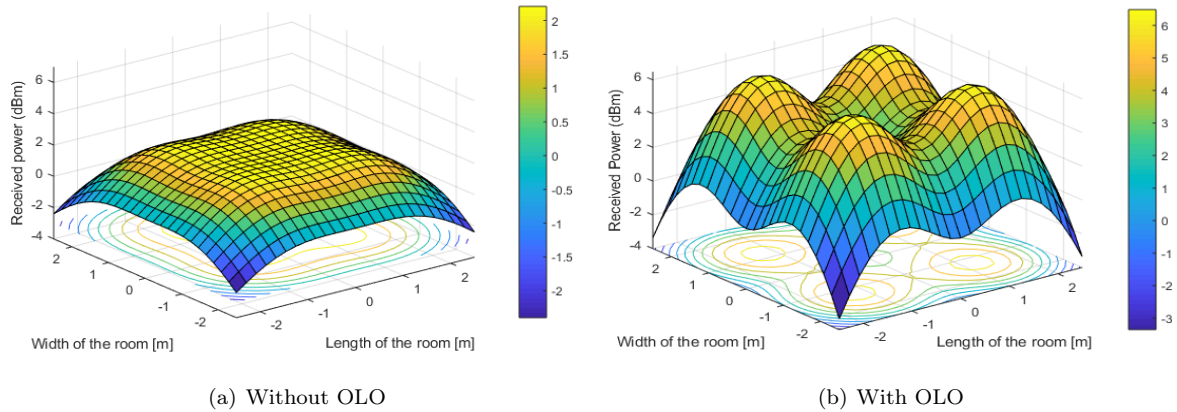


Figure 3.3: Received optical power distribution in rectangular configuration without and with OLO.

Figs. 3.3(a) and 3.3(b) compare the received optical power distribution (ROPD) for rectangular placement of four LEDs without and with OLO respectively. From Fig. 3.3(a), we notice that for the case of ‘without OLO’ for which the LED irradiance angle is 60° and the Lambertian order $m = 1$, the received optical power varies from -2 dBm to 2.5 dBm with mean value of 1.4 dBm, whereas for the case of ‘with OLO’ for which the LED irradiance angle calculated from is 56° and the OLO $m_{opt} = 5.57$, the received optical power varies from -3 dBm to 6 dBm with mean value of 3.2 dBm. It is observed that OLO allows additional 1.8 dBm increase in the mean received optical power. The quality factor (Q), measures the received optical power distribution and

Table 3.1: Hybrid RF-VLC System Model Parameters

Parameter	Value
Room size	5 m × 5 m × 3 m
Location of T_x (Four LED system) (x, y, z)	(1.25, 1.25, 3), (1.25, 3.75, 3), (3.75, 1.25, 3), (3.75, 3.75, 3)
LED transmitted power	200 mw
Wall reflection ρ	0.8
LED irradiance angle	60°
OLO	58°
Height of Receiver plane	0.85 m
Receiver elevation	90°
Receiver active area	1 cm ²
Field of views (FOVs) of receiver	60°, 50°, 40°, 30°.
Responsivity \mathcal{R}	0.5 $\frac{A}{W}$
Noise bandwidth factor I_2	0.562
Background current I_{bg}	100 μA
Distance between BTS to VLC AP	1 km
Mode number at the Transmitter	45
Responsivity RGB	[0.42 0.32 0.22] A/W
Distance between BTS to RF AP	1 km
Effective people density	(0.17; 0.37; 1.11) people/m ²
Rayleigh distribution scale parameter	(0.98; 1.33; 1.77)

is used to evaluate the fairness of whole system to all users and is given as [150]:

$$Q_{ROPD} = \frac{Mean_{ROPD}}{2\sqrt{Var_{ROPD}}}. \quad (3.27)$$

For the case of ‘without OLO’, the measured quality factor is 0.6 whereas ‘with OLO’, the measured quality factor is 0.8. It can be summarized that ‘with OLO’ results in increased average received optical power and better quality factor than ‘without OLO’ configuration for a given room which in turn reduces the outage area and improves fairness among the users.

3.6.2 RMS Delay Spread

The channel time dispersion has also been investigated for the proposed configurations as receiver performance is affected by delay spread causing intersymbol interference (ISI). Figs. 3.4(a) and 3.4(b) show D_{rms} for the indoor room without and with OLO respectively. For four LEDs rectangular configuration ‘without OLO’, the D_{rms} varies from 0 to 0.39 ns with mean value of 0.15 ns and variance of 0.008 ns. In the case of ‘with OLO’, D_{rms} varies from 0 to 0.25 ns with mean of 0.06 ns and variance of 0.003 ns. It can be observed that there is a significant reduction in D_{rms} across the room with low variance using OLO, which in turn implies that RMS delay spread is nearly uniform throughout the room as shown in Fig. 3.4(b), resulting in uniform bit rate inside the room.

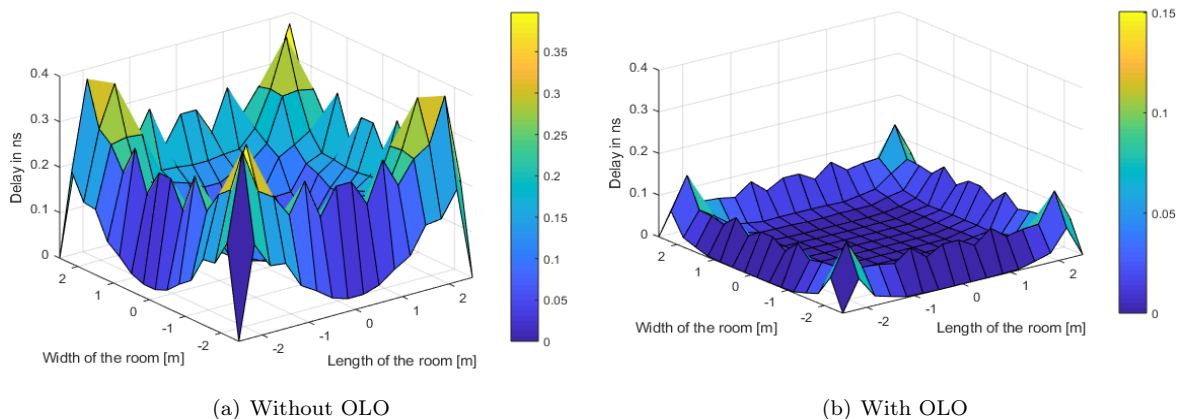


Figure 3.4: RMS channel delay spread inside the room without and with OLO.

3.6.3 Outage Region for Indoor Room Using Static VLC Channel Model

In this subsection, outage performance of the proposed hybrid cellular-VLC link for a target BER (10^{-3}) under static VLC channel model has been analysed. The outage region is defined as the regions where the instantaneous SNR is less than the desired SNR required to achieve the target BER. Figs. 3.5(a) to 3.5(d), show the outage region with four LED rectangular configuration for the proposed system under different FOVs (i.e., 60° , 50° , 40° , 30°) respectively, with optimize irradiance angle of the LEDs (56°).

The outage region is plotted as the difference between instantaneous SNR and desired SNR inside the room at various locations. Numerical values in the contour show the offset in the received SNR with respect to the desired SNR in dB. The negative value region indicates the region where a hybrid cellular-VLC link is in the outage. It is to be noted that reducing FOV, improves the optical channel gain (see(2.7)) and reduces the ISI which in turn results in better performance. However, reducing the FOV below 40° at receivers often introduces blind spots as shown in Fig. 3.5(d). These blind spots limit the connectivity in the indoor VLC system. It is also be noted that as FOV reduces, the received SNR increases but at the cost of restricted coverage.

Fig. 3.6 compares the outage area for four LEDs rectangular configurations at different FOV without and with OLO. Figs. 3.6(a) and 3.6(b), show the outage area comparison for the proposed system without and with OLO. It is clear that reducing the FOV results in an increase of outage region. For the worst case i.e., at FOV 30° , the outage area without OLO and with OLO is approximately 40% and 30% respectively. Similarly, for the best case i.e., FOV 60° , the outage area without OLO and with OLO is approximately 8% and 1% respectively. It is concluded that four LEDs rectangular configuration with OLO at receiver FOV of 60° is the best configuration to minimize the outage region while maintaining the satisfactory quality of service throughout the room.

3.6.4 Outage Analysis Under VLC Channel Model with User Movement

In Fig. 3.7(a), the outage probability of the hybrid cellular-VLC link and direct cellular has been plotted. The good agreement between theoretical and simulation results validates the efficacy of the proposed analytical

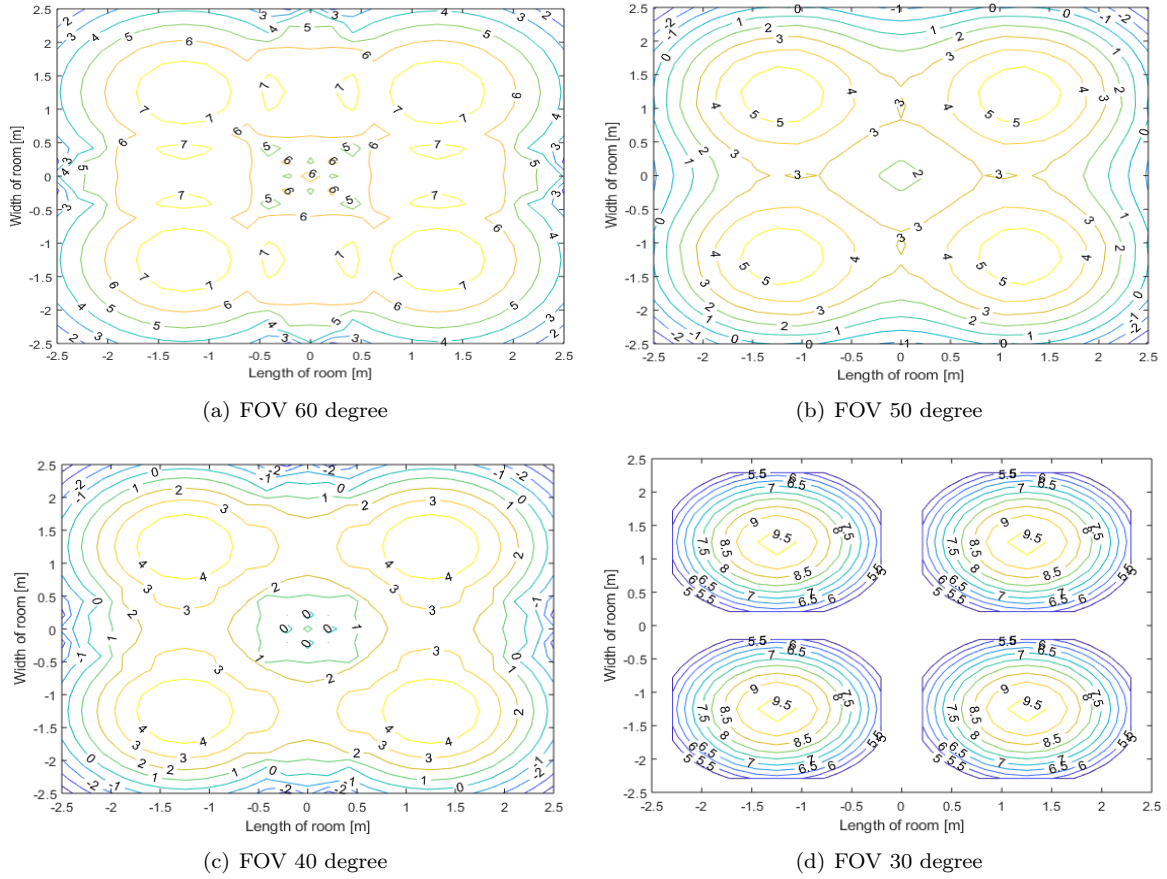


Figure 3.5: Outage region contours inside the room with 4 LED and using OLO with different FOV.

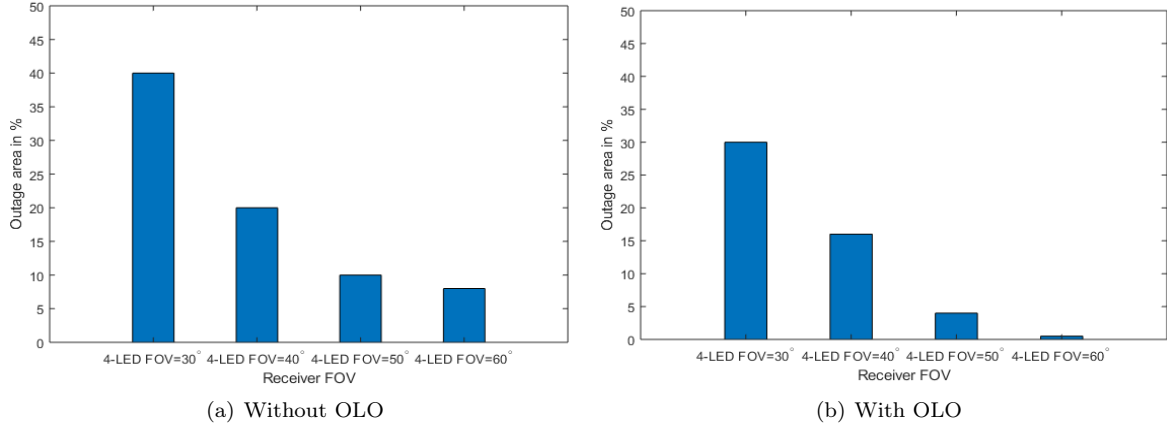
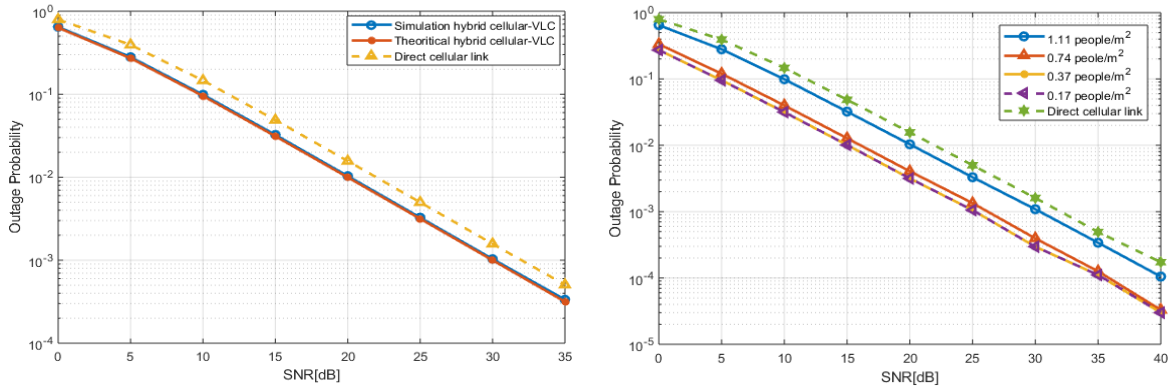


Figure 3.6: Outage area comparison without and with OLO.

methodology. However, as compared to the direct cellular link, the outage performance of hybrid cellular-VLC link is better. For instance, to achieve an outage rate of 10^{-3} , required SNR using the hybrid cellular-VLC link is 30 dB whereas for the direct cellular link, the required SNR is approximately 33 dB.

Fig. 3.7(b) shows the outage performance for the hybrid cellular-VLC link for different indoor conditions (i.e., non-furnished room, furnished room) considering user movement inside the room. The results have also

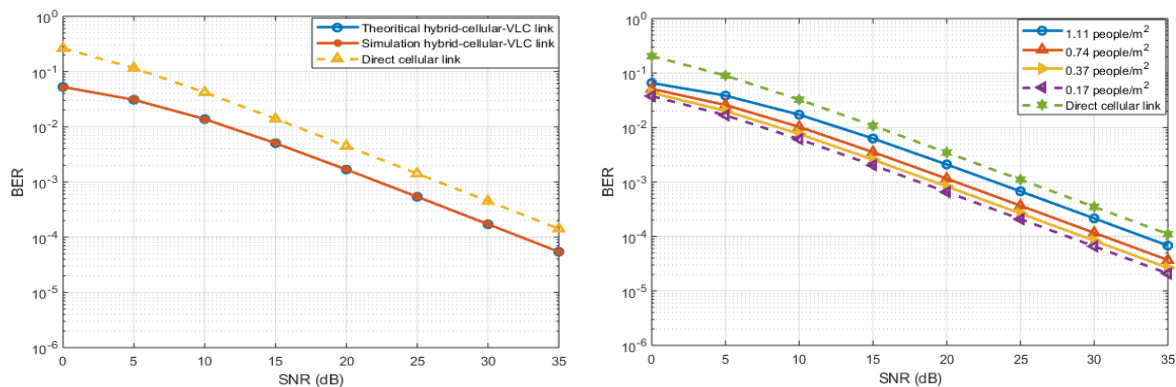


(a) Outage Probability in hybrid cellular-VLC link and direct cellular link. (b) Outage Probability in hybrid cellular-VLC link with different user movement.

Figure 3.7: Outage Probability

been compared with the direct cellular link. It can be noticed that the outage performance for an indoor room non-furnished (lower effective people density) is much better than furnished (higher effective people density) room for the proposed hybrid cellular-VLC link. For lower effective people densities like 0.17 people/m² and 0.37 people/m² the outage performance is almost same and requires SNR of 25 dB for outage of 10^{-3} . However, as we go on increasing the effective people density, the performance starts deteriorating, e.g., for higher effective people density of 0.74 people/m² and 1.11 people/m², the required SNR to achieve a target outage is approximately 26 dB and 30 dB respectively. This is due to the fact that as we increase the effective people density inside the room, it increases the value of scale factor (σ) which leads to a decrease in the received SNR (see (3.26)). However, the outage performance in a hybrid cellular-VLC link is still better than the direct cellular link.

3.6.5 BER Performance Under VLC Channel Model with User Movement



(a) BER performance of hybrid cellular-VLC link with OOK and direct cellular link. (b) BER performance of hybrid cellular-VLC link with different user movement.

Figure 3.8: BER Performance

Fig. 3.8(a) shows the BER performance of the proposed hybrid cellular-VLC link. It is evident that the derived BER expressions and the simulation results are in close agreement, which validates the mathematical

derivations and justifies the approximations made in (3.20). It can also be observed in Fig. 3.8(a) that hybrid cellular-VLC link gives better BER performance than a direct cellular link. For instance, to achieve a BER of 10^{-3} , required SNR using the hybrid cellular-VLC link is nearly 23 dB whereas, for the direct cellular link, the required SNR is nearly 26 dB.

Fig. 3.8(b) compares the BER performance with user movement at different effective people density with the direct cellular link from BTS to the end user. It can be observed that the BER performance degrades as user movement (people density) inside the room increases because higher the movement of people, will result in higher value of σ and lower received SNR e.g., for effective people density of 0.17 people/m², 0.37 people/m², 0.74 people/m² and 1.11 people/m², the required SNR to achieve a target BER of 10^{-3} is approximately 18, 19, 21, 23 dB respectively. However, the proposed hybrid link is performing better than the direct cellular link even with the increase in effective people density.

3.6.6 Performance Under Dimming

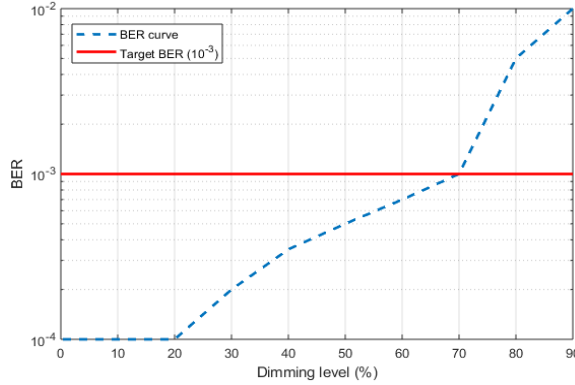


Figure 3.9: BER performance at different dimming level.

In the VLC system, the adequate lighting of LED light should be adjusted based on the users need as well as for saving energy [151],[152]. One of the simplest ways to achieve dimming control is by changing DC bias to provide a particular dimming level which is referred to as analog dimming. The second digital dimming technique generally uses pulse width modulation (PWM), in which a digitally modulated pulse train drives the LED at a constant current level. The average duty cycle represents the equivalent dimming level and is varied proportionally to acquire the desired dimming percentage [153].

Under the dimming constraint, using digital dimming technique the system model is evaluated to find out the possible dimming range to maintain the desired BER of 10^{-3} or better. Fig. 3.9 shows the BER performance of the system under a dimming constraint. It is quite clear that the proposed system can support up to 70% dimming range.

3.6.7 Power Saving with respect to Cellular-VLC Link

In this subsection, the amount of power saving by replacing last wireless link with the VLC link for a given BER performance has been analysed. The power saving is calculated as a power difference between the direct

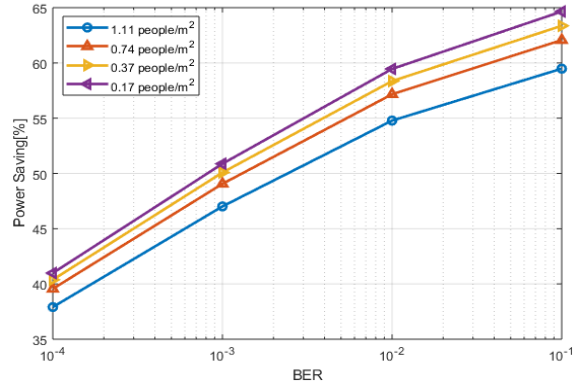


Figure 3.10: Power saving at different BER with user movement.

cellular link and the hybrid cellular-VLC link to achieve the target BER (10^{-3}) performance. Fig. 3.10 shows the percentage of power saving at the BTS by using a hybrid cellular-VLC link as compared to direct-cellular link. The proposed scheme requires approximately 51% less power with respect to the direct cellular link to achieve the desired BER performance with effective people density of 0.17 people/m². It may also be noted that as the effective people density inside the room increases the received SNR at the end user decreases, which in turn slightly reduces the power saving at BTS to maintain the required performance. For instance, with increasing effective people density 0.37 people/m², 0.74 people/m² and 1.11 people/m², the power saving at BTS is 49, 48 and 46% respectively. Further, it can also be seen that power saving at BTS reduces as BER limit is decreased.

3.6.8 SER Performance

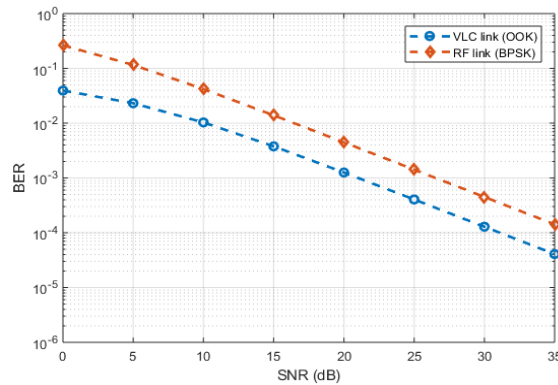


Figure 3.11: SNR vs BER for indoor VLC and RF link for 2 constellation points modulation scheme

The SER comparison between BPSK (RF) and OOK (VLC) is shown in Fig. 3.11. The comparison is made fairer by taking the same power at the transmitter end of both the links and an equal number of constellation points in the modulation scheme. Clearly, VLC gives an advantage of 5 dB over RF link at BER 10^{-3} . Further, Figs 3.12 and 3.13 shows the symbol-error-rate (SER) comparison for 4 points constellation modulation scheme, e.g., 4-CSK for VLC and 4-QAM for RF. Fig. 3.12 with 4-CSK for VLC and 4-QAM modulation shows the SER

performance of indoor VLC system without considering the effect of people blockage density, and it is observed that at SER 10^{-3} , VLC performs better than RF by 4 dB. The result shows the performance of the distance-based model for 4-CSK and the Rayleigh-based model for 4-QAM with reference to SNR at different SER. Also, there is good agreement between the respective theoretical and simulation plots of modulation schemes. Similarly, Fig. 3.13 displays the performance of the VLC 4-CSK modulation scheme in a dynamic channel with people density. The simulation result shows that even after considering people's movement, the performance of VLC is comparable to the RF link. It can be observed that the SER performance with people density in Fig. 3.13 degraded due to the effect of shadowing. However, it can also be seen that the proposed VLC modulation schemes outperform the 4-QAM RF schemes in the highly people-dense environment.

Furthermore, the SER comparison between 4-QAM DCO-OFDM for VLC and 4-QAM OFDM for RF is shown in Fig. 3.14. The comparison is made fairer by taking the same power at the transmitter end of both the links and an equal number of constellation points in the modulation scheme. It can be observed that the VLC link with 4-QAM DCO-OFDM gives an advantage of 2-3 dB over the RF link for the same modulation scheme 4-QAM OFDM at SER of 10^{-3} . The reason behind this is the huge difference in the value of noise in RF, and the VLC system gives VLC link an advantage over the RF link. Further, we believe that the SER gap between VLC and RF decreases as the constellation size increases.

3.6.9 Power saving with respect to Modulation Schemes

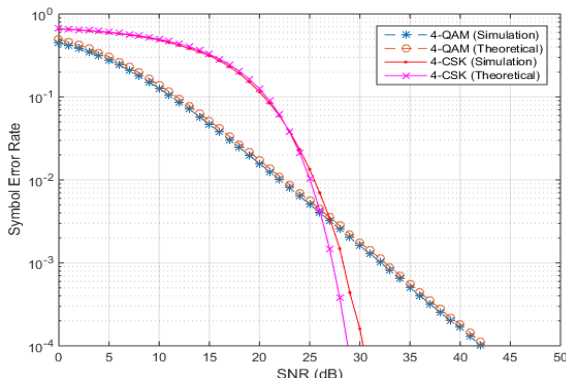


Figure 3.12: SNR vs SER for indoor VLC 4-CSK and RF 4-QAM Rayleigh.

The power saving plot reveals the difference in the power requirement of RF and VLC link at a particular SER. Fig. 3.15 shows the power saving of 4-CSK with different VLC channel models over the RF link. It is observed that VLC saves significant power in comparison to RF. One important observation from the power saving plot is that on increasing SER, the power saving decreases. This behavior can be explained from Figs. 3.12 and 3.13, as the SER decreases the SNR value increases and hence signal power also increases. The signal power increases both in VLC and RF system, but the noise is much less in VLC as compared to RF link, so the increment in VLC signal power is much less than RF. Thus, on decreasing SER, the difference in RF and VLC average signal power also increases. The power saving percentage is defined as $\left(\frac{\text{Power(RF)} - \text{Power(VLC)}}{\text{Power(RF)}}\right) \times 100$, which follows the same trend as above. The power saving in RF-CSK static case is 5% at SER 10^{-1} and

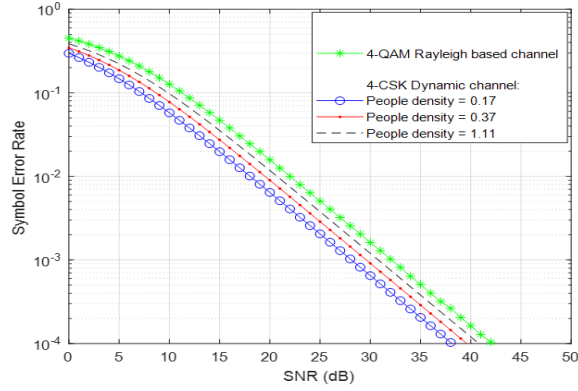


Figure 3.13: SNR vs SER for 4-CSK in indoor VLC Dynamic channel with varying people density

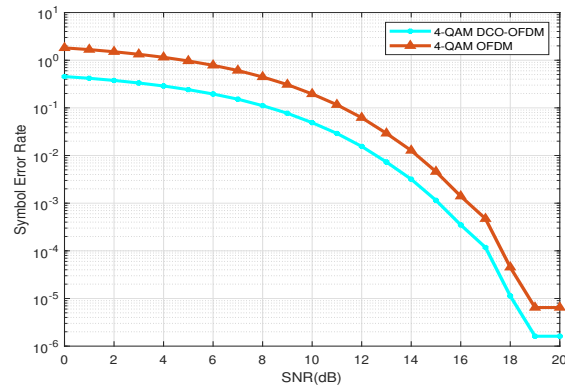


Figure 3.14: SNR vs SER for indoor VLC 4-QAM DCO-OFDM and RF 4-QAM OFDM RF.

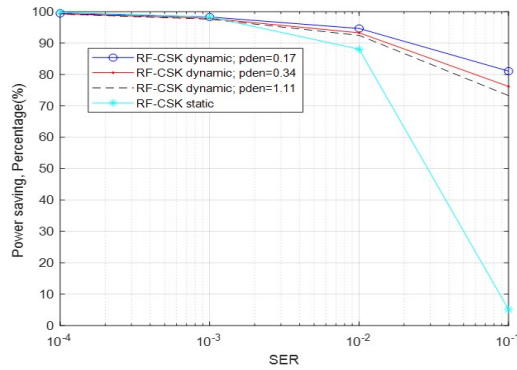


Figure 3.15: Power saving of different VLC modulation schemes over different channel models over RF link.

approaches 99.81% at SER 10^{-4} . Additionally, power saving in terms of dBm is shown in Fig. 3.16.

3.7 Summary

In this Chapter, we proposed a hybrid cellular-VLC link and compared its performance with the direct-cellular link. The closed-form expressions of outage probability and BER using OOK modulation for VLC is derived under dynamic user movement. The results are in close agreement with the simulation results, and the results

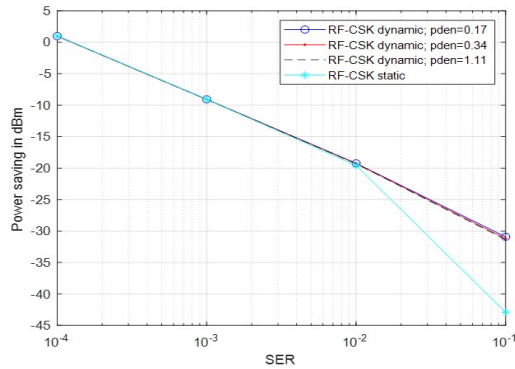


Figure 3.16: Power saving of different VLC modulation schemes over different channel models over RF link in dBm.

showed that even for the higher effective people density, the hybrid cellular-VLC link is performing better than the direct cellular link. The optimal Lambertian order with four LEDs rectangular scenario has been analyzed to make delay spread uniform and to increase the average received optical power in the room. Further, the outage region inside the room is plotted for different FOVs at optimal irradiance angle of LED under the static VLC channel, it was found that the rectangular configuration with OLO is the best configuration with minimum area in outage. The proposed scheme also results in a significant amount of power saving as compared to direct-cellular link at BTS. The proposed work also established that the hybrid link can support up to 70% dimming range of visible light.

Furthermore, this Chapter also compares the SER performance of the same constellation-based modulation schemes in the RF and VLC link in an indoor room. As one looks for better performance, i.e., beyond SER 10^{-3} , the performance of VLC in all its channel models is much better than RF. Further, the SER gap between VLC and RF decreases as the constellation size increases. This work shows that there is a significant amount of power saving using VLC link as compared to RF link inside a room, and at higher SNR the power saving approaches to a very high percentage of 99.81. The huge difference in the value of noise in RF and VLC system gives us a large power saving. One can generalize that VLC performs far better than RF regarding power saving. So, one can opt a VLC system even without source or channel coding for indoor communication. Also, the high SNR requirement for better performance covers the need for illumination. The performance of dynamic VLC link will increase further as compared to RF if one considers all the indoor effects in the RF link.

Chapter 4

Indoor VLC System Under Random Placement of LEDs with Non-imaging and Imaging Receiver

In this Chapter, we have shown the performance of indoor VLC systems with random placement of LEDs with imaging and non-imaging receiver configuration. It is a widely known fact that in a conventional VLC system, the SNR profile inside the room varies with respect to the LED placement and the PDs position. Consequently, the proposed work attempts to achieve uniform SNR across the room by utilizing MHCP-based LED placement at the transmitter and a non-imaging receiver with four PDs using 1-FOV, 2-FOV, and imaging receiver configurations.

The rest of the Chapter is organized as follows. We discuss the motivation behind this work and outline our contributions in Section 4.1. Section 4.2 describes the system model for the proposed MHCP LED deployment and the receiver structure. Further, in Section 4.3, the optimal and distance-based power allocation schemes for the LEDs are explained. The Closed-form expression of BER for the proposed system is derived in Section 4.4. The analytical and simulation results have been discussed in Section 4.5. Finally, Section 4.6 summarizes the Chapter.

4.1 Motivation and Contribution

4.1.1 Motivation

The illumination in most indoor scenarios is provided by multiple LEDs are located at specified intervals on the ceiling. Consequently, at most locations within a room, light can be received from more than one source. When these luminaires are used as data transmitters, they can be configured in many ways. The simplest is to transmit the same signal from each luminaire. This potentially provides the best coverage but at the cost of diminished overall capacity. Alternatively, a cellular system can be constructed where each luminaire transmits data destined for the nearest receiver [154, 155]. The above approach can be extended wherein the transmitters can be used in a MIMO configuration [156]. In MIMO configuration, the receiver must be able to separate signals from different sources. It has been shown in [157] that receivers with different FOV can be used to

separate the channel gains. This Chapter further builds on the work in [157] and investigates the performance of random deployment of LEDs using the MHCP by employing PDs with two different FOVs (2-FOV receivers) and the PDs with the same FOV (1-FOV receiver) referred to as non-imaging receivers.

4.1.2 Contribution

Motivated by these earlier works (ref. Section 1.6.3) on LED deployment, in this Chapter, we utilize MHCP to propose a random placement of LEDs in an indoor scenario to achieve uniform SNR and improved BER performance at the receiver. It has been shown that MHCP is a desirable and more appropriate approach for LED placement.

The main contributions of this Chapter are summarized as follows:

- We propose a random placement scheme of LEDs using MHCP, which results in more uniform SNR throughout the room. The performance of the proposed scheme has been evaluated under two types of receiver structure with four PDs using 1-FOV and 2-FOV. Both non-imaging and imaging receiver configurations are considered in the analysis.
- An optimal and distance-based power allocation scheme is proposed to distribute the power across each LED. The proposed power allocation schemes have shown improved performance with respect to conventional equal power allocation scheme.
- The closed-form expression of BER for the MHCP based LED placement scheme for both optimal and distance-based power allocation with multiple PDs using 1-FOV and 2-FOV configurations has been derived.
- Further, the performance of imaging and non-imaging receiver for different power allocation schemes has been shown by plotting the cumulative distribution function (CDF) of the received power.

4.2 System Model

We have considered a standard room size of $5\text{m} \times 5\text{m} \times 3\text{m}$. The 16 LEDs are placed in a random manner using MHCP process, as shown in Fig. 4.1. The receiver structure consists of $K = 4$ PDs lying in a plane parallel to the LED array plane. We have used two types of receiver structure, a non-imaging receiver structure in which four PDs are arranged in a square panel with different FOVs and another one is an imaging receiver.

In the following subsections, we will discuss in detail the LED placement using MHCP as well as different receiver configurations.

4.2.1 Random Placement of LEDs

A point process is a collection of points randomly located on the space such as a real line, or a Cartesian plane, etc. It is a powerful tool in statistics for modeling and analyzing the spatial data [158]. These point processes are frequently used in a wireless network for planning the location of base stations (BS) in a given area. Generally, the point processes depends on some random measure. If the random measure follows a Poisson

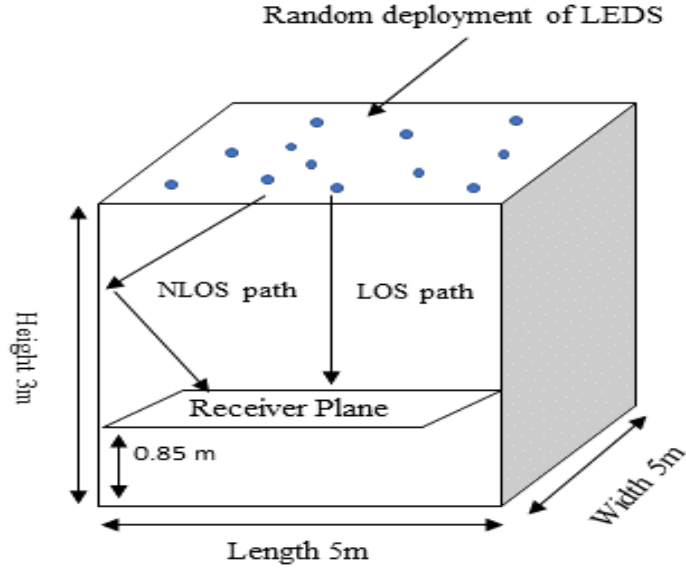


Figure 4.1: Indoor VLC System Model

random variable, such a process is called the Poisson point process (PPP). Further, if the average density of the points in the Poisson process located in some space is constant; then the resulting point process is called a homogeneous or stationary Poisson point process. The other type of process, called as the MHCP, is the hardcore point processes which is clustered point processes where the points are forbidden to be closer than a certain minimum distance. MHCP is also used for planning the locations of base stations and interference calculation in a cellular network [159]. One general way to achieve such a minimum distance between points is to start with a point process that has no such restriction and then remove points that violate the above condition. Fig. 4.2 shows the realization 16 LEDs in MHCP configuration. In this work, we have used the

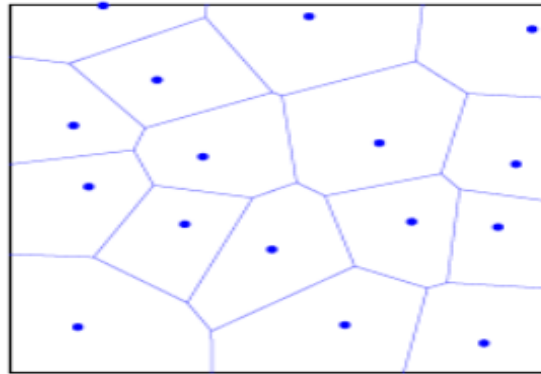


Figure 4.2: Realization of MHCP with 16 LEDs

MHCP process to distribute the LEDs in a plane with intensity λ which is defined by the number of LEDs to be deployed. Here, a random point or mark is associated with each LED, and a mark of the parent Poisson process is deleted if there exists another mark within the hardcore distance δ .

To determine the intensity of the MHCP process, we first condition on a point having a given mark t . This

point is retained with probability of $\exp(-t\pi\delta^2)$. Since $t\lambda_b$ is the density of points with marks smaller than t , the intensity of the resulting process is [160]:

$$\lambda = \lambda_b \int_0^1 \exp(-t\lambda_b\pi\delta^2) dt = \frac{1 - \exp(-\lambda_b\pi\delta^2)}{\pi\delta^2}, \quad (4.1)$$

MHCP can be used for modelling the positions of the simultaneous transmitting nodes. However, the MHCP is a conservative model, it will underestimate the intensity of simultaneous transmitting nodes in a certain degree when the network becomes dense.

4.2.2 Receiver Structure

4.2.2.1 Non-imaging Receiver

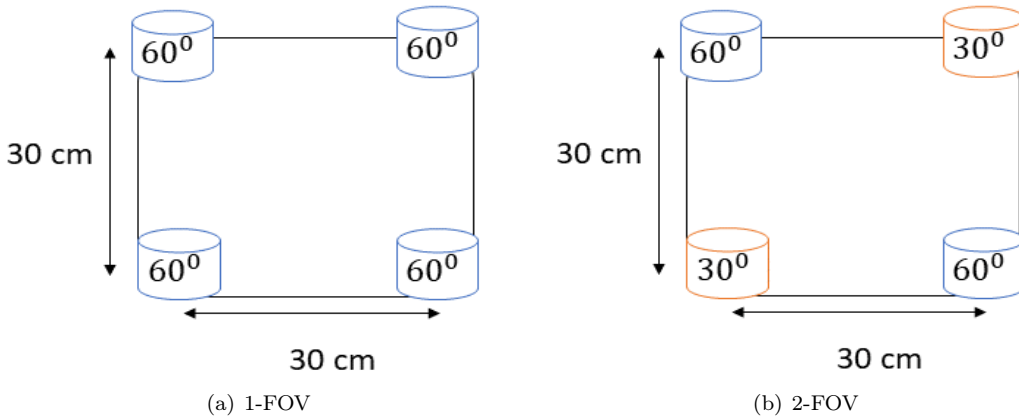


Figure 4.3: Non-imaging receiver structure with four PDs in 1-FOV and 2-FOV configuration.

A good optical MIMO receiver for indoor optical wireless applications should combine two characteristics:

- It should have a large overall FOV so that it has line of sight (LoS) to as many LED transmitters as possible.
- It should provide good diversity so that the signals from different transmitters can be separated [157].

In the 2-FOV receiver, the PDs with large FOV ensure that the receiver has a large overall FOV so that it has LoS to all the LED luminaries from all the possible receiver positions. The PDs with small FOV is used to reduce the similarity between the channel gains in each column of the channel matrix because for most receiver positions some luminaires are outside of the FOV of some PDs and within the FOV of others. Thus, even when the distance between the PDs is small, the channel matrix is well conditioned. In this work, we have used a combination of large FOV 60° and small FOV 30° receiver, as shown in Fig. 4.3. The reason behind using FOV combination of 60° and 30° is because and the large separation between the PD, as it provides a better-conditioned channel matrix than any other FOV combination, which will help the receiver in signal extraction [157].

4.2.2.2 Imaging Receiver

Fig. 4.4 shows the schematic of the imaging receiver with a FOV of 30° in a room with the concentrator (imaging lens) followed by PD array and an amplifier [161]. The PD array collects ambient light from all parts of the room and this creates unwanted photo-current, so a threshold is set for each detector pixel, and if the received photo-current is below this threshold then it is set to zero in the subsequent calculation.

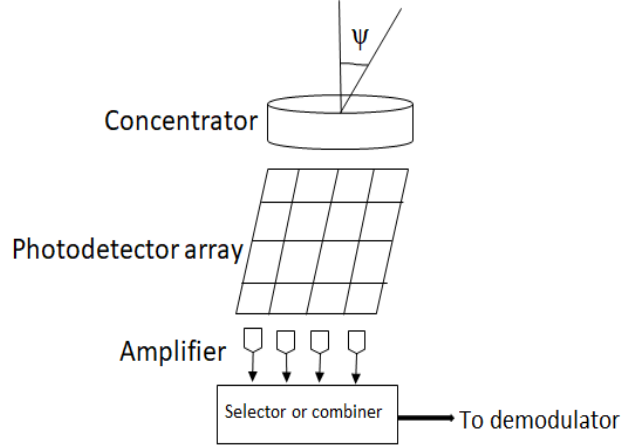


Figure 4.4: Imaging receiver

Light propagates from the transmitter LED arrays to the receiver, and each LED array is imaged onto a detector array, where images may strike any pixels or group of pixels on the array, and be in arbitrary alignment with them. Each pixel on the detector array is a receiver channel, and measuring the channel matrix. By denoting the optical connection between each pixel and each transmitter LED array allows the received signals to be separated.

4.3 LED Power Allocation Schemes

In this work, we have proposed three LED power allocation strategy for MHCP in order to maximize the received power at the receiver plane.

4.3.1 Equal Power Allocation

In the equal LED power allocation strategy, the total LED transmit power is equally divided among N randomly placed LEDs. The total LED transmit power can be expressed as:

$$P_t = \sum_{i=1}^N P_{t_i}. \quad (4.2)$$

where P_{t_i} is the allocated power to the i_{th} LED.

4.3.2 Distance-based Power Allocation

For MHCP configuration, each LED is at a random location, so heuristically the power should also depend on the distance of the LED from the center of the LEDs array. In this power allocation strategy, the total power

is distributed among all the LEDs. The power distribution is the function of the distance of the i_{th} LED to the center of the array. Hence, the power allocated to i_{th} LED is expressed as :

$$P_{t_i} = \frac{d_i^\alpha P}{\sum_{i=1}^N d_i^\alpha}, \quad (4.3)$$

where d_i is the location of i_{th} LED from the centre, P is total transmit power and α is the suitable exponent. This exponent α is calculated in order to maximize the SNR at the receiver. For a MHCP, SNR at the j_{th} PD is:

$$\text{SNR}_j = \text{E} \left[\frac{P_{r_j}}{\sigma_j^2} \right]. \quad (4.4)$$

where E is the expectation with respect to the MHCP with intensity λ . By solving (4.4) α is found out to be 3.1 for the proposed MHCP with 16 LEDs.

4.3.3 Optimum Power Allocation

In order to maintain uniform SNR across the room, it is essential that the mean SNR at the receiver is above a given threshold and the variance of the SNR should be small. Since the PD can be located at any point in the receiver plane, the variance of the received power P_{r_j} at j_{th} PD is considered as an objective function which can be expressed as:

$$\min_{P_{t_i}} \text{E} \left[(P_{r_j} - \text{E}[P_{r_j}])^2 \right] \quad (4.5)$$

subject to following constraints of total power constant and each LED has non negative power.

$$\begin{aligned} \sum_{i=1}^N P_{t_i} &= P. \\ \mathbf{Ax} &= \mathbf{P}. \end{aligned} \quad (4.6)$$

where $\mathbf{A} = [1, \dots, 1]$.

$$P_{t_i} \geq 0, \quad \forall i = 1, \dots, N. \quad (4.7)$$

The above can be formulated as an optimization problem. The objective function in (4.5) is expressed in quadratic form and is a cost function for the proposed optimization problem. The first term in (4.5) is a second order mean of received power at PDs and can be expressed in terms of transmit power as:

$$P_{r_j} = \sum_{i=1}^N H_{ij} P_{t_i}. \quad (4.8)$$

The optimization problem is:

$$\min_x \frac{1}{2} \mathbf{x}^T \mathbf{BP}_x \quad (4.9)$$

Subject to

$$\mathbf{Ax} = \mathbf{P}. \quad (4.10)$$

$$\mathbf{Gx} \leq 0. \quad (4.11)$$

where $\mathbf{G} = \text{diag}(-1, \dots, -1)$, $\mathbf{x} = [P_{t_1}, \dots, P_{t_N}]$, the matrix \mathbf{B} is given by:

$$B = \begin{bmatrix} \beta_{11} & \dots & \beta_{1N} \\ \beta_{N1} & \dots & \beta_{NN} \end{bmatrix} \quad (4.12)$$

and elements β_{uv} are

$$\beta_{uv} = \begin{cases} \frac{2 \sum_{p=1}^K H_{up}^2}{K} - \frac{2(\sum_{p=1}^K H_{up})^2}{K^2}, & u = v \\ \frac{2 \sum_{p=1}^K H_{up} H_{vp}}{K} - \frac{2(\sum_{p=1}^K H_{up})(\sum_{p=1}^K H_{vp})}{K^2}; & u \neq v. \end{cases} \quad (4.13)$$

Here (4.10) and (4.11) corresponds to the two constraint that we stated during problem formulation (4.5). The cost function in (4.9) is convex [162]. It is numerically solved using quadratic programming (QP) through CVXOPT solver in Python.

4.4 BER Performance

We have assumed OOK modulation in the VLC link for deriving the BER expression as this is one of the standard modulation scheme defined in the VLC standard (IEEE 802.15.7) [49]. The optical signal transmitted by the i_{th} LED of the VLC is given by:

$$s_i(t) = P_{t_i}[1 + M_I x_i(t)], \quad (4.14)$$

where P_{t_i} is the transmit power at the i_{th} LED, x_i is the corresponding modulating OOK signal and M_I is the modulating index [163]. Here the former term (P_{t_i}) in (4.14) takes care of illumination while the latter ($P_{t_i} M_I x_i$) is for communication. After photo-detection, assuming that the DC component of the detected electrical signal is filtered out at the receiver, the received signal at photo-detector j is given by

$$y_j = \mathcal{R}P_{r_j} + n_j, \quad (4.15)$$

where \mathcal{R} is photodiode responsivity, n_j is AWGN with $n_j = \mathcal{N}(0, \sigma_j^2)$ and P_{r_j} is expressed as:

$$P_{r_j} = \sum_{i=1}^N H_{ij} P_{t_i} M_I x_i. \quad (4.16)$$

VLC channel coefficient between i_{th} LED and j_{th} PD H_{ij} using (2.7) can be expressed as [12]:

$$H_{ij} = \frac{(m+1)\cos^m(\phi)A\cos(\theta)}{2\pi d_{ij}^2}. \quad (4.17)$$

where ϕ is the angle of incidence of light on the surface and m is the order of Lambertian emission, A is the detector physical area and θ is the angle of incidence with respect to the receiver axis, d_{ij} is the distance between the i_{th} LED and the j_{th} PD.

4.4.1 BER for Equal Power Allocation

For equal power allocation the SNR at the receiver using minimum mean square error (MMSE) equalizer at the output of the PD is expressed as [164]:

$$\text{SNR}_{\text{MMSE}} = \frac{(\mathcal{R}P_t)^2}{\sigma_j^2 \left[\left(\mathbf{H}^T \mathbf{H} + \frac{\sigma_j^2 \mathbf{I}}{(\mathcal{R}P_t)^2} \right)^{-1} \right]}, \quad (4.18)$$

where \mathbf{H} is the channel matrix and can be calculated using (4.17) and \mathbf{I} is the identity matrix. BER for VLC with OOK under AWGN can be defined as [165]:

$$\begin{aligned} \text{BER}_{\text{equalpower}} &= Q\left(\sqrt{\text{SNR}_{\text{MMSE}}}\right) \\ &= Q\left(\sqrt{\frac{(\mathcal{R}P_t)^2}{\sigma_j^2 \left[\left(\mathbf{H}^T \mathbf{H} + \frac{\sigma_j^2 \mathbf{I}}{(\mathcal{R}P_t)^2} \right)^{-1} \right]}}\right). \end{aligned} \quad (4.19)$$

BER calculation is done using (4.19) for both 1-FOV and 2-FOV configuration, where only the channel matrix \mathbf{H} value will change as per the configuration of the receiver.

(4.19) can be used for BER calculation for distance based power allocation, in which the P_t will be calculated according to (4.4). The \mathbf{H} matrix calculation will remain same for both equal and distance-based power allocation schemes.

4.4.2 BER for Distance-based Power Allocation

For distance-based power allocation, the SNR at the receiver can be written as:

$$\text{SNR}_{\text{DBP}} = \sum_{j=1}^K \left[\frac{\left(\mathcal{R} \sum_{i=1}^N H_{ij} P_{t_i} \right)^2}{\sigma_j^2} \right], \quad (4.20)$$

where P_{t_i} will be calculated according to distance-based power allocation strategy, which satisfy (2.4). BER for OOK with distance-based power allocation can be expressed as:

$$\begin{aligned} \text{BER}_{\text{DBP}} &= Q\left(\sqrt{\text{SNR}_{\text{DBP}}}\right) \\ &= Q\left(\sqrt{\sum_{j=1}^K \left[\frac{\left(\mathcal{R} \sum_{i=1}^N H_{ij} P_{t_i} \right)^2}{\sigma_j^2} \right]}\right). \end{aligned} \quad (4.21)$$

The \mathbf{H} matrix calculation will remain same for both equal and distance-based power allocation schemes.

4.4.3 BER for Optimal Power Allocation

For the optimal power allocation the transmit power to the i_{th} LED will be allocated using optimization problem formulated in (4.9), which will depend on the MHCP process. The SNR at the j_{th} PD for optimal power allocation can be written as:

$$\text{SNR}_j = E \left[\frac{\left(\mathcal{R} \sum_{i=1}^N H_{ij} P_{t_i} \right)^2}{\sigma_j^2} \right], \quad (4.22)$$

The SNR at the receiver for optimal allocation can be written as:

$$\text{SNR}_{\text{optimal}} = \frac{\mathcal{R}^2 \sum_{j=1}^K \sum_{i=1}^N H_{ij}^2 P_{t_i}^2}{\sigma_j^2}, \quad (4.23)$$

therefore the BER expression with OOK for optimal power allocation can be expressed as:

$$\begin{aligned} \text{BER}_{\text{optimalpower}} &= Q\left(\sqrt{\text{SNR}_{\text{optimal}}}\right) \\ &= Q\left(\sqrt{\frac{\mathcal{R}^2 \sum_{j=1}^K \sum_{i=1}^N H_{ij}^2 P_{t_i}^2}{\sigma_j^2}}\right). \end{aligned} \quad (4.24)$$

BER calculation for optimal power allocation with 1-FOV and 2-FOV can be done using (4.24). It cannot be further decomposed analytically due to summation included in the point process hence will be evaluated numerically. Moreover, above BER performance can be extended for other modulation techniques like QAM, PAM as well.

4.5 Results and Discussion

In this section, we present simulation and analytical results for the proposed system inside a standard room size of $5\text{m} \times 5\text{m} \times 3\text{m}$ length and width of the room in the figures is represented by $L(\text{m})$ and $B(\text{m})$ respectively. The room consists of 16 LED transmitters placed in a random geometry using MHCP and a receiver consist of 4 PDs in a square geometry with non-imaging (1-FOV and 2-FOV) and an imaging receiver.

4.5.1 Received SNR Profile

In this section, the SNR distribution at the receiver for the proposed MHCP configuration with LED power allocation schemes under 1-FOV, and 2-FOV receiver structure with 4 PDs are shown using simulation results.

4.5.1.1 Equal Power Allocation

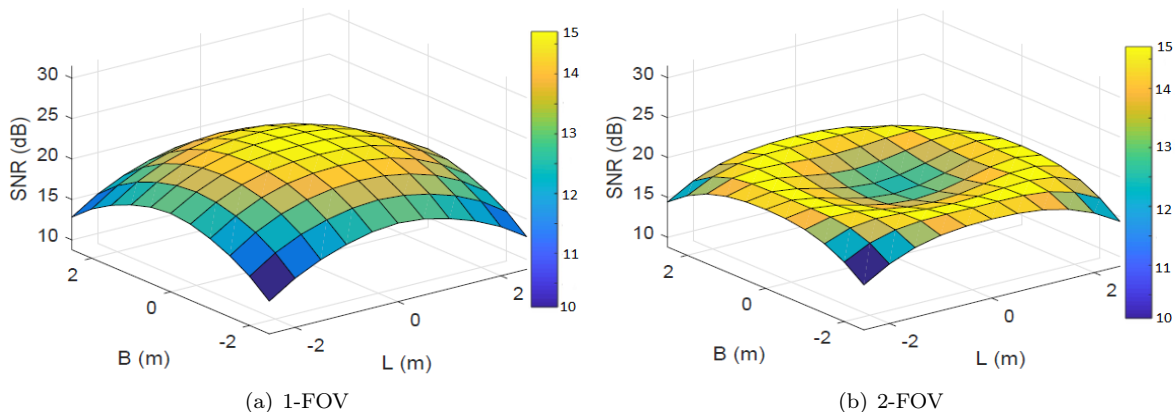


Figure 4.5: Received SNR distribution for 1-FOV and 2-FOV receiver with equal power allocation.

Fig. 4.5 shows the SNR profile at the receiver for proposed MHCP geometry with $N = 16$ LEDs for 1-FOV and 2-FOV receiver with 4 PDs. The total power is equally distributed among LEDs. With the help of the received SNR profile from Figs. 4.5(a) and 4.5(b), it can be calculated that for equal power allocation with 1-FOV receiver, the average SNR at the receiver is 13.50 dB whereas, for 2-FOV receiver the average SNR at the

receiver is 14.20 dB. 1-FOV receiver performance is poor because all of the elements in the channel matrix have very similar values, so the MMSE equalizer causes considerable noise enhancement. In a 2-FOV receiver, the combination of low and high FOV results in a more conditioned channel matrix than 1-FOV receiver, which results in improved channel gain at the receiver.

4.5.1.2 Distance Based Power Allocation

For the proposed MHCP geometry of LED deployment, the LEDs are located at an arbitrary location in the transmitting plane. In the distance-based power allocation strategy, the transmit power will also depend on the distance of the LED from the center of the MHCP array. The total power is distributed across $N = 16$ LEDs using (2.9), which maximizes the SNR at the receiver.

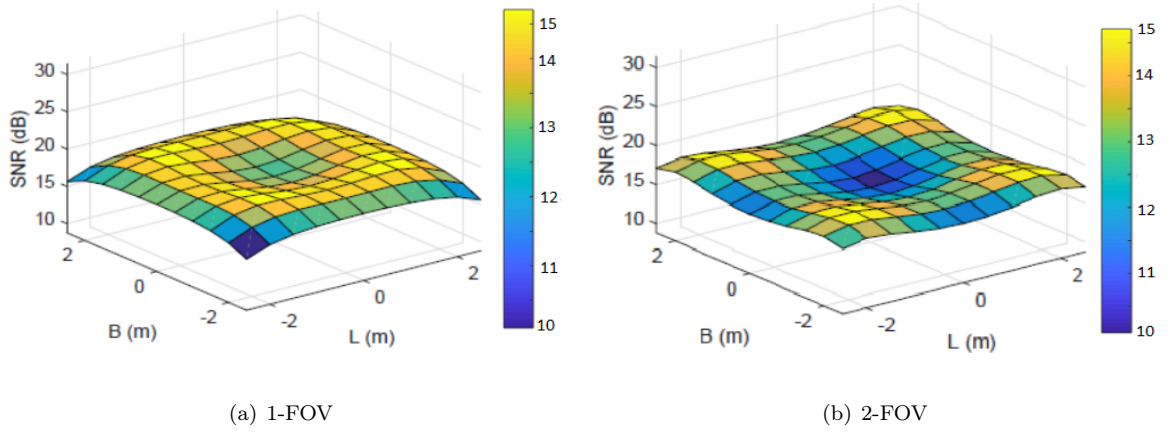


Figure 4.6: Received SNR distribution for 1-FOV and 2-FOV receiver with distance based power allocation.

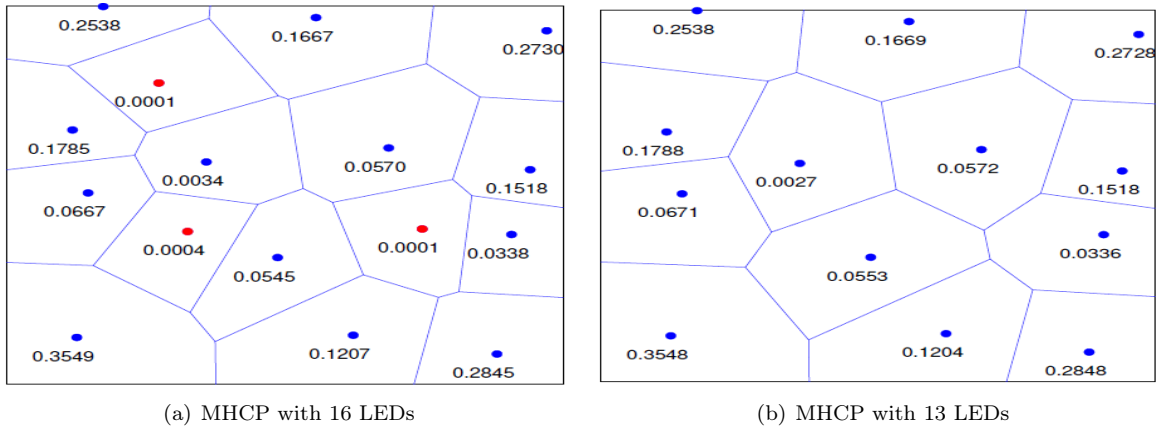


Figure 4.7: Optimal distribution of total transmit power across source LEDs.

Fig. 4.6 shows the SNR profile at the receiver for proposed MHCP with $N = 16$ LEDs with 1-FOV and 2-FOV receiver configuration. For 1-FOV with distance-based power allocation, the average SNR is 17.34 dB, while with 2-FOV receiver, the average SNR is 18.26 dB, as shown in Figs. 4.6(a) and 4.6(b). The 2-FOV receiver structure performs better than the 1-FOV receiver.

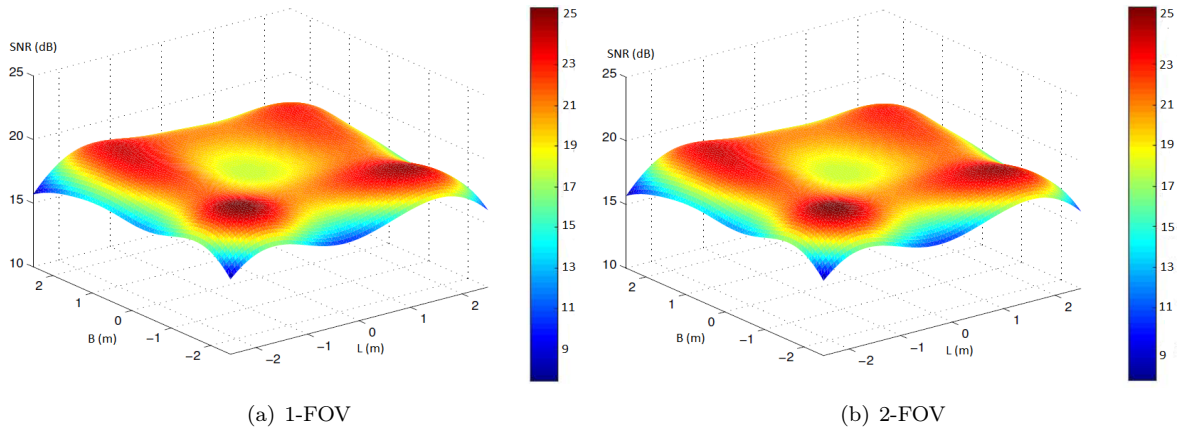


Figure 4.8: Received SNR profile for 1-FOV and 2-FOV receiver with 16 LEDs in MHCP with optimal power allocation .

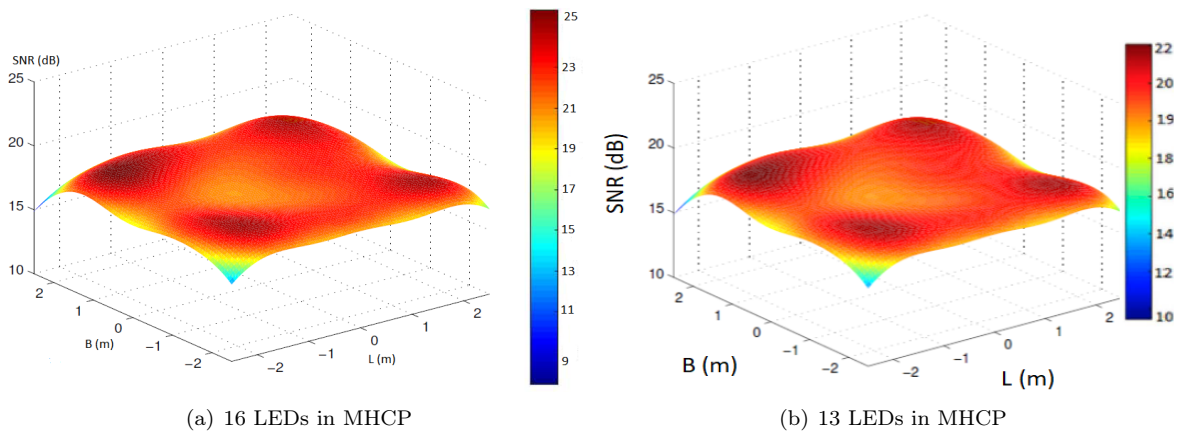
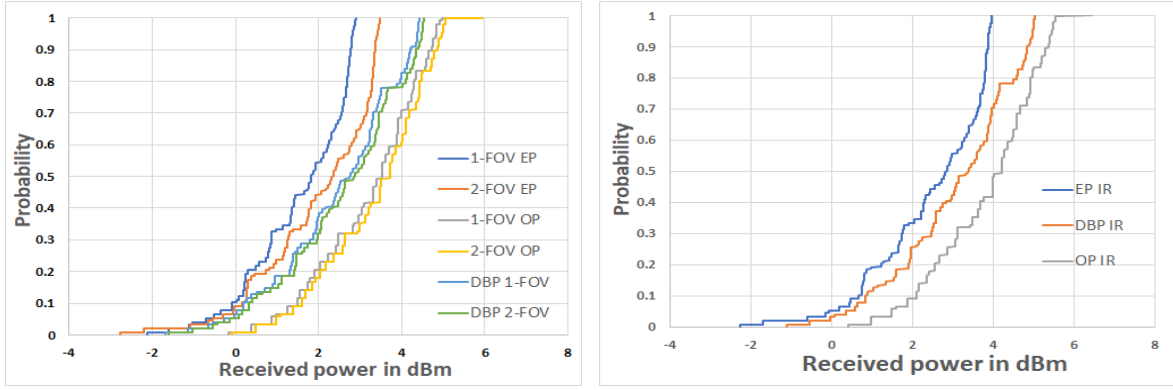


Figure 4.9: Received SNR profile for 1-FOV and 2-FOV receiver with 13 LEDs in MHCP with optimal power allocation .

4.5.1.3 Optimal Power Allocation

Fig. 4.7 shows the realization of LEDs using the MHCP with an optimal power allocation scheme. The total transmit power of P Watt is distributed among 16 LEDs by solving the proposed optimization problem in (4.9). It was observed that three LEDs which are marked as red in Fig. 4.7(a), have very less transmit power distributed compared to others, hence these 3 LEDs can be ignored in realization as shown in Fig. 4.7(b).

Figs. 4.8(a) and 4.8(b) compare the SNR profile at the receiver for 1-FOV and 2-FOV receiver with 16 LEDs in MHCP using optimal power allocation. It can be observed that for optimal power allocation with 16 LEDs, 2-FOV receiver performs better with an average SNR of 21.15 dB with respect to 1-FOV receiver, which has an average SNR of 18.85 dB. Further, by removing 3 LEDs, which are transmitting negligible power as compared to other LEDs and with optimal power allocation among 13 LEDs, it is observed that the SNR profile at the receiver is not affected. It is still comparable to the average SNR of 16 LEDs with low variance, as shown in Figs. 4.9(a) and 4.9(b).



(a) CDF of received power in MHCP with non-imaging receiver (b) CDF of received power in MHCP with imaging receiver

Figure 4.10: CDF of received power in MHCP with equal power (EP), distance-based power (DBP) and optimal power allocation (OP).

It may be noted that illumination is considered as a primary functionality of the LEDs and is given priority over communication [166]. The standard illuminance requirement for indoor room lighting for office work is 300-1500 lux standardized by international standard organization (ISO), which is also calculated and is fulfilled by the proposed geometry [46]. Hence, from the above discussion it can be inferred that the proposed work improves the performance of the system without compromising on the illuminance.

Table 4.1: SNR Performance of LEDs in Circular geometry

Parameter	EP		DBP		OP	
	1-FOV	2-FOV	1-FOV	2-FOV	1-FOV	2-FOV
Mean SNR	12.35 dB	14.50 dB	16.50 dB	17.85 dB	18.25 dB	19.20 dB
Variance (ROPD)	2.75 dBm	2.20 dBm	2.13 dBm	1.65 dBm	0.98 dBm	0.65 dBm
Illumination	340-1300 lux	340-1300 lux	340-1350 lux	340-1350	360-1350 lux	360-1350 lux

Table 4.2: SNR Performance of LEDs with Non-imaging Receiver

Parameter	EP		DBP		OP	
	1-FOV	2-FOV	1-FOV	2-FOV	1-FOV	2-FOV
Mean SNR	13.50 dB	14.20 dB	17.34 dB	18.26 dB	18.85 dB	21.15 dB
Variance (ROPD)	2.67 dBm	2.11 dBm	1.79 dBm	0.82 dBm	0.69 dBm	0.38 dBm
Illumination	330-1320 lux	330-1320 lux	350-1350 lux	350-1350	380-1400 lux	380-1400 lux

Table 4.3: SNR performance of LEDs in MHCP Configuration with Imaging Receiver

Parameter	EP	DBP	OP
Mean SNR	15.30 dB	19.22 dB	22.45 dB
Variance (ROPD)	1.76 dBm	1.05 dBm	0.5. dBm
Illumination	330-1320 lux	350-1350 lux	380-1400 lux

The SNR performance for all three power allocation strategies for the proposed MHCP with 1-FOV and 2-FOV receiver structure is summarized in Table 4.2. We have also compared the performance of MHCP

geometry with circular geometry shown in Table 4.1. We have also examined the MHCP performance with imaging receiver, as shown in Table 4.3. It is obvious that the proposed MHCP based optimal power allocation in LEDs performs better than the circular geometry in equal power and distance based power allocation strategies for 1-FOV and 2-FOV non-imaging receiver.

MHCP with optimum power in imaging receiver performs even better, and it is due to the fact that in imaging receiver both LOS and non-LOS links reduce ambient light noise, receiver thermal noise and multipath distortion, which results in improved SNR at the receiver. To further elaborate the results obtained for MHCP in Table 4.2 and Table 4.3, we have plotted the CDF of received optical power in MHCP configuration, as shown in Fig. 4.10. Fig. 4.10 shows the probability of the received optical power being less than to the corresponding received optical power in dBm. For instance, as shown in Fig. 4.10(a), at the probability of 0.5, the received optical power in equal power 1-FOV, and 2-FOV configuration is less than the 1.83 dBm and 2.35 dBm respectively. Similarly, in imaging receiver at the probability of 0.5, the received optical power for equal, distance based and optimal power allocation is 2.79 dBm, 3.38 dBm and 4.01 respectively. It is obvious from Fig. 4.10 that the MHCP with optimal power allocation is performing better in both non-imaging receiver (1-FOV and 2-FOV) and imaging receiver configurations.

4.5.2 BER Performance

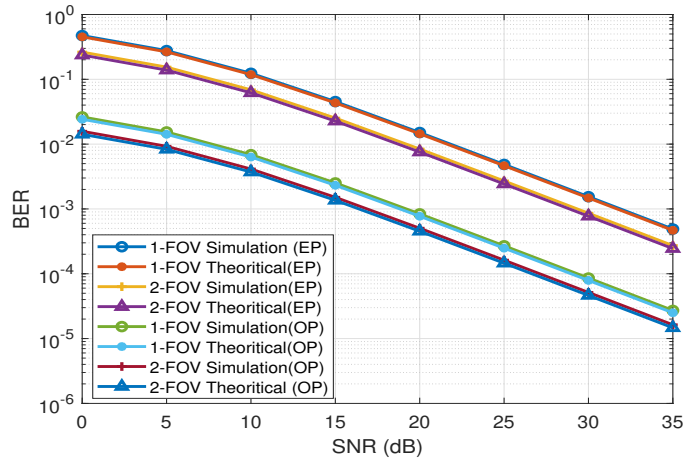


Figure 4.11: BER performance of the MHCP with non-imaging 1-FOV and 2-FOV receiver

Fig. 4.11 shows the BER performance of the proposed system with equal power and optimal allocation for non-imaging 1-FOV and 2-FOV receiver configuration, respectively. The derived BER expressions and the simulation results are in close agreement, which validates the mathematical derivations and justifies the approximations made in (4.19) and (4.24). It can also be observed from Fig. 4.11, that non-imaging 2-FOV receiver performs better than the 1-FOV receiver for equal power allocation. For instance, to achieve the BER of 10^{-3} required SNR with 1-FOV receiver is 32 dB whereas, for 2-FOV, the required SNR is 29 dB. Similarly, for optimal power allocation also, the 2-FOV receiver is better as compared to 1-FOV receiver with required SNR of 17 dB and 19 dB respectively to achieve the BER of 10^{-3} as shown in Fig. 4.11.

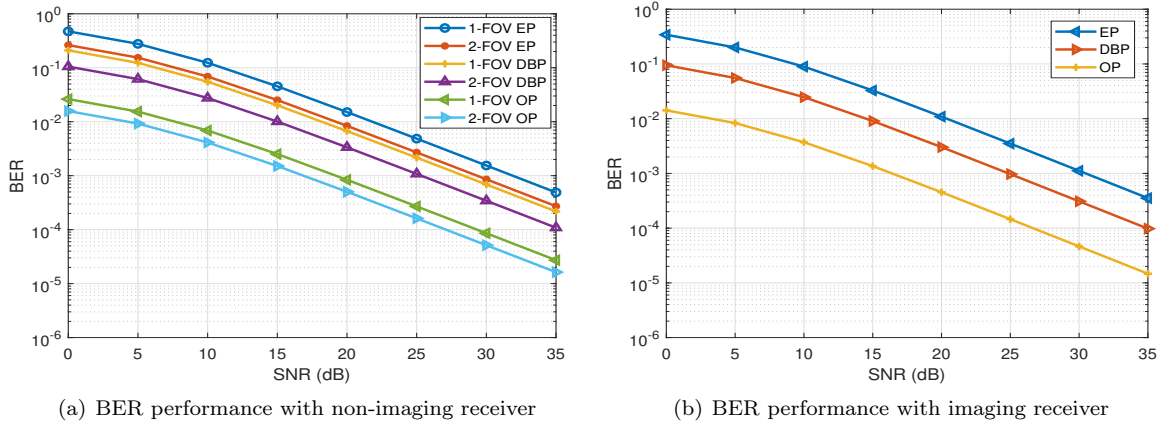


Figure 4.12: BER performance of the MHCP with non-imaging and imaging receiver

Fig. 4.12 shows the BER performance for the proposed MHCP configuration for equal, distance based, and optimal power allocation. It can be observed that optimal power allocation gives better BER performance for both receiver configuration. For instance, 2-FOV receiver with equal and distance based power to achieve the BER of 10^{-3} the required SNR is 29 dB and 25 dB respectively, whereas for optimal power allocation for the same BER the required SNR is 19 dB as shown in Fig. 4.12(a). Fig. 4.12(b) compares the BER performance for imaging receiver with equal, distance based, and optimal power allocation.

4.6 Summary

In this Chapter, a random deployment of LEDs using the MHCP for an indoor VLC system with non-imaging receiver and imaging receiver structures is proposed. It has been shown that MHCP results in more uniform SNR in the room as compared to conventional LED deployments. The results of SNR at the receiver were compared for three different power allocation strategies namely, equal power allocation, distance-based power allocation, and optimal power allocation. The proposed optimal power allocation is shown to provide more uniform SNR across the room with increased average SNR as well as the minimum variance between the two receiver locations inside the room. It has also been shown that the optimal power allocation performs better with the imaging receiver. The closed-form expression with MHCP is derived for the power allocation schemes with 1-FOV and 2-FOV receiver structure. The analytical results are in close agreement with the simulation results, which validates the analytical framework proposed in the Chapter.

Further, the results also demonstrate that MHCP with 2-FOV receiver and imaging receiver outperforms the non-imaging 1-FOV receiver with the proposed power allocation strategy. It has also been shown that the BER performance for optimal power allocation with non-imaging (2-FOV) and imaging receiver is better than equal and distance-based power allocation strategy.

Chapter 5

Indoor Visible Light Communication System with Human Blockages

This Chapter employs a stochastic geometry model-based approach to analyze the downlink performance of an indoor VLC system with human blockages. The system performance is analyzed for a regular placement of LEDs in a rectangular configuration. The proposed analysis is divided into two parts. In the first part, it is assumed that human blockages are static. Further, the analysis is extended for the case where blockage mobility has also been considered.

The rest of the Chapter is organized as follows. We discuss the motivation behind this work and outline our contributions in Section 5.1. In section 5.2, the system model is described, which includes the VLC channel model and spatial model of human blockages. The analytical framework for blockage realization using MHCP is derived in Section 5.3. Section 5.4 gives a characterization of human blockages using the RWP model. The analytical expression of SNR at the receiver with human blockages is derived in Section 5.5. The analytical and simulation results have been discussed in Section 5.6. Finally, Section 5.7 concludes the Chapter.

5.1 Motivation and Contribution

5.1.1 Motivation

Despite the growing literature (ref. Section 1.6.4) on shadowing, one or more of the following aspects are not considered in the above works. The received optical power in the indoor VLC system varies with respect to the distance from respective transmitting LEDs to the intended user inside the room. When there are multiple users inside the room, these users act as a blockage to the intended user. This blockage results in a sudden fall in received optical power as it can block both the LoS and the NLoS signal from the LED to the intended user. The amount of power reduction will depend on the height and width of the blockage. In order to analyze the impact of static and dynamic human blockages in indoor VLC systems performance, we have proposed two models to characterize the blockages. The first model, with MHCP realizes the static blockages wherein two blockages are forbidden to an absolute minimum distance. Further, to include the effect of dynamic human blockages moving with uniform velocity inside the room, the RWP model is used to realize the dynamic blockages.

5.1.2 Contributions

The proposed work analyzes an indoor VLC system under static and dynamic human blockages. The performance is analyzed for fixed placement of LEDs in a rectangular configuration with 4-LEDs and 8-LEDs arrangement. Some of the main contributions of the proposed work are summarized as follows:

- We propose a stochastic geometry-based model to investigate the impact of the static and varying size of human blockages inside the room. For the realization of static human blockage, MHCP is used. Further, to include the mobility of humans, the RWP model is used with uniform velocity.
- The analytical expression of the intensity of human blockages inside the room and the SNR at the receiver for the homogeneous (same size) and heterogeneous (different size) blockages are derived using MHCP for the static realization of human blockages.
- The received optical power with increasing density of human blockages inside the room has been plotted for both MHCP and RWP model with 4-LED and 8-LED configuration.
- Further, the SNR at the receiver with different blockage intensity has been shown by obtaining the cumulative distribution function (CDF) results for 4-LED and 8-LED configuration.

Notations: The vector and the matrix are denoted as \mathbf{x} and \mathbf{X} , respectively. The vectorization of matrix \mathbf{X} is denoted as $\mathbf{X}(:)$. The element corresponding to i^{th} row and j^{th} column of a matrix \mathbf{X} is represented as X_{ij} . The CDF and the PDF of the random variable are denoted as F and f , respectively. The retaining probability for radius r is represented as $P(r)$. The expectation of the random variable is denoted as E . The set of positive real numbers is denoted by \mathbb{R}_+^N and \mathbb{R}^2 denotes the two dimensional space. Φ denotes the set of points in the Poisson point process.

5.2 Characterization of Static Human Blockages Using MHCP

This section discusses the realization of the locations of the stationary human blockages inside the room using MHCP. The effect of homogeneous and heterogeneous blockages is analyzed. In MHCP, two or more points are forbidden to be closer than a certain minimum distance. The MHCP is also used to plan the deployment of base stations in cellular networks and modeling of blockages and interference calculation in wireless networks [159]. One way to achieve such a minimum distance between points is to start with a parent point process with no such restriction and then remove points that violate the above condition. We start with a target number of blockages (N_B) to be considered for the downlink analysis. To model the location of the blockages, we assume a modified version of the type-II MHCP process, wherein, the points are a result of random thinning of a parent PPP Φ_P with intensity λ_P . In particular, for each realization of Φ_P , we assign a random mark $[0, 1]$ to each \mathbf{x}_i in Φ_P . Then, \mathbf{x}_i is deleted if there exists an \mathbf{x}_j , $j \neq i$, such that the mark assigned to \mathbf{x}_j is lower than the mark assigned to \mathbf{x}_i . Let the resulting MHCP so created be denoted by Φ_B with intensity λ_B . Finally, we check the condition $N_B = \Phi_B(A)$, and perform the downlink analysis of the network for only such realizations

in which $N_B = \Phi_B(A)$ holds. we have used above describe MHCP to characterize the locations of stationary homogeneous (same radii r_1 or r_2) and heterogeneous (different radii r_1 and r_2) blockages, where $r_1 < r_2$.

5.2.1 Intensity of Homogeneous Blockages Using MHCP

In this subsection, we have characterized the homogeneous blockage process having radius r_B using MHCP. First, a parent Poisson point process is generated to realize the locations of human blockages in a 2-D plane. A random point or mark is associated with each human blockage, and a point of the parent Poisson process is deleted if there is another mark within the hardcore distance of δ . The intensity of the resulting process is [159]:

$$\lambda_B = \frac{1 - \exp(-\lambda_p \pi \delta^2)}{\pi \delta^2}. \quad (5.1)$$

where λ_p is the intensity of the parent point process. As shown in Fig. 2.5, the link between two nodes located at a distance d_B from each other is blocked if a element of point process falls in the shadow region of the blockage. The probability that the center of at least one blocking object falls in the shaded the area can be calculated using the void probability [167]:

$$P_B(d) = 1 - \exp(-2\lambda_B d_B r_B^2). \quad (5.2)$$

where λ_B is the blockage intensity having same radius and r_B is the blockage radius which can be either r_1 or r_2 .

5.2.2 Intensity Calculation of Heterogeneous Blockages Using MHCP

This subsection has characterized the heterogeneous blockage process with radius r_1 and r_2 using MHCP. The blockages inside the room have been modelled in two steps. In the first step, the points with fixed radius r_1 and r_2 are generated and the respective weights are assigned as $W_1(r_1)$ and $W_1(r_2)$. This marked Poisson process we denoted by Φ , and a point of the marked process in \mathbb{R}^2 is denoted by $[x; r]$.

In the second step, we thin the marked point process by letting all pairs of points whose associated cylinders intersect compete. A point is kept if it has a higher weight in all pairwise comparisons. Given a pair of blockages points $[x_1; r_1], [x_2; r_2] \in \Phi$, we give points independent weights, $W_1(r_1)$ and $W_2(r_2)$ respectively, which will depend on the radius, therefore, for the proposed model ($r_1 < r_2$), W_1 will be less than W_2 . If their associated cylinder intersects, the point with the lower weight is removed, and the point with the higher weight will be retained.

Hence, the retaining probability of a typical point with radius r and weight W after thinning is [168]:

$$P_{retain}(r) = E[\exp\{-\lambda_P \pi r^2 \int_0^\infty \{P(W_1(r) \leq W_2(y)) (r+y)^2 F_{pr}(dy)\}\}], \quad (5.3)$$

where $W_1(r)$ and $W_2(y)$ are independent weights and F_{pr} is the distribution of radius before thinning. A point and its associated d-dimensional cylinder are kept if and only if the sphere meets no larger or equal sized

sphere of the marked point process. Further, $E[P(W_1(r) \leq W_2(y))] = 1$ ($r \leq y$), then the retaining probability can be further written as:

$$P_{retain}(r) = \exp\left(-\lambda_P \pi r^2 \int_r^\infty (r+y)^2 F_{pr}(dy)\right). \quad (5.4)$$

We now consider a heterogeneous model of cylinders (blockages) with two different radius r_1 and r_2 . Let P_1 and P_2 denote the probability of blockage with radius r_1 and r_2 , respectively. The probability after thinning $P_{thin}(r_1)$ for the case $r_2 = 2r_1$, using Theorem 3.2 and Corollary 2.2 [168] in (5.4). The retaining probability of blockage radius r_1 can be expressed as:

$$P_{retain}(r_1) = \frac{P_2 (9P_1 + 16P_2)}{P_1 (4P_1 + 9P_2)^{-1} + P_2 (9P_1 + 16P_2)^{-1}}, \quad (5.5)$$

Similarly, the retaining probability of blockage radius r_2 can be expressed as:

$$P_{retain}(r_2) = \frac{P_1 (4P_1 + 9P_2)}{P_1 (4P_1 + 9P_2)^{-1} + P_2 (9P_1 + 16P_2)^{-1}}. \quad (5.6)$$

The intensity of thinned point process with retaining probability $P_{retain}(r)$ is given by [168]:

$$\lambda_{th} = \lambda_P P_{retain}(r). \quad (5.7)$$

Using (5.5), (5.6) and (5.7), the equivalent blockage density $\lambda_{B2}(r)$ for heterogeneous blockage process are generated which are given as:

$$\lambda_{B2}(r_1) = \lambda_P \frac{P_2 (9P_1 + 16P_2)}{P_1 (4P_1 + 9P_2)^{-1} + P_2 (9P_1 + 16P_2)^{-1}}, \quad (5.8)$$

$$\lambda_{B2}(r_2) = \lambda_P \frac{P_1 (4P_1 + 9P_2)}{P_1 (4P_1 + 9P_2)^{-1} + P_2 (9P_1 + 16P_2)^{-1}}. \quad (5.9)$$

5.3 Characterization of Dynamic Blockages using RWP

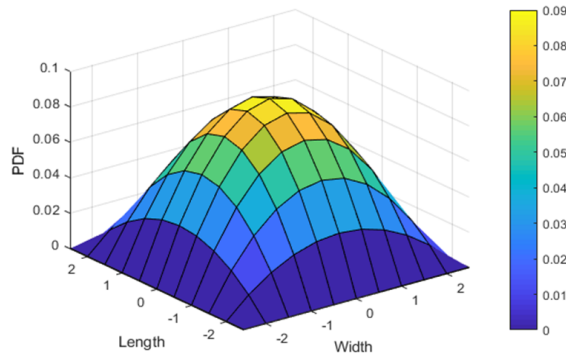


Figure 5.1: Stationary RWP model location PDF

In this section, the dynamic effect of human blockages moving within the room with the uniform velocity has been analyzed. The RWP mobility model is a simple and straightforward stochastic model that describes

a human blockage's movement behavior in given room size. In this model, a blockage randomly chooses a destination point ('waypoint') in the room and moves with uniform velocity on a straight line to the next destination point. After waiting for a specific pause time, it chooses a new destination and moves with uniform velocity to the destination, and so on. Further, we can use non-uniform velocity distribution, but in this work, for ease of analysis and analytical tractability, we have used uniform velocity distribution [169]. As discussed earlier, in a VLC system, the achievable user's data rate is related to the user-AP distance; therefore, including the spatial user distribution becomes essential.

Furthermore, note that human blockages are not necessarily distributed uniformly in typical indoor environments across the network area. On the contrary, their location distribution is characterized by a higher probability of being located near the center of the room than near the walls. Incidentally, the stationary distribution of the RWP model captures such a spatial configuration. For example, as discussed in [89], users' stationary distribution without pause-time in an RWP model can be approximated by an elliptic-paraboloid function.

In the analysis, RWP model is considered in a rectangular area of size $R = a \times a$, a point (waypoint) S_1 is selected randomly in R . A pause time at point S_1 is chosen randomly in an interval $[t_{min}, t_{max}]$, upon the termination of pause time, a new waypoint S_2 is chosen uniformly at random in R , and the node starts moving from S_1 to S_2 along a straight line trajectory with velocity chosen uniformly at random in an interval $[v_{min}, v_{max}]$. The pause and movement process is repeated as above when the node arrives at the destination. For the sake of simplicity and without loss of generality, we have used the RWP model without any pause time. As the users continue to move, the distribution of the position of users approaches a stationary distribution. In particular, for a square area of size, $a \times a$, the stationary distribution of the user locations is:

$$f_X(\mathbf{x}) = f_{XY}(x, y) = \frac{36}{a^6} \left(x^2 - \frac{a^2}{4} \right) \left(y^2 - \frac{a^2}{4} \right), \quad (5.10)$$

where $\frac{-a}{2} \leq x \leq \frac{a}{2}$, $\frac{-a}{2} \leq y \leq \frac{a}{2}$ shows the coordinate of each node in the square area and $\mathbf{x} = [x \ y]$ is the position vector. This stationary distribution is also represented in Fig. 5.1, which confirms the concentration of the users near the center of the room.

5.4 SNR Model

In this section, the received SNR is calculated for the stationary blockage process using MHCP. It is assumed that when the PD is in blockage, it receives no signal. The optical signal transmitted by the i_{th} LED is given by:

$$s_i(t) = P_{t_i} [1 + M_I x_i(t)], \quad (5.11)$$

where P_{t_i} is the transmit power at the i_{th} LED, x_i is the corresponding modulating OOK signal and M_I is the modulating index [163]. Here, the first term (P_{t_i}) in (5.11) takes care of illumination while the second term ($P_{t_i} M_I x_i$) is for communication. After photo-detection, assuming that the DC component of the detected electrical signal is filtered out at the receiver, the received signal at photo-detector j is given by

$$y_j = \mathcal{R}P_{r_j} + n_j, \quad (5.12)$$

where \mathcal{R} is photodiode responsivity, n_j is AWGN with $n_j = \mathcal{N}(0, \sigma_j^2)$ and P_{r_j} is expressed as:

$$P_{r_j} = \sum_{i=1}^N H_{ij} P_{t_i} M_I x_i, \quad (5.13)$$

where N is the number of LEDs and H_{ij} is the VLC channel coefficient between i_{th} LED and j_{th} PD, using (2.7) H_{ij} and can be expressed as [12]:

$$H_{ij} = \frac{(m+1)\cos^m(\phi)\text{Acos}(\theta)}{2\pi d_{ij}^2}. \quad (5.14)$$

where d_{ij} is the distance between the i_{th} LED and the j_{th} PD. If there is human blockage between the LED and the PD at distance d with probability $P_B(d)$ between transmitting LED and the PD the VLC channel gain with blockage can be expressed as:

$$\begin{aligned} H_{ij}^B &= H_{ij} [(1 - P_B(d))] \\ &= \frac{M[\exp(-2\lambda_B d_{ij} r_B^2)]}{2\pi d_{ij}^2}, \end{aligned} \quad (5.15)$$

where $M = (m+1)\cos^m(\phi)\text{Acos}(\theta)$.

The SNR at the receiver in the presence of blockages using (5.14), and (5.15) can be expressed as:

$$SNR_B = \frac{(\mathcal{R} \sum_{i=1}^N H_{ij}^B P_{t_i} M_I x_i)^2}{\sigma_j^2}, \quad (5.16)$$

The noise variance σ_j^2 at j_{th} PD is the total noise comprising of shot noise and thermal noise [170]:

By substituting value of H_{ij}^B from (5.15), it can be rewritten as:

$$SNR_B = \frac{\left[\sum_{i=1}^N \sum_{j=1}^K \frac{\mathcal{R} M P_{t_i} M_I x_i}{2\pi d_{ij}^2} \exp(-2\lambda_B d_{ij} r_B^2) \right]^2}{K \sigma_j^2}. \quad (5.17)$$

For the average SNR calculation, the blockage intensity will be taken as $\lambda_B \in (\lambda_{B_1}, \lambda_{B_2})$ and the blockage radius $r_B \in (r_1, r_2)$ as per the proposed configuration.

5.5 Results and Discussion

In this section, we present the simulation and analytical results for the VLC system with human blockages inside a standard room size of 5 m \times 5 m \times 3 m. The two transmitter configuration of 4 and 8 LEDs in a rectangular geometry are considered. The locations and the orientations of the VLC transmitters and the receiver are provided in Table 5.1. Both LoS and NLoS (with one-point reflection because of higher data rate threshold) [149] signals are considered in the analysis.

5.5.1 Received SNR Profile with Human Blockage

In this subsection, the received SNR profile with human blockages inside the room has been plotted. Figs. 5.2(a) and 5.2(b) show the received SNR profile with 4 LEDs having 6 and 8 human blockages of the same radius inside the room. It can be seen that there is a sudden fall in the received SNR whenever there is a

Table 5.1: Indoor VLC System Model Parameters

Parameter	Value
Room size	5 m × 5 m × 3 m
LED transmitted power	200 mw
Refractive index n	1.5
Optical filter gain T_s	1
Wall reflection ρ	0.8
LED irradiance angle	60°
Receiver plane above the floor (h_R)	0.85 m
Receiver elevation	90°
Receiver active area	1 cm ²
Field of views (FOVs) of receiver	60°.
Blockage radius (r_1 and r_2)	20 cm & 40 cm
Height of the blockage (h_B)	180 cm
Responsivity (\mathcal{R})	0.5 $\frac{\text{A}}{\text{W}}$
Signal bandwidth B_s	10 MHz
Noise bandwidth factor I_2	0.562
Background current I_{bg}	100 μA

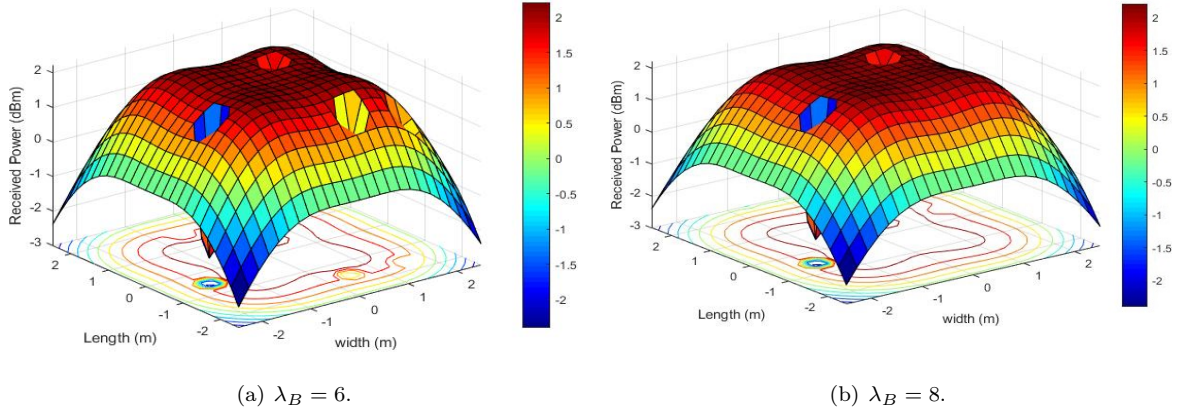
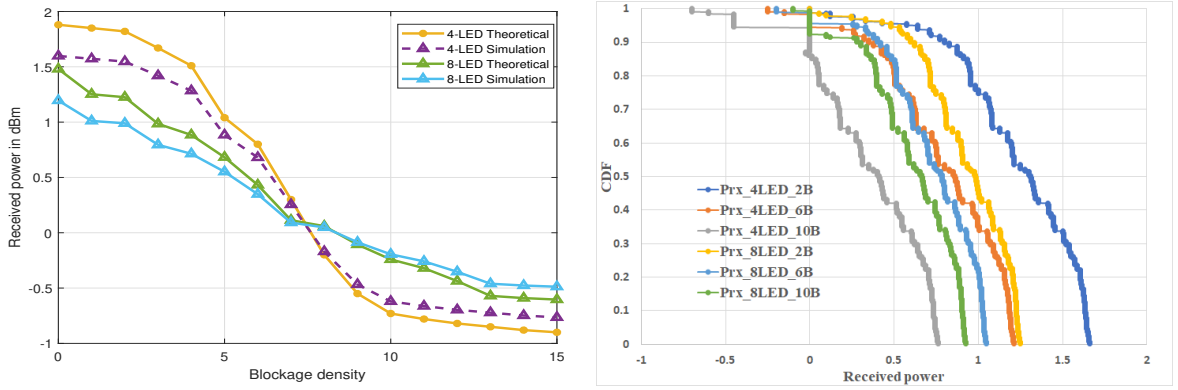


Figure 5.2: Received optical power distribution profile with human blockage intensity.

blockage between the transmitting LED and the user inside the room. Based upon the distance of blockage from the transmitting LED, its shadow region has been calculated using Fig. 2.5. As the distance from LEDs to the blockage increases using (2.16), it can be shown that the shadow region also decreases and vice versa. This results in different size areas of received SNR profile in shadowing due to the blockage and can also be seen in Figs. 5.2(a) and 5.2(b).

5.5.2 Received Power with Varying Homogeneous Blockage Intensity

Figs. 5.3(a) and 5.3(b) show the average received power and CDF of the received power with varying homogeneous blockages intensity inside the room. The human blockages of the same radius $r_1 = 20$ cm has been considered. Fig. 5.3(a) shows the average received power across the room with increasing blockage intensity with 4-LED and 8-LED in a rectangular configuration. The theoretical and simulation results are in good agreement with each other, validating the mathematical derivations and justifying the approximation made in



(a) Average received power versus homogeneous blockage density. (b) CDF of average received power of varying homogeneous blockage density.

Figure 5.3: Received power with varying homogeneous blockage intensity

(5.17).

It may be noted that in order to satisfy the total power constraint and support the fairness among the different configurations, we have used the constant power of 2 Watts for both 4 and 8 LEDs configuration. Thus the per LED transmit power is more in 4 LED configurations, i.e., 0.5 Watt, whereas for the case of 8 LEDs, it is 0.25 Watt. Further, the received power also depends on the relative distance between the LEDs. As mentioned before, the LEDs are placed in rectangular geometry, so in 4 LEDs, the LEDs are separated by more distance with respect to 8 LEDs configuration. In sparse blockages, 4 LEDs provide higher received power because of good LoS condition, which means that more LEDs are blocked in 8 LEDs with respect to 4 LEDs. On the contrary, when the number of blockages increases, in 4 LEDs case, the probability of users in LoS with LED decreases, while for 8 LEDs, this probability increases due to spatial diversity (i.e., because of more number of LEDs) so in 8 LEDs case the received power is more as compared to 4 LEDs.

To validate the above argument, we have plotted the received power CDF with 4 and 8 LED configurations in Fig. 5.3(b). Fig. 5.3(b) respectively shows that the probability of the received optical power being less than some threshold. For instance, at the probability of 0.5, the received optical power in 4 and 8 LED configurations with two blockages inside the room are 0.5 dBm and 1.23 dBm, respectively. Similarly, as blockage density increases, the 8 LED configuration performs better than the 4 LED, which confirms that the obtained CDF profile in 5.3(b) is in agreement with the results obtained in Fig. 5.3(a).

5.5.3 Received Power with Heterogeneous Blockage Intensity Using MHCP

This subsection shows the average received optical power across the room with increasing heterogeneous blockage density for 4-LED and 8-LED configuration. Two size of blockages with radius r_1 and r_2 have been considered, where $r_1 < r_2$. Figs. 5.4(a) and 5.4(b) show the average received power with heterogeneous blockage intensity inside the room with 4 and 8 LEDs, respectively. The blockages are realized using (5.9) MHCP process with radius r_1 , r_2 and mix radii (r_1 and r_2), equal number blockages have been realized for each case with equal probability. For example, in heterogeneous blockage realization, both r_1 and r_2 radius blockages have been

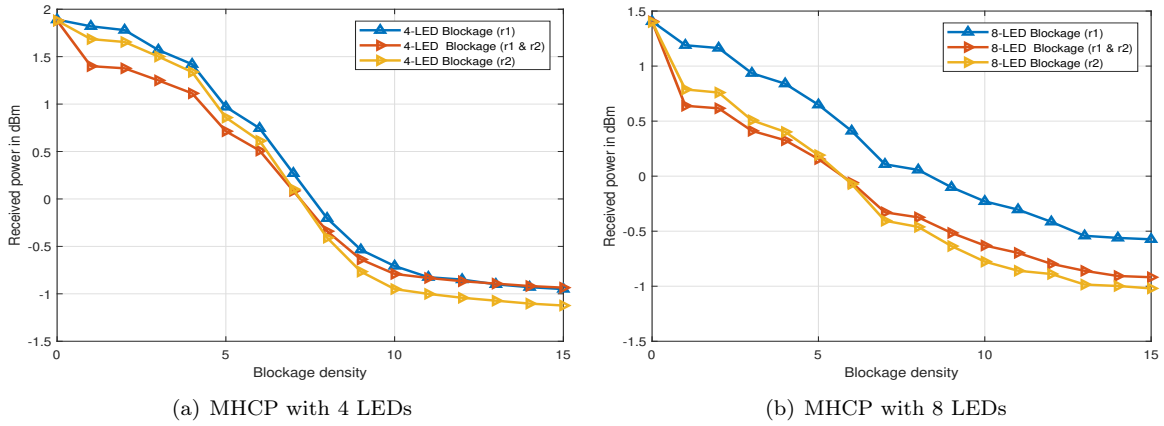


Figure 5.4: Average Received power with varying heterogeneous blockage density inside the room with 4 and 8 LEDs.

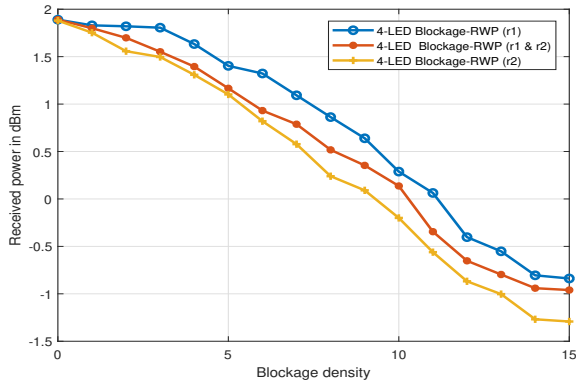
realized with equal probability. The average received power is decreasing with respect to the increasing blockage density. It is evident from the figure that the homogeneous blockages with radius r_1 are performing best among blockage with radius r_2 and mix radii. It is interesting to observe that for lower blockage density, blockage with mixed radii is performing better than the blockage with radius r_2 . However, this trend is reversed for higher blockage density (more than 7), as shown in Figs. 5.4(a) and 5.4(b). It is due to the fact that during the realization of blockages using the MHCP process, the less number of blockages are realized with radius r_2 in comparison to mix radii because of wider radius and thinning process in MHCP.

Further, it can also be observed from Fig. 5.4 that 4-LED configuration is giving better average received power compared to the 8-LED configuration for constant transmit power of 2 Watts for each configuration. However, for the higher blockage density of r_2 and mix radii, the 8-LED configuration gives better performance than the 4-LED configuration.

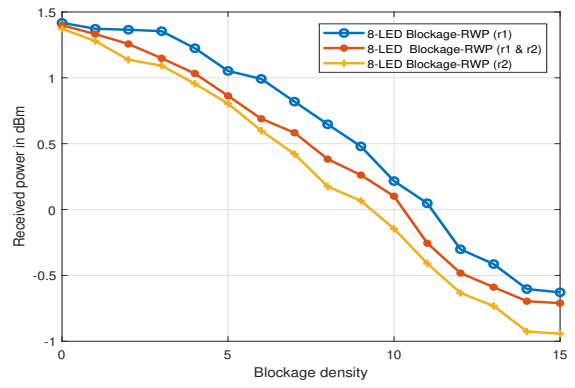
5.5.4 Received Power with Heterogeneous Blockage Intensity Using RWP

In this subsection, we have shown the average received optical power results across the room with heterogeneous blockage density using the RWP model. Figs. 5.5(a) and 5.5(b) show the average received optical power with varying blockage intensity inside the room with 4 and 8 LEDs, respectively. The blockages are realized using RWP mobility model with radius r_1 , r_2 and mix radii. It can be observed that the blockage with radius r_1 is performing better than the r_2 and mix radii for both 4-LED and 8-LED configuration. There is no crossover between r_2 and mix radii blockage realization using MHCP, and there is a clear gap between the received optical power in larger and smaller blockages.

Fig. 5.6 shows the comparison of average received optical power with heterogeneous blockage density inside the room with 4 and 8 LEDs using MHCP and RWP. It can be observed from Fig. 5.6(a) that average received power is decreasing with an increase in blockage density for both MHCP and RWP. The average received power with RWP performs slightly better than the MHCP because in the RWP model using (5.11), the user probability of being in the center is more than in edges or anywhere in the room, which results in a less number of LEDs

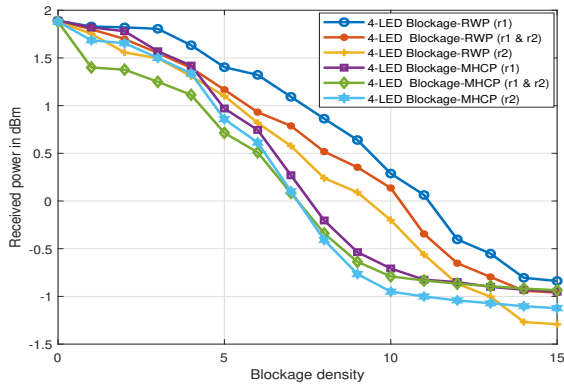


(a) MHCP with 4 LEDs

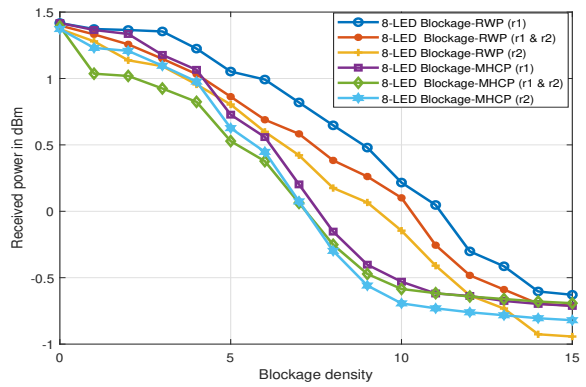


(b) MHCP with 8 LEDs

Figure 5.5: Average Received power with varying heterogeneous blockage density inside the room with 4 and 8 LEDs using RWP.



(a) MHCP with 4 LEDs



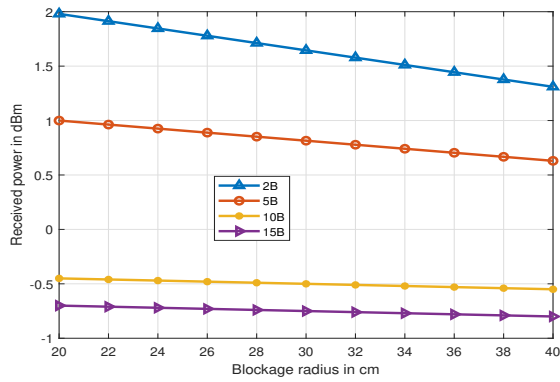
(b) MHCP with 8 LEDs

Figure 5.6: Comparison of average Received power with heterogeneous blockage density inside the room with 4 and 8 LEDs using MHCP and RWP.

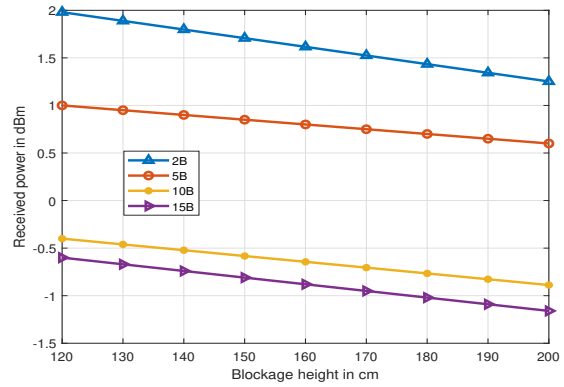
getting blocked in a rectangular configuration. Further, the average received power with the RWP model is continuously decreasing for higher blockage density, while for MHCP, the average power gets saturated for higher blockage density due to the stationary behavior of the MHCP.

5.5.5 Received Power with Varying Blockage Radius and Height

In this section, we have plotted the received power for different height and width of the human blockages, as shown in Fig. 5.7. It may be noted that for modelling static human blockages, we have used the MHCP process. For the width of the human blockage, the radius has been varied from 20 cm to 40 cm to reflect a typical human's waist size, as shown in Fig. 5.7(a). It can be observed that the received power decreases as the human blockages' width increases for different blockage densities. However, for lower number human blockage, the reduction is more as compared to higher human number blockage. Similarly, the height of blockage has been varied from 120 cm to 200 cm to reflect human height, as shown in Fig. 5.7(b). It can be observed that the received power decreases as the height of the human blockages increases due to the larger shadow of the



(a) Received power versus varying blockage radius



(b) Received power versus varying blockage heights

Figure 5.7: Average received power with varying blockage height and radius

blockages.

5.6 Summary

In this Chapter, the performance of an indoor VLC system with human blockages have been analyzed. For the realization of static and dynamic blockages inside the room, the MHCP and RWP model are used, respectively. We have also calculated the analytical expression of the received SNR for varying size human blockages inside the room using MHCP. Further, the effect of varying human height and width also have been analyzed. It can be observed that the received power decreases as the human blockages' width increases for different blockage densities. However, for lower number human blockage, the reduction is more as compared to higher human number blockage. It is concluded that for the higher number of blockages, the 8-LED configuration has been shown to perform better as compared to 4-LED for the same amount of total power from transmitting LEDs.

Chapter 6

Optimum LED semiangle and the receiver FOV selection for Indoor VLC System with Human Blockages

In this Chapter, we have determined the optimum pair of LED semiangle and the receiver FOV in the presence of human blockages for indoor VLC system. Firstly, we have calculated the optimum value of LED semiangle and the receiver FOV independently, keeping the others constant. Secondly, we have jointly optimized both the LED semiangle and the receiver FOV.

The rest of this Chapter is organized in the following way. We discuss the motivation behind this work and outline our contributions in Section 6.1. Section 6.2 discuss our proposed system model followed by VLC parameter optimization in Section 6.3. Section 6.4 discusses the analytical as well as the simulation plots. Lastly, Section 6.5 concludes the Chapter.

6.1 Motivation and Contribution

6.1.1 Motivation

In the earlier analysis of the VLC system, they avoid the impact of human blockages in the room, which will affect the system parameter values due to shadowing. Also, they do not study the impact of several practical system parameters like the order of reflections from the wall and human body reflection in the analysis in order to get the optimum values of VLC parameters. Our work aims to bridge these gaps in the literature (ref. Section 1.6.2). The motivation behind this work is to find the optimum pair of LED semiangle and the receiver FOV in the presence of human blockages, including reflections from the walls up to two-point and reflections from the human body [171] which can contribute to received power. To analyze the impact of human blockages on indoor VLC systems performance, we have employed an MHCP model to realize the static blockages [20]. We have also incorporated the reflections from the human body, essentially the skin and the clothes, in the analysis as it impacts the received power. In order to obtain the optimum value of the LED semiangle and the receiver FOV, we have used the quality factor (Q) as a performance metric. As it ensures the received power distribution is maintained uniformly by minimizing the variance between two points across the room while maximizing the

average power. Which will result in optimal system parameters such as receiver FOV and the LED semiangle.

6.1.2 Contribution

The major contributions of this Chapter are outlined below:

1. This work optimizes the LED semiangle and the receiver FOV for an indoor VLC system in the presence of human blockages for 4 LEDs in a rectangular configuration in order to provide high-quality factor and minimum delay spread across the room.
2. In the analysis of quality factor inside the room, wall reflection up to second-order and reflections from the human body and the clothes are considered.
3. A Joint optimization framework along with single variable optimization have been proposed to provide us the optimum value of VLC parameter (LED semiangle and receiver FOV) considering the impact of human blockages.
4. Further, we investigate the effect of the number of blockages on received quality factor with respect to varying FOV and LED irradiance angles and suggest optimum range (FOV and LED semiangle) of operation subject to the number of blockages inside the room.
5. Moreover, We also analyze the trade-off between the required quality factor and the delay spread across the room with respect to the number of blockages, LED semiangle, and the receiver FOV.

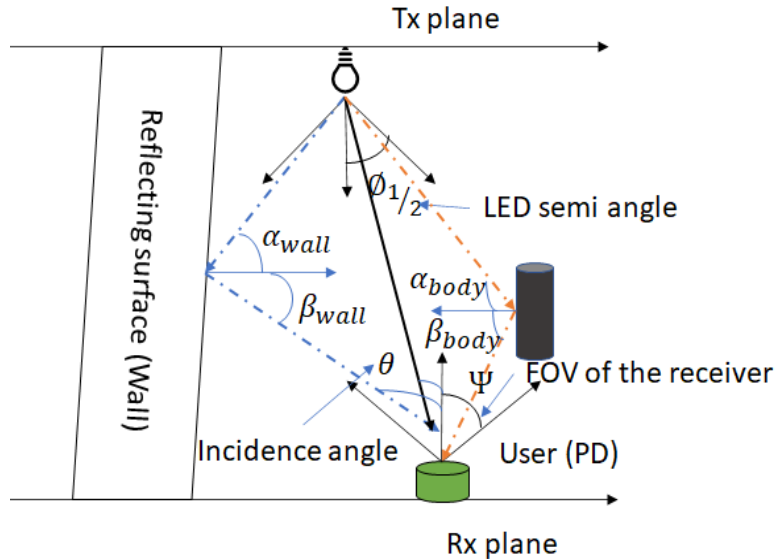


Figure 6.1: Multipath VLC System model

6.2 Multipath VLC System Model with Human Blockage

In this section, we discuss the system model of an indoor VLC system with human blockages inside. We have used the Matern type-II process to distribute the location of the blockages in a plane with an intensity of λ_B respectively. The blockages are assumed to be cylindrical with radius r and the height h_B as shown in Fig.6.1. For the proposed system model, two types of blockages of having radius $r_1 = 20$ cm, $r_2 = 40$ cm which are equivalent to varying sizes of humans with a minimum separation distance of $D_1 = 40$ cm, $D_2 = 20$ cm have been considered. Also, the surface of a human body exposed to light propagation is composed of two main parts, the skin, and the clothes, and their ρ values vary according to the light wavelength. We have used the mean human body reflection value of 0.51 mentioned in [171]. The receiver plane is considered to be 0.85m above the floor. Both LoS and NLoS paths are considered [49]. The receiver plane is divided into 25×25 sub-region to cover the whole room for analysis.

In the following subsections, we discuss in detail the the impact of the human body, and the modeling of human blockages.

6.2.1 Impact of Human Body

We consider geometrical models, one in 2D corresponding to the profile of a generic human body as a cylinder with a height of 180 cm and width of 20 cm and 40 cm, respectively.

As discussed in the above subsection I-B, firstly, we realize the human blockages with the help of the MHCP process. Then for each realization, we calculate the reflections from the human body to the PD using the ray-tracing model [172]. So the received power, including reflections from the human body can be written as:

$$H_{NLoS}^{body} = \begin{cases} \frac{\rho_2(m+1)A}{2\pi D_3^2 D_4^2} \cos^m(\phi) T_s(\psi) g(\psi) \cos(\alpha_{body}) \cos(\beta_{body}) & 0 \leq \Psi \leq \Psi_c \end{cases}, \quad (6.1)$$

Here α_{body} and β_{body} are the incidence and reflectance angle NLoS link make with reflecting surface (wall) have reflection coefficient ρ . D_3, D_4 are the distance travelled by NLoS link to reach the user from the blockages.

For a given transmission power (P_T), the total received power with multiple LEDs, including diffused paths through the walls and the human body using (2.9) and (6.1) can be obtained as:

$$P_r = \sum_{i=1}^N \left[P_T H_{LoS}^{LED} + \sum_{k=1}^K P_T H_{NLoS}^{wall} + \sum_{j=1}^M P_T H_{NLoS}^{body} \right]. \quad (6.2)$$

Here N is the total number of transmitting LEDs, M are the expected number of human blockage realized using MHCP process, K is the total number of reflection point on the wall, and the total power is obtained by integrating both LoS the NLoS link across the room.

6.2.2 Modeling of Human Blockages using MHCP

In this subsection, we have characterized the homogeneous blockage process having radius r_B using MHCP. First, a parent Poisson point process is generated to realize the locations of human blockages in a 2-D plane. A random point or mark is associated with each human blockage, and a point of the parent Poisson process

is deleted if there is another mark within the hardcore distance of δ . The intensity of the resulting process is $\lambda_{B1} = \frac{1 - \exp(-\lambda_p \pi \delta^2)}{\pi \delta^2}$, where λ_p is the intensity of the parent point process [159]. The link between two nodes located at a distance d_B from each other is blocked if an element of the point process falls in the shadow region of the blockage. The probability that the center of at least one blocking object falls in the shaded area can be calculated using the void probability $P_B(d) = 1 - \exp(-2\lambda_B d_B r_B^2)$ where λ_B is the blockage intensity having same radius and r_B is the blockage radius which can be either r_1 or r_2 .

6.3 VLC Parameter Optimization

This section discusses the optimization framework for the LED semiangle and the receiver FOV in the presence of human blockages. Here, our goal is to optimize the power at the receiver in the presence of human blockages considering second-order reflections from the wall and the reflections from the human body [173]. Therefore, we define quality factor as a performance metric, which is defined as the ratio of average received power to the variance of the received power:

$$Q = \frac{\bar{P}_{rec}}{2\sqrt{Var(P_{rec})}}, \quad (6.3)$$

where \bar{P}_{rec} is the average received power across the room and $Var(P_{rec})$ is the variance of received power across the room.

The average received power \bar{P}_{rec} can be defined as:

$$\bar{P}_{rec} = E[P_{rec}] = \frac{1}{A_{floor} \times N} \int_x \int_y P_{rec} dx dy, \quad (6.4)$$

where $A_{floor} = x \times y$ is the indoor room floor area which we have divided into number of grids, x and y represents the length and width of the room respectively.

The variance $Var(P_{rec})$ of the received power across the room can be defined as:

$$\begin{aligned} Var(P_{rec}) &= [E[P_{rec}^2] - [E(P_{rec})]^2] \\ &= \frac{1}{A_{floor}} \int_x \int_y [P_{rec}^2 - (\bar{P}_{rec})^2] dx dy, \end{aligned} \quad (6.5)$$

Using (6.3), (6.4) and (6.5) the quality factor can be expressed as:

$$Q = \frac{\frac{1}{A_{floor} \times N} \int_x \int_y P_{rec} dx dy}{2\sqrt{\frac{1}{A_{floor}} \int_x \int_y [P_{rec}^2 - (\bar{P}_{rec})^2] dx dy}}. \quad (6.6)$$

6.3.1 FOV Optimization

In this section, we describe the optimization of the FOV of the receiver such that the optical power detected on the receiver plane has a high average value and low spatial variations. For the FOV optimization, we have expressed the quality factor as a function of the FOV Ψ_c of the receiver. It can be observed from (6.3) that the quality factor is a function of the received power and variance, which we can write as a function of receiver FOV.

The average receive power $P_{rec}(\Psi_c)$ as a function of receiver FOV Ψ_c :

$$P_{rec}(\Psi_c) = \frac{1}{A_{floor} \times N} \int_x \int_y P_{rec}(\Psi_c) dx dy, \quad (6.7)$$

where $P_{rec}(\Psi_c)$ can be expressed using (2.7), (2.6) and (6.1):

$$\begin{aligned} P_{rec}(\Psi_c) &= \frac{(m+1)AP_T}{2\pi D^2} \cos^m(\phi) T_s g(\psi) \cos(\theta) \\ &= \frac{(m+1)AP_T}{2\pi \left[\sqrt{(x_R - x_T)^2 + (y_R - y_T)^2 + h^2} \right]} \\ &\quad \cos^m(\phi) T_s \cos(\theta) \frac{n^2}{\sin^2(\psi_c)}, \end{aligned} \quad (6.8)$$

where (x_T, y_T) , (x_R, y_R) are the transmitter and receiver location coordinates, respectively and h is the height of the receiver plane from transmitter plane.

Putting the value of $P_{rec}(\Psi_c)$ in (6.7) the average receive power $P_{rec}(\Psi_c)$ as a function of receiver FOV Ψ_c :

$$\begin{aligned} P_{rec}(\Psi_c) &= \frac{1}{A_{floor} \times N} \int_x \int_y \\ &\quad \frac{(m+1)AP_T}{2\pi \left[\sqrt{(x_R - x_T)^2 + (y_R - y_T)^2 + h^2} \right]} \\ &\quad \cos^m(\phi) T_s \cos(\theta) \frac{n^2}{\sin^2(\psi_c)} dx dy, \end{aligned} \quad (6.9)$$

Similarly the variance of the received power can be expressed as a function of receiver FOV Ψ_c :

$$\begin{aligned} Var(\Psi_c) &= E [P_{rec}^2(\Psi_c)] - [E (P_{rec}(\Psi_c))]^2 \\ &= \frac{1}{A_{floor}} \int_x \int_y \left(P_{rec}^2(\Psi_c) - (P_{rec}(\Psi_c))^2 \right) dx dy. \end{aligned} \quad (6.10)$$

Finally, the quality factor Q can be expressed as a function of receiver FOV Ψ_c :

$$Q(\Psi_c) = \frac{P_{rec}(\Psi_c)}{2\sqrt{Var(\Psi_c)}}, \quad (6.11)$$

For optimal solution to find the maximum value of quality factor subject to the receiver FOV Ψ_c

$$\frac{dQ(\Psi_c)}{d(\Psi_c)} = 0, \quad (6.12)$$

Solving the above optimality condition (6.12), the optimality equation subject to receiver FOV can be written as:

$$\frac{dP_{rec}(\Psi_c)}{d(\Psi_c)} \sqrt{Var(\Psi_c)} + \frac{d\sqrt{Var(\Psi_c)}}{d(\Psi_c)} P_{rec}(\Psi_c) = 0. \quad (6.13)$$

Now we can calculate the values of $P_{rec}(\Psi_c)$, $Var(\Psi_c)$, $\frac{dP_{rec}(\Psi_c)}{d(\Psi_c)}$ and $\frac{d\sqrt{Var(\Psi_c)}}{d(\Psi_c)}$ numerically by putting the value of VLC system parameter in the table 6.1.

6.3.2 LED Semiangle Optimization

In this section, the optimization of LED semiangle in the presence of human blockage, keeping the FOV of the receiver constant, has been proposed. In the analysis, the wall reflection up to second-order has been considered. Again the quality factor is considered as a performance metric. Here we are maximizing the quality factor at the receiver subject to LED semiangle.

We have expressed quality factor Q as a function of LED semiangle Φ , which can be defined as:

$$Q(\Psi_c) = \frac{P_{rec}(\Phi)}{2\sqrt{Var(\Phi)}}, \quad (6.14)$$

By using optimality condition $\frac{dQ(\Psi_c)}{d(\Psi_c)} = 0$, we have obtained the LED semiangle optimal equation as:

$$\frac{dP_{rec}(\Phi)}{d(\Phi)}\sqrt{Var(\Phi)} + \frac{d\sqrt{Var(\Phi)}}{d(\Phi)}P_{rec}(\Phi) = 0. \quad (6.15)$$

Now we can calculate the values of $P_{rec}(\Phi)$, $Var(\Phi)$, $\frac{dP_{rec}(\Phi)}{d(\Phi)}$ and $\frac{d\sqrt{Var(\Phi)}}{d(\Phi)}$ numerically by putting the value of VLC system parameter in the table 6.1.

6.3.3 Joint Optimization

In this subsection, we describe the optimization of both LED semiangle and the receiver FOV subject to the maximization of the quality factor. The optical power detected on the receiver plane has a high average value and low spatial variations. Therefore, we first calculate the received power and the variance of the received power as a function of both the LED semiangle Φ and the receiver FOV Ψ_c jointly.

The quality factor Q as a function of LED semiangle and the receiver FOV jointly can be expressed as:

$$Q(\Psi_c, \Phi) = \frac{P_{rec}(\Psi_c, \Phi)}{2\sqrt{Var(\Psi_c, \Phi)}}, \quad (6.16)$$

The optimal value of both LED semiangle and the receiver FOV can be calculated using optimality condition $\frac{dQ(\Psi_c, \Phi)}{d(\Psi_c, \Phi)} = 0$.

$$\frac{\partial \left(\frac{\partial P_{rec}(\Psi_c, \Phi)}{\partial(\Psi_c)}\sqrt{Var(\Psi_c, \Phi)} + \frac{\partial\sqrt{Var(\Psi_c, \Phi)}}{\partial(\Psi_c)}P_{rec}(\Psi_c, \Phi) \right)}{\partial(\Phi)} = 0. \quad (6.17)$$

6.4 Results and Discussion

This section presents and discusses the results obtained using simulation in MATLAB® environment in order to increase the value of quality factor subject to human blockages inside the room. The transmitter configurations of 4 LEDs in a rectangular geometry are considered. The locations and the orientations of the VLC transmitters and the receiver are provided in Table 6.1.

Table 6.1: VLC System Model Parameters

Parameter	Value
Room size	5 m × 5 m × 3 m
LED transmitted power	200 mw
Refractive index n	1.5
Optical filter gain T_s	1
Wall reflection ρ_1	0.8
Human body reflection ρ_2	0.51
LED semiangle	60°
Receiver plane above the floor (h_R)	0.85 m
Receiver elevation	90°
Receiver active area	1 cm ²
Field of views (FOVs) of receiver	60°.
Blockage radius (r_1 and r_2)	20 cm & 40 cm
Height of the blockage (h_B)	180 cm
Responsivity (\mathcal{R})	0.5 $\frac{A}{W}$
Signal bandwidth B_s	10 MHz
Noise bandwidth factor I_2	0.562
Background current I_{bg}	100 μA

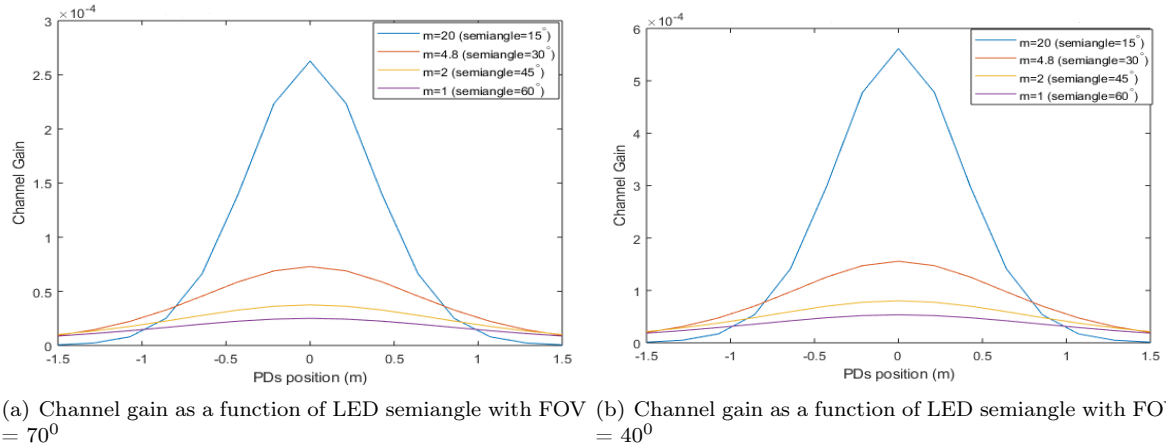


Figure 6.2: Variation in VLC Channel gain as a function of PD's position

6.4.1 VLC Channel Gain as a Function of LED Semiangle and Receiver FOV

Fig. 6.2(a) and Fig. 6.2(b) shows the variation in VLC channel gain at the receiver FOV of 70° and 30° respectively. In both the case the LED semiangle considered is 15°, 30°, 45° and 60°. We can see that the VLC channel gain is maximum at the lower values of LED semiangle (Φ) and FOV (Ψ_c), it starts decreasing with increasing value of Φ and Ψ_c .

It is due to the fact that the VLC channel is a cosine function of Φ and Ψ_c . We can also see that the VLC channel gain decreases as the distance to the LED and PD increases. As in the practical system, there will be obstacles inside the room. The VLC channel gain value will deteriorate due to shadowing, so it is essential to get the optimum pair of Φ and Ψ_c , which will give us better performance across the room.

6.4.2 Average Received Power with Varying FOV in the Presence of Blockage

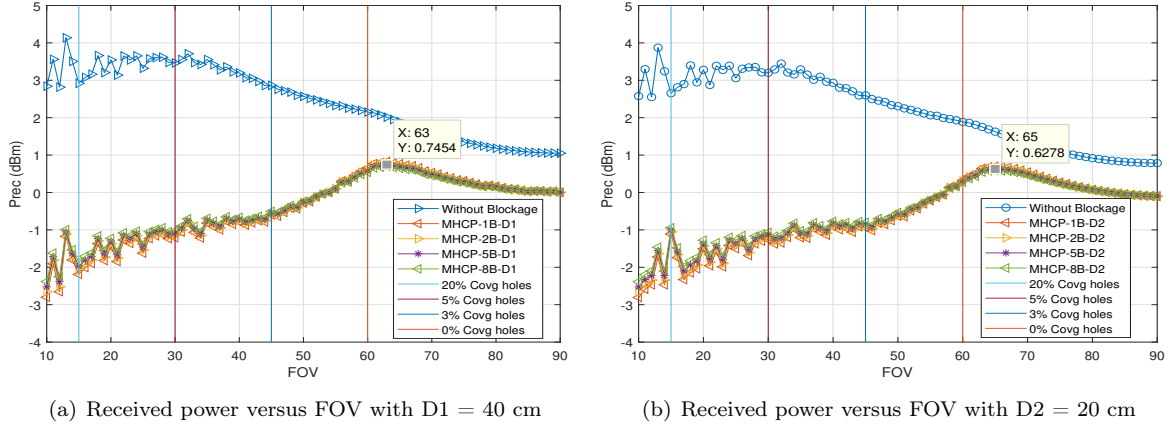


Figure 6.3: Effect of varying FOV and the separation distance between the blockages on the received power

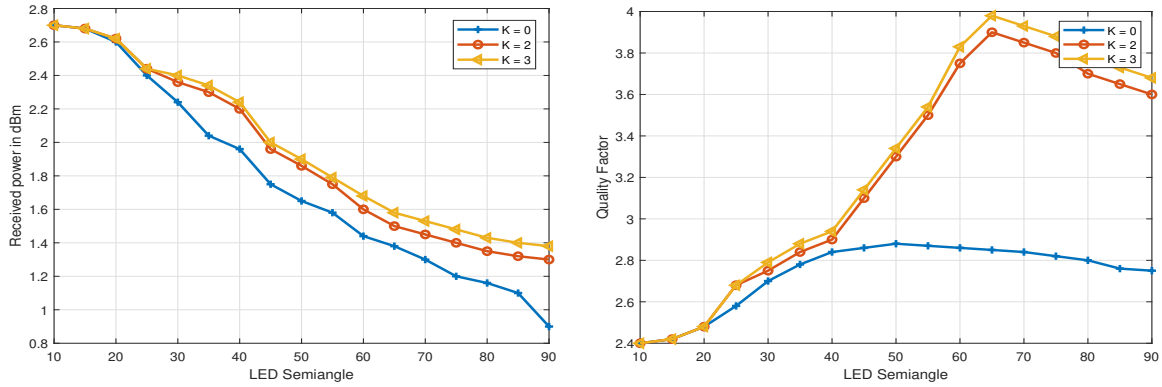
Fig. 6.3(a) and 6.3(b) show the average received power as a function of varying receiver FOV. For without blockage case, as the receiver FOV increases, the average power decreases and becomes constant at the higher value of FOV. However, for with blockage case, the average power first increases, then after achieving its maximum value, it starts decreasing for different blockage densities and minimum separation among them. Because of blockage, the user will be in shadow, so it requires a wider FOV to get the power from other LEDs that are not in shadow. Also, wider FOV capture more and more NLoS signals. It can be observed that for a specific minimum separation distance, we are getting a particular value FOV where the average power is maximizing, like for separation distance of $D_1 = 40$ cm, the optimum FOV value is 63° for all the blockage densities. While for the minimum separation distance of $D_2 = 20$ cm, the optimum value of FOV is 65° for all the blockage density.

It can be concluded that in the presence of blockage, the optimum value of FOV varies as a function of blockage density and the separation distance between them. The optimum FOV value is lower for the larger separation distance due to the non-clustering of blockages because of broader spacing between them. On the other hand, as the minimum separation distance among them decreases, it results in the clustering of blockage. Therefore, it requires wider FOV to increase average power across the room.

6.4.3 Average Received Power and the Received Quality Factor with Varying LED Semiangle

Fig. 6.4(a) and 6.4(b) show the average received power and the quality factor as a function of LED semiangle, keeping the receiver FOV fixed at 60° . Here in the analysis, reflections of up to second-order from the wall have been considered. In Fig. 6.4 $K = 0$ means only the LoS link, $K = 1$ means LoS and first-order NLoS link, and $K = 2$ means LoS with second-order reflection.

As the LED semiangle value increases, the average received power and power decreases as shown in Fig. 6.4(a). Compared to only LoS links, the average received power loss for the case that considers both LoS and



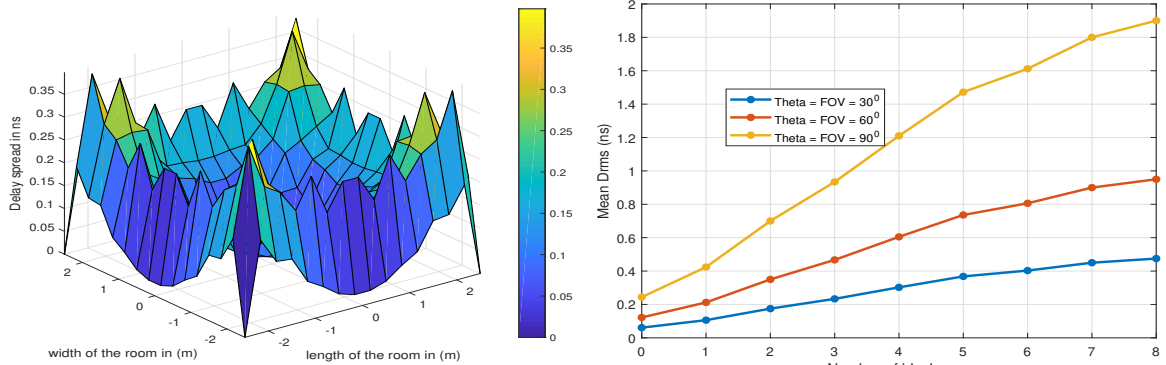
(a) Average received as function of LED semi angle with FOV = 60°

(b) Quality factor as a function of LED semi angle

Figure 6.4: Effect of varying LED semiangle on received power and the quality factor

NLoS is less. Therefore, the average received power should be maximum for the uniform quality of service, and the variance should be minimum. To evaluate the same, we have plotted the quality factor (Q) (see (6.3)) in Fig. 6.4(b) as it includes both averages received power and variance of the power in the analysis. It can be seen from Fig. 6.4(b) as the value of LED semiangle increases initially, the quality factor increases and achieve its maximum value. For the higher values of LED semiangle, it starts decreasing. It can be seen that the quality factor reaches its maximum value at the LED semiangle value of $\Phi = 65^\circ$.

6.4.4 Delay Spread with and without Blockage



(a) Delay spread across the room without blockage

(b) Delay spread with blockage

Figure 6.5: Delay spread Comparison without and with blockage

Fig. 6.5(a) shows the delay spread profile without any blockages across the room in which delay spread ranges from 0 ns to 0.35 ns. It can be observed that the delay spread is minimum in the center of the room and increasing towards the corner of the room because, at the corners, most of the received power is due to NLoS links. Fig.6.5(b) shows the mean RMS delay spread as a function of a number of blockages in the room subject to different receiver FOV and LED semiangle values. For each case, the mean RMS delay spread (see (2.17))

increases with the increasing value of blockages, which is intuitive because the number of blockages more and reflections will be there in the received power because the LoS component will be blocked due to shadowing. For the case of $\Phi = \Psi_c = 30^\circ$ in this case the mean RMS delay spread is ranging from 0.1 ns to 0.25 ns and for the case of $\Phi = \Psi_c = 60^\circ$ in this case the mean RMS delay spread is ranging from 0.15 ns to 0.9 ns similarly for the case of $\Phi = \Psi_c = 60^\circ$ in this case the mean RMS delay spread is ranging from 0.22 ns to 1.9 ns. We can say that for a larger pair of LED semiangle and receiver FOV, the delay spread is more because many NLoS links will be generated due to the wide LED semiangle. The same large number of NLoS links will be captured by the PDs, while for the smaller pair of LED semiangle, fewer NLoS links will be generated because of the small LED semiangle and less captured by the PD due to small FOV.

6.4.5 Quality Factor and Delay Spread Trade-off

Table 6.2: Quality Factor and Delay Spread performance with respect to proposed optimization techniques

Blockage	Ψ_{opt}	Q (Ψ_{opt})	Φ_{opt}	Q (Φ_{opt})	DS	(Ψ_{opt}, Φ_{opt})	Q (Ψ_{opt}, Φ_{opt})	DS (Ψ_{opt}, Φ_{opt})
D1-2B	63°	8.05	65°	8.50	0.25 ns	$(63^\circ, 65^\circ)$	9.05	0.17 ns
D1-5B	63°	7.52	70°	8.06	0.40 ns	$(63^\circ, 70^\circ)$	8.35	0.21 ns
D2-2B	65°	6.09	70°	7.11	0.70 ns	$(65^\circ, 70^\circ)$	7.50	0.38 ns
D2-5B	65°	5.21	75°	2.25	5.54 ns	$(65^\circ, 75^\circ)$	6.15	0.78 ns

In this subsection, we have shown the trade-off between the received quality factor and delay spread as a function of the number of blockages in the room with respect to proposed optimization techniques. Table 6.2 shows the quality factor versus the number of blockages subject to proposed optimization methods. It can be seen that joint optimization (both FOV and LED semiangle optimization) provides us the best quality factor and minimum delay spread compared to single variable optimization LED semiangle and FOV optimization independently.

Table 6.2 shows the comparison of the proposed optimization techniques in terms of obtained quality factor and delay spread. Further, we have also shown the optimum pair of the receiver FOV and the LED semiangle for the respective configuration. For example, with two blockages with a separation distance of $D_1 = 40$ cm, the obtained optimum pair with single and joint optimization is $\Psi_c = 63^\circ$, $\Phi = 65^\circ$ and the respective quality factor value is 8.05 using single variable optimization and 9.05 using joint optimization. Similarly, for the case of 5 blockages, the obtained optimum pair with joint and single optimization is $\Psi_c = 63^\circ$, $\Phi = 70^\circ$ and the respective quality factor value is 8.06 using single variable optimization and 8.35 using joint optimization. Similarly, the delay spread of single variable optimization for 2 and 5 blockages using joint optimization 0.17 ns and 0.21 ns for $D_1 = 40$ cm and 0.38 ns and 0.78 ns for $D_1 = 20$ cm. Thus, we can see that the proposed joint optimization technique gives us the best possible quality factor with minimum delay spread in blockages compared to single variable optimization and without optimization case.

6.5 Summary

In this Chapter, we presented the optimum pair of LED semiangle and the receiver FOV in the presence of human blockages. The quality factor value is maximized to get the optimum value of LED semiangle with the receiver FOV. Further, We also show the effect of wall reflections and the reflection from the human body into the analysis. Results shows that with 2 and 5 blockages, the optimum pair using single and joint optimization is $(63^\circ, 65^\circ)$ and $(63^\circ, 70^\circ)$ for a separation distance of $D_1 = 40$ cm and $(65^\circ, 70^\circ)$ and $(65^\circ, 75^\circ)$ for $D_2 = 20$ cm respectively which provide the highest quality factor with minimum delay spread shown. Furthermore, the optimization analysis can also be mapped to different room sizes and LED placement, with static and dynamic blockages inside the room. Additionally, the results demonstrate that optimized LED semiangle and FOV pair perform better than any other combination.

Chapter 7

Optical IRS-aided Indoor VLC System with Human Blockages Considering Random User Equipment Orientation

This Chapter exploited the use of IRS to enhance the communication quality of indoor VLC systems [174]. It is demonstrated that an IRS can significantly improve the communication links' performance by configuring elements to reflect any incident wave from the transmitter in the receiver's direction. As discussed earlier, in indoor VLC systems, where the communication performance is mainly dependent on the availability of the LoS paths, IRS can compensate for a blocked LoS path by re-configuring the NLoS path. Therefore, we can utilize IRS in order to relax the LoS path requirement in VLC systems [113], [175].

The rest of this Chapter is organized in the following way. We discuss the motivation behind this work and outline our contributions in Section 7.1. Section 7.2 describes a system model consisting of a VLC channel model and an IRS channel model, a model that characterizes humans as a blockage and UE orientation. Section 7.3 describes the user orientation model for OIRS-aided indoor VLC systems. The probability distribution function for received SNR using OIRS is described in Section 7.4. Section 7.5 represents optimal FOV and LED semi-angle calculations for OIRS-aided indoor VLC systems. Section 7.6 discusses the obtained analytical and simulation results. Finally, Section 7.7 concludes the entire Chapter.

7.1 Motivation and Contribution

7.1.1 Motivation

As discussed earlier (ref. Section 1.6.5), IRS seems to have significant abilities in improving the performance of VLC systems. Several issues related to its integration into VLC systems have to be addressed to harness its full potential. Such concerns include deployment in indoor VLC environments, channel state information (CSI) acquisition, configuration optimization (phase shifts and/or rotation angles), and IRS control (feedback of the preferred or the optimized configuration) [176]. In optical IRS (OIRS), a mirror array (MA) is a reflecting surface comprising multiple adjacent small mirrors. Each small mirror can adjust its rotation depending on the user's location, and therefore, it can manipulate the direction of an incident optical wave without changing its

amplitude and polarity.

The focusing capabilities of the OIRS can be exploited to control the propagation of optical beams and, therefore, in alleviating the effect of the random UE orientation and link blockage in VLC systems [111]. Specifically, for a specific channel use, the direct LOS link between certain APs and VLC receivers may not exist due to the random orientation of the UE or blockage resulting from objects or the movement of the users. In such cases, the NLoS VLC links can be established alternatively through OIRS to overcome the LoS link blockage problem, using reflected link through OIRS.

It is evident from the above that the use of OIRS improves the indoor VLC system's performance due to increase in NLoS channel gain from the OIRS. Further, the impact of standalone OIRS in comparison to the wall reflection is not discussed in the literature. There may be possible cases where the NLoS link from the wall performs better than the NLoS link from the IRS when both LoS and IRS links get blocked. In those cases, unguided reflections from the wall may help. Similarly, the prior literature the orientation model of the user equipment for the OIRS-aided indoor VLC system is not analyzed. Further, the optimum VLC parameters such as LED semiangle, receiver FOV, and the OIRS mirror size need to be investigated.

7.1.2 Contribution

To the best of the authors' knowledge, this Chapter makes a novel contribution in investigating the impact of random UE orientation for OIRS-aided indoor VLC systems. The proposed framework also considers multiple human blockages. Some of the major contributions of the proposed work have been summarized below.

1. The Chapter proposed a UE orientation model for an OIRS-aided indoor VLC system with multiple human blockages considering random UE orientation. The receiver statistics, such as critical elevation angle, rotated normal vector with respect to OIRS, and the multiple LEDs have been calculated.
2. The PDF of the received SNR with random UE orientation for the proposed OIRS-aided indoor VLC system in the presence of multiple human blockages has been calculated. Further, the Chapter analyzed the contributions of the OIRS and wall reflections on the received power for the given room size in the presence of multiple human blockages.
3. The Chapter determined the optimum OIRS mirror size with respect to the varying LED semiangle and the receiver FOV for a given room size and the varying number of human blockages.
4. In addition, the optimal value of LED semiangle and the receiver FOV with varying OIRS mirror sizes are calculated in order to improve the received power using OIRS reflected channel gain.
5. Furthermore, the Chapter analyzed the performance of the proposed OIRS-aided indoor VLC system in terms of achievable average data rate and the BER with and without blockages. Also, the minimum number of OIRS elements required to fulfill the BER requirement of 10^{-3} with respect to permissible outages inside the room is determined.

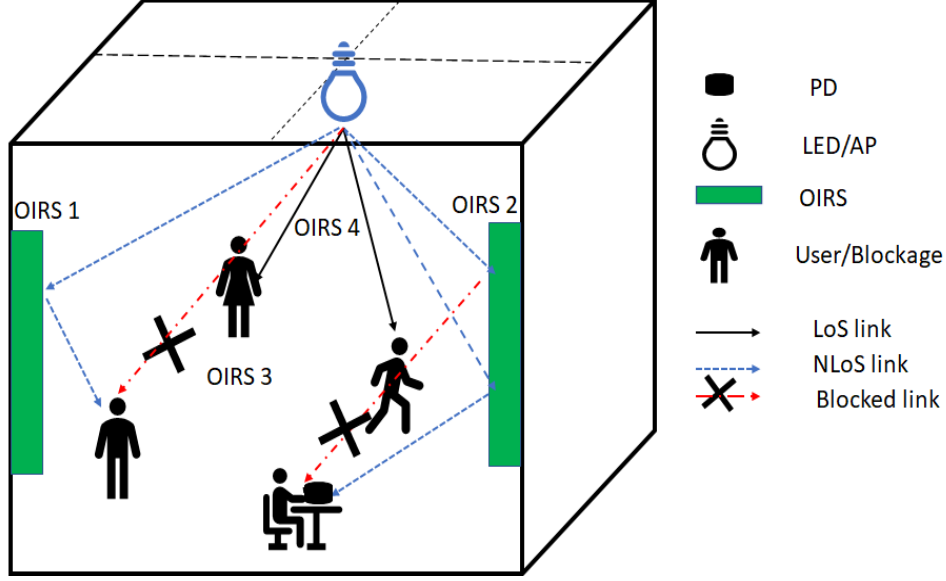


Figure 7.1: OIRS-aided Indoor VLC System with Multiple Human Blockages

7.2 OIRS-aided Indoor VLC System Model

The proposed system model considers 4 LEDs transmitters placed in the rectangular configuration in a room size of $5 \text{ m} \times 5 \text{ m} \times 3 \text{ m}$. The receiver plane is at the height of 0.85 m . In order to see the performance across the room, the whole room is divided into 25×25 grids. A generalized MHCP model (with critical distance δ) has been employed to characterize the distribution of human blockages in a space $[x, y]^2$. The human blockages are modeled as cylinders of height h_B and radius r_B . For the given system model, blockages of different widths (radius r_1 and r_2) have been considered to model the different sizes of people. In the text, the blockers are always assumed to be humans. Blockers could also be other than humans as well, e.g., furniture, large appliances, etc. The 4 OIRS arrays have been deployed at the center of each of the walls, namely OIRS₁, OIRS₂, OIRS₃, and OIRS₄. The total area of each OIRS array is $2.5 \text{ m} \times 2.5 \text{ m}$. The NLoS reflections are also considered from the remaining area of the wall. As depicted in Fig. 7.1, the LoS (from LED) and reflections from the OIRS and wall are denoted by the solid and dotted lines, respectively. Multiple humans present in the room may block the LoS path between the AP and the PD. In addition to the human blockages, self-blockage, which refers to the user's blockage of the optical channel due to random device orientation, is also considered. Unlike many VLC studies, the assumption that the UE is vertically upward is relaxed in this Chapter.

In the following sub-sections, we discuss in detail the OIRS-aided VLC channel, UE orientation.

7.2.1 OIRS-aided VLC channel

In the OIRS-aided indoor VLC system, the channel gain is the sum of LoS channel gain from LED, NLoS channel gain due to reflections from the wall, and reflection gain from OIRS elements.

7.2.1.1 NLoS Channel Gain from OIRS

In this chapter, we consider it as an NLoS one-point reflection model (Lambertian model approach) similar to the wall only, but the OIRS case reflection coefficient ρ_{OIRS} of the OIRS element is higher than the wall along with the guided reflection angle towards the direction of the desired user [177]. The NLoS channel gain of the reflected signal from the n_{th} OIRS (mirror array) element can be expressed as [108, 178]:

$$H_{NLoS}^{OIRS} = \begin{cases} \frac{\rho_{OIRS}(m+1)A_n}{2\pi^2(D_1^n)^2(D_2^n)^2} \cos^m(\phi) T_s(\psi) g(\psi) \cos(\alpha_{OIRS}^n) \cos(\beta_{OIRS}^n) \\ 0 \leq \beta_{OIRS}^n \leq \Psi_c \end{cases} \quad (7.1)$$

Here α_{OIRS} and β_{OIRS} are the incidence and reflectance angle NLoS link form LED make with the OIRS respectively. ρ_{OIRS} is the reflection coefficient of OIRS element. D_1^n, D_2^n are the distance traveled by the NLoS link to reach the user from the n_{th} OIRS element.

The reflection angle of OIRS element and the cosine of the angle of irradiance, which is defined by the yaw (γ) and roll angles (ω) of the mirror array, can be expressed as:

$$\begin{aligned} \cos(\beta_{OIRS}^n) &= \frac{(x_n - x_u)}{D_2^n} \sin(\gamma) \cos(\omega) + \frac{(y_n - y_u)}{D_2^n} \\ &\quad \times \cos(\gamma) \cos(\omega) + \frac{(z_n - z_u)}{D_2^n} \sin(\omega), \end{aligned}$$

where (x_n, y_n, z_n) represent the coordinates of the OIRS elements.

The total OIRS-aided indoor VLC channel gain using (2.9) and (7.1) can be expressed as:

$$H = H_{LoS}^{LED} + \sum_{k=1}^K H_{NLoS}^{wall}(k) + \sum_{n=1}^N H_{NLoS}^{OIRS}(n). \quad (7.2)$$

where K and N are the total number of reflection elements on wall and OIRS respectively.

7.2.2 UE Orientation

The UE orientation can significantly impact the performance of an indoor VLC system. In most of the research on indoor VLC, the UE is always vertically up. Such assumptions is accurate only for a limited number of devices, such as laptops with LiFi dongles. However, most users use devices such as smartphones, and in reality, the user is mobile and tends to hold the device according to comfort. Therefore, considering a random device orientation is a more realistic assumption.

Only a few studies have considered the impact of random orientation in their analysis, see for instance [4, 97, 137] and references therein. All these works incorporate UE orientation. Another important indicator affecting system performance is an optical channel communication link blocked by the user, known as "self-blocking." Or it may be interrupted as a result by other users or objects. The blockage modeling has been done in the prior literature for both millimeter-wave and LiFi systems [20, 138]. In this Chapter, taking into account the above we have considered the random UE orientation for an OIRS-aided indoor VLC systems, as shown in Fig. 7.2.

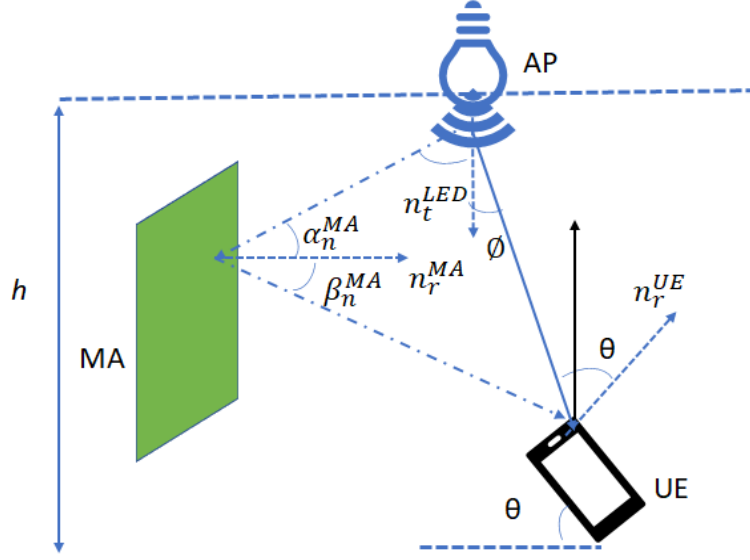


Figure 7.2: OIRS-aided Indoor Visible light Propagation System with UE Orientation [4]

7.3 Orientation Model of Users for OIRS-Aided Indoor VLC System

This section discusses the orientation model of the user equipment. Let the location of the access point (AP) (essentially LED) be defined as:

$$P_a = (x_a, y_a, z_a), \quad (7.3)$$

where x_a, y_a, z_a are the coordinates of the location of AP in x, y and z plane respectively, and the user location is defined as:

$$P_u = (x_u, y_u, z_u). \quad (7.4)$$

Similarly, let the location of OIRS mounted on the wall be defined as:

$$P_{OIRS} = (x_{OIRS}, y_{OIRS}, z_{OIRS}), \quad (7.5)$$

where P_a, P_u and P_{OIRS} are the position vectors of APs, users and the OIRS, respectively. As stated earlier in (2.6) ϕ is the LED irradiance angle, ψ is the VLC LoS link incidence angle, and α is the OIRS link incidence angle. Using geometry as shown Fig. 7.2 we can write the distance vector from LED to the user as:

$$d_{LoS} = P_a - P_u, \quad (7.6)$$

and,

$$\cos(\psi) = \frac{n_r \times d}{\|d_{LoS}\|}, \quad (7.7)$$

$$\cos(\phi) = \frac{n_t \times d}{\|d_{LoS}\|}, \quad (7.8)$$

where n_r and n_t are the normal vector with respect to the AP and the user locations.

Similarly, the distance vector with respect to the OIRS element following the NLoS path can be written as:

$$d_{NLoS}^{OIRS} = P_a - P_{OIRS} - P_u. \quad (7.9)$$

A practical way of defining the orientation is to employ three separate angles showing the rotation about each axes of the rotating local coordinate system or the rotation about the axes of the reference coordinate system. Current smartphones can report the elemental intrinsic rotation angles yaw, pitch and roll denoted as α , β , and γ , respectively [97]. Yaw, pitch, and roll can be described by matrices and are denoted as $R(\alpha)$, $R(\beta)$, and $R(\gamma)$, where each matrices can be written as a function of rotation angles as [4, 97]:

$$R(\alpha) = \begin{bmatrix} \cos(\alpha) & -\sin(\alpha) & 0 \\ \sin(\alpha) & \cos(\alpha) & 0 \\ 0 & 0 & 1 \end{bmatrix}, \quad (7.10)$$

$$R(\beta) = \begin{bmatrix} 1 & 0 & 0 \\ 0 & \cos(\beta) & -\sin(\beta) \\ 0 & \sin(\beta) & \cos(\beta) \end{bmatrix}, \quad (7.11)$$

$$R(\gamma) = \begin{bmatrix} \cos(\gamma) & 0 & \sin(\gamma) \\ 0 & 1 & 0 \\ -\sin(\gamma) & 0 & \cos(\gamma) \end{bmatrix}. \quad (7.12)$$

After the rotation of UE, the generalized unit normal vector is given by:

$$n_r = R(\alpha, \beta, \gamma) = R(\alpha)R(\beta)R(\gamma)n_t^T. \quad (7.13)$$

Here APs are located in z plane so $n_t^{LED} = [0 \ 0 \ 1]$. Using (7.13), the rotated normal vector can be calculated as:

$$n_r^T = \begin{bmatrix} \sin(\alpha)\cos(\gamma)\sin(\beta) - \cos(\alpha)\sin(\gamma) \\ \sin(\alpha)\sin(\gamma) - \cos(\alpha)\cos(\gamma)\sin(\beta) \\ \cos(\beta)\cos(\gamma) \end{bmatrix}. \quad (7.14)$$

The rotated normal vector n_r^T can be represented in the spherical coordinate system (corresponding to XYZ) with the polar angle θ_r . Thus, θ_r is the angle between n_r^T and the positive direction of the Z-axis. Note that $\cos(\theta_r) = n_r^T \frac{Z}{\|n_r^T\|}$ where $Z = [0, 0, 1]^T$ is the unit vector of the Z-axis. Then, from (7.14), the polar angle θ_r can be obtained as:

$$\theta_r = \cos^{-1}(\cos(\beta)\cos(\gamma)). \quad (7.15)$$

It is evident from (7.15) that the polar angle θ_r only depends on the pitch and roll rotation angles which are further associated with the movements of a human's wrists [4]. This is because the LED is deployed on the ceiling (z-plane), so the variation with respect to yaw does not affect the LoS link between LED and the user.

But it is not valid for the case of OIRS-aided indoor VLC systems, as OIRS are deployed on the walls instead of the ceilings. So here, we have analyzed the orientation model with respect to OIRS. The OIRS deployed on each wall acts as virtual APs to the user and correspondingly the polar angle get affected by the UE orientation differently. Similarly, like LED, the unit normal vector considering random UE orientation with respect to OIRS is given by:

$$n_r^{OIRS} = R(\alpha, \beta, \gamma) = R(\alpha)R(\beta)R(\gamma)n_{OIRS}^T, \quad (7.16)$$

where we can write the unit normal vectors of the deployed OIRS on the center of each of the 4 walls as: $n_{OIRS_1} = [0 \ 1 \ 1]$, $n_{OIRS_2} = [1 \ 0 \ 1]$, $n_{OIRS_3} = [0 \ -1 \ 1]$, and $n_{OIRS_4} = [-1 \ 0 \ 1]$, respectively. The generalized unit normal vector for each OIRS has been calculated considering the random orientation of the UE (user) using (7.14) multiplied with their respective unit normal vector using (7.19) is calculated as:

$$n_r^{OIRS_1} = \begin{bmatrix} \sin(\alpha)\cos(\gamma)\sin(\beta) + \cos(\alpha)\sin(\gamma) - \sin(\alpha)\cos(\beta) \\ \sin(\alpha)\sin(\gamma) - \cos(\alpha)\cos(\gamma)\sin(\beta) + \cos(\alpha)\cos(\beta) \\ \sin(\alpha) + \cos(\beta)\cos(\gamma) \end{bmatrix}, \quad (7.17)$$

$$n_r^{OIRS_2} = \begin{bmatrix} \cos(\alpha)\cos(\gamma) + \cos(\alpha)\sin(\gamma) + 2\sin(\alpha)\sin(\beta)\cos(\beta) \\ \sin(\alpha)\cos(\gamma) + \sin(\alpha)\sin(\gamma) - 2\cos(\alpha)\cos(\beta)\sin(\beta) \\ -\sin^2(\alpha) + \cos(\beta)\cos(\alpha) \end{bmatrix}, \quad (7.18)$$

$$n_r^{OIRS_3} = \begin{bmatrix} \cos(\alpha)\sin(\gamma) + \sin(\alpha)(\cos(\beta) + \sin(\beta)\cos(\gamma)) \\ \sin(\alpha)\sin(\gamma) - \cos(\alpha)(\cos(\beta) + \sin(\beta)\cos(\gamma)) \\ -\sin(\beta) + \cos(\beta)\cos(\gamma) \end{bmatrix}, \quad (7.19)$$

$$n_r^{OIRS_4} = \begin{bmatrix} \cos(\alpha)(\sin(\gamma) - \cos(\gamma)) + \sin(\alpha)\sin(\beta)(\sin(\gamma) + \cos(\gamma)) \\ \sin(\alpha)(\sin(\gamma) - \cos(\gamma)) - \sin(\beta)\cos(\alpha)(\sin(\gamma) + \cos(\gamma)) \\ \cos(\beta)\sin(\gamma) + \cos(\beta)\cos(\gamma) \end{bmatrix}. \quad (7.20)$$

Similarly like (7.15) the polar angle of the user with respect to each OIRS can be written as:

$$\theta_{OIRS_1} = \cos^{-1}(\sin(\alpha) + \cos(\beta)\cos(\gamma)), \quad (7.21)$$

$$\theta_{OIRS_2} = \cos^{-1}(-\sin^2(\alpha) + \cos(\beta)\cos(\alpha)), \quad (7.22)$$

$$\theta_{OIRS_3} = \cos^{-1}(\sin(\beta) + \cos(\beta)\cos(\gamma)), \quad (7.23)$$

$$\theta_{OIRS_4} = \cos^{-1}(\cos(\beta)\sin(\gamma) + \cos(\beta)\cos(\gamma)). \quad (7.24)$$

It is obvious from Eqs. (26-29) that in the presence of OIRS in indoor VLC system, unlike the only LED case (see (7.15)) the polar angle depends on all the three rotation angles pitch, roll and yaw.

7.4 PDF of the Received SNR with OIRS

This section discusses the received SNR statistics for the proposed OIRS-aided indoor VLC system in the presence of multiple human blockages. The optical signal $s_i(t)$ transmitted by the i_{th} LED is as follows:

$$s_i(t) = P_{t_i}[1 + M_I x_i(t)], \quad (7.25)$$

where P_{t_i} is the i_{th} LED's transmit power, M_I is the modulating index and $x_i(t)$ is the corresponding on-off-keying (OOK) modulated signal [49, 179]. The primary term in (7.25) (P_{t_i}) is responsible for maintaining the

required illumination inside the room whereas the secondary term ($P_{t_i} M_I x_i(t)$) accounts for the communication part. It is considered that the DC part of the detected electric signal is filtered out at the receiver after photodetection. y_j is the received signal at the j th PD (j th location inside the room) and is expressed as:

$$y_j = \mathcal{R}P_{r_j} + n_j, \quad (7.26)$$

where \mathcal{R} is the responsivity of the PD and n_j is the AWGN with zero mean and σ_j^2 variance. Received power at the j th photo-detector, P_{r_j} is given by:

$$P_{r_j} = \sum_{i=1}^N H_{i,j}^B P_{t_i} M_I x_i. \quad (7.27)$$

The respective received SNR in the presence of human blockages using (5.15) can be written as [180]:

$$\Gamma_r = \frac{(H^B)^2 P_{t_i}^2}{\sigma_r^2}, \quad (7.28)$$

The term in (7.28) of channel gain can be rewritten as [180]:

$$\Gamma_r = \Gamma_0 (r^2 + H^2)^{(-m+2)} \cos^2(\psi) \exp(-2\lambda d_B r_B^2) \text{rect}\left(\frac{\psi}{\Psi}\right), \quad (7.29)$$

where $\Gamma_0 = \rho \mathcal{R} \frac{(m+1) A_{rx} H^m P_T^2}{2\pi}$. It is observed from (7.29) that the received SNR is a function of the blockage probability and the random incidence angles ψ . Let the incidence angle follows the below distribution [180]:

$$X \triangleq \cos^2(\psi), \quad (7.30)$$

where ψ is the incidence angle so X ranges from $l_1 = \cos^2(\Psi)$ and $L_1 = 1$. The PDF of the X can be written as:

$$f_X(x) = \begin{cases} \frac{1}{2\Psi} x^{-\frac{1}{2}} (1-x)^{-\frac{1}{2}}, & l_1 \leq x \leq L_1. \end{cases} \quad (7.31)$$

Similarly, considering the received power as a random variable Y such that

$$Y \triangleq (r^2 + H^2)^{(-m+2)} \exp(-2\lambda d_B r_B^2), \quad (7.32)$$

where Y ranges from $l_2 = (R^2 + H^2)^{(-m+2)} \exp(-2\lambda d_B r_B^2)$ and $L_2 = H^{2(-m+2)}$. Here R is the radius of the room. The PDF of the Y can be written as [181]:

$$f_Y(y) = \begin{cases} \sum_{i=1}^3 p_i y^{-q_i} \exp(-2\lambda d_B r_B^2), & l_2 \leq y \leq L_2, \end{cases} \quad (7.33)$$

where,

$$p_1 = \frac{6}{73(m+2)R^2} \left(27 + 35 \frac{H^2}{R^2} + 8 \frac{H^4}{R^4} \right),$$

$$p_2 = -\frac{6}{73(m+2)R^2} \left(\frac{35}{R^2} + \frac{16H^2}{R^4} \right),$$

$$p_3 = \frac{48}{73(m+2)R^2},$$

$$q_1 = \frac{m+3}{m+2},$$

$$q_2 = \frac{m+4}{m+2},$$

$$\text{and } q_3 = \frac{m+5}{m+2}.$$

Consequently, based on the theorem of product's PDF in [4], the PDF of the received SNR will be:

$$f_{\Gamma_r}(\Gamma) = \begin{cases} \sum_{i=1}^3 c_i \exp(-2\lambda d_B r_B^2) \frac{\Gamma}{\Gamma_0}, & \Gamma_{min} \leq \Gamma \leq \Gamma_{max}, \end{cases} \quad (7.34)$$

where $c_i = \frac{P_i}{2\Gamma_0\Psi}$, $i = 1, 2, 3$.

$$\Gamma_{min} = \Gamma_0 \cos^2(\psi) (R^2 + H^2)^{-(m+2)}, \quad (7.35)$$

and

$$\Gamma_{max} = \frac{\Gamma_0 H^{2(-m+2)} (1 - \exp(-2\lambda d_B r_B^2))}{2\lambda r_B^2}. \quad (7.36)$$

7.5 Optimal LED Semiangle and the Receiver FOV for OIRS-aided Indoor VLC System

This section has optimized the LED semiangle and the receiver FOV for the OIRS-aided indoor VLC system subject to multiple human blockages and the random UE orientation.

7.5.1 Optimal LED Semiangle

In the proposed OIRS-aided indoor VLC systems, the received optical power consists of the LoS path and the reflected paths (both wall and the OIRS). To circumvent the problem of blockages and random UE equipment and to increase the received power across the room, we should maximize the power received from the reflections due to OIRS elements.

The received optical power from the LoS and NLoS paths from OIRS and wall can be calculated using (7.2) to (7.1) for a given transmission power (P_T), and can be expressed as:

$$P_r = \left[P_T H_{LoS} + \sum_{k=1}^K P_T H_{NLoS}^{wall} + \sum_{n=1}^N P_T H_{NLoS}^{OIRS} \right]. \quad (7.37)$$

Here, N is the number of OIRS elements, and K is the number of reflection points on the wall. In order to maximize the received power in the presence of human blockages and the UE orientation, we need to maximize the power received from OIRS. Consequently, we need to maximize the channel gain from the OIRS link H_{NLoS}^{OIRS} with respect to the LED semiangle to find out the optimal LED semiangle.

For LED semiangle optimization, we need to maximize the Lambertian order m , so taking the partial derivative of H_{NLoS}^{OIRS} with respect to m [52].

$$\frac{\delta H_{NLoS}^{OIRS}}{\delta m} = M \cos(\alpha_{OIRS}^n) \cos(\beta_{OIRS}^n) \frac{\delta [(m+1)\cos^m(\phi)]}{\delta m}, \quad (7.38)$$

where $M = \frac{\rho_{OIRS}^A}{2\pi(D_1^n)^2(D_2^n)^2} T_s(\psi)g(\psi)$. Substitute $C_1 = M \cos(\alpha_{OIRS}^n) \cos(\beta_{OIRS}^n)$ Eq. (7.38) can be further simplified as:

$$\frac{\delta H_{NLoS}^{OIRS}}{\delta m} = C_1 \cos^m(\phi) [1 + (m+1)\ln(\cos(\phi))], \quad (7.39)$$

To find the optimum m , we put $\frac{\delta H_{NLoS}^{OIRS}}{\delta m} = 0$, hence the optimal m is calculated as:

$$m_{opt} = \frac{-1}{\ln(\cos(\phi))} - C_1, \quad (7.40)$$

From (2.6) and (7.40), we can calculate the optimum LED semiangle:

$$\Phi_{opt} = \cos^{-1} \left(\exp \left(\frac{-\ln 2}{\frac{-1}{\ln(\cos(\phi))} - C_1} \right) \right), \quad 0 < \Phi_{opt} < 90. \quad (7.41)$$

Using (7.41), the optimized irradiance angle of the LED should be 56° , and its corresponding optimized Lambertian order m_{opt} is found out to be 5.57 for the given room dimension of 5 m \times 5 m \times 3 m with 4 LEDs deployed in rectangular configuration.

7.5.2 FOV Optimization

In this section, we have derived the receiver's optimal FOV with human blockages and random UE orientation for the proposed OIRS-aided indoor VLC system. In order to maximize the received power in the presence of human blockages and the UE orientation, we need to maximize the power received from OIRS. This can be achieved by maximizing the received power from the OIRS (MA) P_{rec}^{OIRS} subject to receiver FOV Ψ_c .

Using (7.1) the received power from NLoS link using OIRS as a function of receiver FOV using (7.29) can be written as:

$$P_{rec}^{OIRS} = \frac{\rho_{OIRS}(m+1)A}{2\pi(D_1^n)^2(D_2^n)^2} \cos^m(\phi) T_s(\psi) g(\psi) \cos(\alpha_{OIRS}^n) \cos(\beta_{OIRS}^n) \cos^2(\Psi_c) \text{rect}\left(\frac{\psi}{\Psi_c}\right), \quad (7.42)$$

Taking partial derivative of P_{rec}^{OIRS} with respect to Ψ_c .

$$\frac{\delta P_{rec}^{OIRS}}{\delta \Psi_c} = \frac{\delta \left[C_2 \frac{n^2}{\sin^2(\Psi_c)} \cos^2(\Psi_c) T_s(\psi) \right]}{\delta \Psi_c}, \quad (7.43)$$

where $C_2 = \frac{\rho_{OIRS}(m+1)A}{2\pi(D_1^n)^2(D_2^n)^2} \cos^m(\phi) \cos(\alpha_{OIRS}^n) \cos(\beta_{OIRS}^n)$. To find the optimum $\Psi_{c_{opt}}$, we put $\frac{\delta P_{rec}^{OIRS}}{\delta \Psi_c} = 0$, hence the optimal FOV is given as:

$$\Psi_{c_{opt}} = \frac{1}{2} \sin^{-1}(T_s(\psi) C_2 g(\psi)). \quad (7.44)$$

Using (7.44), the optimized FOV of the receiver is found out to be 58° for the given room dimension of 5 m \times 5 m \times 3 m with 4 LEDs deployed in rectangular configuration.

7.6 Results and Discussion

We have considered a room size of 5 m \times 5 m \times 3 m with one AP, and multiple users behaving as a blockage to each other. The blockages are realized using MHCP and are modeled as cylinders with 0.30 m diameter and 1.65 m height. The user holds the receiver at a distance of 0.85 m above ground and 0.36 m from the human body. The orientation of the UE is random. For the OIRS-Aided VLC system, the IRS contains $N \times N$ mirrors, and the dimensions of each mirror are 0.1 m \times 0.06 m [108]. The simulation parameters are summarized in Table 7.1.

Table 7.1: OIRS-aided VLC System Model and Simulation Parameters

Parameter	Value
LED transmitted power	200 mw
Refractive index n	1.5
Optical filter gain T_s	1
Wall reflection coefficient ρ_{wall}	0.7
Human body reflection ρ_2	0.51
LED semiangle	60°
Receiver plane above the floor (h_R)	0.85 m
Receiver elevation	90°
Receiver active area	1 cm^2
PD Responsivity (\mathcal{R})	$0.5 \frac{\text{A}}{\text{W}}$
Field of views (FOVs) of receiver	60°
Number of OIRS elements	10 - 150
OIRS reflection coefficient ρ_{OIRS}	0.9
Blockage radius (r_1 and r_2)	20 cm & 40 cm
Height of the blockage (h_B)	180 cm
Number of human blockages (N_B)	1-5

7.6.1 Received Power

In this subsection, as shown in Fig. 7.3 and Fig. 7.4, the received power for OIRS-aided indoor VLC system with and without blockages and UE having random orientations have been plotted. Fig. 7.3 shows the average received power with a varying number of OIRS elements for the LoS link from LED and NLoS link from the wall and OIRS without blockages. It can be observed that, the increase in received power at the UE more for the combined link (LoS (LED) + NLoS (wall) + (OIRS)) with respect to the other two links (LoS (LED) + NLoS (wall)) and (LoS (LED) + (OIRS)) respectively with an increase in the number of OIRS elements. This is because the combined link includes the contributions from both NLoS link from wall and OIRS. However, the NLoS links from the wall are independent of OIRS elements.

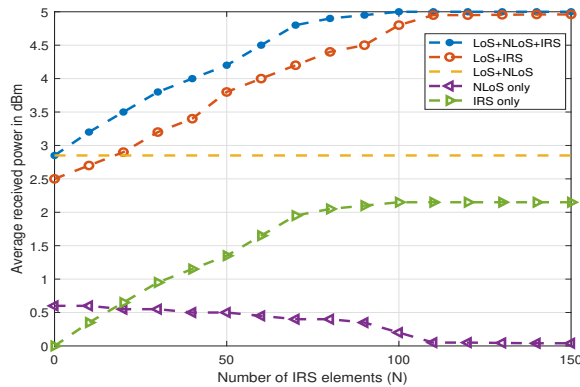


Figure 7.3: Effect on the received power without blockages

Fig. 7.3 also shows the standalone contribution of the NLoS link from the wall and the OIRS link, respectively. It can be observed that without blockage and with fewer OIRS elements such as $N = 20$, the standalone link from the wall (NLoS (wall)) performs better than the reflected OIRS link. It is due to the fact that with less

number of OIRS elements, the larger area of the wall contributes to NLoS links generation, and the NLoS power from the wall is more (see (2.6)). Whereas with an increase in N , the standalone OIRS links start performing better than an NLoS link from the wall. For a larger number of OIRS elements, the NLoS contribution from the wall starts decreasing as the area of the wall for the NLoS link also starts falling as more and more area of the wall is filled by OIRS elements.

7.6.2 Standalone Contribution of OIRS and NLoS (wall) Link in Received Power

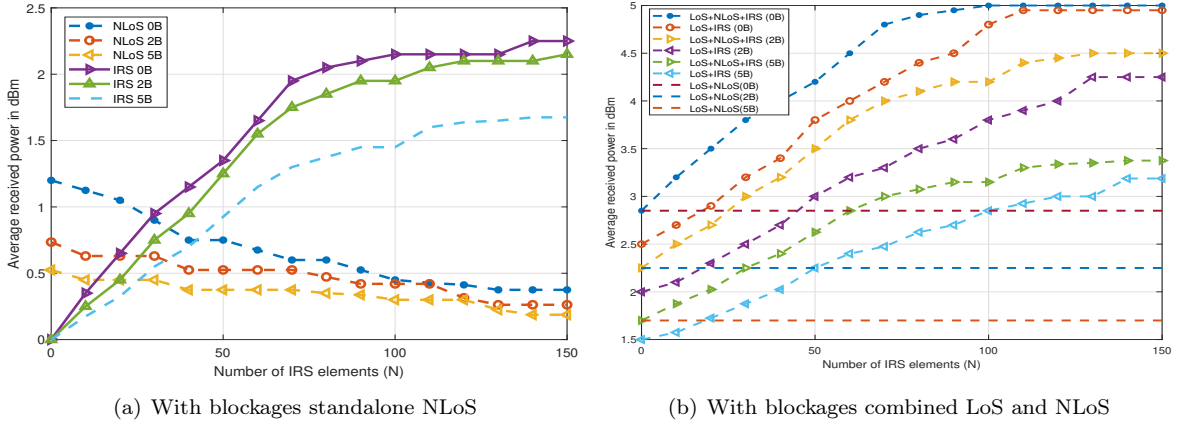
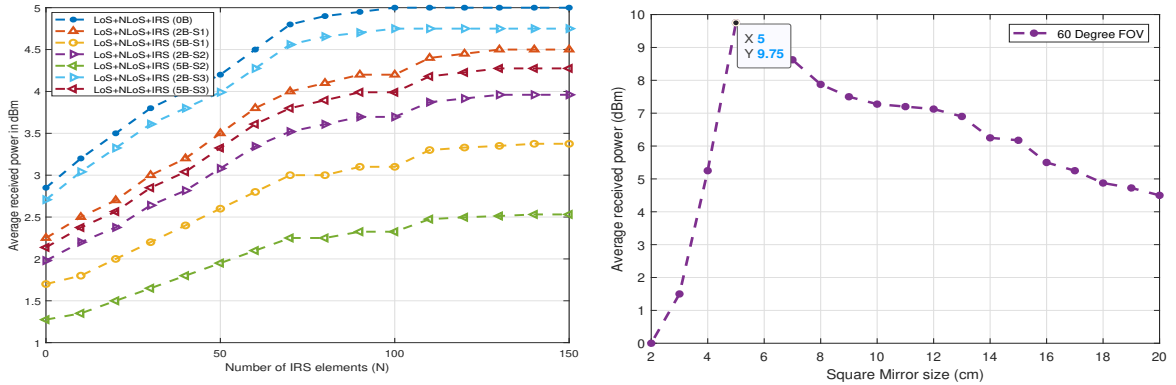


Figure 7.4: Effect on the received power with and without OIRS in the presence of blockages and random UE orientation

This subsection shows the effect of standalone links from the OIRS and NLoS (wall) on the received power with and without blockages. Fig. 7.4(a) shows the standalone contribution of the NLoS link from the wall and OIRS in the presence of blockages. It can be observed that even in the presence of human blockages, with fewer OIRS elements such as $N = 20$, the standalone link from the wall performs better than the standalone OIRS link. However, this difference starts increasing as we increase the number of blockages. As is evident from Fig. 7.37 that, the crossover points shifts towards a higher number of OIRS elements with increased blockages. Such as for the case of no human blockages $N = 20$ and for 2 and 5 blockages $N = 30$ and $N = 40$ respectively. Similarly, Fig. 7.4(b) shows the average received power of the LoS(LED), NLoS (wall), and OIRS with varying numbers of blockages. Further, it can be seen that even in the presence of blockages, the combined link (LoS (LED) + NLoS (wall) + (OIRS)) provides the maximum achieved average data rate with respect to all other links. Therefore, it can be inferred that the use of OIRS improves the indoor VLC system performance in the presence of human blockages with random UE orientation.

7.6.3 Effect of OIRS Mirror Size on the Received Power

This subsection shows the effect of OIRS mirror size on the received power across the room. Initially the size of each OIRS element is considered $S_1 = 0.1 \text{ m} \times 0.06 \text{ m}$ [108]. Now in order to see the effect of varying mirror size on the received power, we have varies the OIRS mirror size to $S_2 = 2 \times S_1$ and $S_3 = \frac{1}{2} \times S_1$ respectively as shown in Fig. 7.5(a). The idea of choosing the double and half size of the mirror is to see the effect of an



(a) Received power versus the number of OIRS elements with varying OIRS element size

(b) Optimum OIRS element size

Figure 7.5: Effect of mirror size on the received power

increase in mirror size and the effect of a decrease in mirror size on the received power. It is observed that for a smaller OIRS mirror size with S_2 , the received power increases as the number of OIRS elements increases for a fixed size of OIRS. It is because, with the increase in OIRS elements, the number of NLoS links generated from OIRS also increased (the OIRS gain $N \times N$ increased), resulting in increased received power. On the other hand, with the increase in OIRS elements size (with S_3), the received power decreases as the number of OIRS elements reduces for a fixed size of OIRS. So getting motivation from these results, we have tried to find out the optimal OIRS mirror size for a given room dimension, giving us the maximum received power in the presence of blockages and random UE orientation.

In order to find the optimum OIRS mirror size for a given room dimension of $5 \text{ m} \times 5 \text{ m} \times 3 \text{ m}$ with a LED semiangle $\Phi_{\frac{1}{2}} = 60^\circ$ and the receiver FOV of $\Psi_c = 60^\circ$, we have plotted the average received power with respect to the OIRS mirror size as shown in Fig. 7.5(b). It can be noticed that with a reduction in OIRS element size, the average received power increases up to the optimum or the possible smallest size. After that further reduction in OIRS size, the power decreases as the OIRS cannot generate sufficient NLoS power with such a small mirror size. Also, with the small OIRS mirror size, most of the OIRS links fall beyond the receiver FOV, which results in no power contribution from those OIRS links. Therefore it is found that for a given room dimension, the optimum square OIRS mirror size is $0.05 \text{ m} \times 0.05 \text{ m}$ with respect to the LED semiangle values of $\Phi_{\frac{1}{2}} = 60^\circ$ and the receiver FOV of $\Psi_c = 60^\circ$.

7.6.4 Effect of Varying LED Semiangle and the Receiver FOV on Received Power

This subsection discusses the effect of varying LED semiangle and the receiver FOV with varying OIRS mirror size on the received power. Fig. 7.6(b) shows the effect of OIRS element size in the received power with varying LED semiangle and the receiver FOV. Fig. 7.6(a) shows the change in average received power with varying OIRS element sizes for different FOV of the receiver and fixed LED semiangle value of $\Phi = 60^\circ$. It has been noticed that the corresponding average received power decreases for the wider FOV of the receiver with the increase in OIRS mirror size. For instance, with the FOV value of 70° the optimum OIRS mirror size is $0.05 \text{ m} \times 0.05 \text{ m}$

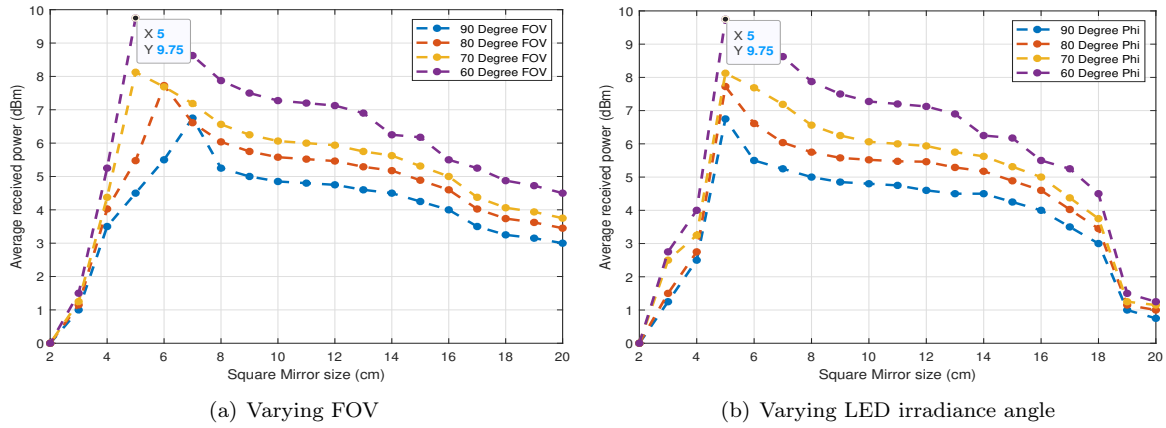


Figure 7.6: Effect of mirror size on the received power with varying LED irradiance angle and the receiver FOV

with the average received power of 7.6 dBm, and for the FOV values of 90° the optimum OIRS mirror size is $0.07 \text{ m} \times 0.07 \text{ m}$ with the average received power of 6.6 dBm. It can be concluded that the wider field of view results in a wider optimum mirror size, and the maximum average received power decreases. Further, subject to optimum OIRS mirror size, we have also found the optimum value of the receiver FOV, which will give us the maximum average received power. It is found out that for a given room dimension of $5 \text{ m} \times 5 \text{ m} \times 3 \text{ m}$, with 5 blockages is ($\Psi_c = 60^\circ$, $S = 0.05 \text{ m} \times 0.05 \text{ m}$) with the average received power of 11.8 dBm.

Similarly, Fig. 7.6(b) shows the change in average received power with varying OIRS mirror sizes for different LED semiangle. It can be seen that the average received power decreases for wider LED semiangle, but the optimum OIRS mirror size remains constant. Whereas for smaller LED semiangle, the average received power increases. Further, it is found out that for a given room dimension of $5 \text{ m} \times 5 \text{ m} \times 3 \text{ m}$, with 5 blockages the optimal LED semiangle value is ($\Phi_{\frac{1}{2}} = 60^\circ$, $S = 0.05 \text{ m} \times 0.05 \text{ m}$) with the average received power of 11.2 dBm. Furthermore, we can see that in both cases, the optimum OIRS element size value to achieve maximum received power is the same, which is $S = 0.05 \text{ m} \times 0.05 \text{ m}$.

7.6.5 Optimization of LED Semiangle and the Receiver FOV

As discussed above in Subsection C, the maximum average received power varies with the change in LED semiangle and the receiver FOV for the proposed OIRS-aided indoor VLC system. Motivating from the above in this subsection, we have analyzed the optimal pair of the LED semiangle and the receiver FOV subject to optimum OIRS mirror size. Fig. 7.7 shows the analytical and simulation results of average received power with varying OIRS mirror sizes. It can be seen that both simulation and theoretical results are in close agreement with each other, which validates the mathematical derivations and justifies the approximations made in (7.41) and (7.44). Fig. 7.7(a) shows the average received power with varying OIRS element size at the optimum FOV value obtained using (7.44). Here we can see that for an optimum FOV of $\Psi_c = 58^\circ$ the maximum received power is 11.22 dBm at an OIRS element width of 5 cm, which validates the optimized OIRS element size. Similarly, Fig. 7.7(b) shows the average received power with varying OIRS element size at the optimum FOV value obtained using (7.41). It can be observed that for the optimum LED semiangle value of $\Phi_{\frac{1}{2}} = 56^\circ$, the

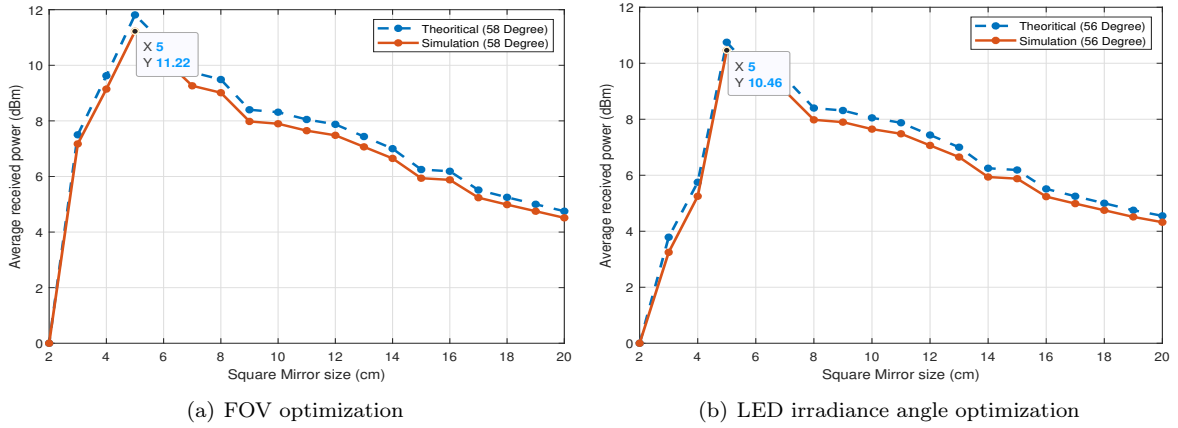


Figure 7.7: Effect of mirror size on the received power with optimized FOV and LED irradiance angle

maximum average received power is 10.46 dBm at the optimum OIRS mirror size is 5 cm. It can be concluded that that the optimum value of LED semiangle and the receiver FOV ($\Phi_{\frac{1}{2}} = 56^\circ$, $\Psi_c = 58^\circ$) with the optimum mirror size of $S = 0.05 \text{ m} \times 0.05 \text{ m}$ for the given room configuration.

7.6.6 Number of IRS Elements Required

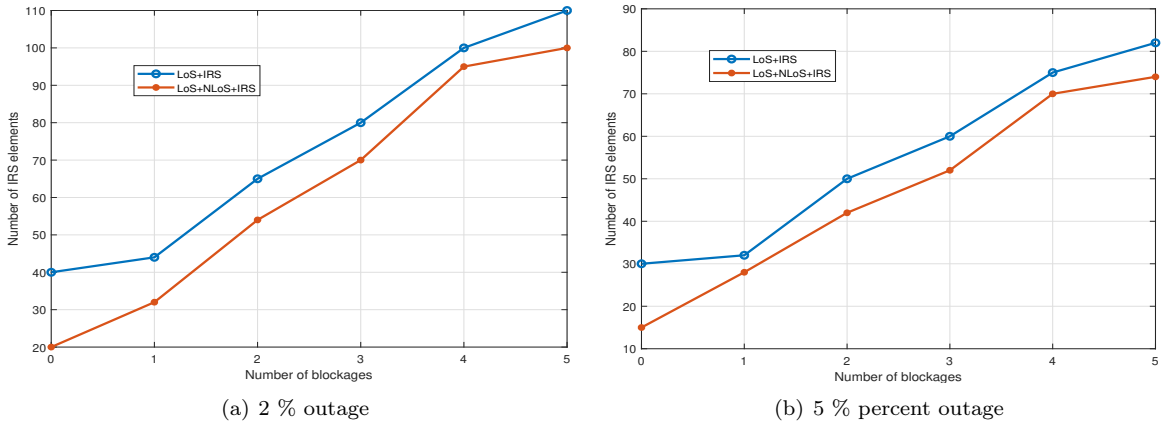


Figure 7.8: Minimum number of OIRS elements required with blockages

In this subsection, we have shown the minimum number of OIRS elements required to fulfill the BER requirement of 10^{-3} subject to 2 % and 5 % outage inside the room. Fig. 7.8(a) shows the number of OIRS elements required with 2 % outage inside the room. It can be seen that for a combined link (LoS (LED) + NLoS (wall) + (OIRS)), the required minimum number of OIRS elements is less with respect to other links. For instance, with 3 blockages, the required number of OIRS elements for a combined link is 70, while without an NLoS link from the wall, it is 80. It can be observed that the required number of IRS elements can be reduced by considering NLoS reflections from the wall. Similarly, Fig. 7.8(b) shows the minimum number of OIRS elements required with blockages for 5 % outage inside the room. Here also, the combined link (LoS (LED) + NLoS (wall) + (OIRS)) requires fewer OIRS elements than without the other links. With 3 blockages, the

required number of OIRS elements for a combined link is 50, while without an NLoS link from the wall, it is 60. With more permissible outages, the required minimum number of OIRS elements are also less. There is a trade-off between a required minimum number of OIRS elements and the allowed outage inside the room. One can opt for the required quality of services like BER, data rate, and the permissible outage inside the room.

7.6.7 BER Performance

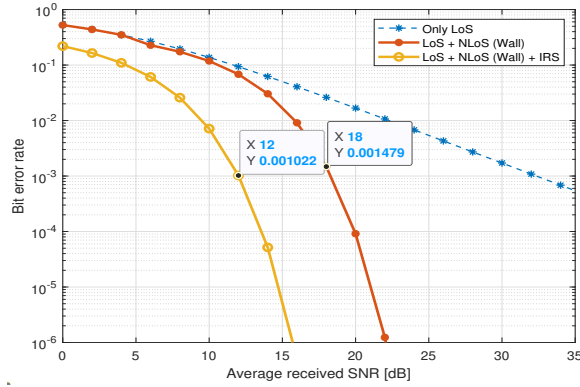


Figure 7.9: BER performance without blockages

In this subsection, we have analyzed the BER performance of an OIRS-aided indoor VLC system with and without blockages with random UE orientation with OOK as modulation scheme [177]. Fig. 7.9 shows the BER performance without blockage case. Here we can see that the combined link (LoS (LED) + NLoS (wall) + (OIRS)) performs better than the without OIRS and stand-alone LoS link. For instance, to achieve the BER of 10^{-3} , the required SNR with OIRS link is 14 dB, whereas, without an OIRS link, it is approximately 18 dB.

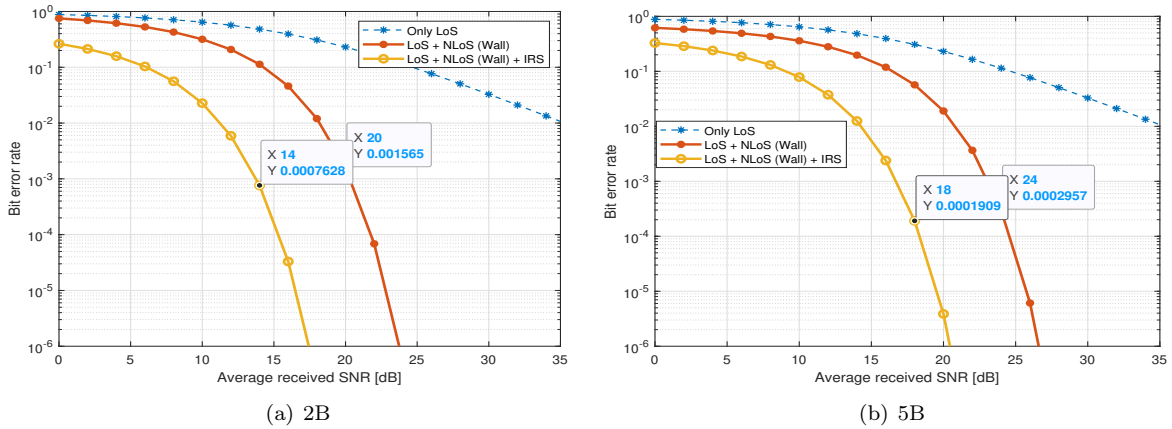


Figure 7.10: BER Performance with Blockages

Similarly, the BER performance of the OIRS-aided indoor VLC system with blockages has been shown in Fig. 7.10. Figs. 7.10(a) and 7.10(b) show the BER performance with 2 blockages and 5 blockages respectively. It can be observed that in both the cases, to achieve the BER performance of 10^{-3} , the required SNR for the OIRS link is less 14 dB and 18 dB, respectively, with respect to the other two links. The required SNR

is approximately 20 dB and 24 dB without an IRS link. It means the gain of 6 dB with the OIRS link is maintained even in the presence of human blockages.

7.6.8 Data Rate Performance

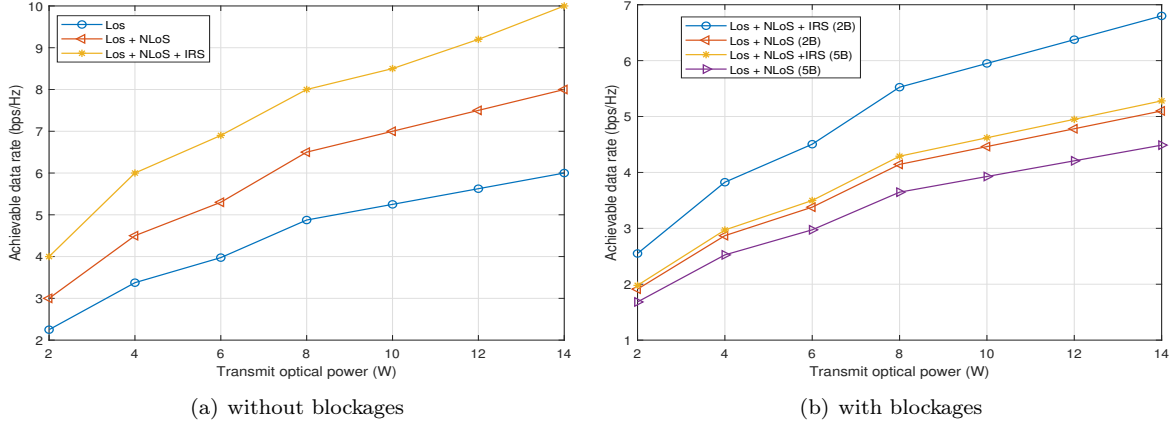


Figure 7.11: Average data rate performance

This subsection analyzes the average data rate performance with and without blockages for the proposed OIRS-aided indoor VLC system. Fig. 7.11 shows the average data rate with respect to the varying transmit optical power without and with human blockages. Fig. 7.11(a) shows the average data rate for without blockage case, and it can be observed that the combined link (LoS (LED) + NLoS (wall) + (OIRS)) without human blockages inside the room performs better with respect to the other two links. For instance, at the transmit optical power of 2 Watt, the achieved data rate with the OIRS link is 4 b/s/Hz, while with the other two links, LoS (LED) and LoS (LED) + NLoS (wall), the achieved data rates are 2.2 and 3 b/s/Hz, respectively.

Similarly, Fig. 7.11(b) shows the average data rate with human blockages. Here we can see that even in the presence of blockages, the combined link (LoS (LED) + NLoS (wall) + (OIRS)) outperforms the other two without OIRS links. At the transmit optical power of 4 watts with 2 and 5 blockages, the (LoS (LED) + NLoS (wall) + (OIRS)) link achieves the average data rate of 4 b/s/Hz and 3 b/s/Hz, respectively. Whereas without the OIRS link (LoS (LED) + NLoS (wall)) for 2 and 5 blockages, the acquired data rates are 2.8 b/s/Hz and 2.4 /b/s/Hz, respectively.

7.7 Summary

In this Chapter, we have investigated an OIRS-aided indoor VLC system with random UE orientation in the presence of multiple human blockages. We have investigated the impact of standalone OIRS and NLoS links from the wall on the received power and determined the minimum number of OIRS elements required for a given BER performance. Further, the orientation model with random UE orientation for an OIRS-aided indoor VLC system has been proposed. We also derived the probability distribution function of the received SNR for the proposed system model. The analysis allows the determination of the optimum LED semiangle and the

receiver FOV for the given system configuration. The results are in close agreement with the simulation results, and it is found that the optimum LED semiangle and the receiver FOV pair give the maximum received power. The numerical results were obtained for a given room geometry to optimize the receiver FOV, LED semiangle, and OIRS mirror size. Further, we can optimize these parameters by optimizing the channel gain with respect to the OIRS link for any given room size and the number of blockages. For a given room size with more than 2 blockages, the received power starts deteriorating without OIRS and can be overcome with the inclusion of an OIRS link. Hence, it is evident that the deployment of OIRS in an indoor VLC system helps to combat the blocking and shadowing effect due to other users as a blockage and self blockage due to random UE orientation.

Further, the effect of varying OIRS mirror sizes on the received power has been analyzed, and it is shown that for the given configuration, the optimum OIRS mirror size is $0.005 \times 0.005 \text{ m}^2$. Also, the minimum number of required OIRS elements has been calculated to maintain the BER performance of 10^{-3} with the given outage. The proposed work also analyzes the BER performance of the system, and it is observed that with OIRS, we can achieve a gain of approximately 6 dB even in the presence of human blockages. Furthermore, the average data rate results suggest that the link with OIRS (LoS (LED) + NLoS (wall) + (OIRS)) outperforms the other without the OIRS link. Moreover, we can also exploit the impact of multi-LED and multi-IRS with both static and dynamic blockages in the future.

Chapter 8

On estimating the Location and the 3-D shape of an Object in an Indoor Environment Using Visible Light

This Chapter builds upon the existing work on VLP and proposes a novel system model for indoor positioning, which can be implemented by utilizing the existing lighting infrastructure. Specifically, the proposed VLP system model can be used to construct a 3-D rendering of a room with multiple objects. The objects in the room are modelled as cylinders¹ with varying heights and radius, leading to well-defined metrics for evaluating the performance of the algorithm [183]. Furthermore, this Chapter also presents a technique for allocating the power available to the LEDs in response to a particular arrangement of objects, further increasing the accuracy of positioning [184].

The rest of this Chapter is organized in the following way. We discuss the motivation behind this work and outline our contributions in Section 8.1. Section 8.2 and 8.3 discuss our system model and spatial model, respectively. Section 8.4 presents our algorithm for visible light positioning. Section 8.5 is related to constructing and training the NN to calculate the height and radius of the objects. Section 8.6 discusses a power allocation scheme for optimum localization accuracy, and the Chapter is concluded in Section 8.7.

8.1 Motivation and Contribution

8.1.1 Motivation

It is noted that in the models presented in existing literature (ref. Section 1.6.6), a single PD is generally used to signify a user and the location of that PD is estimated by maximizing the likelihood of the received power profile matrix obtained from different transmitting LED's [185]. Consequently, most of the existing system models for VLP locate the objects as a point in 3-D space. In contrast, by utilizing the VLP system model proposed in this Chapter, the 3-D shape of the user can be identified. In addition, the proposed model facilitates passive modelling. Specifically, the target, which is being localized, need not possess a PD. For instance, passive objects, such as furniture in the room, can also be modeled by the proposed method.

¹In [136] [182], different geometric models representing the human body have been considered. It has been shown that the human body as a cylinder is the best fit with respect to other models.

In addition, the proposed model can also perform accurate positioning in the presence of multiple objects. Conventional VLP methods generally are inaccurate when multiple objects are present in a room since the objects may block the LOS path between the transmitter and other objects. As this model considers the objects as 3-D shapes, the effects of shadowing in the presence of multiple objects can be clearly observed and corrected. Moreover, in this Chapter, as stated before indoor positioning utilizes RSS based method. In order to obtain the RSS, we need to calculate the received power at the PD. Here, in this Chapter the received power is calculated based on the LED illumination power across the room in the presence of human blockages. Hence for the received power profile calculation, LED need not be a communication source and may just function as a source of illumination Hence, the proposed VLP can facilitate improvement in positioning without significant changes to existing infrastructure.

8.1.2 Contribution

The existing literature on VLP primarily focused on locating the object as a point in 3-D space. Although, this induces less operational overhead, it tends to overlook the information about the shape and size of the object. The estimation of the shape and size of the object is especially important when multiple objects are present in the room. In this work, which builds upon the work presented in [183], we overcome the above drawback by proposing a novel VLP model which estimates an object's 3-D parameters along with its location in an indoor environment. The major contributions of this Chapter are summarised as follows:

1. In this Chapter, we propose a novel system model for VLP, which can be used to estimate the location of objects in a room. Unlike the conventional VLP models, the proposed model can be used to predict the location even in the presence of multiple objects.
2. Further, we also construct and train a neural network (NN) to estimate the height as well as the radius of the objects. The NN, along with the VLP algorithm, can be together employed to construct a 3-D model of the objects in the room.
3. In addition, we propose a method to optimize the power allocation to each LED in a room by exploiting the current location of objects while maintaining the total power constraint on the system. This will lead to efficient power allocation among LED's, based on the instantaneous position of objects in the room for optimum communication performance.

Notations: The vector and the matrix are denoted as \mathbf{x} and \mathbf{X} respectively. The vectorization of matrix \mathbf{X} is denoted as $\mathbf{X}(:)$. The element corresponding to i^{th} row and j^{th} column of a matrix \mathbf{X} is represented as X_{ij} . The blockage probability and the blockage density are denoted as P_B and λ_B , respectively. The actual coordinates of an object is denoted by (x,y) while the predicted coordinated of the object is given by (\hat{x}, \hat{y}) . The variable L and K are used throughout the Chapter to denote the number of LED's and the number of objects in the indoor environment. P denotes the power profile of the room and $H(\tilde{g}, \tilde{l})$ denotes the channel gain between LED (l), and photo diode (g).

8.2 VLC Positioning System Model

In this Chapter, we have considered a standard office room of dimensions, $5 \text{ m} \times 5 \text{ m} \times 3 \text{ m}$,² with 4 LEDs placed on the ceiling. The LEDs are located at the midpoints of the diagonals from the center to the vertices as shown in Fig. 8.1. The room floor is considered to be the receiver plane and is divided into a number of grids with PDs placed at each grid point.

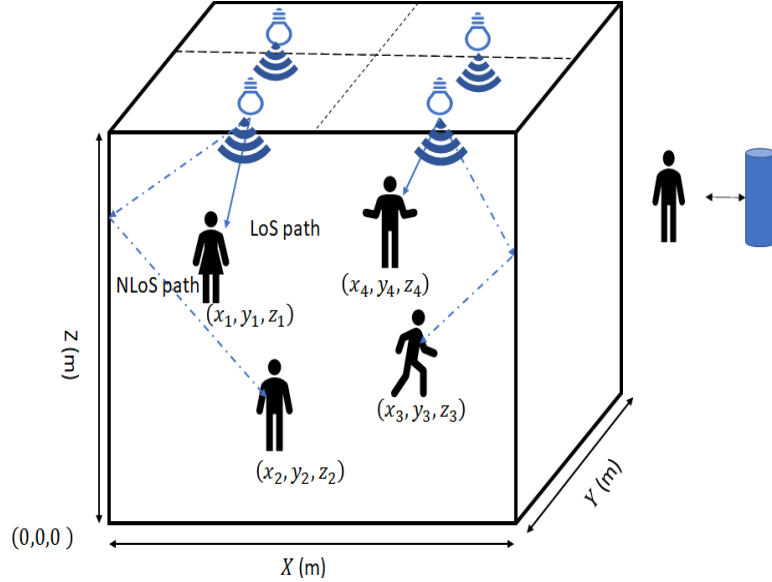


Figure 8.1: Indoor VLP System Model

The received power at each PD depends on the distance between the LED and the PD, the receiving angle, the field of view of the PD etc. The proposed system model simulates the presence of multiple objects and takes into account a single reflection from the room walls as well as the LoS path. The LoS link is exploited to estimate the position of objects in the indoor environment and their broad geometrical properties like height and radius. The received power profile in the absence of an object can be seen in Fig. 8.2, where each lattice point represents the location of a PD.

We have consider a multipath VLC channel model that includes reflections up to first-order (with one-point reflection because of higher data rate threshold) from the wall [149]. We use the integrating-sphere model using (2.14) (ref. Section 2.2.5) to simulate the radiation of the LED light source, which is well established in literature. The given VLC model is used to reproduce both the LoS, and the NLoS light intensity transmitted by each LED [35, 132]. The VLC channel gain is a sum of both the LoS path and the reflections by the walls (NLoS path). The parameters used in this Chapter for the visible light channel are given in Table 8.1.

²The dimensions considered are consistent with that of a standard office room as shown in [129]

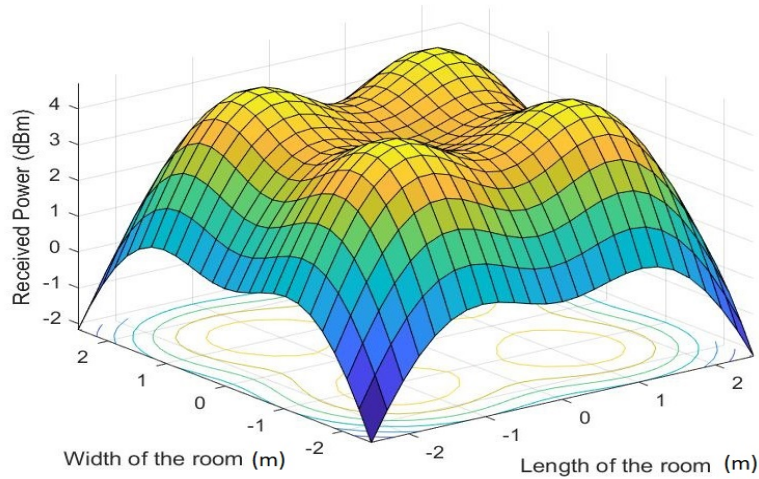


Figure 8.2: Received power profile of the room in the absence of any objects.

Table 8.1: VLP System Model Parameters

Parameter	Value
Total transmitted power P_T	2 W
Refractive index n	1.5
Optical filter gain T_s	1
Wall reflection ρ	0.8
LED semiangle Φ	60°
Receiver active area A	1 cm^2
FOV of the receiver ψ_c	60°

8.3 Spatial Model

In this Chapter, the objects are modelled as cylinders placed randomly within the room [20]. Since we have approximated the objects as cylinders, their geometric shape can be determined by their radius and height only. The height of the objects is sampled uniformly from the range 0 to 2 m, and the radius is sampled uniformly from the range 0 to 0.5 m.³ Unless mentioned otherwise, we will assume the default height and radius of the object to be 1 m and 0.05 m respectively, which are selected keeping in mind the height of the room and the area of the floor.

8.3.1 Regression Model

In this Chapter, we have used the standard Multivariate Linear Regression model, where the hypothesis function is given by (8.1), and the cost function is given by (8.2). Here X represents values obtained from the received power profile, y represents the blockage's height and location, and θ represents the predictive parameters.

$$h_\theta(x) = \theta^T \times X = \theta_0 x_0 + \theta_1 x_1 + \theta_2 x_2 + \dots + \theta_n x_n \quad (8.1)$$

³These ranges were used keeping in mind the average range for the height and width of humans.

$$J(\theta_0, \theta_1, \dots, \theta_n) = \frac{1}{2m} \sum_{i=1}^m [h_{\theta}(x^i) - y^i]^2 \quad (8.2)$$

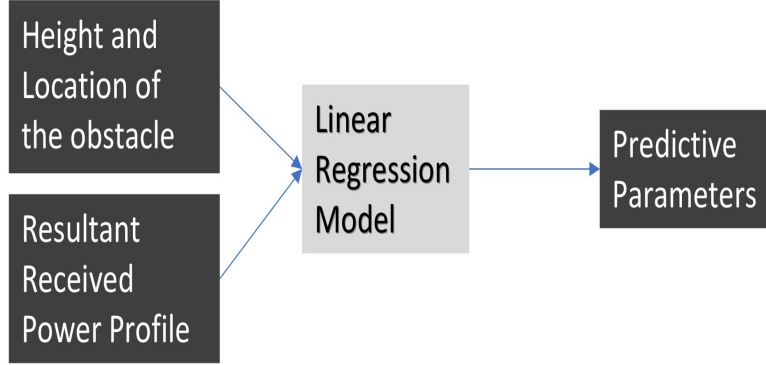


Figure 8.3: Parameter training using Linear Regression

After X and y are obtained from the simulation, gradient descent is used to find the value of θ for which the Cost Function, (8.2), is minimum. This value of θ is taken as the predictive parameters as shown in Fig 8.3.

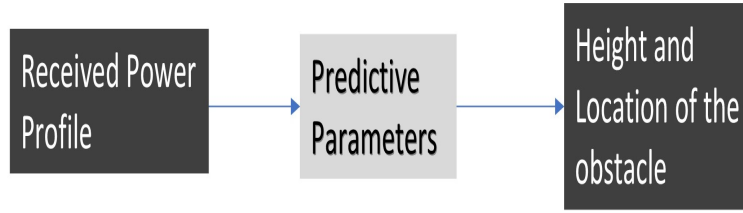


Figure 8.4: Predictive Algorithm obtained from the results of Linear Regression

The value of θ calculated above is used to make a Predictive algorithm that calculates the height and location of the obstacle based on the received power profile, as shown in Fig. 8.4.

8.3.2 Multiple Object Environment

In this Chapter, we have used MHCP to generate multiple objects in an indoor environment. Hard-Core processes are point processes where points are not allowed to be closer than a certain minimum distance. Thus, they are more regular (less clustered) than other point processes. Moreover they realistically emulate real-life scenarios where objects have a finite width and cannot occupy the same space. In this Chapter, we have MHCP Type-I, where we start with a basic uniform Poisson point process (PPP) ϕ_b with intensity λ_b , and then remove all points which have another point within the minimum distance r . The intensity of the type-I process is given by $\lambda_b e^{-\lambda_b \pi r^2}$. [159] [160].

8.4 Proposed Visible Light Positioning (VLP) Model

In this section, the proposed algorithm for locating an object in an indoor environment is presented. The proposed algorithm takes into account the received power profile of the room in the presence of the objects and estimates the positions of objects in an indoor environment.

8.4.1 VLP Model

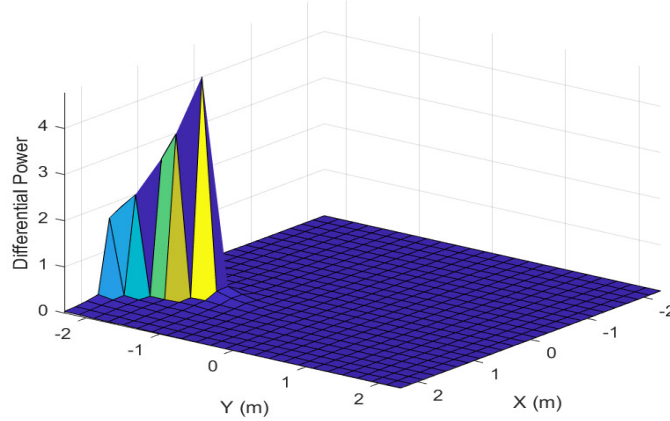


Figure 8.5: Differential power profile for an object at $(0.6507, -1.2414)$ with height of 1.4806 which is used to predict the height of the obstacle

This subsection discusses the proposed VLP model to estimate the location of the object in a multiple-object environment. We have considered an indoor environment having K desired users and L LED light sources. Let P_0 represent the received power profile of the room without any desired users, and P represents the received power profile in the presence of the desired users. Define a function, $\nabla\mathcal{F} = P_0 - P$, which will be referred as the differential power profile in the rest of the Chapter. Then the coordinates of the desired users predicted by the system are given such that:

$$(x, y) : \nabla\mathcal{F} = 0 \text{ and } \nabla^2\mathcal{F} < 0. \quad (8.3)$$

Since the function $\nabla\mathcal{F}$ represents the change in the power profile on the addition of desired users in the room, we can assume that the power profile will incur maximum change at points near the location at which the desired users have been added. This assumption has been validated in the results shown in the Chapter and can be heuristically observed since the desired users block the light reaching the photodiodes in its vicinity and hence have a greater impact on the power profile near their location. For example, Fig. 8.5 shows the plot of $\nabla\mathcal{F}$, and as you can see, the maxima $(0.65, -1.25)$ lies near the actual location of the obstacle.

However, the power profile cannot be calculated over the entire room, so \mathcal{F} is only evaluated at discrete points known as grid points which contain PDs. The spacing between adjacent grid points is known as grid size (this can be seen in Fig. 8.1, where each point on the graph is a grid point).

Let $\tilde{g}, \tilde{l}, \tilde{k}$, represent the coordinates of the grid points, LED's and objects respectively. P_0 and P can be evaluated as:

$$(P_0)_{\tilde{g}} = \sum_{l=1}^L \left[P_l H_0(\tilde{g}, \tilde{l}) + \int_{walls} P_l H_{DIFF}(\tilde{g}, \tilde{l}) \right], \quad (8.4)$$

$$P_{\tilde{g}} = \sum_{l=1}^L \left[P_l H_0(\tilde{g}, \tilde{l}) \left(\prod_{k=1}^K \phi(\tilde{g}, \tilde{l}, \tilde{k}) \right) + \int_{walls} P_l H_{DIFF}(\tilde{g}, \tilde{l}) \left(\prod_{k=1}^K \phi(\tilde{g}, \tilde{l}, \tilde{k}) \right) \right]. \quad (8.5)$$

where, $\phi(\tilde{g}, \tilde{l}, \tilde{k})$ is an indicator variable (0 or 1), which indicates whether the object is In the proposed VLC model, an obstacle is said to block the line of sight to the desired user if :

1. The center of the obstacle is at a distance less than r from the line joining the center of the desired user to the LED, where r is the radius of the obstacle (Please refer to Fig. R1).
2. The height of obstacle is sufficient such that its shadow reaches the desired user, which can also be checked geometrically. As shown in Fig. 2.5, the condition is equivalent to:

$$\frac{h_B - h_R}{d_B} \geq \frac{h_T - h_R}{d_T}$$

where h_B is the height of the obstacle, h_R is the height of the receiver, h_T is the height of LED, and d_T and d_B are the horizontal distances of user and blockages from the transmitting LED respectively.

8.4.2 Performance of VLP Algorithm

In this subsection, the performance of the proposed VLP algorithm has been presented. In order to test the performance, an object is uniformly simulated inside the room with the default shape (height and width) parameters. The location of this object is then estimated using the VLP algorithm, and this process is repeated over 1000 iterations. The average RMSE thus obtained in the measurement is **0.054 m**, where the RMSE is calculated as:

$$\text{RMSE} = \sqrt{\sum_{n=1}^N \frac{(\hat{x} - x)^2 + (\hat{y} - y)^2}{N}}, \quad (8.6)$$

where \hat{x}, \hat{y} represents the predicted location of the desired user and x, y represent the true location of the desired user, and N is the total number of iterations which in the present case is equal to 1000.

8.5 Results and Discussion

In this section, we present the simulation and analytical results for the VLC system with human blockages inside a standard room size of 5 m × 5 m × 3 m. The two transmitter configuration of 1 and 4 LEDs in a rectangular geometry are considered. First, A single block of LED's is considered to be placed at the center of the ceiling – at coordinates (0,0). In the second configuration, four blocks of LED's are placed symmetrically at the centers

of the four lines joining the center to the vertices – at coordinates $(-1.25, -1.25)$, $(-1.25, 1.25)$, $(1.25, -1.25)$ and $(1.25, 1.25)$. The room floor is divided into a 101×101 grid, and the distance between any two adjacent lattice points is 0.05 m. A photodiode receiver is considered to be placed at each lattice point. The locations and the orientations of the VLC transmitters and the receiver are provided in Table 8.1

8.5.1 Received Power Profile with infinitely thin object

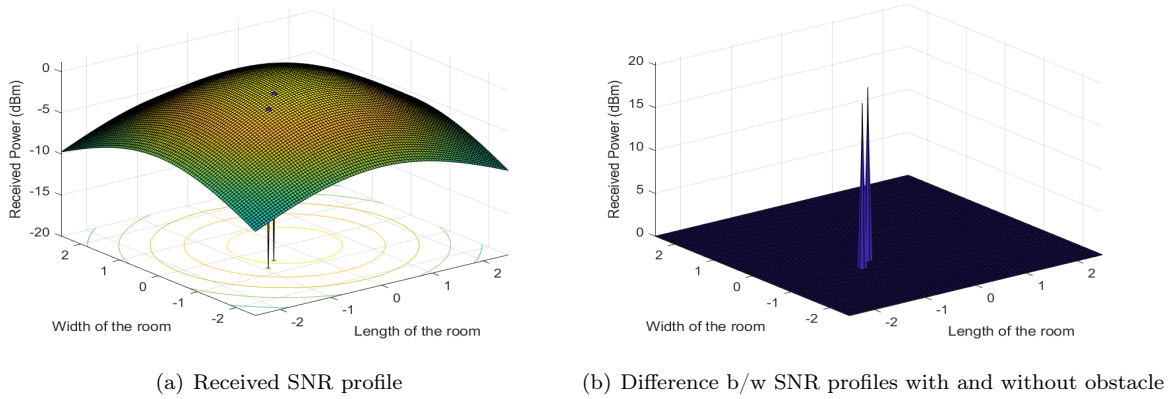


Figure 8.6: Infinitely thin obstacle is at $(-0.6, -0.5)$ with height = 1m for single LED setup

The received power profile for an infinitely thin obstacle kept in a setup with a single LED and four LEDs can be observed in Figs 8.6(a) and 8.6(b) respectively. The accuracy of height is lower because of two reasons. Firstly due to the object being infinitely thin, as only the points which fall exactly behind the obstacle are affected by it, and as a result, the output has very little correlation with the actual height of the obstacle. Secondly, for the points on the room’s fringes, the shadow goes beyond the boundary of the room where there are no receivers, and as a result, objects of height greater than a certain value will give the same result.

8.5.2 Received Power Profile with an object of finite radius

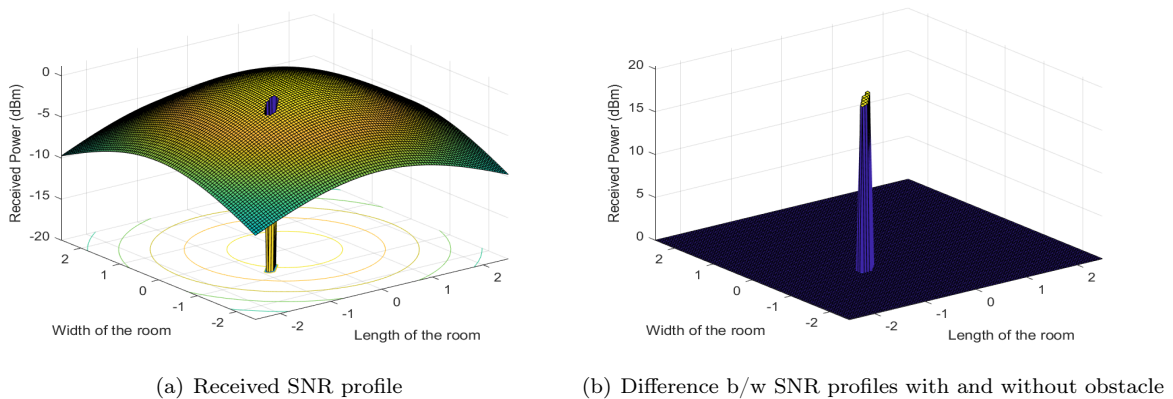


Figure 8.7: Obstacle having finite width(=0.05m) is at $(-0.6, -0.5)$ with height = 1m for single LED setup

The received power profile for an obstacle with a radius of 0.05m kept in a setup with a single LED and with four LEDs can be seen in Figs 8.7(a) and 8.7(b) respectively.

Table 8.2: Accuracy Matrix

Obstacle	Setup A (One LED)		Setup B (Four LED)	
	LA (cm)	HA (cm)	LA (cm)	HA (cm)
Infinitely Thin Object	0.0017	11.5987 (99.85%)	0.0029	14.8995 (99.80%)
Object with finite Radius	0.0026	9.9982 (99.86%)	0.0029	9.6689 (99.87%)

Table 8.2 shows the location accuracy (LA) and height accuracy (HA) for one LED and 4 LED setup. It can be seen that the accuracy of the height increases in the case of an object having a finite radius (=0.05m). This is because the object now casts a definite shadow. This eliminates the first reason listed above as there is now a direct correlation between the length of the shadow and the height of the obstacle.

8.5.3 Variation of VLP System Performance with System Parameters

The proposed algorithm can also be applied to a multiple object environment. However, the interference with the line of sight and shadowing effects in a multiple object scenario would result in lower location accuracy. In this subsection, the impact of grid size and the number of objects on the performance of the proposed VLP algorithm is discussed.

8.5.3.1 Grid Size

In the practical system, the power profile of the room can only be evaluated at discrete points across the room. The grid size (the distance between two adjacent points at which the function is evaluated) is extremely important for two reasons. Firstly, it decides the number of PDs required for the system to function. Larger the grid size, lesser the number of PDs required. However for a smaller grid size the function is evaluated at more number of points, and it approximates the continuous function better. Hence, the error in VLP is expected to increase with grid size.

The effect of varying the grid size on the RMSE, average location error over multiple iterations can be seen in Fig. 8.8. For each value of grid size, 20 iterations of multiple desired user environments are generated using MHCP, and for each iteration, the location error (ϵ) is calculated as:

$$\epsilon = \sum_{k=1}^K \frac{\sqrt{(\hat{x} - x)^2 + (\hat{y} - y)^2}}{K}. \quad (8.7)$$

where, \hat{x}, \hat{y} represent the predicted location of the desired user and x, y represent the true location of desired user, and K represents the number of desired users generated using MHCP in that particular iteration.

Fig. 8.8 shows the variation in location error with varying grid sizes. It can be seen that the location error increases with the increase in grid size which is consistent with our hypothesis considered in the Chapter. It is due to the fact that the smaller the grid size, the better the approximation to the continuous differential power profile and hence our algorithm works better too.

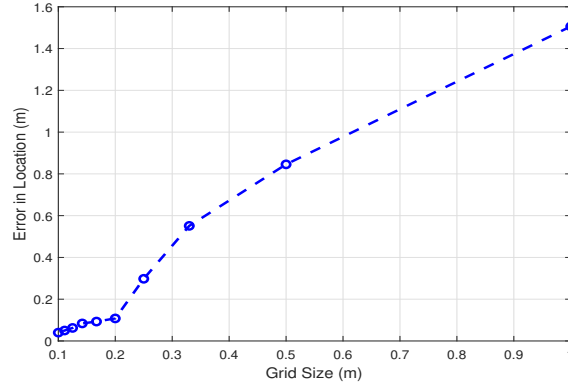


Figure 8.8: Variation of location error with grid size

Unless otherwise mentioned in this Chapter, henceforth we will assume a grid size of 0.2 m as further decrease in grid size increase the operational overload without any proportionate increase in accuracy of the model as seen in Fig. 8.8.

8.5.3.2 Number of Objects

Since the MHCP results in a random number of objects being generated in the room, in order to get a fixed number of objects, we will be using a random point process which assumes a uniform probability of an object being anywhere in the room. Moreover, the objects are distributed independently with the same default shape parameters (height, radius).

Fig. 8.9 depicts the variation of location error with a change in the number of objects. The location error is calculated using (8.7).

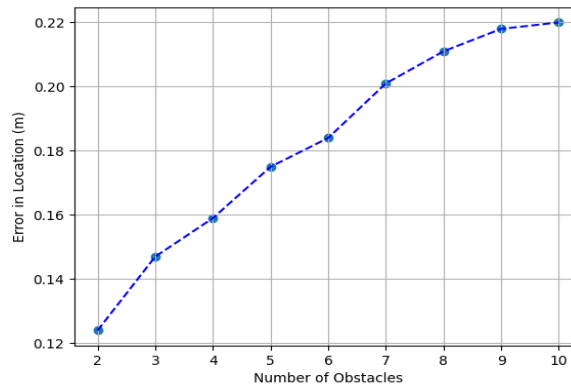


Figure 8.9: Variation of location error with the number of obstacles

As we can see, the value of location error increases with the number of objects. More the number of objects in a room, greater will be the probability of an object being blocked by another's shadow. This overlap would result in some objects not being detected which increases the error in positioning as shown in Fig. 8.9.

8.6 Shape Estimation using Visible Light

This section presents a novel insight into using visible light to construct a 3-D rendering of an indoor environment. This algorithm can be used to develop accurate surveillance systems which makes use of only the current lighting infrastructure of the rooms. Moreover, using LED's is much cheaper than the present methods of height estimation that utilizes microwave or WiFi. Estimating the shape of objects in an indoor environment could help us in constructing a topological map of the room which could be useful for indoor navigation and monitoring.

One of the most significant advantages of the system model presented in this Chapter over the previous system models is its ability to estimate an object/ user's shape in the room's boundaries. Since we are modelling the objects as cylinders, estimating their shape consists of estimating the height and radius of the objects. No extra hardware is required for shape estimation, and instead, it can be done using the same architecture, LEDs as transmitters and PDs as the receiver. However, it can not be done using a fixed algorithm since height and radius estimation are more subjective than location estimation. In this Chapter, we have constructed a NN as shown in Fig. 8.10, that takes the room's received power profile as input and then outputs the predicted height/radius of the object [186–190].

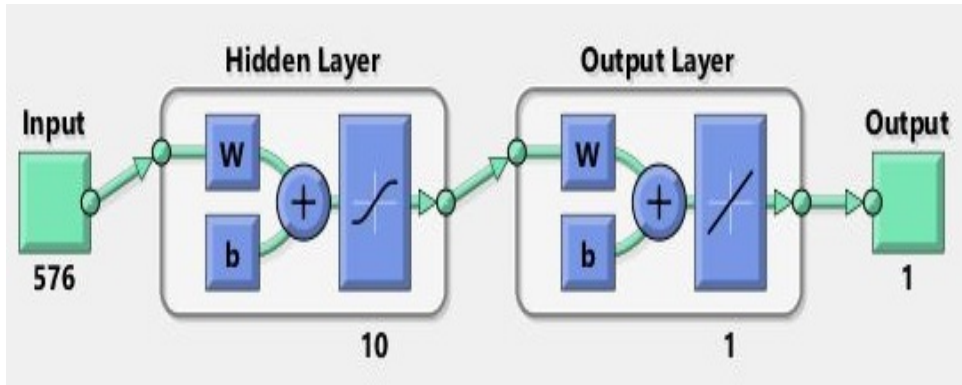


Figure 8.10: Structure of the shallow neural network[5, 6] used for shape estimation

8.6.1 Height Estimation Model

The height of an object in a room is calculated by constructing an artificial NN. It takes the received power profile of the room as an input and predicts the height of the object. The received power profile of the room consists of power received at each grid point in the room. The height of the objects is assumed to be between 0 and 2 m, which is a reasonable range for indoor measurements. The radius of the object is fixed at the default value of 0.05 m.

8.6.1.1 Training Data Generation

In order to make predictions using a NN, the first step is to train the parameters of the NN in order to minimize the error in predicting the height of objects. We simulate an object at a random location in the room with

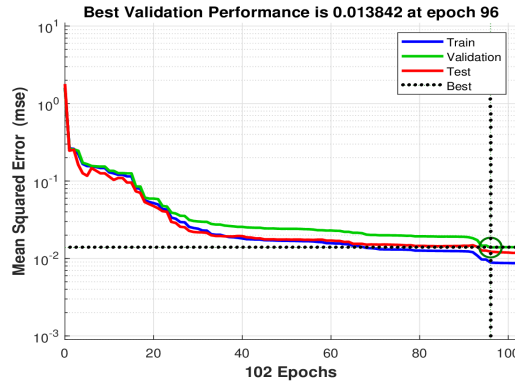


Figure 8.11: Training the neural network

uniform probability across the entire room and sample the object’s height from a uniform distribution between 0 to 2 m. Further, we calculate the differential power profile of the room in the presence of the object. This is repeated over 1000 iterations to get a training dataset. It is seen that the NN works better when the target variable is between $[0,1]$, so the height of the sample is divided by 2 and used to train the network. The height predicted by the NN is then doubled in order to get the actual predicted height.

Where, X and Y represent the length and the width of the room respectively.

8.6.1.2 Training NN

For training, the constructed data set is divided in the proportion of 80:10:10 into the training, validation, and test set. A shallow NN having 10 hidden nodes is constructed and then trained using the Levenburg-Marquadt (LM) algorithm. The LM algorithm iteratively finds the minima of a function that can be expressed as the sum of squares of non-linear functions. It is very useful in solving problems involving non-linear least squares and is a combination of the Gauss-Newton method and Steepest Gradient Descent [191].

8.6.1.3 Results

The NN was trained for over 100 epochs (Fig. 8.11) after which the error obtained in each of the training, validation and testing sets is represented below in Table 8.3. The best performance of the NN is seen at epoch 102, that is minimum RMSE was seen in the test set.

Table 8.3: Distributed Error in Prediction

Data type	Samples	RMSE	R-value
Training	800	4.38854e-2	9.421e-1
Validation	100	6.08677e-2	9.1654e-1
Testing	100	5.60280e-2	9.0426e-1

RMSE is defined as the average squared difference between the outputs of the NN and targets, which are the true values. Lower values of RMSE means a more accurate prediction by the NN. Regression (R) values is

indicative of the correlation between targets and outputs [192]. An R value close to 1 means that the output and the target are strongly co related that is there exists a simple bijective mapping between the two. On the other hand, an R value of 0 indicates a random relationship. The performance of the NN is better represented by Figs. 8.12 and 8.13.

Fig. 8.12 depicts the distribution of errors over the training, validation and test set. It is an histogram with the height of the bar equal to the number of instances with error equal to the range on the x axis. As you can see that the error distribution is sharply peaked around zero error and the number of instances become close to zero as the amount of error increases. This shows that the neural network model is working correctly and predicting values close to the intended target. Fig. 8.13 shows us the regression value for the training, validation and test set as well as over the entire dataset. As you can see that we get an almost direct correlation between the outputs predicted by the neural network and the target variables. This shows that the model is working correctly in predicting the target variable.

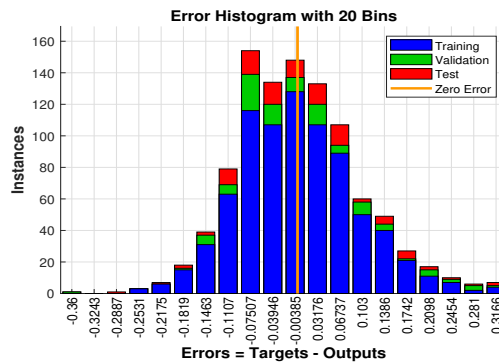


Figure 8.12: Distribution of error (in meters) in prediction by the NN

8.6.2 Radius Estimation Model

The radius of an object in a room is calculated by constructing an artificial NN. That takes the power profile of the room as an input and predicts the radius of the object. The power profile of the room consists of power received at each grid point in a room that contains a PD. The radius of the objects is taken between 0 and 0.5 m, which is a reasonable range for indoor measurements. The height of the object is fixed at the default value of 1 m.

8.6.2.1 Creating Training Data

In order to make predictions using a NN, the first step is to train the parameters of the NN in order to minimize the error in predicting the height of objects. An object is repeatedly simulated for 1000 iterations at a random location in the room with uniform probability over the entire room. The object radius is sampled from a uniform distribution between 0 to 0.5 m. The power profile of the room is then taken as input to the NN to calculate the object radius. It is seen that the NN works better when the target variable is between [0,1], so the height

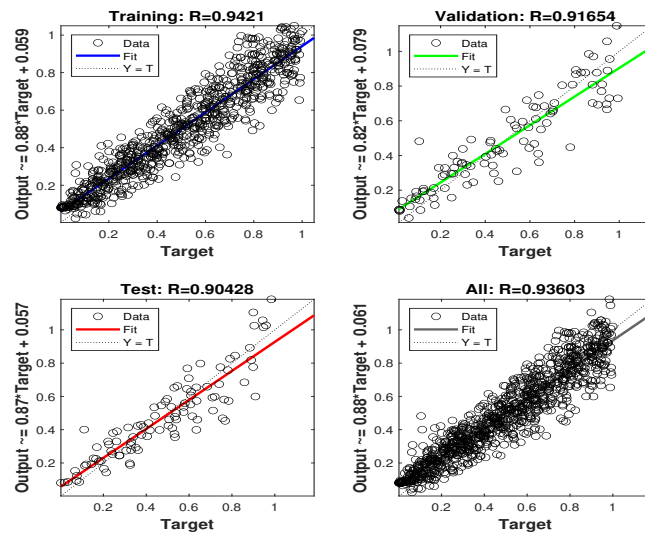


Figure 8.13: R values for the data in each of the training, validation and test set as well as the entire dataset

of the sample is doubled and used to train the network. The radius calculated by the NN is then halved to get the actual predicted radius.

8.6.2.2 Training NN

For training, the constructed data set is divided in the proportion of 80:10:10 into the training, validation, and test set. A shallow NN with 10 hidden nodes is then constructed and trained using the Bayesian regularization algorithm.(Fig. 8.14)

Bayesian regularization is a commonly used process to train Neural networks and is especially used to convert non linear regression into a simple ridge regression. It offers many advantages such as: the models are more robust, the validation process is faster and models become difficult to overtrain and overfit [193].

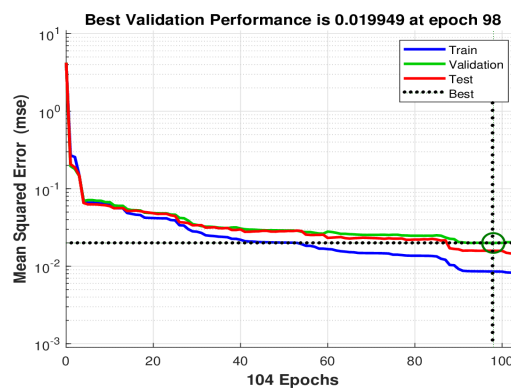


Figure 8.14: Training the neural network

Table 8.4: Error in Prediction

Data type	Samples	RMSE	R-value
Training	800	1.26084e-2	9.027e-1
Validation	100	1.14627e-2	8.5783e-2
Testing	100	1.47891e-2	8.757e-1

8.6.2.3 Results

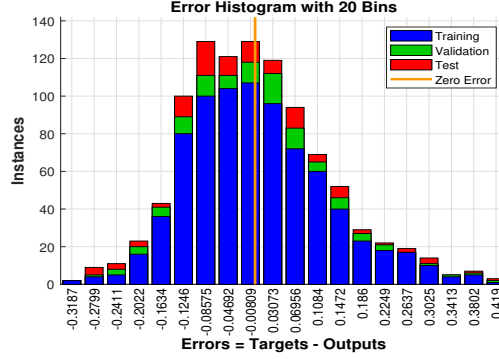


Figure 8.15: Distribution of error (in meters) in prediction by the NN

The NN was trained for over 100 epochs after which the error obtained in each of the training, validation and testing sets is represented in Table 8.4. The best performance of the NN was seen at Epoch 104, that is the minimum RMSE was seen in the test set. Lower values of RMSE means a more accurate prediction by the NN. Regression (R) values is indicative of the correlation between targets and outputs [192]. An R value close to 1 means that the output and the target are strongly co related that is there exists a simple objective mapping between the two. On the other hand, an R value of 0 indicates a random relationship. The performance of the NN is better represented in Figs. 8.15 and 8.16.

Similar observations can be seen in Fig. 8.15 and 8.16 to height estimation. The error (in meters) for radius estimation is also sharply peaked around zero error and becomes no of instances become rarer as the amount of error increases. The regression values shown in Fig. 8.16 are also very close to 1 showing a direct correlation between the outputs of the neural network and the target variable. Based on the above two points, we can safely say that our radius estimation model is working correctly and is predicting values close to the target variable. One observation that we can draw from the Fig. 8.15 is that the network tends to underestimate the radius more often which may be due to the shadowing effects of other objects.

8.7 Optimising VLP by changing Power Allocation to LED's

In this section, we have analyzed the performance of the proposed VLP system by optimizing the power allocation to LEDs. We have used the attocell approach by locating the obstacle within the LiFi attocell, and the VLC parameter can be tuned to improve the overall communication performance. A LiFi attocell network uses the

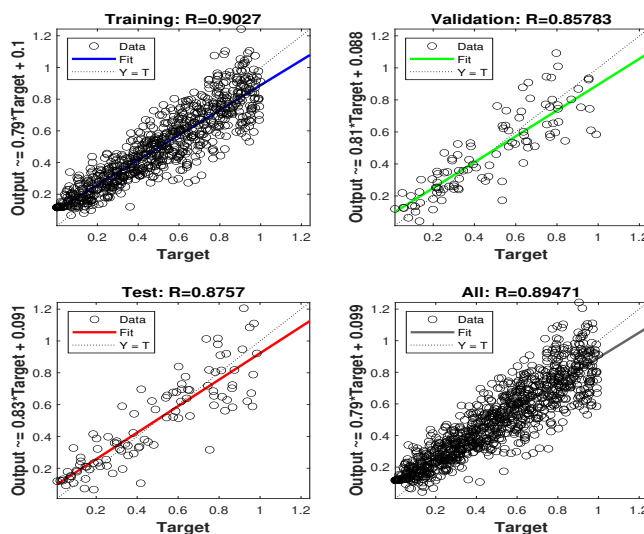


Figure 8.16: R values for the data in each of the training, validation and test set as well as the entire data set

lighting system to provide wireless access to multiple light fixtures that each LED functions as a very small radio base station. The result is a network of very small cells called 'optical attocells.' They are analogous to femtocells in RF communications, which cover a small area and are, therefore, classed as 'small cells'. Based on the approach mentioned above, the LED with a large number of users associated is given more power than the LEDs with fewer users as per the location information. We believe that this position information can be exploited to improve communication performance in the presence of different obstacles inside the room. Moreover, the LED power allocation can be optimized to maximize the data rate or minimize the BER by exploiting this location information. Here, we have considered VLP in an indoor $5\text{ m} \times 5\text{ m} \times 3\text{ m}$ room with 4 LEDs placed symmetrically on the roof. Moreover, we have considered that each LED has been allocated constant power, 2W. However, this system appears sub-optimal as the power of each individual LED remains constant irrespective of the placement of objects in the room. Instead, suppose we could allocate power to each LED based on the position of the objects while maintaining the total power constraint. In that case, we could perhaps decrease the error in positioning further.

Let us consider the power allocated to the LED in the form of a four-dimensional vector, P , where each entry represents the power allocated to that LED.

$$P = \begin{bmatrix} P_1 \\ P_2 \\ P_3 \\ P_4 \end{bmatrix}, \quad (8.8)$$

where, P_i is the power allocated to the i^{th} LED, $i = \{1, 2, 3, 4\}$. Subject to the total power constraint:

$$\sum_i P_i = P_t, \quad (8.9)$$

where P_t is the total power. When no information about the location of the user (also the obstacle for the other users) is available, power is allocated equally to all the LED's. Once the location information is available, initially, total power is allocated to one particular LED at a time while leaving the other 3 LEDs with no power, and the location error is calculated as shown in Fig 8.17. Then the process is repeated for all the LEDs until the location information of each user is obtained. Afterwards, power is allocated in such a way that the LED serving the more users will get more power giving the minimum location error with respect to other LEDs having fewer users, respectively.

The power allocation algorithm is given by:

Algorithm 1: Power Allocation Algorithm

Result: Optimum power allocation vector, Φ

Initial power allocation vector, \mathbf{P} $P_i = \frac{P_t}{4} \quad \forall i = \{1, 2, 3, 4\}$

For $j = \{1, 2, 3, 4\}$

- Set Power allocation vector, \mathbf{P}^j , such that $P_i^j = P_t \delta_{ij}$
- Simulate the received power profile of the room and then calculate Location_Error_j using Section 8.4

Set,

$$\Phi_i = \frac{1}{\text{Location_Error}_i} \cdot \frac{1}{\sum_{j=1}^4 \frac{1}{\text{Location_Error}_j}}$$

where, δ_{ij} is the dirac delta function.

$$\delta_{ij} = \begin{cases} 0 & i \neq j \\ 1 & i = j \end{cases} \quad (8.10)$$

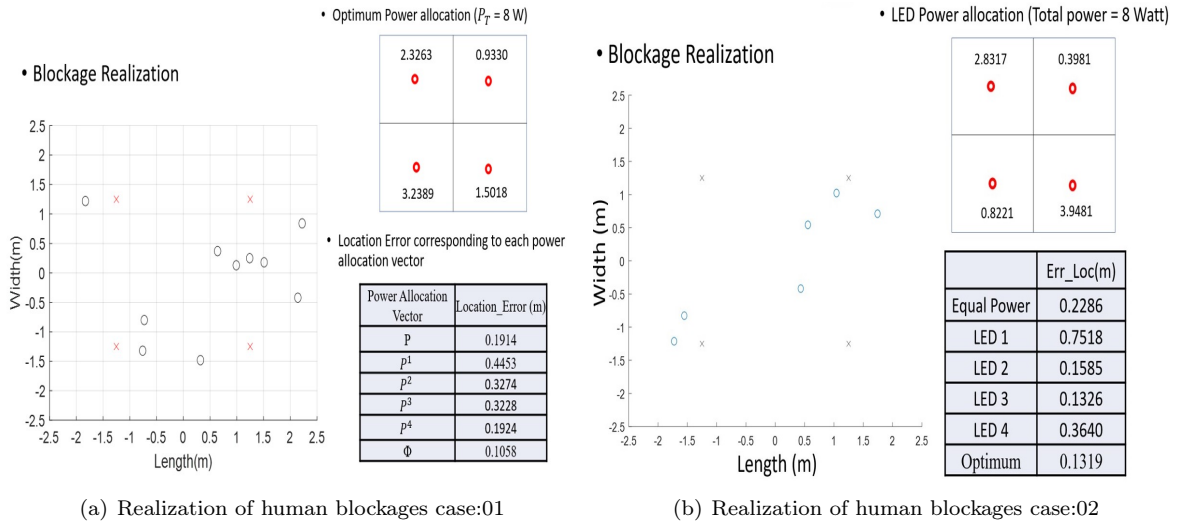


Figure 8.17: Position of objects, power allocated to the LED's and the location error

This power allocation algorithm was applied over many iterations, where each iteration has a different number and arrangement of obstacles, to improve positioning by optimizing the power allocation to LED's. Over 100 iterations, the power allocation optimization was applied, and the algorithm showed improvements

in location accuracy in 20 iterations, with the accuracy remaining unchanged in the rest. We can conclude that there is a saturation point for the accuracy after which application of the algorithm provides no further improvement. The saturation point varies widely for different arrangements of the objects in the room and it is difficult to quantify it. The optimization algorithm resulted in an average net improvement of 22.068 % (9.2 cm) in location accuracy.

8.8 Summary

This Chapter presented a predictive system for estimating the height and location of an obstacle. This is realized by an RSS-based method using modulated LEDs. The system is simulated firstly using an infinitely thin blockage and then with a blockage having a constant finite radius ($= 0.05\text{m}$). Based on the simulation results, a predictive algorithm is built using Multivariate Linear Regression. The accuracy of the predictive algorithm developed is reasonably high as it predicts the location of the obstacle within 0.03 cm and the height within 15 cm.

Further, this Chapter also introduces a novel VLP model which can be used to predict the location of an object even in multiple object environments. It is seen that the minimum squared error for positioning is 6.7 cm. Moreover, the effect of grid size (the distance between two adjacent PD's) and the number of objects on the location error is also observed. In addition, this Chapter also presents a neural network-based algorithm for measuring the height and radius of objects in an indoor environment such that a 3-D rendering of the room can be constructed. The RMSE for the height and radius of the objects is 4.67 and 1.27 cm, respectively. Moreover, the regression values obtained for both height and radius show a clear dependence between the output of the neural network and the target value.

Furthermore, in this Chapter, we have discussed a method for optimizing the power allocation to the LEDs in the room, such that optimum location accuracy can be obtained, keeping the total power of LEDs constant. The algorithm proposed shows an improvement in 20% of the cases, with an average improvement of 9.2 cm. An important point to be noted is that on the application of the algorithm, the error in positioning either decreases or remains the same, it never increases. In addition to the results presented above, this Chapter opens the doors to many exciting research prospects like using the above methods to estimate the radius and height of the obstacles jointly. The proposed algorithm could find applications in remote surveillance and monitoring of indoor environments using just LEDs and PDs.

Chapter 9

Optimal LED Power Allocation Framework for a Location-Assisted Indoor VLC system

This Chapter utilizes the location information in order to improve the indoor VLC system performance in the presence of obstacles considering random user equipment orientation [194].

The rest of this Chapter is organized in the following way. We discuss the motivation behind this work and outline our contributions in Section 9.1. Section 9.2 presents the system model, consisting of the VLC system model and the characterization of the dynamic human blockages using generalized MHCP. In Section 9.3, we have discussed the proposed optimal LED power allocation employing user location. We explain the shadowing effect and develop a model to find the blockage probability for any dynamic user in the indoor VLC system. The analytical expression for received power and BER is discussed in Section 9.4. Section 9.5 discusses the analytical as well as the simulation plots. Lastly, Section 9.6 concludes the Chapter.

9.1 Motivation and Contribution

9.1.1 Motivation

In an indoor VLC system, the received optical power depends on various factors, such as the location of the emitting LEDs, the desired user's location, and the different types of obstacles present in the room. In an indoor room with multiple-user cases, other users act as a blockage for the desired user. Sometimes other users may pause between movements for a specific time, called a pause time. These pauses taken by moving users can obstruct LoS and NLoS signals from the transmitter to the receiver, and hence can abruptly drop the received power. The height and the radius of the blockages play a significant role in this sudden reduction of the received power [20]. Consequently, the motivation behind this work is to exploit the location information obtained in the presence of obstacles to facilitate better communication services meeting BER better than 10^{-3} and illumination in the range of 300-1500 lux [46, 195].

9.1.2 Contribution

As evident from previous literature discussed in (ref. Section 1.6.6), the existing work on VLP and primarily focused on minimizing the error in localization by exploiting different positioning methods. Similarly, the work in VLC power optimization (ref. Section 1.6.7) have not considered location information in the analysis. Further, in earlier work, utilization of this location information for indoor communication has not been explored. We believe that this position information can be exploited to improve communication performance in the presence of different obstacles inside the room. Moreover, the LED power allocation can be optimized to maximize the data rate or minimize the BER by exploiting this location information. The proposed work has the following major contributions.

1. We propose a location-assisted indoor VLC system, wherein the location information is exploited to enhance the communication performance of the user. Specifically, we propose an optimal LED power management scheme to maximize the average data rate across the room subject to predefined communication constraints as well as number of blockages inside the room.
2. We have also formulated a power-saving optimization framework to maximize the power savings among the LEDs with respect to the number of blockages and permissible localization error. The effect of dimming on the above is also investigated.
3. The closed-form expression of BER for optimal LED power allocation with blockages and localization is derived.
4. Further, to see the effect of a high rate modulation scheme in the proposed system model, we have analyzed the BER performance and the localization error with DCO-OFDM and human blockage. The effect of random device orientation on the BER performance is also analyzed.
5. In addition, we have also analyzed the trade-off between the localization error and the performance metrics such as BER and illumination for the proposed location-assisted indoor VLC system.

9.2 System Model

The system model considers 4 LEDs transmitters placed in the rectangular configuration in a room size of $x \times y \times z$ (m \times m \times m). The receiver plane is at the height of 0.85 m. Generalized RWP model (with pause time t_p) has been employed to characterize the distribution of dynamic blockages in a space $[x, y]^2$. The human blockages are modelled as cylinders of height h_B and radius r_B , as shown in Fig. 8.1 (ref. Section 8.2). For the given system model, blockages of different widths (radius r_1 and r_2) have been considered to replicate the different sizes of people. We have used standard OOK modulation in the proposed VLC system for determining the power and SNR expression. Also, to see the effect of state-of-the-art high data rate modulation schemes such as DCO-OFDM on the proposed LED power allocation framework, we have analyzed the BER performance, and the maximum allowed localization error using DCO-OFDM [196].

The proposed system model can be generalized to a room of any arbitrary size. However, for ease of analysis and without the loss of generality, we consider a square room size of $5 \times 5 \times 3$ (m \times m \times m), where the LEDs 1, 2, 3, and 4 are placed at the height of 3m at (1.25, 3.75), (3.75, 3.75), (1.25, 1.25), (3.75, 1.25) respectively. It is assumed that the location information of the human blockages is available beforehand by utilizing the methods discussed in Chapter 8.

9.3 LED Power Allocation Optimization Problem

This section proposes the optimal LED power management framework based on human blockage estimation inside the room. The objective is to maximize the average bit rate among the users subject to the illumination and BER constraints. Here, we consider multiple LEDs and multiple user scenario wherein each user will act as a human blockage to others. The average bit rate is the function of the average received SNR at the receiver in the presence of human blockages [197]. The average bit rate is maximized by optimally allocating the transmit power P_{t_i} among LEDs and can be expressed as:

$$\max_{P_{t_i}} \log_2 \mathbb{E} \left[1 + \left[\frac{\left(\mathcal{R} \sum_{i=1}^N H_{i,j}^B P_{t_i} \right)^2}{\sigma_j^2} \right] \right] \quad (9.1)$$

$H_{i,j}^B$ is the VLC channel coefficient between i^{th} LED and j^{th} PD in the presence of human blockages and σ_j^2 is the noise variance at j^{th} PD. The objective function is subjected to following constraints:

1. The sum of power of each LED is upper-bounded by P_T

$$\begin{aligned} \sum_{i=1}^N P_{t_i} &\leq P_T, \\ \Rightarrow \mathbf{1}_N \mathbf{x} &\leq P_T. \end{aligned} \quad (9.2)$$

where, $\mathbf{1}_N$ is a N dimensional unit vector and $\mathbf{x} = [P_{t_1}, \dots, P_{t_N}]^T$ is N dimensional column vector of decision variables.

2. The power of each LED is non-negative.

$$P_{t_i} \geq 0 \quad \forall i = 1, \dots, N, \quad (9.3)$$

$$\Rightarrow \mathbf{G} \mathbf{x} \geq 0. \quad (9.4)$$

where $\mathbf{G} = \text{diag}(1, \dots, 1)$.

3. BER should be $P_e \leq 10^{-3}$

$$Q \left(\mathbb{E} \sqrt{\frac{\left(\mathcal{R} \sum_{i=1}^N H_{i,j}^B P_{t_i} \right)^2}{\sigma_j^2}} \right) \leq 10^{-3}. \quad (9.5)$$

4. The illumination across the room must be within a predefined range

$$1500 \text{ lux} \geq \left[\frac{P_{t_i} \cos^{m+1}(\phi) \cos(\theta)}{4\pi r^2} \right] \geq 300 \text{ lux} \quad (9.6)$$

where r is the attocell radius.

The second term inside the log function in optimization function (9.1) is the expected SNR at the receiver in the presence of blockage and can be calculated as:

$$\mathbb{E} \left[\frac{\left(\mathcal{R} \sum_{i=1}^N H_{i,j}^B P_{t_i} \right)^2}{\sigma_j^2} \right] = \mathcal{R}^2 \mathbb{E} \left[\left(\frac{P_{r_j}}{\sigma_j^2} \right)^2 \right], \quad (9.7)$$

$$\begin{aligned} \mathcal{R}^2 \mathbb{E} \left[\left(\frac{P_{r_j}}{\sigma_j^2} \right)^2 \right] &= \mathcal{R}^2 \mathbb{E} \left[\frac{\sum_{i=1}^N (H_{i,j}^B)^2 P_{t_i}^2}{\sigma_j^2} + 2 \frac{\sum_{i=1}^N \sum_{q=i+1}^N H_{i,j}^B H_{q,j}^B P_{t_i} P_{t_q}}{\sigma_j^2} \right] \\ &= \mathcal{R}^2 \left[\frac{\sum_{j=1}^K \sum_{i=1}^N (H_{i,j}^B)^2 P_{t_i}^2}{K \sigma_j^2} + \frac{\sum_{j=1}^K 2 \sum_{i=1}^N \sum_{q=i+1}^N H_{i,j}^B H_{q,j}^B P_{t_i} P_{t_q}}{K \sigma_j^2} \right], \quad (9.8) \\ &= \mathcal{R}^2 \left[\frac{\sum_{i=1}^N \mu_{i,i}^B P_{t_i}^2 + 2 \sum_{i=1}^N \sum_{q=i+1}^N \mu_{i,q}^B P_{t_i} P_{t_q}}{K \sigma_j^2} \right], \end{aligned}$$

where $\mu_{i,q}^B = \sum_{j=1}^K H_{i,j}^B H_{q,j}^B$ and K is total number of PD. By substituting the value of received SNR in (9.1) the average data rate for N_u users can be expressed as:

$$\begin{aligned} \log_2 \left[1 + \frac{\left(\mathcal{R} \sum_{i=1}^N H_{i,j}^B P_{t_i} \right)^2}{\sigma_j^2} \right] &= \log_2 \left[1 + \mathcal{R}^2 \mathbb{E} \left[\left(\frac{P_{r_j}}{\sigma_j^2} \right)^2 \right] \right] \\ &= \frac{1}{N_u} \left[P_{t_1}, \dots, P_{t_N} \right] \\ &\quad \begin{bmatrix} \beta_{11} & \dots & \beta_{1N} \\ \dots & \dots & \dots \\ \beta_{N1} & \dots & \beta_{NN} \end{bmatrix} \begin{bmatrix} P_{t_1} \\ \dots \\ P_{t_N} \end{bmatrix}, \end{aligned} \quad (9.9)$$

Using (9.1) and (9.9), the proposed optimization problem can be expressed in matrix form as:

$$\max_{\mathbf{x}} \frac{1}{N_u} \mathbf{x}^T \mathbf{B} \mathbf{x}, \quad (9.10)$$

where the matrix \mathbf{B} is given by

$$\mathbf{B} = \begin{bmatrix} \beta_{1,1} & \dots & \beta_{1,N} \\ \dots & \dots & \dots \\ \beta_{N,1} & \dots & \beta_{N,N} \end{bmatrix}. \quad (9.11)$$

and elements $\beta_{i,q}$ are

$$\beta_{i,q} = \left[\frac{\sum_{i=1}^N \mu_{i,i}^B P_{t_i}^2 + 2 \sum_{i=1}^N \sum_{q=i+1}^N \mu_{i,q}^B P_{t_i} P_{t_q}}{K \sigma_j^2} \right], \quad (9.12)$$

The objective function in (18) is convex because \mathbf{B} is positive-definite [162]. Since the variance of received power $\mathbf{x}^T \mathbf{B} \mathbf{x} > 0 \forall \mathbf{R}_+^N$, \mathbf{B} is positive-definite. Also, the linear functions are both convex and concave, and all constraints are convex. Therefore, the optimization problem in (9.1) gives a quadratic and the convex optimization problem.

9.3.1 Power Saving Optimization

In this sub-section, we formulate an optimization problem to maximize the power saving among the LEDs based on localization information. The optimization problem also takes into account the human blockages inside the room. Specifically, we derive the total power to be distributed among the LEDs based on the optimal LED power management framework described in Section III in order to fulfill both illumination and BER constraints. The objective power saving function is the total allotted power based on equal power allocation to all the LEDs subtracted from the total allocated power (using optimal LED power allocation framework), fulfilling both illumination and BER constraints, i.e.,

$$\max_{N_B} [P_T - P_A], \quad (9.13)$$

Here, P_A the minimum required allocated power to the LEDs for a given number of blockages using the proposed optimal LED power allocation scheme. P_T the total power required with equal power allocation to maintain the constraints like, average BER should be $\leq 10^{-3}$. The illumination across the room should be $1500 \text{ lux} \geq I_{avg} \geq 300 \text{ lux}$. The total power constraint of the system being $\sum P_{t_i} \leq P_T$.

9.4 BER Performance

In this section, we analyze the BER of the VLC channel in the presence of dynamic blockages characterized by MHCP. To calculate the blockage probability $P_B(d_B)$, it is assumed that no signal is received whenever the PD is blocked by the obstacle. The optical signal $s_i(t)$ transmitted by the i_{th} LED is as follows:

$$s_i(t) = P_{t_i}[1 + M_I x_i(t)], \quad (9.14)$$

where P_{t_i} is the i_{th} LED's the transmit power, M_I is the modulating index and $x_i(t)$ is the corresponding OOK modulated signal [179]. The first term in (9.14) (P_{t_i}) accounts for the illumination whereas the second term ($P_{t_i} M_I x_i(t)$) for the communication part. It is assumed that the DC component of the detected electric signal is filtered out at the Rx after photo detection. y_j is the received signal at the photo-detector j , and is expressed as:

$$y_j = \mathcal{R}P_{r_j} + n_j, \quad (9.15)$$

where \mathcal{R} is the responsivity of the PD and n_j is the additive white Gaussian noise (AWGN) with zero mean and σ_j^2 variance. Thus, we can write the AWGN as $n_j = \mathcal{N}(0, \sigma_j^2)$. Received power at the j^{th} photo-detector, P_{r_j} is given by:

$$P_{r_j} = \sum_{i=1}^N H_{i,j}^B P_{t_i} M_I x_i. \quad (9.16)$$

$$P_{r_j} = \sum_{i=1}^N \frac{P_{t_i} (m+1) A h_T^{m+1} M_I x_i [\exp(-2\lambda_B d_{i,j} r_B^2)]}{2\pi (\sqrt{h_T^2 + r_i^2})^{m+3}}, \quad (9.17)$$

Here, h_T is the height of transmitter plane and r_i location of the i^{th} LED from the centre. As we know the location of blockages, as well as that of the PD, the transmitting power from the LED, will be given by vector $P_{t_i} = B_i P_T$ get from (9.10) the optimal LED power allocation.

$$P_{r_j} = \sum_{i=1}^N \frac{B_i P(m+1) A h_T^{m+1} M_I x_i [\exp(-2\lambda_B d_{i,j} r_B^2)]}{2\pi (\sqrt{h_T^2 + r_i^2})^{m+3}}, \quad (9.18)$$

where B_i is the i_{th} LED power allocation vector derived using optimization in (9.16). Let,

$$C_1 = \frac{P(m+1) A h_T^{m+1}}{2\pi}, \quad (9.19)$$

and

$$V_i = \frac{B_i x_i [\exp(-2\lambda_B d_{i,j} r_B^2)]}{(\sqrt{h_T^2 + r_i^2})^{m+3}}. \quad (9.20)$$

Now P_{r_j} can be expressed as:

$$P_{r_j} = C_1 \sum_{i=1}^N V_i, \quad (9.21)$$

Hence the output signal can be written as:

$$y_j = \mathcal{R} C_1 \sum_{i=1}^N V_i + n_j, \quad (9.22)$$

Here n_j is the noise σ_j^2 at j^{th} the PD is the total noise power comprising of shot noise power (σ_{shot}^2) and thermal noise power ($\sigma_{\text{thermal}}^2$) which can be expressed as:

$$\sigma_j^2 = \sigma_{\text{shot}}^2 + \sigma_{\text{thermal}}^2. \quad (9.23)$$

Using (9.22), the BER for OOK modulation scheme with the optimal LED power allocation with human blockages can be expressed as:

$$P_e = Q\left(\frac{\mathcal{R} C_1 \sum_{i=1}^N V_i}{\sigma_j}\right). \quad (9.24)$$

Further, the above BER analysis can be extended for other modulations schemes such as QAM, PAM, etc.

9.5 Results and Discussion

In this section, the simulation and analytical results for the proposed indoor VLC broadcast system inside a standard room sizes of $5 \text{ m} \times 5 \text{ m} \times 3 \text{ m}$ and $10 \text{ m} \times 10 \text{ m} \times 3 \text{ m}$ have been presented. Each room consists of either 4 and 8 LED transmitters placed in a rectangular geometry. A Monte Carlo simulation of 10^4 independent trials is conducted, where for each trial, a random location of blockages has been generated. The locations of the VLC transmitters, receiver and the orientations are provided in Table 9.1.

In the proposed optimal LED power allocation framework, in order to update the LED power in real-time with respect to the user's location inside the room, we require estimation of the user location, which is further fed into the LED controller, which distributes the power among LEDs as per the proposed optimal LED power allocation. Here we can use a microcontroller-based LED controller circuit to facilitate the power management (varying light intensity) of the LEDs based on the user's location information inside the room.

Table 9.1: System Model & Simulation Parameters

Parameter	Value
Total transmitted power P_T	200 mw
Refractive index n	1.5
Optical filter gain T_s	1
Wall reflection ρ	0.8
Number of user N_u	1-8
Number of receiver location K	625
LED semiangle Φ	60°
Receiver plane above the floor h_R	0.85 m
Receiver elevation	90°
Receiver active area A	1 cm ²
FOV of the receiver ψ_c	60°
Blockage radius r_1 and r_2	20 cm & 40 cm
Height of the blockage h_B	180 cm
Responsivity \mathcal{R}	0.5 $\frac{A}{W}$
Signal bandwidth B_s	10 MHz
Noise bandwidth factor I_2	0.562
Background current I_{bg}	100 μA

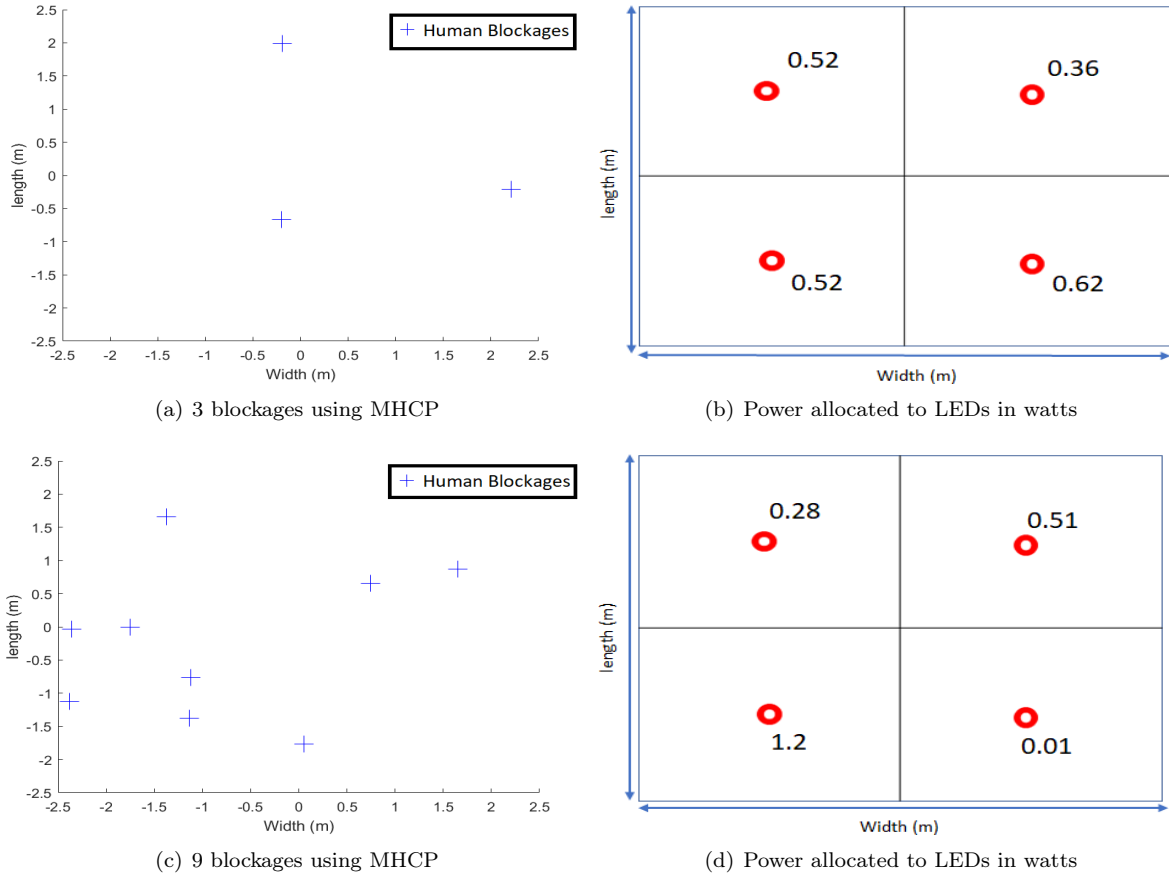


Figure 9.1: Optimal LED power allocation in the presence of blockages with total power of 2 watts

9.5.1 Optimal LED Power Allocation

This sub-section shows the results of the proposed optimal LED power allocation scheme to maximize the average data rate with respect to the number of blockages subject to illumination and BER constraints. The realization blockage using MHCP and their respective allotted power to the LEDs has been shown in Fig. 9.1. Figs. 9.1(a) and 9.1(b) show the realization of 3 human blockages and their respective power subject to the total power constraint of 2 W, which is distributed among 4 LEDs using optimal LED power allocation in (9.2). Similarly, Figs. 9.1(c) and 9.1(d) show the realization of 9 human blockages and their respective power allocation.

It can be seen from Fig. 9.1 that depending on the location of the human blockages, the respective LED power varies in order to fulfill the above constraints. For example, in Figs. 9.1(c) and 9.1(d) with 9 human blockages inside the room, 6 blockages are clustered near the 3rd LED attocell, and the allotted power to the respective LED is 1.2 W. While the 1st and 3rd LEDs have been assigned 0.28 W and 0.51 W of power to serve the remaining 3 users. Similarly, the 4th LED has 0 blockages in its attocell, so it has been allotted a minimum required power of 0.1 W to maintain the illumination constraints. Therefore, it can be observed that based on the location information of the users, the respective LED power varies to maximize the data rate subject to the proposed constraints. Figs. 9.2(a) and 9.2(b) show the change in allocated optimal LED power

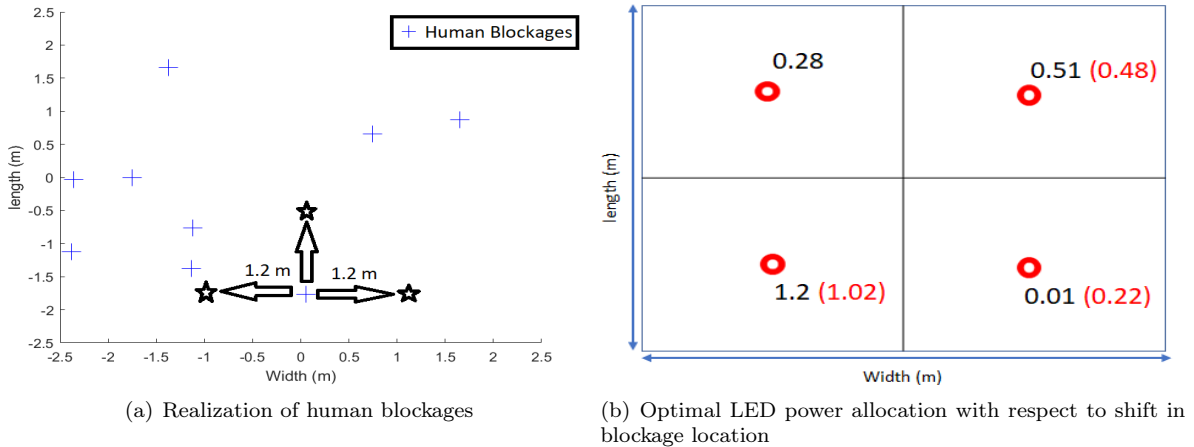


Figure 9.2: Optimal LED power allocation with respect to shift in blockage location (the values in red color shows the updated LED power values due to shift)

allocation values due to a shift in blockage location. The primary objective is to find the maximum allowed shift in blockage location that will not alter the current LED power allocation which depends on the current location of the blockage as well as the minimum distance required to move out of the coverage area of the respective LED attocell. As shown in Fig. 9.2(a) that the maximum allowed shift for a given blockage realization is found to be 120 cm.

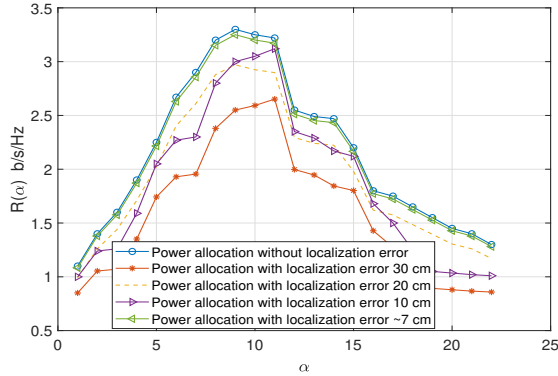


Figure 9.3: Convergence of achieved average data rate for different localization error with respect to all possible solution (α)

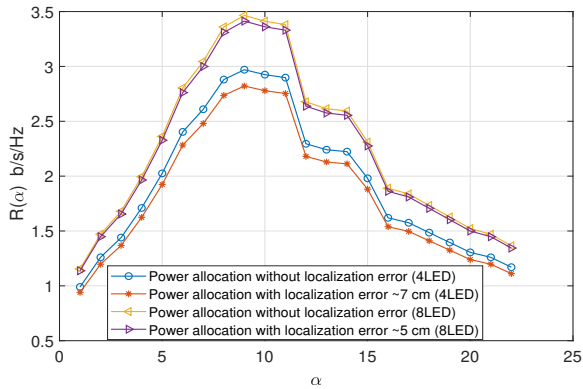
9.5.2 Convergence of the Proposed LED Power Allocation Framework

This sub-section shows the convergence of the proposed optimal LED power allocation scheme in the presence of human blockages based on location information. The maximum allowed error in localization with respect to LED and room configuration has also been analyzed. Fig. 9.3 shows the maximum achievable average data rate for the proposed optimization framework (9.1) for the given realization of human blockages as shown in Fig. 9.1(c). The index number of all possible solutions (α) has been chosen such that the maximum average data rate is achieved. It can also be observed from Fig. 9.3 that as the localization error increases, the maximum achievable data rate decreases as it results in less accurate estimation of the blockage, which will affect the proposed optimization solution. Therefore, we can see that for 4 LEDs configuration with nine blockages in a room size of $5 \text{ m} \times 5 \text{ m} \times 3 \text{ m}$, the maximum allowed localization error is 7 cm with the maximum achieved data rate of 3.28 b/s/Hz. Further, if localization error increases, the achieved data rate decreases. For example, for the localization error of 10 and 20 cm, the maximum achieved data rate reduces to 3.1 and 2.85 b/s/Hz respectively.

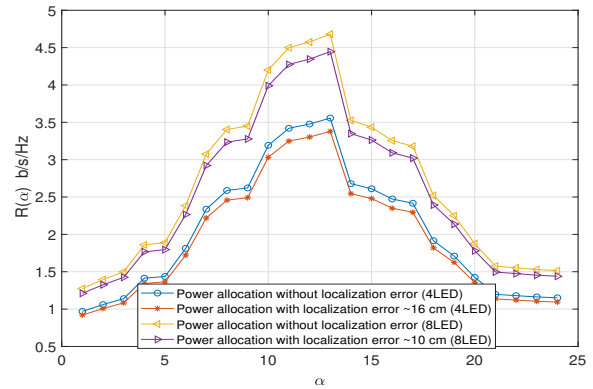
9.5.3 Optimal LED power allocation framework for 4 and 8 LED configuration with varying room size

Fig. 9.4 shows the maximum achievable average data rate subject to different localization error for 4 and 8 LED configuration with a room size of $5 \text{ m} \times 5 \text{ m} \times 3 \text{ m}$ and $10 \text{ m} \times 10 \text{ m} \times 3 \text{ m}$.

Fig. 9.4(a) shows the average achieved data rate for a room size of $5 \text{ m} \times 5 \text{ m} \times 3 \text{ m}$ with 4 and 8 LEDs. As the number of LEDs increases from 4 to 8 LED, the respective maximum allowed localization error decreases from 7 cm to 5 cm. This reduction in localization error is due to the fact that with an increase in the number of LEDs, the separation between the two LEDs decreases the attocell coverage area. Similarly, Fig. 9.4(a) shows the average achieved data rate for a room size of $10 \text{ m} \times 10 \text{ m} \times 3 \text{ m}$ with 4 and 8 LEDs. It can be observed that the maximum allowed localization error value increases due to increased separation between two LEDs with an increase in room size. The maximum allowed localization error for 4 LED and 8 LED cases are 16 cm and 10 cm respectively. Therefore, it is obvious that increase in the number of LEDs results in a decrease in



(a) Achieved average data rate with 4 and 8 LEDs for room $5 \text{ m} \times 5 \text{ m} \times 3 \text{ m}$

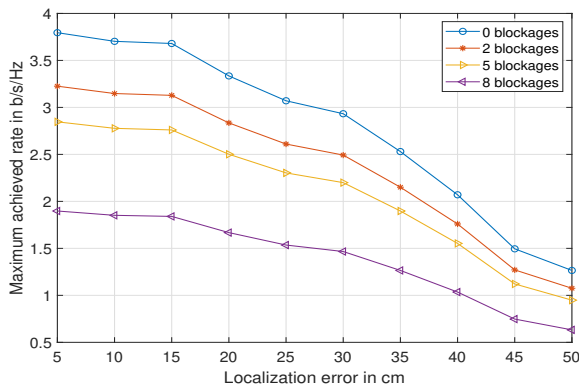


(b) Achieved average data rate with 4 and 8 LEDs for room $10 \text{ m} \times 10 \text{ m} \times 3 \text{ m}$

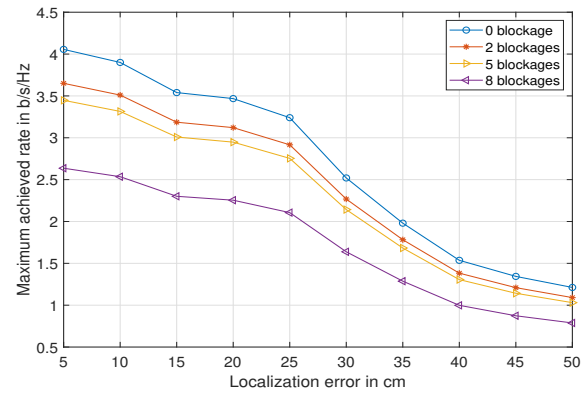
Figure 9.4: Achieved average data rate with localization error for 4 and 8 LEDs and two room dimensions

the maximum allowed localization error with an increase in average data rate. While with the increase in room dimension, the maximum allowed localization error increase for the same number of LEDs with a decrease in the maximum achievable average data rate. Hence, it can be inferred that there exists a trade-off between the maximum achievable average data rate and the maximum allowed localization error and the operator can tune the system as per the requirement.

9.5.4 Maximum Achieved Data Rate for Different Localization Error with respect to Number of Blockages



(a) Maximum achieved data rate with 4 LEDs



(b) Maximum achieved data rate with 8 LEDs

Figure 9.5: Maximum achieved data rate for different localization error with 4 and 8 LEDs

This sub-section shows the maximum achieved data rate by the proposed scheme in the presence of human blockages for varying localization error subject to fulfilling both illumination and BER constraints for a room size of $5 \text{ m} \times 5 \text{ m} \times 3 \text{ m}$. Fig. 9.5 shows the maximum achievable data rate as a function of localization error for increasing number of blockages for 4 and 8 LED configurations. It can be seen that as the number of human blockages increases, the maximum achievable data rate decreases along with maximum localization error for 4

LED configuration as shown in Fig. 9.5(a). For example, with 2 blockages and an allowed localization error of 5 cm, the maximum achieved data rate is 3.25 b/s/Hz. For the same number of blockages with an increase in localization error to 20 cm, the maximum achieved data rate is reduced to 2.75 b/s/Hz. Similarly, in Fig. 9.5(b) with 8 LED configurations, the effect is nearly the same. It can be observed that with 2 blockages and with allowed localization error of 5 cm, the maximum achievable data rate is 3.65 b/s/Hz, while for the same number of blockages and increase in localization error to 20 cm, the maximum achievable data rate reduces to 3.05 b/s/Hz. It is due to the fact that for 8 LED configuration, there is less separation between the LEDs, the transmit power is more uniformly distributed but at the same time, the localization error also increases due to more overlapping regions in their respective attocell.

From the above results, it can be inferred that the maximum achieved data rate decreases with the increase in localization error and the number of blockages. Hence, depending on the requirement of the system with a given number of blockages and errors in the localization, one can deploy either the 4 or 8 LED configuration.

9.5.5 Effect of LED Semiangle in the Maximum Allowed Localization Error

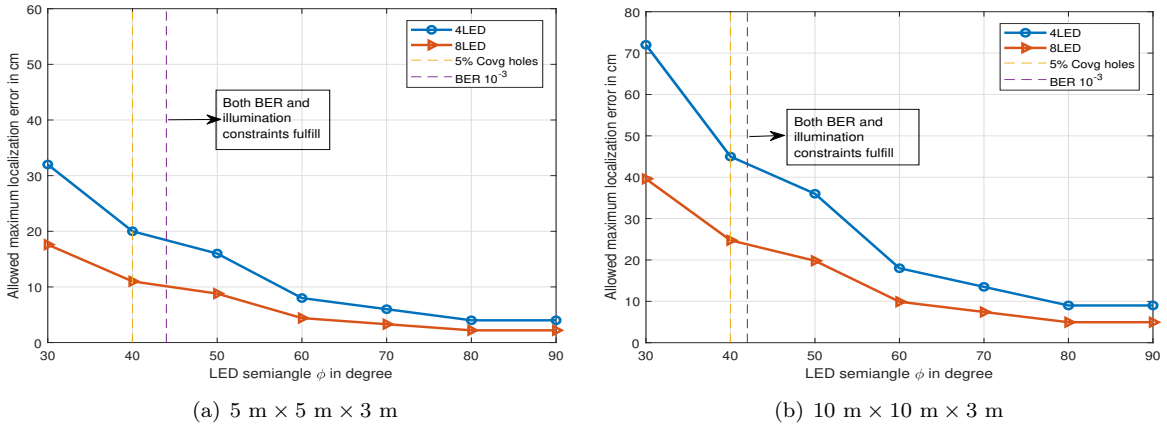


Figure 9.6: Maximum allowed Localization error versus the LED semiangle with 4 and 8 LED configuration

In this sub-section, The effect of LED semiangle on the maximum allowed error in localization has been shown in Fig. 9.6. The increased LED semiangle results in an increase in attocell size. The increase in attocell size leads to more overlapping regions among LEDs and, affects the maximum allowed localization error. Figs. 9.6(a) and 9.6(b) show the maximum allowed localization error with 4 and 8 LEDs for a room size of 5 m x 5 m x 3 m and 10 m x 10 m x 3 m respectively. In both cases, the maximum allowed localization error decreases with an increase in LED semiangle. For the case of 5 m x 5 m x 3 m room size, the minimum required LED semiangle is 44° with maximum allowed localization error of 10 cm and 18 cm while maintaining the illumination and BER constraints for 4 and 8 LEDs respectively. Similarly, for the case of room size of 10 m x 10 m x 3 m minimum required LED semiangle is 42.8° with maximum allowed localization error of 22 cm and 43 cm for 4 LED and 8 LED respectively. It is worth mentioning that wider LED semiangle results in more uniform received power and better BER across the room while decreasing the maximum allowed localization error and vice versa. Therefore, it can be inferred that there is a trade-off between the allowed maximum localization error versus

the illumination and BER constraints. Wider LED semiangle satisfies the illumination and BER constraints with good margin but suffers in maximum allowed localization error and vice versa.

9.5.6 Power Saving with and without Illumination Constraint Under the Effect of Dimming

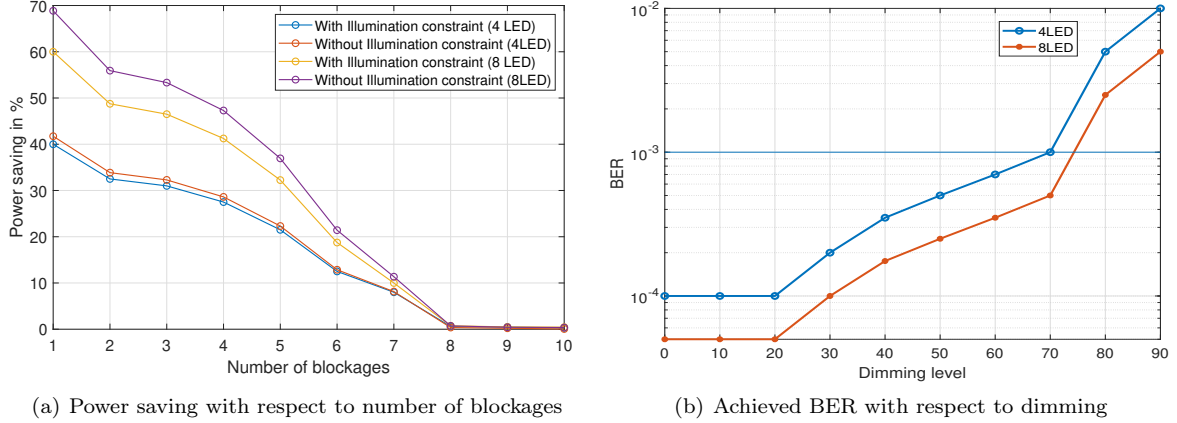


Figure 9.7: Power saving and dimming performance with and without illumination constraints

In this sub-section, we have shown the maximum possible power saving for the proposed optimal LED power allocation scheme with and without illumination constraints for 4 and 8 LEDs configuration for a room size of 5 m × 5 m × 3 m. The power-saving is calculated using the (9.13) subject to the number of blockages. In order to calculate the power saving in percentage in the denominator, we have taken the constant power P_T . The formula for the percentage of power-saving P_S is written as:

$$P_S = \frac{\max_{N_B} [P_T - P_A]}{P_T} \times 100, \quad (9.25)$$

Denominator P_T is fixed for all lighting scenarios to maintain the fair comparison with constant power. We have taken 2 Watt constant power for 4 and 8 LEDs arranged in rectangular configurations. Fig. 9.7(a) shows the power saving with varying number of human blockages for with and without illumination constraints for the optimization problem formulated in (9.15). It can be seen that for 4 LED case with one blockage, the maximum power saving achieved with and without illumination constraint is nearly the same which is approximately 40 %. Further, it is observed that the power saving decreases with an increase in the number of blockages. While for the case of 8 LED, the maximum power saving without any blockages and illumination constraint is 70 %, and with illumination constraint, it is reduced to 60 %. It is observed that the power saving decreases with an increase in the number of blockages for both cases. It goes to zero with blockages more than 7. For the given room size, this is the maximum number of blockages that can be served. Therefore, it can be inferred that for a given room size of 5 m × 5 m × 3 m, the maximum allowed human blockages are ≤ 7 to save the power.

In the VLC system, the illumination due to LED should be adjusted based on the user's need as well as for saving energy [151],[152]. Fig. 9.7(b) shows the achieved BER with respect to the dimming percentage for

4 and 8 LEDs with 5 blockages. As the dimming percentage increases, the respective BER starts increasing for both cases. As the dimming percentage increases, the received power decreases, which results in an error in localization, and the effective SNR decreases. It can be seen that for 4 LED case, the maximum allowed dimming is 70 %, while for 8 LED case, it is approximately 75 %.

9.5.7 BER Performance with Optimal LED Power Allocation

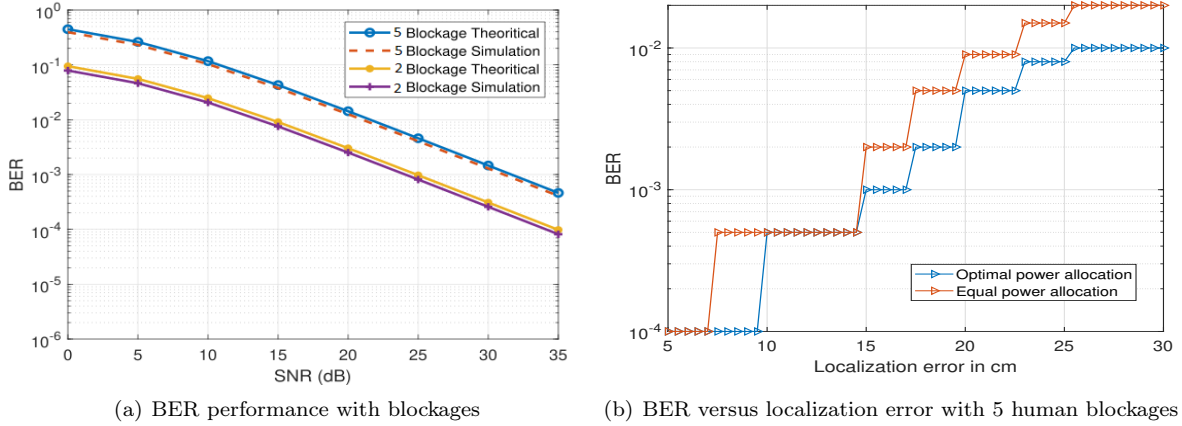


Figure 9.8: BER Performance

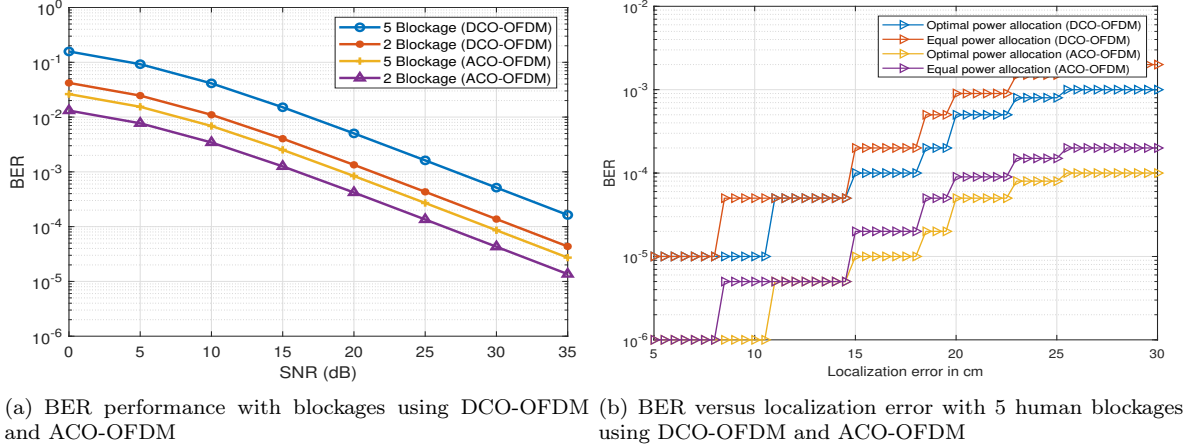


Figure 9.9: BER Performance with DCO-OFDM and ACO-OFDM

This sub-section shows the BER performance of the proposed system with equal and optimal power allocation schemes. Fig. 9.8(a) shows the BER performance in the presence of human blockages. The derived BER expressions and the simulation results are in close agreement, which validates the mathematical derivations and justifies the approximations in (9.24).

Fig. 9.8(b) shows the BER with respect to localization error in estimation with equal power allocation and proposed optimal LED power allocation schemes. It can be seen that as the localization error increases, the BER decreases in both cases. However, it is interesting to observe that the system with optimal LED power

allocation can tolerate more error in localization as compared to equal power allocation scheme for the same BER values. We have also plotted the BER performance results with blockages using DCO-OFDM as shown in Fig. 9.9 and compared it with standard OOK modulation as shown in Fig. 9.8.

It can be seen from Fig. 9.8(a) and Fig. 9.9(a) the BER performance with blockages using OOK and DCO-OFDM and ACO-OFDM, respectively, using location information. To achieve the BER of 10^{-3} with 2 blockages, the SNR required using OOK is approximately 23 dB, whereas, in the case of DCO-OFDM and ACO-OFDM, it is around 20 dB and 15 dB, respectively. Similarly, for 5 blockages, the required SNR is 30 dB, whereas, in the case of DCO-OFDM, it is approximately 27 dB and 21 dB, respectively. DCO-OFDM and ACO-OFDM provide a gain of 3 dB and 8 dB, respectively, with respect to OOK. It is because, with DCO-OFDM and ACO-OFDM, the data stream is parallelized and sent through orthogonal subcarriers. Each sub-stream can be modulated using a high-order modulation such as PSK or QAM. Furthermore, external narrow-band interference will most probably impact only a limited number of subcarriers while the other subcarriers will remain unaltered, which in turn leads to better-received power and better error rate performances [198].

Table 9.2: Performance Comparison

Modulation Scheme	SNR for BER of 10^{-3}	Localization Error
OOK with 2B	23 dB	9 cm
DCO-OFDM with 2B	20 dB	11 cm
ACO-OFDM with 2B	15 dB	13 cm
OOK with 5B	30 dB	7 cm
DCO-OFDM with 5B	27 dB	9 cm
DCO-OFDM with 5B	21 dB	11 cm

Similarly, Fig. 9.8(b) and Fig. 9.9(b) show the BER versus the localization error with equal and optimal power allocation scheme using OOK and DCO-OFDM, respectively. As the optimum power allocation vector is calculated using received power as a reference, the LED optimal power allocation vector in a change in modulation scheme remains the same. Only the BER ranges widen for DCO-OFDM in respect of the standard OOK scheme. For example, with DCO-OFDM, we can maintain BER of 10^{-5} up to the localization error of 11 cm, while in the case of OOK, it is around 9 cm. We can say that with higher-order modulation schemes such as DCO-OFDM, we can reduce the range of SNR with respect to the required BER performance as shown in Table 9.2.

9.5.8 BER Performance with Random UE orientation

In this subsection, we have considered the impact of random orientation in their analysis, for instance, and references therein [97, 199]. All these works signify the importance of incorporating user equipment (UE) orientation. In the previous BER performance, we are considering that the PD is facing directly upward for ease of analysis. The above assumption has been made to simplify the proper orientation model and make the analysis tractable. To address the effect of random device orientation on the proposed system, we have plotted the BER performance considering the random device orientation of the receiver and compared it without device orientation, as shown in Fig. 9.10. It can be seen that by considering random device orientation, the BER

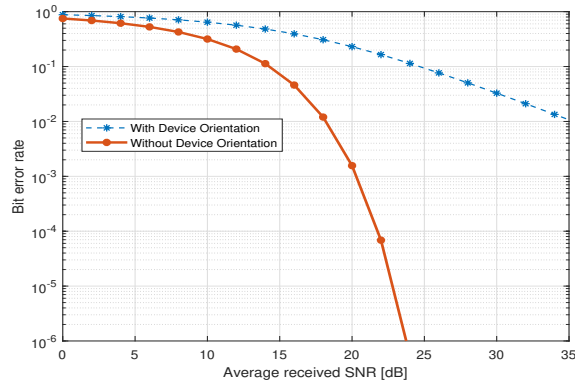


Figure 9.10: BER performance with and without UE orientation

performance degraded even with the location information. It is due to the fact that the acquiring location information does not confirm the direction of the receiver, and the random device orientation results in self blockage, sometimes affecting the received power.

9.6 Summary

In this Chapter, a location-assisted VLC system with human blockages has been analyzed. We have proposed the optimal LED power allocation scheme based on location information, resulting in a better indoor communication system in terms of BER, achieved data rate, and illumination across the room. The closed-form expression for BER with MHCP is derived for the optimal LED power allocation schemes with human blockages. The analytical results are in close agreement with the simulation results, which validates the analytical framework proposed in the article. The proposed work also established that with the proposed optimal LED power allocation scheme can support up to 70 % and 75 % dimming range of visible light with 4 and 8 LED respectively. Further, we have also proposed an optimization framework to maximize power saving with and without dimming among the LEDs while satisfying the communication constraints. Further, to see the effect of a high rate modulation scheme in the proposed system model, we have analyzed the BER performance and the localization error with DCO-OFDM and human blockage.

This work also analyzed the maximum allowed localization error for varying room sizes and the number of LEDs with respect to blockages. In addition, the proposed work also studied the trade-off between the achieved data rate with respect to allowed localization error as a function of LED semiangle. It is shown that for a room size of 5 m × 5 m × 3 m, the minimum required LED semiangle is 44° for 4 and 8 LED configuration and for room size of 10 m × 10 m × 3 m, it is 42.8° to maintain both illumination and BER constraints. Furthermore, through the obtained results it is observed that maximum achieved data rate is subject to varying localization error and is a function of number of human blockages inside the room. Further, the proposed framework can be easily extended for other used cases such as factories and shopping malls with different lighting requirements. The proposed optimization problem can be modified with the required constraints to provide both illumination and communication.

Chapter 10

Conclusion

In this chapter, we present the various conclusions drawn from our research work reported in this thesis. We also outline the possible directions for future work based on our work.

10.1 Conclusion

Due to unprecedented growth in Internet traffic over the last few decades, there is a pressing need to develop new communication technologies that utilize the untapped regions of the electromagnetic spectrum. To this end, a lot of research is being undertaken in the area of wireless optical communication, particularly VLC, which utilizes the illumination infrastructure of LEDs for data communication. Indoor VLC combines illumination and data transmission, thereby facilitating green and sustainable energy solutions. The effort of using VLC for an in-home access solution started with the IEEE P802.15.7 standard for short-range wireless optical communication. However, the physical layer solutions proposed therein are limited to 96 Mb/s and thus should be further optimized to keep pace with the ever-increasing BW requirements: for example, 5G solutions already require a minimum per-user bit rate of 100 Mb/s or peak bit rates of 20 Gb/s, latency below 1 ms, and a density of 10 Mb/s/m². These requirements are very ambitious, and thus, an optimal indoor VLC technology should be evolved on various aspects, as addressed in this thesis by tackling the related challenges that hamper the judicious implementation of indoor VLC systems.

We first analyze the performance of a hybrid cellular-VLC downlink where the outdoor coverage is provided via the cellular network, and the indoor coverage is provided through a VLC system [200, 201]. It has been shown that by using the proposed hybrid cellular-VLC downlink, it is possible to achieve a significant amount of power-saving (approximately 51%) at BTS as compared to a direct cellular link. Also, this thesis compares the SER performance of the same constellation-based modulation schemes in the RF and VLC link in an indoor room. As one looks for better performance, i.e., beyond SER 10^{-3} , the performance of VLC in all its channel models is much better than RF. Further, the SER gap between VLC and RF decreases as the constellation size increases [202]. Finally, the dimming range is calculated for the proposed system under dimming constraints. Results show that a dimming range of up to 70% can be achieved in the hybrid cellular-VLC link.

Further, this thesis analyzes the performance of the MIMO indoor VLC system by randomly deploying the LEDs using MHCP. PDs with two different FOVs have been utilized for imaging as well as non-imaging receiver

structures [118, 203]. Consequently, the proposed work attempts to achieve uniform SNR across the room by utilizing MHCP-based LED placement at the transmitter and a non-imaging receiver with four PDs using 1-FOV, 2-FOV, and imaging receiver configurations. Simulation results show that random deployment of LED using MHCP configuration results in a more uniform SNR profile inside the room as compared to regular LED deployment schemes. Three different power allocation schemes for LEDs, namely equal power, distance-based power, and an optimal power allocation, are proposed. The average SNR and the variance of the received optical power inside the room are derived and compared for the different power allocation schemes. In addition, the closed-form expression for the BER probability is derived for the proposed MHCP configuration using OOK as a modulation scheme. Results show improvement in BER performance with the optimal power allocation compared to other power allocation schemes for imaging and non-imaging receiver configuration.

We also infer that for a realization of static and dynamic human blockages, the MHCP and the RWP model are the best fit as they provide close to the practical realization of blockages [20]. We compared the indoor VLC system performance in terms of received SNR for 4 and 8 LED configurations under predefined total power constraints. It is observed that at a lower density of human blockages in the room, the 4-LED configuration outperforms the 8-LED configuration. However, at a higher density of human blockages in the room, the 8-LED configuration outperforms the 4-LED configuration for the same total power constraint. Hence the proposed analysis will be useful for designing a VLC-based indoor communication system wherein the system designer can switch between these two configurations depending on the number of blockages.

Furthermore, in this thesis, we have obtained the optimum value of the LED semiangle and the receiver FOV in the presence of human blockages, using the quality factor (Q) as a performance metric [204]. The analytical expression for the achieved quality factor is derived for both single variable and joint optimization formulation. Results shows that with 2 and 5 blockages, the optimum pair using single and joint optimization is $(63^\circ, 65^\circ)$ and $(63^\circ, 70^\circ)$ for a separation distance of $D_1 = 40$ cm and $(65^\circ, 70^\circ)$ and $(65^\circ, 75^\circ)$ for $D_2 = 20$ cm respectively which provide the highest quality factor with minimum delay spread shown. Furthermore, the optimization analysis can also be mapped to different room sizes and LED placement, with static and dynamic blockages inside the room.

The performance of VLC may severely deteriorate when the LoS link gets blocked due to other users/obstacles. Further, the received power may also fluctuate due to the random orientation of UE (self-blockage) and as NLoS power varies. In this thesis, in order to combat the shadowing due to obstacles and the UE orientation, we employ OIRS in indoor VLC systems in the presence of multiple human blockages. Moreover, we also propose the UE orientation model of users for an OIRS-aided indoor VLC system. The LoS channel gain statistics are calculated, and the orientation of UE is modeled as a random process. The impact of the random UE orientation and human blockages on the SNR performance of VLC systems is evaluated by utilizing the OIRS. Moreover, the PDF of the received SNR with OIRS is also calculated. The proposed analysis also deduces the optimum LED semiangle and the receiver FOV for the OIRS-aided indoor VLC system. Additionally, for the proposed system model, we have found out the optimum OIRS element size is for a given room size of $5 \text{ m} \times 5 \text{ m} \times 3 \text{ m}$ with 4 LEDs deployed in a rectangular configuration. The optimum OIRS element size will vary with the system

model and user configurations. Finally, BER and the average data rate performance with and without blockage cases have been analyzed for the proposed OIRS-aided indoor VLC system.

Further, we study the application of VLC in indoor positioning and navigation. We propose a novel optical identification algorithm to circumvent the use of active devices in IPSs, thereby enabling a passive IPS with higher energy efficiency, more flexibility, less cost, and enhanced robustness. The recent interest in using visible light as a means of communication has opened up possibilities for using visible light for other applications as well, such as indoor positioning. Visible light offers higher bandwidth, immunity from electromagnetic radiation, and most importantly, it can be seamlessly integrated into the existing lighting infrastructure. This thesis proposes a visible light-based positioning model for estimating an object's 3-D parameters, such as height and radius, in addition to the location in an indoor environment [184]. The model is built using neural networks, trained by simulating numerous multiple object scenarios in an indoor environment. It also takes into account the shadowing effects so it can be implemented in a multiple obstacle environment. The proposed algorithm has numerous applications, such as positioning assisted communication, suspicious object monitoring, and surveillance in an indoor environment. The proposed model achieves a location accuracy of 6.7 cm, which could be further improved to 4 cm at the expense of extra hardware. The accuracy in measuring the height and radius of the objects using the proposed framework is observed to be 4.67 cm and 1.27 cm, respectively. In addition, we also propose a methodology to optimize the power distribution to the LEDs in order to get the optimum location accuracy while maintaining the total power constraint on the system. This method could be utilized to update the power allocated to the LEDs by exploiting the current location of the objects in the room to improve communication uplink by employing VAPs. The proposed VLC-based IPS is a very inexpensive and promising technique to accurately locate and identify a very large number of targets in an energy-efficient manner.

Recent studies have shown that determining the position of a person or an object in a room can use the signals transmitted by LEDs. Finally, in this thesis, we exploit the location information obtained via LEDs to improve the communication performance of an indoor VLC system. Specifically, we propose an optimal LED power management framework to maximize the average data rate across the room while satisfying the BER and illumination constraints across the room [194]. The maximum allowed localization error, as a function of the number of blockages and the LED irradiance angle, have been calculated. In addition, the closed-form expression for the BER is derived for the proposed optimal LED power allocation scheme. We have also formulated an optimization problem that will maximize the power savings among the LEDs with respect to the number of blockages and permissible errors in localization. It has been shown that employing the proposed optimal LED power allocation will result in a significant amount of power-saving, which is approximately 40% for 4 LEDs configuration and 70% for 8 LEDs configuration as compared to equal power allocation. Further, the maximum allowed localization error is found to be approximately 7 cm and 18 cm with 4 and 8 LEDs, respectively, to achieve the maximum achievable data rate. Finally, it is shown that the proposed system can achieve a dimming range of up to 70%.

10.2 Future Work

The work presented in this thesis can be extended in many ways. Some exciting directions for future work arising out of this thesis are listed below.

- An interesting direction could be the analysis of an indoor VLC system with dynamic human blockages considering pause time in the investigation, which will give more practical insights into designing the practical system.
- The power dissipation by other devices, such as LED Driver circuits, and its comparison with other technologies can be done.
- The BER analysis can be extended for higher-order modulation schemes such as QAM and OFDM.
- In Chapter 3, the channel between the BTS and the VLC AP can be considered a frequency-selective Rayleigh faded channel.
- The NLoS reflection up to 3rd order can be considered in the analysis of the NLoS link from the wall.
- In Chapter 5, the analysis of indoor VLC systems with human blockages can be extended with the random deployment of LEDs as well.
- Also, the proposed indoor VLC system insights can be extended for different room sizes like corridors, factory environments, and shopping malls where both static and dynamic obstacles are present in different configurations.
- An exciting direction could be to study other dimming-based modulation schemes and channel equalization techniques. Moreover, the effect of physical parameters (like LED semiangle, detector FOV, detector size, etc.) on the performance of dimmable VLC systems can also be studied.
- Further, the modeling and characterization of VLC links can be augmented by including the effect of limited BW of LED sources on the achievable data rates. This would give more realistic results and practical target data rates.
- The analysis of the received SNR in Chapter 7, Section 7.4 can be extended for the other modulation schemes such as QAM, PAM.
- An interesting direction for an OIRS-aided indoor VLC system could be the multi-LED, multi-OIRS, and multi-user scenarios. It can be considered with a practical room layout (window and door), including static obstacles such as furniture and dynamic obstacles (humans). Furthermore, find a geometry-dependent solution, a specific pattern of the OIRS so that we do not need to steer the OIRS every time the user location changes.
- The effect of self-blockage of the user can be considered in the OIRS-aided indoor VLC system.

- In addition, for the multi-LED and multi-IRS scenario finding the optimum LED-IRS pair in the presence of static and dynamic blockages with random UE orientation and also discovering the optimum LED tilting (orientation of the LED) of LED towards OIRS so that illumination across the room is maintained.
- Finally, the passive IPS proposed in this thesis can be extended to 3D positioning by taking into account the amplitude of the power peaks in the color snaps of different wavelengths.

Bibliography

- [1] P. H. Pathak, X. Feng, P. Hu, and P. Mohapatra, “Visible light communication, networking, and sensing: A survey, potential and challenges,” *IEEE communications surveys & tutorials*, vol. 17, no. 4, pp. 2047–2077, 2015.
- [2] J. M. Kahn and J. R. Barry, “Wireless infrared communications,” *Proceedings of the IEEE*, vol. 85, no. 2, pp. 265–298, 1997.
- [3] Y. Qiu, H.-H. Chen, and W.-X. Meng, “Channel modeling for visible light communications—a survey,” *Wireless Communications and Mobile Computing*, vol. 16, no. 14, pp. 2016–2034, 2016.
- [4] M. D. Soltani, A. A. Purwita, Z. Zeng, H. Haas, and M. Safari, “Modeling the random orientation of mobile devices: Measurement, analysis and LiFi use case,” *IEEE Transactions on Communications*, vol. 67, no. 3, pp. 2157–2172, 2018.
- [5] W. S. McCulloch and W. Pitts, “A logical calculus of the ideas immanent in nervous activity,” *The bulletin of mathematical biophysics*, vol. 5, no. 4, pp. 115–133, 1943.
- [6] J. E. Dayhoff, *Neural network architectures: an introduction*. Van Nostrand Reinhold Co., 1990.
- [7] L. Feng, R. Q. Hu, J. Wang, P. Xu, and Y. Qian, “Applying VLC in 5g networks: Architectures and key technologies,” *IEEE Network*, vol. 30, no. 6, pp. 77–83, November 2016.
- [8] L. Shi, W. Li, X. Zhang, Y. Zhang, G. Chen, and A. Vladimirescu, “Experimental 5G new radio integration with VLC,” in *2018 25th IEEE International Conference on Electronics, Circuits and Systems (ICECS)*, Dec 2018, pp. 61–64.
- [9] J. E. Mitchell, “Integrated wireless backhaul over optical access networks,” *Journal of Lightwave Technology*, vol. 32, no. 20, pp. 3373–3382, 2014.
- [10] A. Khreishah, S. Shao, A. Gharaibeh, M. Ayyash, H. Elgala, and N. Ansari, “A hybrid RF-VLC system for energy efficient wireless access,” *IEEE Transactions on Green Communications and Networking*, vol. 2, no. 4, pp. 932–944, Dec 2018.
- [11] Z. Ghassemlooy, M. Uysal, M. A. Khalighi, V. Ribeiro, F. Moll, S. Zvanovec, and A. Belmonte, “An overview of optical wireless communications,” *Optical Wireless Communications*, pp. 1–23, 2016.

- [12] T. Komine and M. Nakagawa, "Fundamental analysis for visible-light communication system using LED lights," *IEEE transactions on Consumer Electronics*, vol. 50, no. 1, pp. 100–107, 2004.
- [13] P.-C. Song, Z.-Y. Wu, X.-D. An, and J. Wang, "Energy efficiency analysis of light-emitting diodes with high modulation bandwidth," *IEEE Electron Device Letters*, vol. 42, no. 7, pp. 1025–1028, 2021.
- [14] J. S. B. Perlaza, J. C. T. Zafra, M. Morales-Cespedes, A. A. Qidan, B. Bentura, A. G. Armada, and J. M. S. Pena, "Measurement of the modulation bandwidth of high-power chip-on-board leds for vlc systems," in *2022 13th International Symposium on Communication Systems, Networks and Digital Signal Processing (CSNDSP)*, 2022, pp. 38–42.
- [15] J. Grubor, S. Randel, K.-D. Langer, and J. W. Walewski, "Broadband information broadcasting using LED-based interior lighting," *Journal of Lightwave technology*, vol. 26, no. 24, pp. 3883–3892, 2008.
- [16] L. Feng, R. Q. Hu, J. Wang, P. Xu, and Y. Qian, "Applying VLC in 5G networks: Architectures and key technologies," *IEEE Network*, vol. 30, no. 6, pp. 77–83, 2016.
- [17] A. Jovicic, J. Li, and T. Richardson, "Visible light communication: opportunities, challenges and the path to market," *IEEE Communications Magazine*, vol. 51, no. 12, pp. 26–32, 2013.
- [18] D. Karunatilaka, F. Zafar, V. Kalavally, and R. Parthiban, "LED based indoor visible light communications: State of the art," *IEEE Communications Surveys & Tutorials*, vol. 17, no. 3, pp. 1649–1678, 2015.
- [19] H. Elgala, R. Mesleh, and H. Haas, "Indoor optical wireless communication: potential and state-of-the-art," *IEEE Communications Magazine*, vol. 49, no. 9, pp. 56–62, 2011.
- [20] A. Singh, G. Ghatak, A. Srivastava, V. A. Bohara, and A. K. Jagadeesan, "Performance analysis of indoor communication system using off-the-shelf LEDs with human blockages," *IEEE Open Journal of the Communications Society*, vol. 2, pp. 187–198, 2021.
- [21] P. A. Haigh, S. T. Le, S. Zvanovec, Z. Ghassemlooy, P. Luo, T. Xu, P. Chvojka, T. Kanesan, E. Giacomidis, P. Canyelles-Pericas, H. L. Minh, W. Popoola, S. Rajbhandari, I. Papakonstantinou, and I. Darwazeh, "Multi-band carrier-less amplitude and phase modulation for bandlimited visible light communications systems," *IEEE Wireless Communications*, vol. 22, no. 2, pp. 46–53, 2015.
- [22] N. Chi, Y. Zhou, Y. Wei, and F. Hu, "Visible light communication in 6g: Advances, challenges, and prospects," *IEEE Vehicular Technology Magazine*, vol. 15, no. 4, pp. 93–102, 2020.
- [23] H. Ma, L. Lampe, and S. Hranilovic, "Integration of indoor visible light and power line communication systems," in *2013 IEEE 17th International Symposium on Power Line Communications and Its Applications*. IEEE, 2013, pp. 291–296.
- [24] M. Zhang and Z. Zhang, "Fractionally spaced equalization in visible light communication," in *2013 IEEE Wireless Communications and Networking Conference (WCNC)*. IEEE, 2013, pp. 4282–4287.

- [25] C.-W. Chow, C. Yeh, Y. Liu, and Y. Liu, “Improved modulation speed of LED visible light communication system integrated to main electricity network,” *Electronics letters*, vol. 47, no. 15, pp. 867–868, 2011.
- [26] M. Kavehrad, “Sustainable energy-efficient wireless applications using light,” *IEEE Communications Magazine*, vol. 48, no. 12, pp. 66–73, 2010.
- [27] J. K. Kim and E. F. Schubert, “Transcending the replacement paradigm of solid-state lighting,” *Optics Express*, vol. 16, no. 26, pp. 21 835–21 842, 2008.
- [28] N. Bardsley, S. Bland, L. Pattison, M. Pattison, K. Stober, F. Welsh, and M. Yamada, “Solid-state lighting research and development multi-year program plan,” *US Department of Energy*, 2014.
- [29] D. Karunatilaka, F. Zafar, V. Kalavally, and R. Parthiban, “LED based indoor visible light communications: State of the art,” *IEEE Communications Surveys & Tutorials*, vol. 17, no. 3, pp. 1649–1678, 2015.
- [30] S. U. Rehman, S. Ullah, P. H. J. Chong, S. Yongchareon, and D. Komosny, “Visible light communication: a system perspective—overview and challenges,” *Sensors*, vol. 19, no. 5, p. 1153, 2019.
- [31] J. Armstrong, R. J. Green, and M. D. Higgins, “Comparison of three receiver designs for optical wireless communications using white LEDs,” *IEEE communications letters*, vol. 16, no. 5, pp. 748–751, 2012.
- [32] I. E. Lee, M. L. Sim, and F. W.-L. Kung, “Performance enhancement of outdoor visible-light communication system using selective combining receiver,” *IET optoelectronics*, vol. 3, no. 1, pp. 30–39, 2009.
- [33] J. Vučić, C. Kottke, S. Nerreter, K.-D. Langer, and J. W. Walewski, “513 Mbit/s visible light communications link based on DMT-modulation of a white LED,” *Journal of lightwave technology*, vol. 28, no. 24, pp. 3512–3518, 2010.
- [34] A. H. Azhar, T.-A. Tran, and D. O’Brien, “A gigabit/s indoor wireless transmission using MIMO-OFDM visible-light communications,” *IEEE photonics technology letters*, vol. 25, no. 2, pp. 171–174, 2012.
- [35] F. R. Gfeller and U. Bapst, “Wireless in-house data communication via diffuse infrared radiation,” *Proceedings of the IEEE*, vol. 67, no. 11, pp. 1474–1486, 1979.
- [36] A. J. Moreira, R. T. Valadas, and A. de Oliveira Duarte, “Optical interference produced by artificial light,” *Wireless Networks*, vol. 3, no. 2, pp. 131–140, 1997.
- [37] Y. Zeng, P. H. Pathak, C. Xu, and P. Mohapatra, “Your AP knows how you move: fine-grained device motion recognition through WiFi,” in *Proceedings of the 1st ACM workshop on Hot topics in wireless*, 2014, pp. 49–54.
- [38] J. Wang, D. Vasisth, and D. Katabi, “RF-IDraw: Virtual touch screen in the air using RF signals,” *ACM SIGCOMM Computer Communication Review*, vol. 44, no. 4, pp. 235–246, 2014.

- [39] D. H. Kwon and R. Gebhardt, “An affordable, accessible human motion controlled interactive robot and simulation through ROS and azure kinect,” in *Companion of the 2021 ACM/IEEE International Conference on Human-Robot Interaction*, 2021, pp. 649–650.
- [40] M. Uysal, Z. Ghassemlooy, A. Bekkali, A. Kadri, and H. Menouar, “Visible light communication for vehicular networking: Performance study of a V2V system using a measured headlamp beam pattern model,” *IEEE Vehicular Technology Magazine*, vol. 10, no. 4, pp. 45–53, 2015.
- [41] M. Karbalayghareh, F. Miramirkhani, H. B. Eldeeb, R. C. Kizilirmak, S. M. Sait, and M. Uysal, “Channel modelling and performance limits of vehicular visible light communication systems,” *IEEE Transactions on Vehicular Technology*, vol. 69, no. 7, pp. 6891–6901, 2020.
- [42] Y. Zhuang, L. Hua, L. Qi, J. Yang, P. Cao, Y. Cao, Y. Wu, J. Thompson, and H. Haas, “A survey of positioning systems using visible LED lights,” *IEEE Communications Surveys & Tutorials*, vol. 20, no. 3, pp. 1963–1988, 2018.
- [43] J. Luo, L. Fan, and H. Li, “Indoor positioning systems based on visible light communication: State of the art,” *IEEE Communications Surveys & Tutorials*, vol. 19, no. 4, pp. 2871–2893, 2017.
- [44] K. Saxena, R. Raj, and A. Dixit, “A novel optimization approach for transmitter semi-angle and multiple transmitter configurations in indoor visible light communication links,” in *2018 9th International Conference on Computing, Communication and Networking Technologies (ICCCNT)*. IEEE, 2018, pp. 1–7.
- [45] M. S. Shur and R. Zukauskas, “Solid-state lighting: toward superior illumination,” *Proceedings of the IEEE*, vol. 93, no. 10, pp. 1691–1703, 2005.
- [46] I. Din and H. Kim, “Energy-efficient brightness control and data transmission for visible light communication,” *IEEE photonics technology letters*, vol. 26, no. 8, pp. 781–784, 2014.
- [47] E. T. Won, “IEEE 802.15 WPAN™ task group 7 (TG7) visible light communication,” 2009.
- [48] N. T. Dang and V. V. Mai, “A PHY/MAC cross-layer analysis for IEEE 802.15. 7 uplink visible local area network,” *IEEE Photonics Journal*, vol. 11, no. 3, pp. 1–17, 2019.
- [49] S. Rajagopal, R. D. Roberts, and S.-K. Lim, “IEEE 802.15. 7 visible light communication: modulation schemes and dimming support,” *IEEE Communications Magazine*, vol. 50, no. 3, pp. 72–82, 2012.
- [50] A. Wilkins, J. Veitch, and B. Lehman, “LED lighting flicker and potential health concerns: IEEE standard PAR1789 update,” in *2010 IEEE Energy Conversion Congress and Exposition*. IEEE, 2010, pp. 171–178.
- [51] S. M. Berman, D. S. Greenhouse, I. L. Bailey, R. D. Clear, and T. W. Raasch, “Human electroretinogram responses to video displays, fluorescent lighting, and other high frequency sources.” *Optometry and vision science: official publication of the American Academy of Optometry*, vol. 68, no. 8, pp. 645–662, 1991.

- [52] D. Wu, Z. Ghassemlooy, H. Le Minh, S. Rajbhandari, M. A. Khalighi, and X. Tang, "Optimisation of lambertian order for indoor non-directed optical wireless communication," in *2012 1st IEEE International Conference on Communications in China Workshops (ICCC)*, 2012, pp. 43–48.
- [53] L. E. M. Matheus, A. B. Vieira, L. F. Vieira, M. A. Vieira, and O. Gnawali, "Visible light communication: concepts, applications and challenges," *IEEE Communications Surveys & Tutorials*, vol. 21, no. 4, pp. 3204–3237, 2019.
- [54] G. Pang, T. Kwan, C.-H. Chan, and H. Liu, "LED traffic light as a communications device," in *Proceedings 199 IEEE/IEEJ/JSAI International Conference on Intelligent Transportation Systems (Cat. No. 99TH8383)*. IEEE, 1999, pp. 788–793.
- [55] K. Kulhavy, "Home: ronja," *RONJA*, 2012.
- [56] Y. Tanaka, S. Haruyama, and M. Nakagawa, "Wireless optical transmissions with white colored LED for wireless home links," in *11th IEEE International Symposium on Personal Indoor and Mobile Radio Communications. PIMRC 2000. Proceedings (Cat. No. 00TH8525)*, vol. 2. IEEE, 2000, pp. 1325–1329.
- [57] J. Vucic, C. Kottke, S. Nerreter, K. Habel, A. Buttner, K.-D. Langer, and J. Walewski, "125 Mbit/s over 5 m wireless distance by use of OOK-modulated phosphorescent white LEDs," in *2009 35th European Conference on Optical Communication*. IEEE, 2009, pp. 1–2.
- [58] J. Vučić, C. Kottke, K. Habel, and K.-D. Langer, "803 Mbit/s visible light WDM link based on DMT modulation of a single RGB LED luminary," in *Optical Fiber Communication Conference*. Optical Society of America, 2011, p. OWB6.
- [59] C. Kottke, K. Habel, L. Grobe, J. Hilt, L. F. del Rosal, A. Paraskevopoulos, and K.-D. Langer, "Single-channel wireless transmission at 806 Mbit/s using a white-light LED and a PIN-based receiver," in *2012 14th International Conference on Transparent Optical Networks (ICTON)*. IEEE, 2012, pp. 1–4.
- [60] Z. Wang, J. Chen, W.-D. Zhong, C. Yu, and W. Chen, "User-oriented visible light communication system with dimming control scheme," in *Optical Communications and Networks (ICOON), 2012 11th International Conference on*. IEEE, 2012, pp. 1–4.
- [61] S. I. Hussain, M. M. Abdallah, and K. A. Qaraq, "Hybrid radio-visible light downlink performance in RF sensitive indoor environments," in *Communications, Control and Signal Processing (ISCCSP), 2014 6th International Symposium on*. IEEE, 2014, pp. 81–84.
- [62] P. Pešek, S. Zvanovec, P. Chvojka, M. R. Bhatnagar, Z. Ghassemlooy, and P. Saxena, "Mobile user connectivity in relay-assisted visible light communications," *Sensors*, vol. 18, no. 4, 1125, 07.04.2018.
- [63] R. C. Kizilirmak, O. Narmanlioglu, and M. Uysal, "Relay-assisted OFDM-based visible light communications," *IEEE Transactions on Communications*, vol. 63, no. 10, pp. 3765–3778, 2015.

- [64] O. Narmanlioglu, R. C. Kizilirmak, F. Miramirkhani, and M. Uysal, “Cooperative visible light communications with full-duplex relaying,” *IEEE Photonics Journal*, vol. 9, no. 3, pp. 1–11, June 2017.
- [65] D. A. Basnayaka and H. Haas, “Hybrid RF and VLC systems: Improving user data rate performance of VLC systems,” in *Vehicular Technology Conference (VTC Spring), 2015 IEEE 81st*. IEEE, 2015, pp. 1–5.
- [66] M. Hammouda, S. Akin, A. M. Vegni, H. Haas, and J. Peissig, “Link selection in hybrid RF/VLC systems under statistical queueing constraints,” *IEEE Transactions on Wireless Communications*, vol. 17, no. 4, pp. 2738–2754, April 2018.
- [67] M. Kashef, M. Ismail, M. Abdallah, K. Qaraqe, and E. Serpedin, “Power allocation for maximizing energy efficiency of mixed RF/VLC wireless networks,” in *2015 23rd European Signal Processing Conference (EUSIPCO)*, Aug 2015, pp. 1441–1445.
- [68] M. Kashef, M. Ismail, M. Abdallah, K. A. Qaraqe, and E. Serpedin, “Energy efficient resource allocation for mixed RF/VLC heterogeneous wireless networks,” *IEEE Journal on Selected Areas in Communications*, vol. 34, no. 4, pp. 883–893, 2016.
- [69] X. Liu, S. Chandrasekhar, T. Wood, R. Tkach, P. Winzer, E. Burrows, and A. Chraplyvy, “M-ary pulse-position modulation and frequency-shift keying with additional polarization/phase modulation for high-sensitivity optical transmission,” *Optics Express*, vol. 19, no. 26, pp. B868–B881, 2011.
- [70] X. Liu, T. H. Wood, R. W. Tkach, and S. Chandrasekhar, “Demonstration of record sensitivities in optically preamplified receivers by combining PDM-QPSK and M-Ary pulse-position modulation,” *Journal of Lightwave Technology*, vol. 30, no. 4, pp. 406–413, Feb 2012.
- [71] H. Selmy, H. M. H. Shalaby, and Z. Kawasaki, “Proposal and performance evaluation of a hybrid BPSK-modified MPPM technique for optical fiber communications systems,” *Journal of Lightwave Technology*, vol. 31, no. 22, pp. 3535–3545, Nov 2013.
- [72] —, “Performance enhancement of QPSK modulation using hybrid QPSK-modified MPPM in optical fiber communications,” in *2013 Second International Japan-Egypt Conference on Electronics, Communications and Computers (JEC-ECC)*, Dec 2013, pp. 140–142.
- [73] H. S. Khallaf, H. M. H. Shalaby, and Z. Kawasaki, “Proposal of a hybrid OFDM-PPM technique for free space optical communications systems,” in *2013 IEEE Photonics Conference*, Sept 2013, pp. 287–288.
- [74] H. S. Khallaf, H. M. Shalaby, J. M. Garrido-Balsells, and S. Sampei, “Performance analysis of a hybrid QAM-MPPM technique over turbulence-free and gamma-gamma free-space optical channels,” *IEEE/OSA Journal of Optical Communications and Networking*, vol. 9, no. 2, pp. 161–171, 2017.
- [75] P. Lei, Q. Wang, and H. Zou, “Designing LED array for uniform illumination based on local search algorithm,” *Journal of the European Optical Society-Rapid publications*, vol. 9, 2014.

- [76] Z. Wang, W.-D. Zhong, C. Yu, and J. Chen, "A novel LED arrangement to reduce SNR fluctuation for multi-user in visible light communication systems," in *2011 8th International Conference on Information, Communications & Signal Processing*. IEEE, 2011, pp. 1–4.
- [77] G. P. Varma, R. Sushma, V. Sharma, A. Kumar, and G. Sharma, "Power allocation for uniform illumination with stochastic LED arrays," *Optics express*, vol. 25, no. 8, pp. 8659–8669, 2017.
- [78] I. Stefan and H. Haas, "Analysis of optimal placement of LED arrays for visible light communication," in *2013 IEEE 77th Vehicular Technology Conference (VTC Spring)*, June 2013, pp. 1–5.
- [79] S. Pal, "Optimization of LED array for uniform illumination over a target plane by evolutionary programming," *Applied optics*, vol. 54, no. 27, pp. 8221–8227, 2015.
- [80] R. Guan, J.-Y. Wang, Y.-P. Wen, J.-B. Wang, and M. Chen, "PSO-based LED deployment optimization for visible light communications," in *2013 International Conference on Wireless Communications and Signal Processing*. IEEE, 2013, pp. 1–6.
- [81] M. T. Niaz, F. Imdad, S. Kim, and H. S. Kim, "Deployment methods of visible light communication lights for energy efficient buildings," *Optical Engineering*, vol. 55, no. 10, p. 106113, 2016.
- [82] S. Pergoloni, M. Biagi, S. Colonnese, R. Cusani, and G. Scarano, "Optimized LEDs footprinting for indoor visible light communication networks," *IEEE Photonics Technology Letters*, vol. 28, no. 4, pp. 532–535, Feb 2016.
- [83] Y. Liu, Y. Peng, Y. Liu, and K. Long, "Optimization of receiving power distribution using genetic algorithm for visible light communication," in *AOPC 2015: Optical Fiber Sensors and Applications*, vol. 9679. International Society for Optics and Photonics, 2015, p. 96790I.
- [84] T. Tang, T. Shang, and Q. Li, "Impact of multiple shadows on visible light communication channel," *IEEE Communications Letters*, vol. 25, no. 2, pp. 513–517, 2021.
- [85] C. Chen, D. A. Basnayaka, and H. Haas, "Downlink performance of optical attocell networks," *Journal of Lightwave Technology*, vol. 34, no. 1, pp. 137–156, 2016.
- [86] H. Tabassum and E. Hossain, "Coverage and rate analysis for co-existing RF/VLC downlink cellular networks," *IEEE Transactions on Wireless Communications*, vol. 17, no. 4, pp. 2588–2601, 2018.
- [87] M. Gapeyenko, A. Samuylov, M. Gerasimenko, D. Moltchanov, S. Singh, E. Aryafar, S.-p. Yeh, N. Himayat, S. Andreev, and Y. Koucheryavy, "Analysis of human-body blockage in urban millimeter-wave cellular communications," in *2016 IEEE International Conference on Communications (ICC)*. IEEE, 2016, pp. 1–7.
- [88] M. A. Dastgheib, H. Beyranvand, and J. A. Salehi, "Optimal visible light communication access point placement under stationary distribution of users' mobility," in *2018 9th International Symposium on Telecommunications (IST)*. IEEE, 2018, pp. 96–101.

- [89] C. Bettstetter, H. Hartenstein, and X. Pérez-Costa, “Stochastic properties of the random waypoint mobility model,” *Wireless Networks*, vol. 10, no. 5, pp. 555–567, 2004.
- [90] M. A. Dastgheib, H. Beyranvand, J. A. Salehi, and M. Maier, “Mobility-aware resource allocation in VLC networks using t-step look-ahead policy,” *Journal of Lightwave Technology*, vol. 36, no. 23, pp. 5358–5370, Dec 2018.
- [91] L. Feng, R. Q. Hu, J. Wang, and Y. Qian, “Deployment issues and performance study in a relay-assisted indoor visible light communication system,” *IEEE Systems Journal*, vol. 13, no. 1, pp. 562–570, March 2019.
- [92] X. Hong, M. Gerla, G. Pei, and C.-C. Chiang, “A group mobility model for ad hoc wireless networks,” in *Proceedings of the 2nd ACM international workshop on Modeling, analysis and simulation of wireless and mobile systems*, 1999, pp. 53–60.
- [93] I. Rhee, M. Shin, S. Hong, K. Lee, S. J. Kim, and S. Chong, “On the levy-walk nature of human mobility,” *IEEE/ACM transactions on networking*, vol. 19, no. 3, pp. 630–643, 2011.
- [94] F. Ashtiani, J. A. Salehi, and M. R. Aref, “Mobility modeling and analytical solution for spatial traffic distribution in wireless multimedia networks,” *IEEE Journal on Selected Areas in Communications*, vol. 21, no. 10, pp. 1699–1709, 2003.
- [95] G. H. Mohimani, F. Ashtiani, A. Javanmard, and M. Hamdi, “Mobility modeling, spatial traffic distribution, and probability of connectivity for sparse and dense vehicular ad hoc networks,” *IEEE Transactions on Vehicular Technology*, vol. 58, no. 4, pp. 1998–2007, 2008.
- [96] T. Camp, J. Boleng, and V. Davies, “A survey of mobility models for ad hoc network research,” *Wireless communications and mobile computing*, vol. 2, no. 5, pp. 483–502, 2002.
- [97] M. D. Soltani, Z. Zeng, I. Tavakkolnia, H. Haas, and M. Safari, “Random receiver orientation effect on channel gain in LiFi systems,” in *2019 IEEE Wireless Communications and Networking Conference (WCNC)*. IEEE, 2019, pp. 1–6.
- [98] M. D. Soltani, X. Wu, M. Safari, and H. Haas, “Access point selection in Li-Fi cellular networks with arbitrary receiver orientation,” in *2016 IEEE 27th Annual International Symposium on Personal, Indoor, and Mobile Radio Communications (PIMRC)*. IEEE, 2016, pp. 1–6.
- [99] J.-Y. Wang, Q.-L. Li, J.-X. Zhu, and Y. Wang, “Impact of receiver’s tilted angle on channel capacity in VLCs,” *Electronics Letters*, vol. 53, no. 6, pp. 421–423, 2017.
- [100] J. Zhao, “A survey of intelligent reflecting surfaces (IRSs): Towards 6G wireless communication networks,” *arXiv preprint arXiv:1907.04789*, 2019.
- [101] Q. Wu and R. Zhang, “Towards smart and reconfigurable environment: Intelligent reflecting surface aided wireless network,” *IEEE Communications Magazine*, vol. 58, no. 1, pp. 106–112, 2019.

- [102] X. Yuan, Y.-J. A. Zhang, Y. Shi, W. Yan, and H. Liu, “Reconfigurable-intelligent-surface empowered wireless communications: Challenges and opportunities,” *IEEE Wireless Communications*, vol. 28, no. 2, pp. 136–143, 2021.
- [103] E. Basar, M. Di Renzo, J. De Rosny, M. Debbah, M.-S. Alouini, and R. Zhang, “Wireless communications through reconfigurable intelligent surfaces,” *IEEE access*, vol. 7, pp. 116 753–116 773, 2019.
- [104] Ö. Özdogan, E. Björnson, and E. G. Larsson, “Intelligent reflecting surfaces: Physics, propagation, and pathloss modeling,” *IEEE Wireless Communications Letters*, vol. 9, no. 5, pp. 581–585, 2019.
- [105] A. M. Abdelhady, O. Amin, A. Chaaban, B. Shihada, and M.-S. Alouini, “Downlink resource allocation for dynamic TDMA-based VLC systems,” *IEEE Transactions on Wireless Communications*, vol. 18, no. 1, pp. 108–120, 2018.
- [106] —, “Spectral-efficiency—illumination pareto front for energy harvesting enabled VLC systems,” *IEEE Transactions on Communications*, vol. 67, no. 12, pp. 8557–8572, 2019.
- [107] A. M. Abdelhady, O. Amin, B. Shihada, and M.-S. Alouini, “Spectral efficiency and energy harvesting in multi-cell SLIPT systems,” *IEEE Transactions on Wireless Communications*, vol. 19, no. 5, pp. 3304–3318, 2020.
- [108] A. M. Abdelhady, A. K. S. Salem, O. Amin, B. Shihada, and M.-S. Alouini, “Visible light communications via intelligent reflecting surfaces: Metasurfaces vs mirror arrays,” *IEEE Open Journal of the Communications Society*, vol. 2, pp. 1–20, 2021.
- [109] L. Qian, X. Chi, L. Zhao, and A. Chaaban, “Secure visible light communications via intelligent reflecting surfaces,” in *ICC 2021 - IEEE International Conference on Communications*, 2021, pp. 1–6.
- [110] B. Cao, M. Chen, Z. Yang, M. Zhang, J. Zhao, and M. Chen, “Reflecting the light: Energy efficient visible light communication with reconfigurable intelligent surface,” in *2020 IEEE 92nd Vehicular Technology Conference (VTC2020-Fall)*, 2020, pp. 1–5.
- [111] M. A. Arfaoui, A. Ghrayeb, and C. Assi, “Integration of IRS in indoor VLC systems: Challenges, potential and promising solutions,” *arXiv preprint arXiv:2101.05927*, 2021.
- [112] S. Aboagye, T. M. N. Ngatched, O. A. Dobre, and A. R. Ndjiongue, “Intelligent reflecting surface-aided indoor visible light communication systems,” *IEEE Communications Letters*, vol. 25, no. 12, pp. 3913–3917, 2021.
- [113] M. Najafi, B. Schmauss, and R. Schober, “Intelligent reflecting surfaces for free space optical communication systems,” *IEEE Transactions on Communications*, vol. 69, no. 9, pp. 6134–6151, 2021.
- [114] M. Najafi and R. Schober, “Intelligent reflecting surfaces for free space optical communications,” in *2019 IEEE Global Communications Conference (GLOBECOM)*, 2019, pp. 1–7.

- [115] P. Huynh and M. Yoo, "VLC-based positioning system for an indoor environment using an image sensor and an accelerometer sensor," *Sensors*, vol. 16, no. 6, p. 783, 2016.
- [116] L. Li, P. Hu, C. Peng, G. Shen, and F. Zhao, "Epsilon: A visible light based positioning system," in *11th USENIX Symposium on Networked Systems Design and Implementation (NSDI 14)*, 2014, pp. 331–343.
- [117] S.-Y. Jung and C.-S. Park, "Lighting LEDs based indoor positioning system using received signal strength ratio," *Proceedings of 3DSA2013*, vol. 8, no. 5, 2013.
- [118] A. Singh, A. Srivastava, V. A. Bohara, and A. K. Jagadeesan, "Performance of indoor VLC system under random placement of LEDs with nonimaging and imaging receiver," *IEEE Systems Journal*, pp. 1–12, 2020.
- [119] Y. Gu, A. Lo, and I. Niemegeers, "A survey of indoor positioning systems for wireless personal networks," *IEEE Communications surveys & tutorials*, vol. 11, no. 1, pp. 13–32, 2009.
- [120] M. Obeed, A. M. Salhab, M.-S. Alouini, and S. A. Zummo, "On optimizing VLC networks for downlink multi-user transmission: A survey," *IEEE Communications Surveys & Tutorials*, vol. 21, no. 3, pp. 2947–2976, 2019.
- [121] M. Dehghani Soltani, X. Wu, M. Safari, and H. Haas, "Access point selection in Li-Fi cellular networks with arbitrary receiver orientation," in *2016 IEEE 27th Annual International Symposium on Personal, Indoor, and Mobile Radio Communications (PIMRC)*, 2016, pp. 1–6.
- [122] X. Wu, M. Safari, and H. Haas, "Bidirectional allocation game in visible light communications," in *2016 IEEE 83rd Vehicular Technology Conference (VTC Spring)*, 2016, pp. 1–5.
- [123] R. Zhang, Y. Cui, H. Claussen, H. Haas, and L. Hanzo, "Anticipatory association for indoor visible light communications: Light, follow me!" *IEEE Transactions on Wireless Communications*, vol. 17, no. 4, pp. 2499–2510, 2018.
- [124] R. Jiang, Q. Wang, H. Haas, and Z. Wang, "Joint user association and power allocation for cell-free visible light communication networks," *IEEE Journal on Selected Areas in Communications*, vol. 36, no. 1, pp. 136–148, 2018.
- [125] C. Chen, D. A. Basnayaka, and H. Haas, "Downlink performance of optical attocell networks," *Journal of Lightwave Technology*, vol. 34, no. 1, pp. 137–156, 2016.
- [126] S. Cincotta, A. Neild, and J. Armstrong, "Luminaire reference points (LRP) in visible light positioning using hybrid imaging-photodiode (HIP) receivers," in *2019 International Conference on Indoor Positioning and Indoor Navigation (IPIN)*, 2019, pp. 1–8.
- [127] M. S. Demir and M. Uysal, "A cross-layer design for dynamic resource management of VLC networks," *IEEE Transactions on Communications*, vol. 69, no. 3, pp. 1858–1867, 2021.

- [128] S. Aboagye, T. M. N. Ngatched, O. A. Dobre, and A. Ibrahim, “Joint access point assignment and power allocation in multi-tier hybrid RF/VLC hetnets,” *IEEE Transactions on Wireless Communications*, vol. 20, no. 10, pp. 6329–6342, 2021.
- [129] P. Chvojka, S. Zvanovec, P. A. Haigh, and Z. Ghassemlooy, “Channel characteristics of visible light communications within dynamic indoor environment,” *Journal of Lightwave Technology*, vol. 33, no. 9, pp. 1719–1725, 2015.
- [130] C. Chen, D. A. Basnayaka, X. Wu, and H. Haas, “Efficient analytical calculation of non-line-of-sight channel impulse response in visible light communications,” *Journal of Lightwave Technology*, vol. 36, no. 9, pp. 1666–1682, 2017.
- [131] F. Miramirkhani and M. Uysal, “Channel modeling and characterization for visible light communications,” *IEEE Photonics Journal*, vol. 7, no. 6, pp. 1–16, 2015.
- [132] V. Pohl, V. Jungnickel, and C. Von Helmolt, “Integrating-sphere diffuser for wireless infrared communication,” *IEE Proceedings-Optoelectronics*, vol. 147, no. 4, pp. 281–285, 2000.
- [133] S.-i. Choi, “Analysis of VLC channel based on the shapes of white-light LED lighting,” in *2012 Fourth International Conference on Ubiquitous and Future Networks (ICUFN)*. IEEE, 2012, pp. 1–5.
- [134] J. Ding, K. Wang, and Z. Xu, “Accuracy analysis of different modeling schemes in indoor visible light communications with distributed array sources,” in *2014 9th International Symposium on Communication Systems, Networks & Digital Sign (CSNDSP)*. IEEE, 2014, pp. 1005–1010.
- [135] K. Majeed and S. Hranilovic, “Performance bounds on passive indoor positioning using visible light,” *Journal of Lightwave Technology*, vol. 38, no. 8, pp. 2190–2200, 2020.
- [136] M. Jacob, S. Priebe, T. Kürner, M. Peter, M. Wisotzki, R. Felbecker, and W. Keusgen, “Fundamental analyses of 60 GHz human blockage,” in *2013 7th European Conference on Antennas and Propagation (EuCAP)*. IEEE, 2013, pp. 117–121.
- [137] A. A. Purwita, M. D. Soltani, M. Safari, and H. Haas, “Handover probability of hybrid LiFi/RF-based networks with randomly-oriented devices,” in *2018 IEEE 87th Vehicular Technology Conference (VTC Spring)*. IEEE, 2018, pp. 1–5.
- [138] S. Jivkova and M. Kavehrad, “Shadowing and blockage in indoor optical wireless communications,” in *GLOBECOM’03. IEEE Global Telecommunications Conference (IEEE Cat. No. 03CH37489)*, vol. 6. IEEE, 2003, pp. 3269–3273.
- [139] S. Rajagopal, R. D. Roberts, and S. Lim, “IEEE 802.15.7 visible light communication: modulation schemes and dimming support,” *IEEE Communications Magazine*, vol. 50, no. 3, pp. 72–82, March 2012.
- [140] Z. Ghassemlooy, W. Popoola, and S. Rajbhandari, *Optical wireless communications: system and channel modelling with Matlab®*. CRC press, 2012.

- [141] F. Miramirkhani and M. Uysal, "Channel modeling and characterization for visible light communications," *IEEE Photonics Journal*, vol. 7, no. 6, pp. 1–16, 2015.
- [142] Y. d. J. Bultitude and T. Rautiainen, "IST-4-027756 WINNER II D1. 1.2 V1. 2 WINNER II channel models," *EBITG, TUI, UOULU, CU/CRC, NOKIA, Tech. Rep., Tech. Rep.*, 2007.
- [143] D. Wu, Z. Ghassemlooy, H. Le Minh, S. Rajbhandari, M.-A. Khalighi, and X. Tang, "Optimisation of lambertian order for indoor non-directed optical wireless communication," in *2012 1st IEEE International Conference on Communications in China Workshops (ICCC)*. IEEE, 2012, pp. 43–48.
- [144] A. Al-Kinani, C. Wang, L. Zhou, and W. Zhang, "Optical wireless communication channel measurements and models," *IEEE Communications Surveys Tutorials*, vol. 20, no. 3, pp. 1939–1962, thirdquarter 2018.
- [145] A. B. Sediq and H. Yanikomeroğlu, "Performance analysis of selection combining of signals with different modulation levels in cooperative communications," *IEEE Transactions on Vehicular Technology*, vol. 60, no. 4, pp. 1880–1887, May 2011.
- [146] S. Arnon, *Visible Light Communication*, 1st ed. New York, NY, USA: Cambridge University Press, 2015.
- [147] J. N. Laneman, D. N. Tse, and G. W. Wornell, "Cooperative diversity in wireless networks: Efficient protocols and outage behavior," *IEEE Transactions on Information theory*, vol. 50, no. 12, pp. 3062–3080, 2004.
- [148] Y. Han, A. Pandharipande, and S. H. Ting, "Cooperative decode-and-forward relaying for secondary spectrum access," *IEEE Transactions on Wireless Communications*, vol. 8, no. 10, 2009.
- [149] Y. Zhu, C. Gong, J. Luo, M. Jin, X. Jin, and Z. Xu, "Indoor non-line of sight visible light communication with a bi-lstm neural network," in *2020 IEEE International Conference on Communications Workshops (ICC Workshops)*, 2020, pp. 1–6.
- [150] Z. Wang, C. Yu, W.-D. Zhong, J. Chen, and W. Chen, "Performance of a novel LED lamp arrangement to reduce SNR fluctuation for multi-user visible light communication systems," *Optics express*, vol. 20, no. 4, pp. 4564–4573, 2012.
- [151] Z. Feng, G. Papageorgiou, Q. Gao, A. F. Atya, S. V. Krishnamurthy, and G. Chen, "Performance of visible light communications with dimming controls," in *Wireless Communications and Networking Conference (WCNC), 2014 IEEE*. IEEE, 2014, pp. 1756–1761.
- [152] Y. Yang, Z. Zeng, J. Cheng, and C. Guo, "An enhanced DCO-OFDM scheme for dimming control in visible light communication systems," *IEEE Photonics Journal*, vol. 8, no. 3, pp. 1–13, 2016.
- [153] F. Zafar, D. Karunatilaka, and R. Parthiban, "Dimming schemes for visible light communication: the state of research," *IEEE Wireless Communications*, vol. 22, no. 2, pp. 29–35, April 2015.

- [154] B. Glushko, D. Kin, and A. Shar, "High bandwidth optical wireless network for gigabit communication," in *IEEE Global High Tech Congress on Electronics*, 2013, pp. 114–120.
- [155] Z. Chen, D. Tsonev, and H. Haas, "Improving SINR in indoor cellular visible light communication networks," in *Proceedings of IEEE International Conference on Communications (ICC)*, 2014, pp. 3383–3388.
- [156] A. Nuwanpriya, S. Ho, and C. S. Chen, "Indoor MIMO visible light communications: Novel angle diversity receivers for mobile users," *IEEE Journal on Selected Areas in Communications*, vol. 33, no. 9, pp. 1780–1792, 2015.
- [157] C. He, T. Q. Wang, and J. Armstrong, "Performance of optical receivers using photodetectors with different fields of view in a MIMO ACO-OFDM system," *Journal of Lightwave Technology*, vol. 33, no. 23, pp. 4957–4967, 2015.
- [158] M. Haenggi, "User point processes in cellular networks," *IEEE Wireless Communications Letters*, vol. 6, no. 2, pp. 258–261, April 2017.
- [159] B. Matérn, *Spatial variation*. Springer Science & Business Media, 2013, vol. 36.
- [160] J. Teichmann, F. Ballani, and K. G. van den Boogaart, "Generalizations of matérn's hard-core point processes," *Spatial Statistics*, vol. 3, pp. 33–53, 2013.
- [161] J. M. Kahn, R. You, P. Djahani, A. G. Weisbin, Beh Kian Teik, and A. Tang, "Imaging diversity receivers for high-speed infrared wireless communication," *IEEE Communications Magazine*, vol. 36, no. 12, pp. 88–94, Dec 1998.
- [162] S. Boyd, S. P. Boyd, and L. Vandenberghe, *Convex optimization*. Cambridge university press, 2004.
- [163] I. Neokosmidis, T. Kamalakis, J. W. Walewski, B. Inan, and T. Sphicopoulos, "Impact of nonlinear LED transfer function on discrete multitone modulation: Analytical approach," *IEEE/OSA Journal of Lightwave technology*, vol. 27, no. 22, pp. 4970–4978, 2009.
- [164] Y. Jiang, M. K. Varanasi, and J. Li, "Performance analysis of ZF and MMSE equalizers for MIMO systems: An in-depth study of the high SNR regime," *IEEE Transactions on Information Theory*, vol. 57, no. 4, pp. 2008–2026, April 2011.
- [165] Z. Ghassemlooy, W. Popoola, and S. Rajbhandari, *Optical wireless communications: system and channel modelling with Matlab®*. CRC press, 2017.
- [166] T.-C. Bui, S. Kiravittaya, K. Sripimanwat, and N.-H. Nguyen, "A comprehensive lighting configuration for efficient indoor visible light communication networks," *International journal of optics*, vol. 2016, 2016.
- [167] S. N. Chiu, D. Stoyan, W. S. Kendall, and J. Mecke, *Stochastic geometry and its applications*. John Wiley & Sons, 2013.

- [168] M. Månsson and M. Rudemo, “Random patterns of nonoverlapping convex grains,” *Advances in Applied Probability*, vol. 34, no. 4, pp. 718–738, 2002.
- [169] Z. Zeng, M. Dehghani Soltani, Y. Wang, X. Wu, and H. Haas, “Realistic indoor hybrid wifi and ofdma-based lifi networks,” *IEEE Transactions on Communications*, vol. 68, no. 5, pp. 2978–2991, 2020.
- [170] L. Hua, Y. Zhuang, L. Qi, J. Yang, and L. Shi, “Noise analysis and modeling in visible light communication using allan variance,” *IEEE Access*, vol. 6, pp. 74 320–74 327, 2018.
- [171] C. Le Bas, S. Sahuguede, A. Julien-Vergonjanne, A. Behloui, P. Combeau, and L. Aveneau, “Human body impact on mobile visible light communication link,” in *2016 10th International Symposium on Communication Systems, Networks and Digital Signal Processing (CSNDSP)*. IEEE, 2016, pp. 1–6.
- [172] —, “Impact of receiver orientation and position on visible light communication link performance,” in *2015 4th International Workshop on Optical Wireless Communications (IWOW)*. IEEE, 2015, pp. 1–5.
- [173] R. Ahmad, M. D. Soltani, M. Safari, A. Srivastava, and A. Das, “Reinforcement learning based load balancing for hybrid lifi wifi networks,” *IEEE Access*, vol. 8, pp. 132 273–132 284, 2020.
- [174] Y. Liu, X. Liu, X. Mu, T. Hou, J. Xu, M. Di Renzo, and N. Al-Dhahir, “Reconfigurable intelligent surfaces: Principles and opportunities,” *IEEE Communications Surveys Tutorials*, vol. 23, no. 3, pp. 1546–1577, 2021.
- [175] M. Di Renzo, A. Zappone, M. Debbah, M.-S. Alouini, C. Yuen, J. de Rosny, and S. Tretyakov, “Smart radio environments empowered by reconfigurable intelligent surfaces: How it works, state of research, and the road ahead,” *IEEE Journal on Selected Areas in Communications*, vol. 38, no. 11, pp. 2450–2525, 2020.
- [176] M. Najafi, B. Schmauss, and R. Schober, “Intelligent reflecting surfaces for free space optical communication systems,” *IEEE Transactions on Communications*, vol. 69, no. 9, pp. 6134–6151, 2021.
- [177] A. M. Abdelhady, O. Amin, A. K. S. Salem, M.-S. Alouini, and B. Shihada, “Channel characterization of irs-based visible light communication systems,” *IEEE Transactions on Communications*, vol. 70, no. 3, pp. 1913–1926, 2022.
- [178] F. Aieta, A. Kabiri, P. Genevet, N. Yu, M. A. Kats, Z. Gaburro, and F. Capasso, “Reflection and refraction of light from metasurfaces with phase discontinuities,” *Journal of Nanophotonics*, vol. 6, no. 1, p. 063532, 2012.
- [179] I. Neokosmidis, T. Kamalakis, J. W. Walewski, B. Inan, and T. Sphicopoulos, “Impact of nonlinear LED transfer function on discrete multitone modulation: Analytical approach,” *Journal of Lightwave Technology*, vol. 27, no. 22, pp. 4970–4978, 2009.

- [180] M. A. Arfaoui, M. D. Soltani, I. Tavakkolnia, A. Ghrayeb, C. Assi, H. Haas, and M. Safari, "SNR statistics of indoor mobile VLC users with random device orientation," in *2019 IEEE International Conference on Communications Workshops (ICC Workshops)*, 2019, pp. 1–6.
- [181] V. A. Aalo, C. Mukasa, and G. P. Efthymoglou, "Effect of mobility on the outage and BER performances of digital transmissions over nakagami- m fading channels," *IEEE Transactions on Vehicular Technology*, vol. 65, no. 4, pp. 2715–2721, 2015.
- [182] M. Gapeyenko, A. Samuylov, M. Gerasimenko, D. Moltchanov, S. Singh, E. Aryafar, S.-p. Yeh, N. Himayat, S. Andreev, and Y. Koucheryavy, "Analysis of human-body blockage in urban millimeter-wave cellular communications," in *2016 IEEE International Conference on Communications (ICC)*, 2016, pp. 1–7.
- [183] A. Chakraborty, A. Singh, V. A. Bohara, and A. Srivastava, "A visible light communication based predictive system for the height and location estimation of an obstacle," in *2020 IEEE International Conference on Advanced Networks and Telecommunications Systems (ANTS)*, 2020, pp. 1–6.
- [184] —, "On estimating the location and the 3-D shape of an object in an indoor environment using visible light," *IEEE Photonics Journal*, pp. 1–11, 2022.
- [185] A. Şahin, Y. S. Eroğlu, I. Güvenç, N. Pala, and M. Yüksel, "Hybrid 3-D localization for visible light communication systems," *Journal of Lightwave Technology*, vol. 33, no. 22, pp. 4589–4599, 2015.
- [186] R. Rojas, "The backpropagation algorithm," in *Neural networks*. Springer, 1996, pp. 149–182.
- [187] J. Li, J.-h. Cheng, J.-y. Shi, and F. Huang, "Brief introduction of back propagation (BP) neural network algorithm and its improvement," in *Advances in computer science and information engineering*. Springer, 2012, pp. 553–558.
- [188] Y. Li and Y. Yuan, "Convergence analysis of two-layer neural networks with relu activation," *arXiv preprint arXiv:1705.09886*, 2017.
- [189] X. Yu, M. O. Efe, and O. Kaynak, "A general backpropagation algorithm for feedforward neural networks learning," *IEEE transactions on neural networks*, vol. 13, no. 1, pp. 251–254, 2002.
- [190] J. Jantzen, "Introduction to perceptron networks," *Technical University of Denmark, Lyngby, Denmark, Technical Report*, 1998.
- [191] A. Ranganathan, "The levenberg-marquardt algorithm," *Tutorial on LM algorithm*, vol. 11, no. 1, pp. 101–110, 2004.
- [192] C. Cheng, K. Chau, Y. Sun, and J. Lin, "Long-term prediction of discharges in manwan reservoir using artificial neural network models," in *International Symposium on Neural Networks*. Springer, 2005, pp. 1040–1045.

- [193] F. Burden and D. Winkler, "Bayesian regularization of neural networks," *Artificial neural networks*, pp. 23–42, 2008.
- [194] A. Singh, A. Srivastava, V. A. Bohara, and A. K. Jagadeesan, "Optimal LED power allocation framework for a location-assisted indoor visible light communication system," *IEEE Photonics Journal*, vol. 14, no. 3, pp. 1–14, 2022.
- [195] P. M. Butala, H. Elgala, and T. D. C. Little, "SVD-VLC: A novel capacity maximizing VLC MIMO system architecture under illumination constraints," in *2013 IEEE Globecom Workshops (GC Wkshps)*, 2013, pp. 1087–1092.
- [196] Z. Feng, C. Guo, Z. Ghassemlooy, and Y. Yang, "The spatial dimming scheme for the MU-MIMO-OFDM VLC system," *IEEE Photonics Journal*, vol. 10, no. 5, pp. 1–13, 2018.
- [197] L. Wu, Y. Shen, Z. Zhang, J. Dang, H. Liu, and J. Wang, "Receiver algorithms for single-carrier OSM based high-rate indoor visible light communications," *IEEE Transactions on Wireless Communications*, vol. 19, no. 2, pp. 1113–1126, 2020.
- [198] B. Béchadergue, W.-H. Shen, and H.-M. Tsai, "Comparison of OFDM and OOK modulations for vehicle-to-vehicle visible light communication in real-world driving scenarios," *Ad Hoc Networks*, vol. 94, p. 101944, 2019.
- [199] M. D. Soltani, X. Wu, M. Safari, and H. Haas, "Bidirectional user throughput maximization based on feedback reduction in LiFi networks," *IEEE Transactions on Communications*, vol. 66, no. 7, pp. 3172–3186, 2018.
- [200] A. Singh, A. Srivastava, V. A. Bohara, and G. S. V. Rao, "Outage and power saving analysis for hybrid cellular-visible light communication and direct cellular downlink," in *2018 20th International Conference on Transparent Optical Networks (ICTON)*, July 2018, pp. 1–4.
- [201] A. Singh, A. Srivastava, V. A. Bohara, and G. S. V. Rao, "Outage and power saving analysis for hybrid cellular-visible light communication and direct cellular downlink," in *2018 20th International Conference on Transparent Optical Networks (ICTON)*. IEEE, 2018, pp. 1–4.
- [202] A. Singh, A. Srivastava, V. A. Bohara, G. S. V. Rao *et al.*, "Power and SER analysis of VLC-and RF-based links in indoor environment," in *Broadband Access Communication Technologies XIII*, vol. 10945. International Society for Optics and Photonics, 2019, p. 109450R.
- [203] A. Singh, A. Srivastava, V. A. Bohara, and G. S. V. Rao, "Performance of hybrid cellular-VLC link for indoor environments under dynamic user movement," *Physical Communication*, vol. 36, p. 100816, 2019.
- [204] A. Singh, A. Srivastava, and V. A. Bohara, "Optimum led semiangle and the receiver fov selection for indoor vlc system with human blockages," in *2022 IEEE 95th Vehicular Technology Conference: (VTC2022-Spring)*, 2022, pp. 1–7.